TOUGHNESS OF FERRITIC STAINLESS STEELS

R. A. LULA, *editor*

TOUGHNESS OF FERRITIC STAINLESS STEELS

A symposium
sponsored by
the Metals Properties Council and
AMERICAN SOCIETY FOR
TESTING AND MATERIALS
San Francisco, Calif., 23–24 May 1979

Foreword

This publication, *Toughness of Ferritic Stainless Steels*, contains papers presented at the Symposium on Ferritic Stainless Steels which was held in San Francisco, California, 23-24 May 1979. The symposium was sponsored by the Metals Properties Council and American Society for Testing and Materials. R. A. Lula, Allegheny Ludlum Steel Corporation, presided as symposium chairman and was the editor of this publication.

Related
ASTM Publications

Part-Through Crack Fatigue Life Prediction, STP 687 (1979), $26.25, 04-687000-30

Properties of Austenitic Stainless Steels and Their Weld Metals (Influence of Slight Chemistry Variations), STP 679 (1979), $13.50, 04-679000-02

Fracture Mechanics Applied to Brittle Materials, STP 678 (1979), $25.00, 04-678000-30

Fracture Mechanics, STP 677 (1979), $60.00, 04-677000-30

Fatigue Testing of Weldments, STP 648 (1978), $28.50, 04-648000-30

Structures, Constitution, and General Characteristics of Wrought Ferritic Stainless Steels, STP 619 (1976), $7.50, 04-619000-02

Compilation and Index of Trade Names, Specifications, and Producers of Stainless Alloys and Superalloys, DS 45A (1972), $5.25, 05-045010-02

A Note of Appreciation
to Reviewers

Editorial Staff

Contents

Introduction

The ferritic stainless steels have been known and used in various applications for more than 50 years. Compared with the austenitic stainless steels. They are resistant to corrosion by reducing acids, they are resistant to chloride stress corrosion cracking, they are amenable, through alloy associated with the interstitial elements, carbon and nitrogen (C + N). Recent advances in melting technology have permitted the economical production of ferritic stainless steels with very low (C + N) content and, hence, improved toughness, opening a new vista for these materials. The ferritic steels have some very valuable features when compared with the austenitic steels. They are resistant to corrosion by reducing acids; they are resistant to chloride stress corrosion cracking, they are amenable, through alloy development, to achieve corrosion resistance superior to that of the austenitic steels, and they are more raw-material efficient in the sense that they can attain a certain level of corrosion resistance with a lower content of critical alloying elements than the austenitic steels.

The recently achieved ability to melt low (C + N) steels has resulted in an intense alloy development activity in the United States, Japan, and Europe. Several new ferritic stainless steels have been developed: 18Cr-2Mo-Ti, E-BRITE[1] 26Cr-1Mo, 26Cr-1Mo-Ti, 28Cr-2-Mo, 29Cr-4Mo, and 28Cr-4Mo-2Ni. The corrosion properties and the metallurgical characteristics of these alloys have been extensively investigated and have received ample coverage in the technical literature. The mechanical properties and the toughness, in particular, have not received attention commensurate with their importance in the design fabrication and operation of processing equipment.

The organization of this symposium was intended to fill this gap by concentrating on the toughness of ferritic stainless steels and the various factors that influence it. The papers presented cover the whole range of ferritic steels from 12 percent to 30 percent chromium content. A balance was accomplished between fundamental and applied research by obtaining papers from universities and processing and fabricating industries. Six of the 17 papers presented are from Japan, Canada, Sweden, and the United Kingdom, conferring to the symposium an international flavor.

This symposium has been sponsored by the Materials Properties Council-Adolph O. Schaefer, executive director, and by Subcommittee 7 on Fracture Toughness, of this organization.

R. A. Lula

Allegheny Ludlum Steel Corp., Brackenridge, Pa., 15014; editor.

[1] Registered trademark, Allegheny Ludlum Steel Corp.

1

R. N. Wright[1]

Toughness of Ferritic Stainless Steels

ABSTRACT: A comprehensive review of the factors fundamental to ferritic stainless steel toughness has been undertaken. Emphasis has been placed on the micromechanisms of fracture and their effects on the ductile-to-brittle transition consistent with the Cottrell crack nucleation model. The general effects of strain rate, plastic constraint (including gage effect), and grain size are set forth. The basic fracture behavior of body-centered-cubic metals, iron and iron-chromium solid solutions, is summarized. Primary emphasis is placed on the role of second phases in the ferritic stainless steel fracture process, and carbides, nitrides, martensite, α'-precipitation, and σ- and χ-phases are discussed extensively. The role of titanium and columbium as gettering agents for carbon and nitrogen is considered. The effects of cold-work are set forth and a brief outline is made of annealing guidelines for optimized toughness. Finally, the fracture behavior of welds and weld heat-affected zones is discussed and approaches to improved as-welded toughness are reviewed.

KEY WORDS: toughness, fracture, stainless steel, microstructure, ferritic stainless steels, fracture toughness

Ferritic stainless steels have been a subject of steadily increasing interest. The latitude of ferritic alloy design ranges to compositions of excellent general corrosion resistance and oxidation resistance. Moreover, the ferritic stainless steels are relatively resistant to stress corrosion cracking, and the alloying elements are generally inexpensive in comparison with the nickel-bearing austenitic grades. The principal limitation of the ferritic stainless steels concerns their lack of toughness, particularly when compared with the austenitic grades. Practical application of the ferritic stainless steels requires careful management of toughness with attention to optimizing composition, processing, and design.

Several comprehensive reviews of the ferritic stainless steels have been published [1-5][2], including the rather recent survey of Demo [5]. It is the

[1]Associate professor, Materials Engineering Department, Rensselaer Polytechnic Institute, Troy, N. Y. 12181.
[2]The italic numbers in brackets refer to the list of references appended to this paper.

2

purpose of this paper to address the subject of the toughness of ferritic stainless steel, per se, with emphasis on the relationship of its behavior to general body-centered-cubic (BCC) metal behavior as well as on the micromechanisms of fracture.

The analysis of Cottrell [6–8] provides a useful basis for discussing the micromechanics of brittle fracture even though, strictly speaking, the Cottrell model does not encompass all of the practical modes of crack initiation. To project a criterion for plastically induced crack nucleation, an energy balance is made between the work done on a slipband and the surface energy produced by opening a crack. The ductile-to-brittle transition is said to occur in the Cottrell model when

$$\sigma_y k_y d^{1/2} = k_y{}^2 + \sigma_0 k_y d^{1/2} \geq C\mu\gamma \qquad (1)$$

where

σ_y = flow or fracture stress or both,
k_y = Hall-Petch slope,
d = grain size,
σ_0 = lattice friction stress,
μ = shear modulus,
γ = effective surface energy of the implied crack, and
C = a constant related to stress state and average ratio of normal to shear stress on the slip plane.

Process and compositional manipulations can directly affect σ_y, k_y, d, σ_0, and γ, and discussions of the significance of such metallurgical changes on the fracture process will be channeled through the foregoing equation.

Generally, the toughness of the ferritic stainless steels will be assessed in terms of a ductile-to-brittle transition temperature (DBTT), or a temperature below which Eq 1 appears to be satisfied for a given material and mechanical test. The satisfaction of Eq 1 with decreasing temperature is generally associated with the tendency for flow stress to increase with decreasing temperature. Petch has explored this point for the case of mild steel [8]. DBTT values can vary greatly from one type of test to another. High strain rates and constraints to plastic flow have the effect of raising the flow stress and lowering the value of C and, thus, promoting satisfaction of Eq 1. Thus, Charpy test DBTT values will generally be higher than notched tension test DBTT values, which, in turn, will be higher than DBTT values for unnotched tension tests. In ferritic stainless steels it may be observed that metallurgical conditions with higher overall DBTT values display greater DBTT sensitivity to strain rate and constraint. Furnace-cooled Fe-26Cr alloys[3] can show a differential as high as 185°C between tension and Charpy test DBTT values

---

[3]All compositions are given in weight percent or ppm by weight.

[9] and a similar differential has been observed in a 475°C embrittled Fe-26Cr alloy [10]. However, more benign metallurgical conditions may be associated with DBTT variations of only a few degrees.

It is obvious from Eq 1 that grain size has a direct effect on DBTT and, in fact, many alloying effects on toughness are confounded by changes in grain size. Reasonable theoretical and experimental justification [8,11,12] exists for the relation

$$\text{DBTT} = D \ln d^{1/2} \qquad (2)$$

where D is a constant. In the case of ferritic stainless steels, Plumtree and Gullberg [13] noted DBTT variations with grain size that turn out to be consistent with Eq 2 for the case of a 150-ppm total carbon and nitrogen, Fe-26Cr alloy. Over a range of grain sizes from ASTM 3.5 to 6.5, a shift of 26 deg C per ASTM grain size number was noted. Less-pure Fe-26Cr compositions displayed much less sensitivity to grain size than shown in Eq 2 with shifts of 6 deg C per ASTM grain size number being common. Semchyshen [14] has noted a shift in ferritic stainless steel DBTT of roughly 20 deg C per ASTM grain size and Nichol [15] has reported a change of about 11 deg C per ASTM grain size over a range of grain sizes from 2.8 to 0 in a high-purity Fe-29Cr-4Mo-2Ni alloy. In general the effect of grain size on ferritic stainless steel DBTT may be somewhat less than projected by Eq 2. Clear-cut effects are nonetheless quite demonstrable.

Another significant factor affecting the DBTT level is that of gage or specimen thickness. Generally, thinner material displays decreased DBTT to a point where very light gages may display no practical toughness limitation [15–17]. *Part* of this effect results from grain size refinement with continued processing. For example, ferritic stainless hot-rolled band, annealed at 0.3 cm, may have an ASTM grain size of 4, whereas 0.15 and 0.05 cm cold-rolled and annealed stock may display respective grain sizes of 6 and 8. However, the bulk of the effect on Charpy test DBTT values is *mechanical* rather than metallurgical. At thin gages, the metal at the notch tip is not substantially constrained in the direction perpendicular to the strip plane (the stress state approaches that of plane stress). As gage increases, constraint occurs in this perpendicular direction and the stress state becomes triaxial at the crack tip (at great enough thickness the stress state begins to resemble that of plane strain). The increased constraint of thicker gage has the effect of lowering C in Eq 1 and results in higher DBTT values, independent of any role of changing grain size. In fact, Nichol has directly compared machined-to-gage and rolled-to-gage specimens of Fe-29Cr-4Mo-2Ni and found that the results could be plotted on a common curve with the effect of gage thus being totally mechanical [15]. Lula [17] has compared the effect of gage on DBTT for seveal ferritic stainless steels, as shown in Fig. 1. Specimens tested at a gage of 0.15 cm typically display DBTT values 150 to

Transition temperature, F(c)
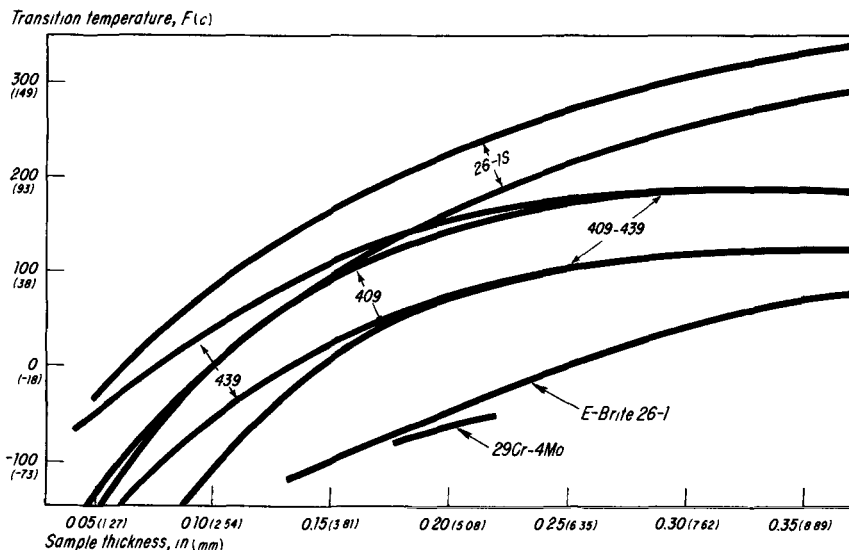
FIG. 1—*DBTT values for several ferritic stainless steels as a function of section thickness* [17].

200 deg C below those of specimens tested at the full-size Charpy thickness of 1 cm. Similar effects are, of course, observed in many other alloy systems.

BCC Behavior of Iron and Iron Chromium

Much of the problem with ferritic stainless steel toughness lies in the fact that the crystal structure is body centered cubic (bcc). While this is little more than a fact of life, designers who take austenitic-type (face centered cubic—fcc) toughness for granted will have to make adjustments, even to the lowest transition temperature bcc alloys. For a general discussion of bcc fracture the reader is directed to the review of Stoloff [11]. Bcc metals display a marked increase in σ_0, the lattice friction stress, with decreasing temperature. This directly contributes to the flow stress and to the satisfaction of Eq 1, often in temperature ranges of engineering interest. In contrast, relatively pure fcc metals and alloys may never manifest conditions satisfying Eq 1.

The basic cause of bcc brittleness appears to lie in the sensitivity of the structure to even the smallest levels of interstitial impurities. Zone-refined bcc polycrystals can be ductile at −269°C [18,19]. However, even slightly less-pure alloys have relatively high DBTT levels. Interstitials in solid solution appear to be progressively embrittling and in the Group *V-a* metals the relative order of importance has been suggested to be hydrogen, oxygen,

nitrogen, and carbon, in decreasing order [20]. The partitioning of the solute to the grain boundaries may be important. Oxygen at levels of only 20 to 30 ppm produces intergranular embrittlement in iron [21,22], an effect that is considerably mitigated by the presence of carbon [23,24].

The solubility levels of the interstitial elements in bcc alloys are sufficiently low that it is rarely possible to clearly separate solute effects from the effects of carbide, nitride, or oxide precipitates [25]. Indeed, the precipitates may be even more important than the solute, particularly as the interstitial element content significantly exceeds the solubility limit [26].

Thus, for iron, as a bcc metal, one observes ductility at −269°C with zone refining [18], but (001) cleavage at −196°C and above as carbon and nitrogen contents increase [25]. Oxygen in small quantities (in the absence of carbon) can lead to intergranular embrittlement, raising the DBTT even above 0°C [27]. Carbon and nitrogen contents well beyond the solubility limits further increase the DBTT. Much of the effect has to do with the number and size of carbides and nitrides formed at the grain boundaries. The precipitates may be strong barriers to slip propagation across grain boundaries and may thus raise k_y [28]. The precipitates may tend to crack and lead to crack propagation in the adjacent ferrite, in effect lowering γ in Eq 1. McMahon and Cohen have shown cleavage cracks in low-carbon ferrite to originate at cracked 1- to 3-μm carbide particles [26]. Grain boundary carbide and nitride precipitation can be suppressed by rapid cooling from above the solution temperatures. However, resulting fine intragranular precipitation may increase the DBTT by increasing the lattice friction stress, σ_0.

The addition of chromium in large quantities has a relatively minor effect on the DBTT values of iron. It is, of course, difficult to separate the effect of chromium as a solid-solution solute element from its effect as a carbide and nitride former and from possible effects on grain size. However, the recent work of Kelley and Stoloff [29] makes it clear that chromium up to 11.2 weight percent has no effect on the tension test DBTT and very limited effect on the increase of σ_y with decreasing temperature. For further comparison, full-size impact test DBTT values for low carbon and nitrogen (C + N) iron are generally in the range from −25 to −75°C [27,30,31] and a tension test DBTT value of perhaps −180°C is representative [29,32] (except for ultrapure zone-refined metal). In comparison, quenched low (C + N) Fe-26Cr alloys display full-size Charpy V-notch DBTT values in the −55 to −65°C range [13,16,33], even with coarse grain size, and tension test DBTT values as low as −195°C have been cited [10] for such binary compositions. Of course, grossly increased DBTT values can be engendered in low (C + N) iron and chromium alloys (as dealt with in the following). However, the simple addition of large amounts of chromium solute appears to present no necessary problem.

While the effects of individual alloying elements on ferritic stainless steel toughness are dealt with in detail later, some comment is pertinent at this point regarding the comparative effects of molybdenum, nickel, and aluminum on the DBTT range of iron. Molybdenum, like chromium, is remarkably benign as a simple solute addition [14,34]. Better yet, nickel displays a decidedly beneficial effect. Gensamer has shown, for example, a 50 deg C suppression of the Charpy test DBTT to be associated with 3.6Ni addition [31]. McEvily has suggested that the beneficial effect of nickel is related to its distortion of the ferrite lattice and thus its consequent entrapment of interstitial solute [11]. A decrease in the magnitude of dislocation locking with nickel addition is suggested by internal friction measurements [35] and by yield-point observation [36]. Aluminum shows a marked tendency to increase the DBTT in ferrite. The effect has been attributed to cross-slip inhibition (and related flow stress increase) and tension test DBTT increases of 85 deg C can be associated with an 8Al addition [32]. On the other hand, in the presence of nitrogen, aluminum can have the beneficial effect of tying up nitrogen as aluminum-nitride, thus lowering the lattice friction stress and refining grain size as well. The much more interesting use of titanium and columbium to tie up interstitial elements is discussed in the following.

At this point, though, it can be seen that the iron-chromium or iron-chromium-molybdenum compositions basic to ferritic stainless steel alloy design do not necessarily present fracture problems much different from those of low-carbon iron. Unfortunately, processing and service excursions and more complex alloy designs can lead to a variety of "second" phases which can sharply raise the DBTT. Foremost among these second-phase effects are the problems associated with carbides and nitrides.

Second-Phase Effects in Ferritic Stainless Steels

The second-phase effects that are most important to the ferritic stainless steel DBTT are those of the carbides, nitrides, and oxides; martensite; α'; and σ and χ. Beyond these, certain phases related to unusual alloying additions may present themselves and, in many instances, the morphology and size of the additional phase may be important.

Carbides, Nitrides, and Oxides

The qualitative relation of (C + N) to ferritic stainless steel toughness has long been known. The concept that high-chromium ferritic stainless steels can be rendered tough enough for practical applications by reducing the (C + N) content can be traced to the work of Hochman [37] and Binder and Spendelow [38]. These latter authors demonstrated, for example, that

practical values of as-annealed impact resistance could be developed in an Fe-30Cr alloy if total (C + N) were held below 200 ppm. In general the requirements for low (C + N) become more stringent as chromium content increases. The widely cited data of Binder and Spendelow are shown in Fig. 2. With the advent of modern melting techniques and under the pressure of high technology demands, a number of high-chromium, low-carbon, and nitrogen alloys have become commercially available. Total (C + N) contents below 200 ppm are common, and in the as-annealed-*and-quenched* condition the alloys commonly exhibit Charpy V-notch DBTT values well below 0°C.

Unfortunately, the DBTT values associated with a given low (C + N) level can be grossly altered by heat treatment and much of this effect involves changes in the *state* of (C + N). In particular, the DBTT is sensitive to postanneal (or postweld) cooling rates and the effect is quite different depending on the (C + N) level. As shown in Fig. 3, rapid cooling rates enhance the toughness of alloys with total (C + N) in the 150-ppm range [*16,33,39*] and the beneficial effect of rapid cooling or quenching has been observed in Fe-26Cr alloys at total (C + N) levels as high as 900 ppm [*16*]. However, as the (C + N) level increases, the effect is reduced, and at high (C + N) levels *rapid* cooling from temperatures above 1000°C raises the DBTT, as observed by Demo with a T446 alloy containing 350-ppm
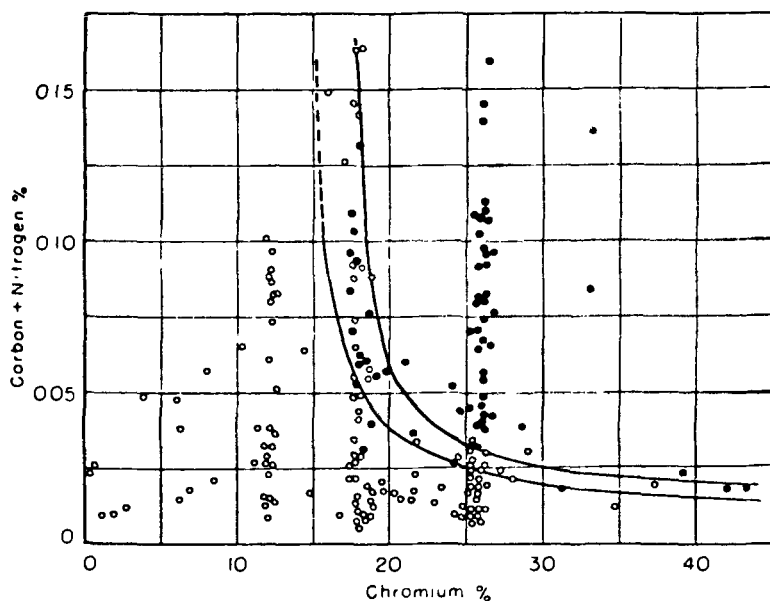
FIG. 2—*Influence of (C + N) on the toughness of iron-chromium alloys. Open circles: high-impact-strength alloys; solid circles: low-impact-strength alloys* [38].

nitrogen and 950-ppm carbon [40] and by Semchyshen et al [14] on a wide range of iron-chromium alloys. Annealing of the high (C + N) alloys in the 850°C range does not lead to such DBTT increases.

The embrittlement associated with the slower cooling of low (C + N) compositions is clearly carbide and nitride related. Plumtree and Gullberg have associated Fe-26Cr embrittlement with the formation of chromium nitrides and carbides at the grain boundaries [13]. Slower cooling of lower (C + N) content alloys fosters grain boundary carbide and nitride precipitation. More rapid cooling leads to a dispersed, intragranular precipitation or to actual retention of (C + N) in solution. Although the (C + N) in solution must have some embrittling effect, relative to pure iron, the effect of solute (C + N) in low (C + N) ferritic stainless steels seems to be quite benign in comparison with the effect of carbide and nitride precipitates. Pollard [41] has noted that the appearance of grain boundary carbonitrides coincides with the loss of ductility in low (C + N) Fe-26Cr and Richter and Finke [43] have noted such precipitates are sites of crack initiation. The embrittlement associated with rapid cooling in high (C + N) level alloys has been suggested by Thielsch [43] to be due to the retention of clustered (C + N) atoms in a grossly supersaturated ferrite matrix. Alternatively, Demo [40] has observed that such quenching embrittlement is associated with fine precipitation on dislocations and presumed low mobile dislocation density. In either case the effect would be to increase the lattice friction stress, σ_0, and the flow stress, σ_y.

As chromium level increases, the levels of carbon and nitrogen consistent with good toughness decrease. This relationship is almost certainly due to the decrease in (C + N) solubility with increased chromium content [44].
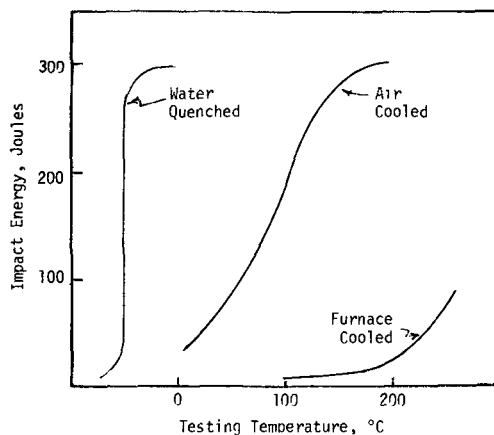
FIG. 3—*Impact energy curves for an Fe-26Cr alloy containing 150-ppm total (C + N) as a function of cooling rate from an 850°C anneal* [39].

The detailed role of (C + N) has been set forth in the very recent work of Grubb and Wright [9] on two Fe-26Cr alloys with combined (C + N) levels of 67 and 570 ppm, respectively. Through heat treatment alone, DBTT variations greater than 200 deg C were achieved in each alloy. At the 67-ppm (C + N) level, carbide and nitride precipitation was entirely suppressed by rapid quenching and, at a gage of 0.15 cm, the Charpy V-notch DBTT was at −130°C. The DBTT became considerably higher when carbide and nitride precipitation was induced through isothermal annealing at low and intermediate temperatures or through slow cooling. Carbide precipitation occurs generally above 850°C; nitride precipitation develops at much lower temperatures [41]. C + N solubilities are displayed in Fig. 4. Grain boundary carbide precipitation in the 67-ppm (C + N) alloy resulted in an increase of the DBTT to −60 to −70°C, and plate-like intragranular precipitation of Cr_2N could be associated with DBTT levels as high as 90°C. The grain boundary precipitates and the plate-like nitrides are shown in Figs. 5 and 6, respectively, for the 67-ppm (C + N) alloy. At the 570 ppm (C + N) level the grain boundary carbides and the plate-like nitrides were again sources of embrittlement. However, quenching to suppress carbide and nitride precipitation leads to a great increase in DBTT. The lowest DBTT value, 0°C for 0.15-cm gage, was associated with a mixture of grain boundary and intragranular carbides and nitrides. Quenched structures displayed DBTT values up to 100°C and furnace-cooled material was even
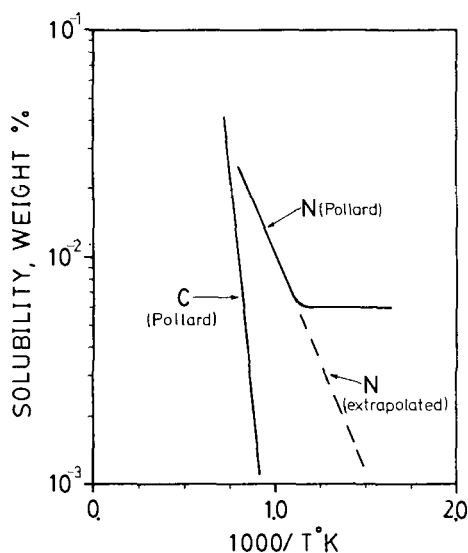
FIG. 4—*Solubility of* (C + N) *in Fe-26Cr. Solid lines represent data of Pollard* [4]. *Dotted line represents an extrapolation of Pollard's data based on Henry's law* [45] *(from Grubb and Wright* [9]).
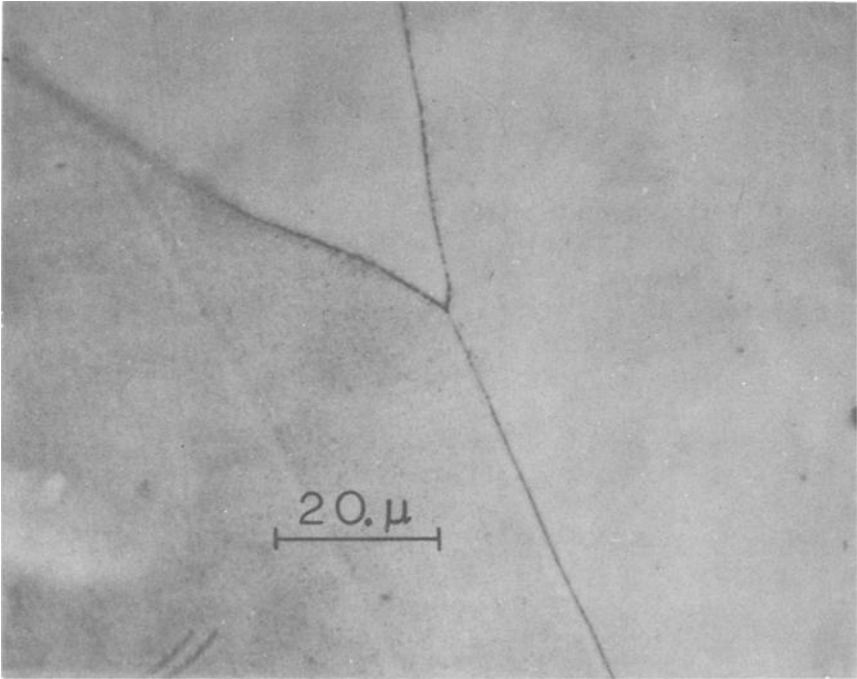
FIG. 5—*Light micrograph showing grain boundary precipitate in an Fe-26Cr alloy annealed at 705°C. Total (C + N) level is 67 ppm* [9].

worse, with a DBTT level of 205°C. The heavy grain boundary precipitates produced by furnace cooling are shown in Fig. 7.

The plate-like Cr_2N precipitates were observed by Grubb and Wright to readily open during plastic deformation and thus embrittle by greatly lowering the value of γ, the effective surface energy of the crack. Beyond this the fine, plate-like precipitation results in an increase in σ_0 and, hence, in σ_y. Thus, the reasons for the big effect on DBTT seem fairly clear. A secondary crack associated with a plate-like nitride is shown in Fig. 8. The grain boundary precipitates were seen to crack as well and to provide macro-crack initiation sites through grain boundary cracking or through propagation of the precipitate crack into the matrix. Thus their role in lowering γ and in concentrating stress seems clear. Beyond this, the solute redistribution and grain boundary precipitation associated with extended low-temperature exposure generally increase k_y, but with possible simultaneous lowering of σ_0 [13,39]. Thus the effect of grain boundary precipitation on σ_y is problematical, although increased k_y promotes brittle fracture over and above its effect on σ_y. The DBTT increase associated with quenching the higher

FIG. 6—*Light micrograph showing plate-like nitride precipitate in an Fe-26Cr alloy furnace-cooled from 1290°C. Total (C + N) level is 67 ppm* [9].

(C + N) alloy is consistent with the earlier work of Demo [40] and may be related to increases in σ_0 and σ_y, as mentioned earlier.

While it is not always easy to identify the carbide and nitride precipitates that develop in ferritic stainless steels, the compounds seen in the higher chromium alloys are Cr_2N, $Cr_2(C,N)$, $Cr_{23}C_6$, and, possibly, CrN [39,41, 46,47]. $Cr_{23}C_6$ predominates at high carbon to nitrogen ratios while Cr_2N [or $Cr_2(C,N)$] predominates at low carbon to nitrogen ratios [4]. The plate-like intragranular precipitate which forms at low temperatures has been observed and identified by Lena and Hawkes as Cr_2N [47].

Of course, the debilitating effects of such carbide and nitride formation can be reduced if not eliminated by maintaining (C + N) at extremely low levels. A more economical approach is to alloy with titanium (or columbium). With titanium addition, (C + N) is tied up as Ti(C,N), largely in the molten steel. The Ti(C,N) is readily identified as a blocky, randomly distributed precipitate. Weight ratios of titanium to (C + N) of 10 or more are generally regarded as adequate to tie up the vast majority of (C + N) [48]. Even so, some (C + N) often remains in solution and lower-temperature precipitation can occur in titanium-stabilized steels. Moreover, it seems unlikely that titanium is involved in such precipitation and the lower-
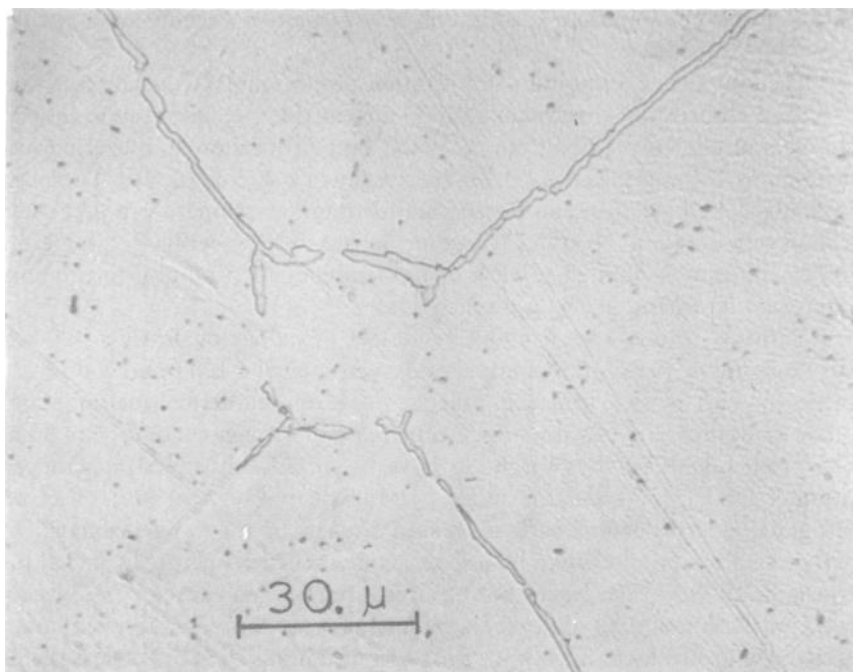
FIG. 7—*Light micrograph showing heavy grain boundary precipitate produced by furnace cooling from 1290°C in an Fe-26Cr alloy with 570-ppm total (C + N)* [9].
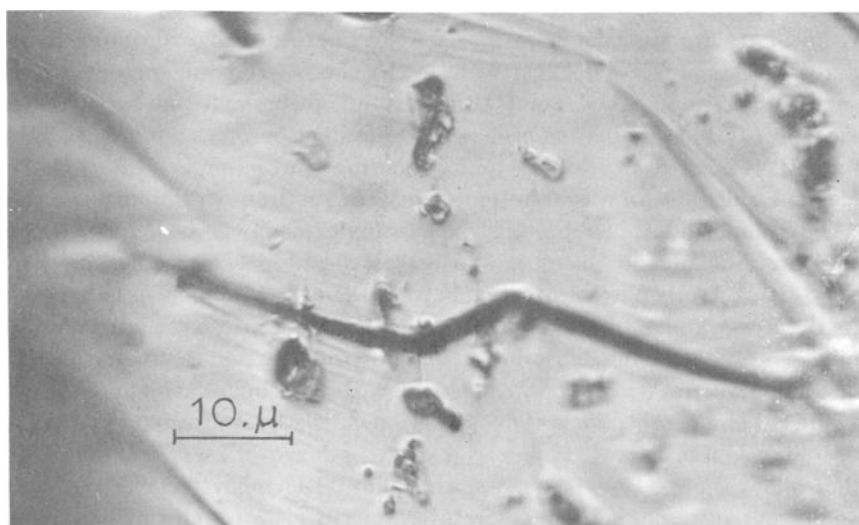

FIG. 8—*Light micrograph of electropolished tension specimen showing secondary crack nucleated from a plate-like nitride in an Fe-26Cr alloy* [9].

temperature precipitation is still that of *chromium* carbide and nitride [*10,41*].

Titanium and columbium stabilization does reduce considerably the extent of embrittling chromium carbide and nitride precipitation in ferritic stainless steels. In the 550 ppm (C + N) range, titanium stabilization has been shown to lower the DBTT of Fe-26Cr as much as 115 deg C [*10*]. Titanium is similarly beneficial in eliminating embrittling low-temperature precipitation in very low (C + N) alloys. However, its use in alloys with (C + N) levels under 100 ppm is limited in view of the tendency for titanium to promote intergranular fracture [*10*], as discussed later.

Relatively little is known about the effect of oxides on ferritic stainless steel toughness, particularly in the low oxygen range (≤ 100 ppm) commonly achieved with electric furnace practice, vacuum induction melting, and other modern melting techniques. An increase of oxygen content from 90 to 535 ppm was shown by Wright to have essentially no effect on wrought product DBTT [*16*]. On the other hand, Kanamaru et al [*49*] observed mitigated embrittlement with decreased oxygen in the range from 20 to 300 ppm. Richter and Finke [*41*] noted oxide inclusions acting as nuclei for transgranular cleavage cracks but observed that oxygen caused considerably less embrittlement than did carbon and nitrogen. In any case, preoccupation with oxide involvement in commercial ferritic stainless steel brittleness seems unwarranted.

Martensite

The effects of (C + N) on iron-chromium toughness become greatly reduced at chromium levels in the 17 weight percent range and lower [*38*], and it is this range that is germane to the classical ferritic stainless alloys such as T430 and T434. Some benefit is still to be achieved by (C + N) control [*14*], but elimination of martensite content becomes a more practical pursuit. It is, of course, widely understood that chromium is a "ferritizing" element and that an austenite loop exists in the iron-chromium diagram. Alloy compositions just beyond the austenite loop will be ferritic at all temperatures and no austenite and martensite need be feared. Moreover, only 12Cr or so is needed to move beyond the austenite loop in alloys with total carbon and nitrogen contents below 50 ppm. However, carbon and nitrogen are powerful "austenitizers" and conventional commercial levels of total (C + N) ($\simeq 700$ ppm) push the $\gamma + \gamma/\alpha$ boundary out as far as 21½Cr. For a detailed look at this behavior the reader is directed to the work of Baerlecken et al [*44*]. Part of this work is shown in Fig. 9. The point is that alloys such as the 17 percent chromium T430 may form as much as 40 percent austenite in the temperature range of 1100°C and small amounts of γ as low as 950°C. The problem is, of course, far worse at lower chromium levels. Thus, welds, weld heat-affected zones (HAZ's), hot-rolled band, and
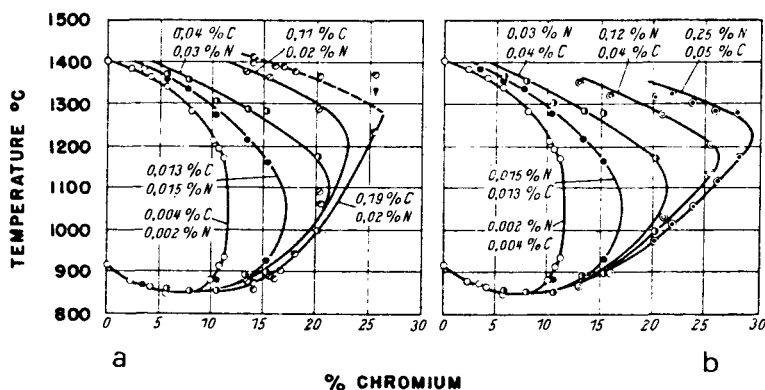
FIG. 9—*Shifting of the boundary line* $\gamma + \gamma/\gamma$ *in the iron-chromium system with increasing* $(C + N)$ *content* [44].

even some annealed stock can contain untempered martensite. The presence of this martensite leads to increased DBTT. The effect is most likely due to strain concentrations in the relatively soft ferrite adjacent to the hard martensite particles. The martensite, per se, is unlikely to be any more brittle than the ferrite [50].

Martensite-related embrittlement can be avoided either by "tempering" or simply annealing the duplex ferrite-martensite structure. Ferritic stainless steel hot-rolled band is commonly annealed for this reason, among others. Beyond this, alloying additions are frequently made to change the phase balance and move the composition away from the austenite loop. In this regard alloying elements are grouped as "ferritizers" (tending to promote a fully ferritic structure) and "austenitizers" (tending to increase the size of the austenite phase field). The common austenitizers are carbon, nitrogen, manganese, nickel, and copper, whereas the common ferritizers are chromium, silicon, titanium, molybdenum, and aluminum.

The net effect of alloying additions and residual impurities on phase balance may be expressed as a "chromium equivalent" in the manner of Thielemann [51]. A reasonably accurate modification of Thielemann's approach is [50]

$$\%\text{Cr equivalent} = \%\text{Cr} + 5(\%\text{Si}) + 7(\%\text{Ti}) + 4(\%\text{Mo}) + 12(\%\text{Al})$$

$$-40(\%\text{C} + \text{N}) - 2(\%\text{Mn}) - 3(\%\text{Ni}) - \%\text{Cu} \qquad (3)$$

where the compositions are in weight percent. Roughly speaking, chromium equivalents of 12 percent or higher are necessary in order to move the composition outside the austenite loop at all temperatures (just as 12 percent chromium is, itself, required in a high-purity binary iron-chromium alloy).

It is important to note that residual impurities can make an important contribution to the chromium equivalent.

One of the first alloys to involve an addition substantially for the purpose of avoiding austenite and subsequent martensite was T405, involving an aluminum addition. This alloy has been more or less superceded by 11 percent chromium compositions such as T409 wherein a titanium addition (at perhaps 10 times total C + N) renders the alloy totally ferritic at essentially all temperatures. Not only is titanium a potent ferritizer, but it also ties up the powerful austenitizers carbon and nitrogen. At the 17 percent chromium level 'it is important to note that molybdenum is a ferritizer and that T434 (17Cr-1Mo) or an 18Cr-2Mo ferritic stainless steel will form significantly less martensite than T430. In that regard, T439 (18Cr-0.5Ti) lies well outside the austenite loop.

It is remarkable that little fundamental work has been done to quantify the effect of martensite on DBTT. One hopes that, in fact, a scientific description of the effect would be consistent with the apparent engineering significance. An example of the martensitic second phase is shown in Fig. 10.

α' (475°C) Embrittlement

Prolonged exposure of ferritic stainless steels to the temperature range from 400°C (or perhaps even 300°C) to 550°C results in a considerable increase in DBTT. The effect is most pronounced in the range of 475°C or 885°F and the response is widely known as "475°C (or 885°F) embrittlement." The effect on the DBTT can be very great and exposure of an Fe-26Cr alloy to 475°C for 500 h has been shown to result in at least a 500 deg C increase in Charpy V-notch transition temperature [39]. The embrittlement presents few problems in processing, but imposes considerable limitations to service applications, particularly with regard to heat-exchange apparatus. The 475°C embrittlement phenomenon is a consequence of the precipitation of a chromium-rich bcc phase, α', which forms due to the miscibility gap in the iron-chromium equilibrium system [46,52-55]. The miscibility gap can be clearly seen in Fig. 11 [56,57]. Roughly speaking, the gap exists from perhaps 10Cr to 90Cr. A spinodal exists within the miscibility gap [58]. The precipitation of α' is thought to occur by a nucleation-and-growth mode outside the spinodal and by spinodal decomposition within [58-62]. Reasonable evidence for nucleation-and-growth behavior has been set forth for 19Cr, 21Cr, and 24Cr alloys [54,58,62]. Behavior suggestive of spinodal decomposition has been noted for 29Cr alloys and higher [55,58,61,62]. In addition to increasing DBTT, the α'-precipitate increases hardness and strength. Of course, the α'-precipitation and the related embrittlement can be removed by simply annealing the steel in the normal range (850°C). However, this is often of little assistance to the embrittlement of parts in service.

The α'-precipitation may occur simultaneously with other embrittling
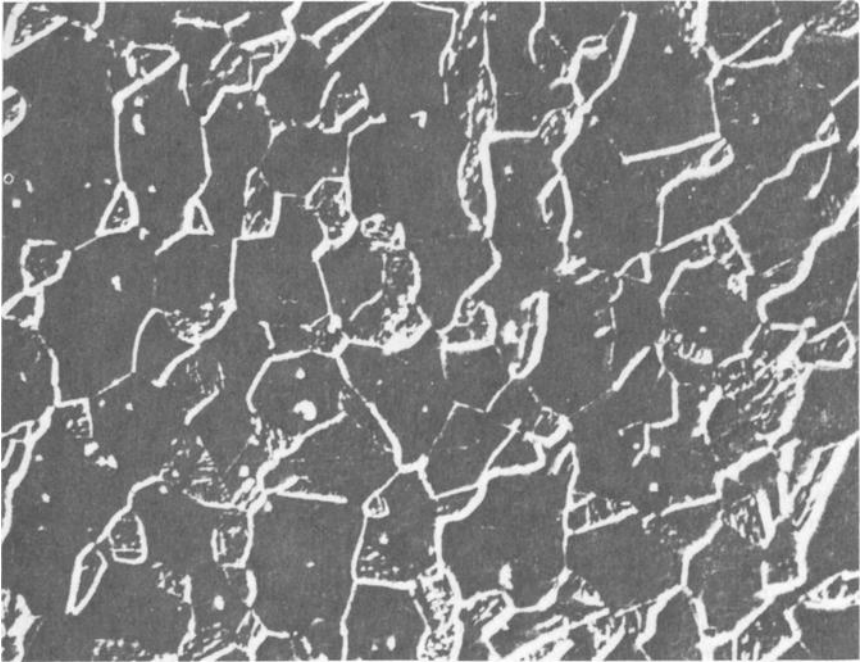
FIG. 10—*Micrograph of T430 ferritic stainless steel heat-treated at 1150°C for 10 min and water quenched. Martensite appears as a mottled phase (×500).*
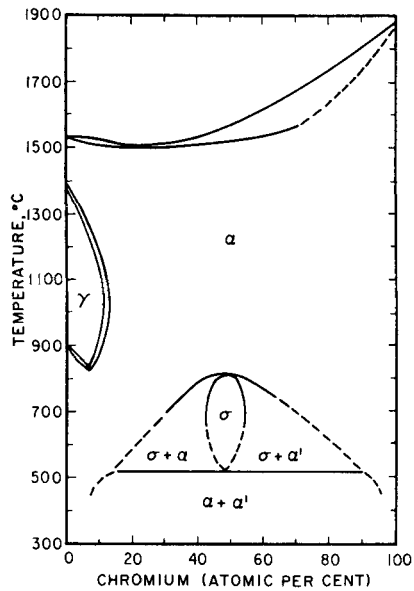
FIG. 11—*General iron-chromium equilibrium diagram.* [56,57].

reactions and this has confused many investigators. In cold-worked structures σ-phase may be precipitated along with α' [52]. Moreover, it is obvious that chromium carbonitride precipitation can occur readily at temperatures as low as 475 °C, and the relatively rapid carbonitride embrittlement has no doubt often been cited as an early stage of 475°C embrittlement. The problem of distinguishing between carbonitride and α'-precipitation effects has been dealt with in detail by Plumtree and Gullberg [39]. From their work on a 26Cr alloy it seems clear that the effects of carbonitride precipitation should be largely manifest after an hour or so at 475°C, with α'-precipitation not becoming significant until perhaps *ten* hours. Moreover, the effect of α'-precipitation on DBTT becomes increasingly severe as time passes. For the 26Cr level, one sees after 10 h at 475°C a DBTT increase of 95 deg C [10], part of which is probably relatable to carbonitride precipitation. After 100 h, the increase in DBTT is 220 deg C [10] and after 500 h an increase of as much as 500 deg C has been indicated [39]. A good feeling for the embrittlement kinetics can be obtained from the work of Nichol [15] on Fe-29Cr-4Mo-2Ni, as shown in Fig. 12. The *lower* noses bracket the time at which the α'-precipitation embrittlement moves the DBTT through the room temperature range (starting from a DBTT level of about -20°C). The kinetics are rather more rapid for this highly alloyed composition than for the Fe-26Cr material discussed earlier. The nose at 475°C clearly indicates α'-precipitation, however, since carbonitride effects would develop more rapidly at, say, 550°C than at 475°C.

The increased α'-embrittlement kinetics with alloying addition is an apparently general effect and a gross impediment to alloy development. Essentially all impurities hasten the embrittling reaction [1,59,63–65]. Alloy development studies have offered no remedy except in pointing to reduced
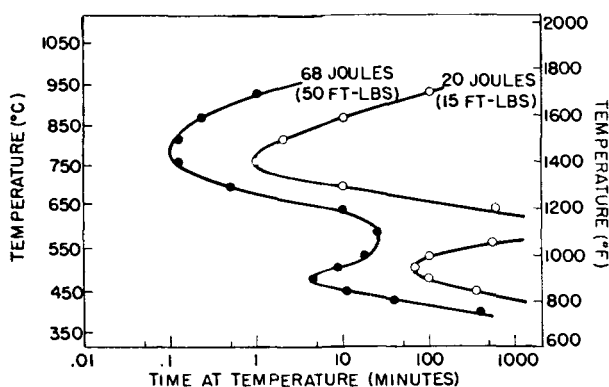
FIG. 12—*Room-temperature Charpy V-notch toughness as a function of isothermal exposures of water-quenched Fe-29Cr-4Mo-2Ni alloy* [15].

embrittlement in higher-purity, lower-chromium content compositions. Some disagreement exists on the precise effects of cold and warm work [1,46,47,66] but very recent work by Grobner and Steigerwald [67] makes it clear that cold work has no really practical effect on the α'-embrittlement process.

In the spinodal reaction composition range, the precipitation should be, in principle, quite general and independent of defect structure [60]. However, preferential precipitation at dislocations and grain boundaries has been noted in the nucleation-and-growth range [54,59] and even into the spinodal [46]. The α'-phase cannot be detected by ordinary light microscopy but is readily resolved by appropriate transmission electron microscopy (TEM) [39,53]. In the studies of low-chromium alloys, Grobner suggested that the mechanical effects of the α'-precipitate are due to dislocation locking [59], whereas Marcinkowski et al cited the lattice friction of the α'-phase, the chemical interface energy, coherency strains, and elastic modulus differences as sources of increased strength in an aged 47Cr alloy [53]. Several authors have noted widespread twinning upon deformation of the α'-embrittled structure [15,53,54]. The predominant fracture mode is intragranular cleavage [54].

The bulk of the evidence points to a gross effect of α'-precipitation on the lattice friction stress, σ_0, as the prime embrittling factor. This could be as a result of outright dislocation locking or intermediate range impedance to dislocation motion presented by the multitude of precipitate barriers. This view has been substantiated by the recent work of Grubb, Wright, and Farrar [10]. These authors noted little or no subcritical microcrack formation in a 475°C embrittled Fe-26Cr alloy. Thus, they inferred that the flow stress elevation of the α'-precipitation (an elevation of about 300 MPa) had led directly to fracture criterion satisfaction without the involvement of local stress- or strain-raising effects, such as are important in carbonitride-related fracture. Beyond this, Grubb et al noted that α'-precipitation greatly altered slip character. The profuse, multiple slip normally observed was replaced by a relatively few, extremely intense slipbands, perhaps reflecting the development of microinstability in the α'-precipitated lattice.

σ and χ Phase Embrittlement

Very high chromium content stainless steels (including austenitics) may be embrittled by precipitation of σ-phase in the 500 to 900°C range. The range of σ-phase stability for the binary iron-chromium system is clearly evident in Fig. 11. This phase is not readily formed in alloys containing less than 20Cr and forms only very sluggishly at higher chromium contents. For example, about 10 h is required for a 26Cr alloy at 650°C and even for a 35Cr alloy a time of, say, 15 min is required [68]. Unfortunately, the kinetics are much more rapid in many practical situations. Cold work greatly increases the

transformation rate [52,69–73]. Moreover, important alloying (or residual) elements such as molybdenum, nickel, manganese, and silicon shift the σ-phase region to lower chromium contents [68,69,74,75]. This is particularly important in the case of molybdenum, as detailed in the ternary diagram isothermal section shown in Fig. 13 [76]. Figure 13 also shows the presence of the χ-phase which may develop along with the σ-phase in molybdenum-bearing, high-chromium ferritic stainless steel. The χ-phase is also a source of embrittlement.

Thus in Fig. 12 the higher-temperature noses bracket the time at which the σ and χ phase precipitation embrittlement moves the DBTT through the room-temperature range (again, starting from a DBTT level of about $-20°C$). Times of less than 1 min are significant for the highly alloyed metal, even in the absence of cold work. In the case of Fig. 12 it is likely that the higher-temperature embrittlement is predominantly due to χ-phase [15,77]. A nickel-free version of the alloy shows a greater tendency for forming σ-phase as well as χ-phase [77]. The temperature range of rapid σ and χ formation coincides with the normal ferritic stainless steel annealing range and, consequently, highly alloyed ferritic stainless steels such as Fe-29Cr-4Mo-2Ni must be annealed in the austenitic range of 1050°C and quickly cooled through the 500 to 900 °C range in order to avoid σ and χ phase

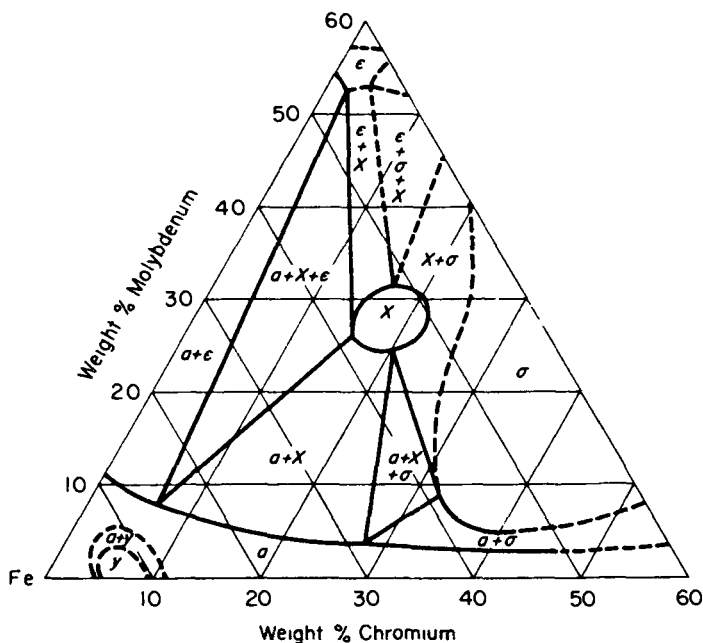
FIG. 13—*Isothermal section at 850°C in the ternary alloy system iron-chromium-molybdenum* [76].

embrittlement. There is also the potential for σ and χ phase formation in welds and weld HAZ's. However, the likelihood of such σ and χ phase embrittlement is small for all but the most highly alloyed ferritic stainless steels. If σ or χ phase does form, the alloy can, of course, be reheated to dissolve the phases and quickly cooled to avoid their re-formation.

Sigma-phase is a hard, brittle intermetallic with a tetragonal structure and a nominal FeCr composition. Chi-phase is also quite brittle and is a complex cubic phase of the α-manganese type, corresponding to the formula $Fe_{36}Cr_{12}Mo_{10}$ [78, 79]. There is a general tendency for the phases to precipitate at ferrite grain boundaries although some intragranular formation of χ-phase has been reported [77]. Figure 14 displays a microstructure from the work of Streicher on the Fe-29Cr-4Mo system showing grain boundary σ-precipitation which has been surrounded by χ-phase [77]. Transverse microcracking of the duplex $\sigma - \chi$ grain boundary layer is quite evident in Fig. 14.

The formation of σ and χ phase does not necessarily result in an increase in flow stress [15]. Rather, it seems that the embrittlement effect must be that of a decrease in γ, the effective surface energy of an initial crack, or an increase in resistance to slip propagation across grain boundaries, or a stress concentration brought about by the irregular, hard intermetallic phases (or cracks therein). In any case, fracture occurs in a predominantly inter-granular mode upon embrittlement by σ and χ phase precipitation [15].

Other Second-Phase Considerations

While the second phases cited in the preceding are the ones most commonly encountered in ferritic stainless steel embrittlement problems, others can be important to specific alloy compositions. For example, retained austenite is occasionally noted in T446 and certain other high-chromium compositions [40,44,80] and it has been suggested that embrittling stress concentrations could occur at the ferrite-austenite interface [81].

The highly oxidation-resistant Fe-16Cr-5Al-0.3Y composition, known as Fecralloy [92,83,84], presents some unique second-phase embrittlement considerations. First of all, the alloy displays a Charpy V-notch DBTT range roughly 80 deg C higher than straight chromium grades of similar (C + N) content. Part of this embrittlement no doubt stems from the effects of aluminum on the ferrite solid solution. However, study of electropolished strips pulled to fracture in the DBTT range reveals that fracture initiation occurs primarily by cleavage of globular, 20-μm particles of the nominal composition YFe_9 [85]. It is interesting that the globular YFe_9 particles are more predisposed to crack initiation than lengthy stringers of YFe_9 crushed during hot rolling. In fact, "stringers" are of little consequence in many ferritic stainless steel DBTT measurements, in spite of effects they may have on ductile fracture, per se. Transverse and longitudinal DBTT values are often comparable.
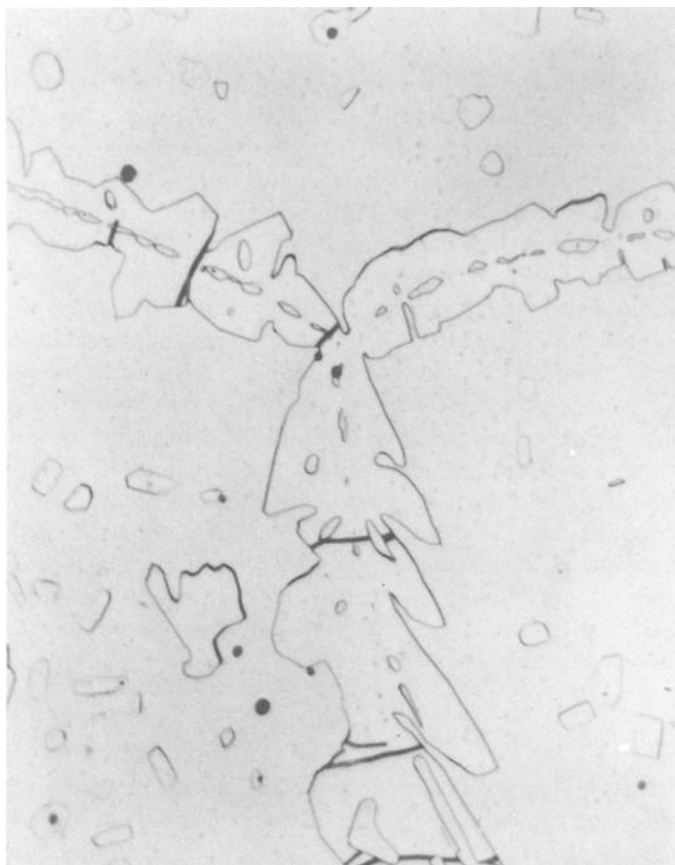
FIG. 14—*Micrograph of Fe-29Cr-4Mo alloy heated for 100 h at 815°C. Fine grain boundary particles are σ-phase; coarse surrounding layers are χ-phase, as are the intragranular precipitates. Note cracks in σ-χ structure (×750)* [77].

It is, though, a recurring theme that toughness is as dependent on the *size* and *distribution* of the second phase as it is on the intrinsic properties of the phase. Fine intragranular carbides and nitrides produce behavior quite different from grain boundary precipitates. Martensite presumably embrittles ferrite, yet it has been shown that a *fine-structured* duplex ferritic-martensitic alloy has a lower DBTT than either the ferrite or martensite in monolithic form [50].

Of course, a wide range of unmentioned second phases can, in principle, be composed from the residual impurities that are found in most commercial ferritic stainless steels. Moreover, the solid-solution strengthening effects of the residuals must not be overlooked as at least some factor in promoting satisfaction of Eq 1. Residual element contributions to flow stress of 60 MPa

are not uncommon [16]. Residual impurity levels primarily reflect scrap sources and melting deoxidation practice. Conventional ferritic stainless steels contain *very roughly* the following residual element levels: 0.5Mn, 0.5Si, 0.15Ni, 0.15Cu, 0.015P, 0.010S, and trace amounts of a number of other elements in addition to the carbon, nitrogen, and oxygen levels discussed in the preceding. Through selective choice of scrap, use of relatively pure starting stock, and through avant-garde melting techniques such as electron beam refining, it is possible to greatly lower these residual levels, although at considerable cost.

Cold-Working and Toughness

Cold-working unquestionably raises the DBTT, but the effect is neither as consistent nor as great as might be expected. Differences is cold working temperature and the extent of preferred grain orientation no doubt confuse the issue. In any case, cold working increases the flow stress. The ferritic stainless steel strain-hardening exponent is, typically, 0.18 to 0.23, and σ_y can readily be doubled by heavy cold rolling [15,33]. Thus, cold rolling should significantly promote satisfaction of Eq 1.

Tensile ductility is considerably reduced by the first stages of cold rolling and this suggests to many a marked effect on DBTT. There is, however, little direct correlation. First of all, the great differences in strain rate and constraint complicate any association of tension test data and Charpy test data. Beyond this, the tensile elongation is mostly uniform elongation and is primarily limited by the onset of necking at the point where the true stress equals the slope of the true-stress versus true-strain curve. Thus the effect of cold rolling on the *slope* of the stress-strain curve may be the primary factor affecting elongation. Of course, ductility calculated from area reduction at fracture will not reflect variations in uniform elongation. The effect of cold-rolling on area reduction at fracture may still not directly relate to DBTT (at least in the absence of cleavage). Rather, it relates to a reduction of the upper threshold level in the impact energy-transition temperature curve. The upper threshold may not be reduced below practical levels of toughness, and only a minor increase in DBTT may accompany a great loss in tensile ductility.

Some interpretive differences of cold-work effects arise depending on whether one defines the DBTT at a given level of impact energy or as a midpoint in toughness between the upper-shelf energy and zero. Moreover, the effect of cold work must be considered at constant gage.

If one defines, however, the DBTT at the midpoint in fracture energy between the brittle range and the upper threshold, the general effect of cold work seems to be that of a DBTT increase of 1 to 2 deg C per percent rolling reduction [49,67]. The embrittlement effect is probably that of a flow stress increase and in some cases the increase in DBTT becomes less severe as

reduction increases, just as the rate of work hardening, itself, decreases [49]. In some cases hard second phases may be cracked or separated from the matrix during cold rolling. However, the high hydrostatic pressures of rolling tend to minimize such damage.

Cold work may complicate other forms of embrittlement. The most striking case is the acceleration of σ-phase formation [52, 69-73]. The possible effects of cold-work on other embrittling reactions are not so clear, although little practical effect on α'-embrittlement can be demonstrated [67].

Annealing Practice and Toughness

Much of the fundamental behavior germane to commercial annealing practice has been reviewed in the preceding. The practical guidelines are, briefly, as follows. Though heavily cold-rolled ferritic stainless steel may be recrystallized in a very few minutes as low as 700°C [16], typical commercial practice is nearer 850°C. The major exception to this is the annealing of *very high* chromium-molybdenum compositions, wherein σ (and χ) phase form rapidly in this range. In this case, annealing is undertaken in the 1050°C "austenitic" range (or somewhat lower), followed by rapid cooling through the 900 to 500°C range. For a mill handling large quantities of austenitic alloys this presents no problem. The high-temperature anneal does run some risk of sensitization and rapid grain growth can be expected. Above 850°C, ferritic grain growth markedly exceeds that of austenite [47, 79]. Fortunately, the modern alloys susceptible to σ and χ-phase formation can be prepared with (C + N) levels low enough to obviate concern about sensitization and grain-size-related DBTT increase.

In the more moderate high-chromium alloys (chromium contents between 20 and 26 weight percent), the 850°C temperature is quite satisfactory and attention is focussed on postanneal cooling rate. With total (C + N) below, say, 500 ppm, quenching generally produces optimum toughness. With higher (C + N) levels nothing is gained by quenching, and, if the anneal is performed as high as 1000 °C, rapid cooling can lead to embrittlement. This rapid cooling embrittlement is substantially reduced by titanium stabilization.

In the lower, conventional chromium range of 11 to 18 weight percent, postanneal cooling rate is not normally a factor. The principal concern is to make sure the anneal cycle is below the austenite loop. The normal anneal temperature of 850°C is actually quite near the base of the loop and continuous annealing systems, in particular, must be carefully monitored if martensite formation is to be avoided.

Of course, there are many other considerations in the annealing of ferritic stainless steels than optimizing toughness. Avoidance of sensitization and vulnerability to subsequent intergranular attack is certainly a major considera-tion. While the subject of sensitization is outside the scope of this review (see Demo [5] for a contemporary discussion of sensitization), intergranular

attack of sensitized steels can lead to a *de facto* embrittlement. The problem arises in lighter gages when a sensitizing anneal is followed by improper pickling, or some other corrosive exposure, such that the sharply attacked grain boundaries become crack-like and grossly reduce the fracture strength of the strip.

Welding and Toughness

Welded structures are often less tough than the base plate and the ferritic stainless steels are no exception. With proper alloy design, though, satisfactory welds can be made with careful tungsten inert-gas (TIG) technique, as well as with the use of various filler metals. The use of dissimilar filler metals, particularly austenitic grades [49,86], presents a complicated metallurgy that is beyond the scope of this review. Moreover, service corrosion resistance requirements often preclude use of filler metal substantially different from the ferritic base plate [86]. This paper focusses on the requirements for good toughness in TIG welded structures.

The subject of welding and toughness is confused somewhat by reliance on slow-bend-test data for toughness assessment. Obviously, important changes in notch impact toughness may not be registered by a bend test. Some Charpy V-notch measurements have been made, however, and the effect of the welding process is reasonably clear.

If nothing else, welds are plagued by coarse grain size. Too much has been made of this in the past, but it is indisputable that *some* increase in local DBTT can be expected from grain growth in the heat-affected zone and from the coarseness of the dendritic weld structure, *per se.*

The thermal cycle experienced by the HAZ results in a response that can be inferred from the earlier discussions. The most serious problems concern (1) the rapid cooling of ferrite from above the (C + N) solution range and (2) the development of austenite. In the higher-chromium alloys where austenite formation does not occur, the problem is mainly one of (C + N) control. If too much (C + N) is present, the rapid cooling experienced by the HAZ results in an embrittlement probably related to fine intergranular carbide and nitride precipitation and resulting lattice friction stress increase [40]. Microhardness traverses of the weld region will generally make this strengthening quite obvious. At sufficiently low (C + N) levels, this effect is minor and the HAZ may retain toughness remarkably similar to the baseplate.

With alloys that traverse the austenite loop, primary HAZ concern is focussed on embrittlement through martensite formation. Of course, alloying additions are often made simply for the purpose of moving the composition outside the austenite loop (aluminum in T405, titanium in T409, etc.). However, for alloys like T430 that do lie inside the austenite loop, the martensite formation must simply be tolerated and a postweld anneal is

necessary to restore toughness. An hour at 750°C will normally suffice [86]. In fact, such an anneal will greatly improve the toughness of totally ferritic structures that have been embrittled by rapid cooling from above the (C + N) solution temperature [9, 40].

The weld zone itself presents some of the same embrittlement problems as the HAZ. However, the melting presents the added problems of chemical segregation and dendritic texture. Moreover, other chemical changes such as contamination and breakdown of high-melting-point second phases (titanium nitride, for example) may complicate the analysis. The role that these additional considerations play in the fracture process is little understood in ferritic stainless steels, however, and alloy development principles for improved weldability are primarily rationalized in terms of the factors already outlined for the HAZ.

The simplest approach to ensuring good as-welded toughness involves limiting (C + N). The limits necessary, however, are more severe than needed for good toughness in rolled and annealed metal. While good DBTT comparisons are not available, the data in Table 1 from Demo [5, 87] and Binder and Spendelow [38] are instructive. The requirement for good impact resistance is conceivably a more severe mechanical stipulation than is good bend ductility. Thus it is not necessarily surprising that the (C + N) limits for the lower chromium levels are lower for the as-annealed case than for the as-welded case. At 30Cr and higher, though, it is clear that far lower (C + N) limits are necessary to insure acceptable as-welded toughness. The deleterious effect of (C + N) is presumed to relate to intergranular carbide and nitride precipitation, as discussed in the foregoing, particularly in light of the effect of chromium in reducing (C + N) solubility.

Some Charpy test DBTT data do exist for Fe-26Cr-1Mo TIG welded at the relatively light gage of 0.15 cm [16]. The averaged results from 11 compositions are summarized in Table 2. For the titanium-free compositions the welding process is seen to raise the DBTT as much as 35 deg C or as little as 0 deg C, and the as-welded DBTT values do increase markedly with (C + N) increase. The bend test results are consistent with the projec-

TABLE 1—(C + N) limits for impact resistance and ductility in as-annealed and as-welded iron-chromium alloys.

Cr Level, weight %	(C + N) Limit for High Room-Temperature Impact Resistance in As-Annealed Form [38], ppm	(C + N) Limit for High Room-Temperature Bend Ductility in As-Welded Form [87], ppm
19	400 to 700	>700
26	250 to 300	200 to 500
30	200 to 250	80 to 100
35	150 to 200	<20

tions of Demo in Table 1. The 0.15-cm-gage Charpy test results display much greater toughness than implied by Table 1, consistent with the general tendency of greatly increased DBTT with decreasing gage. The unnotched bend test reflects little in the way of a gage effect. The point should be made that a severe bend test (such as the 180 deg, 1/2-thickness test employed) may be a stricter criterion for as-welded toughness than a Charpy V-notch test at these lighter gages. Of course, the gross plastic deformation required to pass the 180 deg, 1/2-thickness test will not always be demanded of a welded joint and such a test may reflect resistance to ductile fracture as much as a ductile-to-brittle transition.

The general approach of limiting (C + N) to achieve as-welded toughness has resulted in several commercial alloys which possess reasonable weldability Several practical limitations exist. Firstly, contamination during strip processing or welding can raise the (C + N) content beyond the levels needed for weldability. Secondly, (C + N) requirements for minimized as-welded sensitization will be more severe than those for as-welded toughness when chromium levels are below, say, 28 weight percent [87]. Lastly, the required (C + N) levels are not easily achieved without use of relatively costly scrap selection or melting techniques or both.

These factors have led to considerable evaluation of titanium- or columbium-stabilized grades. Titanium and columbium is of considerable value in mitigating sensitization, and, relative to this review, promotes good as-welded toughness at (C + N) levels well above the limits cited in Table 1 [16,49,87]. In addition to affecting (C + N) control, some reduction in HAZ grain growth and weld grain size is achieved by the stabilizing addition [16]. The data in Table 2 show the efficacy of titanium stabilization. Great improvements in as-welded toughness are promoted at the 300 and 850 ppm (C + N) levels. The effect on as-welded toughness is greater than the effect on

TABLE 2—*Charpy V-Notch DBTT levels and bend test results for Fe-26Cr-1Mo alloys subjected to TIG welding at a gage of 0.15 cm* [16].

(C + N) Level, ppm	Charpy V-Notch DBTT for 0.15-cm Gage, °C		Weld Bend Test Performance in 180 deg, 1/2-Thickness Test
	Baseplate	Weld	
≈ 65	−75	−75	passed
≈ 130	−75	−75	passed
≈ 315	−55	−20	failed
≈ 880	−20	+5	failed
≈ 110 (1200 ppm Ti)	−75	−30	failed
≈ 300 (2200 ppm Ti)	−45	−75	passed
≈ 850 (4500 ppm Ti)	−45	−30	passed

baseplate toughness. At the 110-ppm (C + N) level the effect of titanium stabilization is quite different. Not only is the baseplate DBTT somewhat increased by the titanium addition, but the as-welded DBTT is markedly increased and bend ductility has been lost.

The detrimental effect of titanium on toughness at very low (C + N) levels and the general failure of titanium stabilization to result in DBTT levels fully consistent with those of very low (C + N) alloys have been studied recently by Grubb et al [10]. In Fe-26Cr an embrittling effect of titanium could be associated with intergranular microcrack formation. This may reflect embrittling titanium segregation to the grain boundaries, or, more probably, oxygen intergranular embrittlement due to extensive carbon gettering [21–24]. The embrittling effects of titanium may not be confined to very low (C + N) levels but may be associated with the Ti/(C + N) ratio. While ratios of at least 6 are necessary for practical improvement in as-welded toughness and corrosion resistance [5], ratios somewhat above 10 begin to diminish as-welded toughness [14,16,49]. Thus, maximum as well as minimum ratios of Ti/(C + N) are stipulated for optimum stabilization [87]. Beyond the possibility of titanium-related or oxygen-related grain boundary embrittlement noted in the foregoing, it should be mentioned that titanium beyond the amount needed for stabilization can lead to formation of an embrittling intermetallic grain boundary phase in iron-chromium-molybdenum alloys [5,14]. The phase has been presumed by some observers to be χ [5].

The effects of columbium on weld toughness are not unlike those of titanium. The minimum Cb/(C + N) ratio prescribed for acceptable postweld ductility and corrosion resistance is 8 to 11 times [5]. A point of diminishing returns for columbium additions seems to exist in the range of a Cb/(C + N) ratio of 15 [14]. In one study columbium seemed to be somewhat detrimental to as-annealed DBTT, with a 40 deg C increase being associable with an 0.8 weight percent addition to a commerical-purity 18Cr-2Mo alloy [14]. In another case columbium was reported to be more efficient than titanium in reducing as-welded DBTT in a 26Cr steel containing 250-ppm total (C + N) [49]. An 0.4Cb addition lowered the as-welded DBTT some 60 deg C whereas a lowering of 30 deg C was noted for an 0.25Ti addition. As an aside, it should be noted that a principal advantage of columbium is the fact that columbium-stabilized alloys resist intergranular attack in highly oxidizing solutions, whereas disolution of Ti(C,N) may lead to such attack with titanium-stabilized alloys [88–92].

An increasing number of titanium- and columbium-stabilized alloys are being commercially evaluated. The use of titanium for carbide and nitride stabilization can apparently be abetted through the addition aluminum of [87]. By combining titanium and aluminum in a gettering action, alloys with acceptable as-welded toughness and corrosion resistance can be produced

at increased levels of chromium or higher levels of (C + N) than would be possible with titanium alone.

A novel approach to improving as-welded toughness involves the addition of "weld ductilizing additives" [93]. Low amounts of aluminum, copper, platinum, palladium, and silver, either singly, in combination with each other, or in combination with vanadium, enhance the toughness of high-chromium ferritic stainless steel welds. It is claimed that a 37Cr alloy with as much as 700-ppm (C + N) will be ductile in the as-welded condition through the addition of 0.1 to 1.3 weight percent of the ductilizing additives. The criterion for such additives is that the atomic radius be within 15 percent of the average for the ferrite matrix [87]. Perhaps the additions entrap interstitials in the way suggested by McEvily for nickel in iron [11].

Recommended Research and Development

A principal area for development concerns the generation of toughness data more amenable to contemporary engineering design. Specifically, the great array of Charpy and tension test DBTT values, bend test data, and the like must be supplemented by careful fracture toughness (stress-intensity factor) measurements. It is a pity that many ferritic stainless steel applications are thwarted by designers with vague fears that the ferritic stainless steels are not as tough as T304. Yet in the absence of more precise descriptions of fracture resistance, it is difficult to establish confidence. Of course, many of the applications are for gages at which plane-strain fracture toughness testing probably cannot be undertaken and at which toughness may change rapidly with gage. Even so, much more work is to be encouraged in this direction.

Much more effort is needed to develop quantitative relations of the chemical state of (C + N) to thermal cycles and related DBTT values. Attention must be paid to specific HAZ cycles, weld cycles, and commercial anneal cycles. Commercial continuous anneal cycles should be addressed in particular. Much of the laboratory work to date has focused on isothermal heat treatments coupled to various cooling rates. The Gleeble testing apparatus is ideally suited to simulate the *transient* thermal exposures of more technological interest [94].

The metallurgy of the ferritic stainless steel weld zone requires much more elucidation, with emphasis on chemical inhomogeneity, dendritic structure, and the behavior of titanium and columbium carbonitrides in the weld pool.

It is likely that the role of residual elements other than (C + N) has been given too little consideration. For example, aluminum and copper are listed as "ductilizing additives" which can greatly enhance as-welded ductility in high-chromium alloys even at levels as low as 0.1 weight percent [87,93]. Interestingly enough, conventional commercial ferritic stainless

steels contain levels of (Al + Cu) generally in excess of 0.1 weight percent even though the modern high-purity alloys may not. The costs involved in judicious manipulation of residual elements may be no more than the costs presently incurred in high-quality scrap procurement, vacuum induction melting, electron beam melting, and so on.

Lastly, one hopes that in the rush to develop new, weldable ferritic compositions we have not overlooked the cost-effectiveness of postweld annealing. The disadvantages are painfully obvious, yet a postweld anneal is remarkably effective in eliminating the embrittlement associated with rapid cooling from above the (C + N) solution temperature and with martensite formation. For some applications, enlightened development of a practical postweld annealing technique may be a more effective focus than wholesale alloy upgrading.

Summary

The toughness of ferritic stainless steels in seen to depend not so much on the intrinsic nature of iron-chromium or iron-chromium-molybdenum, but rather on the presence of certain second phases. The effects of carbides and nitrides are perhaps the most important. Grain boundary carbonitrides, plate-like intragranular nitrides, and fine intragranular dispersions of carbonitrides can all result in a significantly increased DBTT. The harmful action of (C + N) can be preempted by gettering with titanium and columbium. Excessive gettering can result in other forms of embrittlement, however.

Untempered martensite is often the major factor increasing the DBTT in alloys which lie inside the austenite loop. Extended time exposure in the 475 °C range results in DBTT increase due to the precipitation of α'. The 475 °C embrittlement becomes more rapid as chromium increases, and alloying additions and impurities generally hasten the reaction. Very high chromium and chromium-molybdenum compositions are susceptible to embrittlement through σ and χ phase precipitation at the grain boundaries in the 500 to 900 °C range.

In many instances the size and distribution of the second phase are of paramount concern. The usual effects of grain size, cold-working, and, particularly, gage are not to be overlooked in assessing ferritic stainless steel toughness.

A thorough knowledge of the factors affecting the DBTT is required to prescribe proper annealing practice and to assess the limited toughness of welds and weld heat-affected zones. Enhanced as-welded toughness is primarily achieved by using compositions that are outside the austenite loop, by severely restricting the carbon and nitrogen content, and by gettering with titanium and columbium.

References

[1] Thielsch, H., *Welding Journal Research Supplement*, Vol. 30, 1951, p. 209s.

[2] Rajkay, L., *Proceedings*, American Society for Testing and Materials, Vol. 67, 1967, p. 158.

[3] Kaltenhauser, R. H., *Metals Engineering Quarterly*, Vol. 11, 1971, p. 41.

[4] Demo, J. J. and Bond, A. P., *Corrosion*, Vol. 31, 1975, p. 21.

[5] Demo, J. J. in *Structures. Constitution and General Characteristics of Wrought Ferritic Stainless Steels, ASTM STP 619*, American Society of Testing and Materials, 1977, p. 1.

[6] Cottrell, A. H., *Transactions, TMS-AIME*, 1958, Vol. 212, p. 192.

[7] Petch, N. J., *Philosophical Magazine*, Vol. 3, 1958, p. 1089.

[8] Petch, N. J. in *Fracture*, B. L. Averbach et al, Eds, Wiley, New York, 1959, p. 54.

[9] Grubb, J. F. and Wright, R. N., "The Role of C and N in the Brittle Fracture of Fe-26 Cr," to appear in *Metallurgical Transactions*, 1979.

[10] Grubb, J. F., Wright, R. N., and Farrar, P., this publication, pp. 56–76.

[11] Stoloff, N. S. in *Fracture*, H. Liebowitz, Ed., Vol. 6, Academic Press, New York, 1969, p. 1.

[12] Jordan, K. R., Ph.D. Dissertation, Rensselaer Polytechnic Institute, Troy, N.Y., 1967.

[13] Plumtree, A. and Gullberg, R., *Journal of Testing and Evaluation*, Vol. 2, 1974, No. 5, p. 331.

[14] Semchyshen, M., Bond, A. P., and Dundas, H. J. in *Proceedings, Symposium Toward Improved Ductility and Toughness*, Kyoto, Japan, 1971, p. 239.

[15] Nichol, T. J., *Metallurgical Transactions*, Vol. 8A, 1977, p. 229.

[16] Wright, R. N., *Welding Journal Research Supplement*, Vol. 50, 1971, p. 434s.

[17] Lula, R. A., *Metal Progress*, Vol. 110, No. 2, 1976, p. 24.

[18] Smith, R. L. and Rutherford, J. L., *Transactions, TMS-AIME*, Vol. 209, 1957, p. 857.

[19] Lawley, A., Van den Sype, J., and Maddin, R., *Journal of the Institute of Metals*, Vol. 91, 1962, p. 23.

[20] Loomis, B. A. and Carlson, O. N., *Reactive Metals*, Wiley (Interscience), New York, 1959, p. 227.

[21] Rees, W. P. and Hopkins, B. E., *Journal of the Iron and Steel Institute*, Vol. 172, 1952, p. 403.

[22] Low, J. R., Jr. and Feustal, R. G., *Acta Metallurgica*, Vol. 1, 1953, p. 185.

[23] Honda, R. and Taga, H., *Metal Science Journal*, Vol. 2, 1968, p. 172.

[24] Low, J. R., Jr., *Transactions. TMS-AIME*, Vol. 245, 1969, p. 2481.

[25] Allen, N. P., *Iron and Its Dilute Solid Solutions*, Wiley (Interscience), New York, 1963, p. 271.

[26] McMahon, C. J. and Cohen, M., *Acta Metallurgica*, Vol. 13, 1965, p. 591.

[27] Biggs, W. D., *Brittle Fracture of Steel*, MacDonald & Evans, London, 1960.

[28] Johnston, T. L. in *Fracture: Proceedings*, 4th Annual Symposium on Materials Science, Plenum Press, New York, 1966, p. 1.

[29] Kelley, M. J. and Stoloff, N. S., *Metallurgical Transactions*. Vol. 7A, 1976, p. 331.

[30] Rinebolt, J. J. and Harris, W. J., *Transactions*, American Society for Metals, Vol. 43, 1951, p. 1175.

[31] Gensamer, M., *Transactions. TMS-AIME*, Vol. 215, 1959, p. 2.

[32] Stoloff, N. S. in *Proceedings, Conference on the Physical Basis of Yield and Fracture*, Physical Society, London, 1966, p. 68.

[33] Franson, I. A., *Metallurgical Transactions*, Vol. 5, 1974, p. 2257.

[34] Rees, W. P., Hopkins, B. E., and Tipler, H. R., *Journal of the Iron and Steel Institute* (London), Vol. 177, 1954, p. 93.

[35] Jackson, J. K., and Winchell, P. G., *Transactions, TMS-AIME*, Vol. 230, 1964, p. 216.

[36] Stoloff, N. S. in *Fracture: Proceedings*, 4th Annual Symposium on Materials Science, Plenum Press, New York, 1966, p. 197.

[37] Hochman, J., *Comptes Rendus Hebdomadaires des Seances de l'Academie des Sciences*, Vol. 226, 1948, p. 2150.

[38] Binder, W. O. and Spendelow, H. R., Jr., *Transactions*, American Society for Metals, Vol. 43, 1951, p. 759.

[39] Plumtree, A. and Gullberg, R., *Metallurgical Transactions*, Vol. 7A, 1976, p. 1451.

[40] Demo, J. J., *Corrosion*, Vol. 27, No. 12, 1971, p. 531.

[41] Pollard, B., *Metals Technology*, Vol. 1, 1974, p. 31.

[42] Richter, J. and Finke, P., *Freiberger Forschungschefte Metallurgie*. Vol. B172, 1976, p. 55.

[43] Thielsch, H., *Welding Journal*, Vol. 34, 1955, p. 225.

[44] Baerlecken, E. B., Fisher, W. A., and Lorenz, K., *Stahl und Eisen*, Vol. 81, No. 12, 1961, p. 768.

[45] Swalin, R. A., *Thermodynamics of Solids*, Wiley, New York, 1962, p. 134.

[46] Lagneborg, R., *Transactions*, American Society for Metals, Vol. 60, 1967, p. 67.

[47] Lena, A. J. and Hawkes, M. F., *Transactions, AIME, Journal of Metals*, Vol. 200, 1954, p. 607.

[48] Woltron, K., *Berg- und Hüttenmaennische Monatschefte*, Vol. 116, 1972, p. 429.

[49] Kanamaru, T., Takahashi, N., Kawatani, K., Ihara, S., and Yamamoto, O., *Tetsu to Hagané*, Vol. 62, No. 4, 1976, p. s218 (Brutcher Translation HB9824).

[50] Wright, R. N. and Wood, J. R., *Metallurgical Transactions*, Vol. 8A, 1977, p. 2007.

[51] Thielemann, R. H., *Proceedings*, American Society for Testing and Materials, Vol. 40, 1940, p. 788.

[52] Fisher, R. M., Dulis, E. J., and Carrol, K. G., *Journal of Metals, Transactions, AIME*, Vol. 197, 1953, p. 690.

[53] Marcinkowski, M. J., Fisher, R. M., and Szirmae, A., *Transactions TMS-AIME*, Vol. 230, 1964, p. 676.

[54] Blackburn, M. J. and Nutting, J., *Journal of the Iron and Steel Institute*, Vol. 202, 1964, p. 610.

[55] Lagneborg, R., *Transactions*, American Society for Metals, Vol. 60, 1967, p. 67.

[56] *The Making, Shaping, and Treating of Steel*, U. S. Steel Corp., Pittsburgh, Pa., 1971, p. 1166.

[57] Elliot, R. P., *Constitution of Binary Alloys*, 1st Supplement, McGraw-Hill, New York, 1965.

[58] Chandra, D. and Schwartz, L. H., *Metallurgical Transactions*, Vol. 2, 1971, p. 511.

[59] Grobner, P. J., *Metallurgical Transactions*, Vol. 4, 1973, p. 251.

[60] Cahn, J. W., *Transactions, TMS-AIME*, Vol. 242, 1968, p. 166.

[61] Vintoykin, Ye. Z., Dmitriyev, V. N., and Kolontsov, V. Yu., *Fizika Metallov I Metallovedenie*, Vol. 29, 1970, p. 1257.

[62] DeNys, T. and Gielen P. M., *Metallurgical Transactions*, Vol. 2, 1971, p. 1423.

[63] Heger, J. J., *Metal Progress*, Aug. 1951, p. 55.

[64] Riedrich, G. and Loib, E., *Archiv fuer das Eisenhuttenwesen*, Vol. 15, 1941–1942, p. 175 (Brutcher Translation No. 1249).

[65] Courtnall, M. and Pickering, F. B., *Metal Science*, 1976, p. 273.

[66] Williams, R. O. and Paxton, H. W., *Journal of the Iron and Steel Institute*, Vol. 185, 1957, p. 358.

[67] Grobner, P. J. and Steigerwald, R. F., *Journal of Metals*, Vol. 29, No. 7, 1977, p. 17.

[68] Shortsleeve, F. J. and Nicholson, M. E., *Transactions*, American Society of Metals, Vol. 43, 1951, p. 142.

[69] Jette, E. R. and Foote, F., *Metals and Alloys*, Vol. 7, 1936, p. 207.

[70] Heger, J. J., *Metal Progress*, Vol. 49, 1946, 976B.

[71] Heger, J. J. in *Symposium on the Nature, Occurrence, and Effects of Sigma Phase, ASTM STP 110*, American Society for Testing and Materials, 1951, p. 75.

[72] Gilman, J. J., *Transactions*, American Society for Metals, Vol. 43, 1951, p. 101.

[73] Zapffe, C. A. and Worden, C. O., *Welding Journal Research Supplement*, Vol. 30, 1951, p. 47s.

[74] Anderson, A. G. H. and Jette, E. R., *Transactions*, American Society of Metals, Vol. 24, 1936, p. 375.

[75] Colombier, L. and Hochmann, J., *Stainless and Heat Resisting Steels,* Edward Arnolds Ltd., Publishers, England, 1967.

[76] McMullin, J. G., Reiter, S. F., and Ebeling, D. G., *Transactions,* American Society of Metals, Vol. 46, 1954, p. 799.

[77] Streicher, M. A., *Corrosion,* Vol. 30, No. 4, 1974, p. 115.

[78] Andrews, K. W., *Nature,* Vol. 164, 1949, p. 1015.

[79] Speidel, M. O., *Stress Corrosion Cracking of Ferritic Stainless Steels,* Handbook on Stress Corrosion Cracking, Advanced Research Projects Agency (National Science Foundation), 1977.

[80] Nehrenberg, A. E. and Lillys, P., *Transactions,* American Society of Metals, Vol. 46, 1954, p. 1176 and p. 1203.

[81] Mogford, I. L., *Metallurgical Reviews,* Vol. 12, 1967, p. 49.

[82] Wukusick, C. S. and Collins, J. F., *Materials Research and Standards,* Vol. 4, 1964, p. 637.

[83] Wukusick, C. S., "The Physical Metallurgy and Oxidation Behavior of Fe-Cr-Al-Y Alloys," USAEC Contract No. AT(40-1)-2847, General Electric Co. NMPO Report No. GEMP-414, 1966.

[84] Bartos, J., Perkins, R., and Robertshaw, F., "Mechanical Properties of Fe-Cr-Al-Y Alloys,"USAEC Contract No. AT(40-1)-2847, General Electric Co. NMPO Report No. GEMP-711, 1969.

[85] Rosenberger, G. J. and Wright, R. N., this publication, pp. 297–312.

[86] Thielsch, H., *Welding Journal Research Supplement,* Vol. 34, 1955, p. 22s.

[87] Demo, J. J., *Metallurgical Transactions,* Vol. 5, 1974, p. 2253.

[88] Bond, A. P. and Lizlovs, E. A., *Journal of the Electrochemical Society,* Vol. 116, 1969, p. 1305.

[89] Lula, R. A., Lena, A. J., and Keifer, G. C., *Transactions,* American Society for Metals, Vol. 46, 1954, p. 197.

[90] Hersleb, G., *Werkstoffe und Korrosion,* Vol. 19, No. 5, 1968, p. 406.

[91] Baumel, A., *Stahl und Eisen,* Vol. 84, 1964, p. 798.

[92] Cowling, R. D. and Hintermann, H. E., *Journal of the Electrochemical Society,* Vol. 117, 1970, p. 1447.

[93] Sipos, D. J., Steigerwald, R. F., and Whitcomb, N. E., U. S. Patent No. 3, 672, 876, 1972.

[94] Savage, W. F., *High Speed Testing,* Vol. 3, Interscience, New York, 1962, p. 55.

A. Plumtree[1] and R. Gullberg[2]

Influence of Interstitial and Some Substitutional Alloying Elements

ABSTRACT: The toughness of several vacuum-melted Fe-25Cr and Fe-18Cr-2Mo ferritic stainless steels containing between 40 and 1000 ppm combined carbon and nitrogen has been investigated in the water-quenched condition. The toughness of these alloys has been assessed using notched-bar impact tests. For a given interstitial content, the ductile-to-brittle transition temperature and the impact shelf energy were not influenced by the presence of 2 percent molybdenum or the change in chromium content from 18 to 25 percent. In order to achieve a low transition temperature and high shelf energy, the combined carbon and nitrogen (C + N) content should be maintained below 150 ppm, in which case the interstitial amount has no effect. Exceeding this threshold level results in a marked increase in transition temperature and decrease in shelf energy. At higher interstitial levels [~ 600 ppm (C + N)] further increases are not as significant. Addition of nickel resulted in a decrease in transition temperature, but this was accompanied by a decrease in shelf energy when compared with plain chromium steels with the same interstitial content. The addition of titanium, however, caused an improvement in both transition temperature and impact shelf energy.

It is shown that increasing the interstitial content of these ferritic stainless steels is associated with an increase in the amount of second phase present, particularly at the grain boundaries. Such particles enhance cleavage fracture by reducing the surface energy. The tendency toward a more brittle condition with increased interstitial content and larger grain size is explained in terms of the Cottrell theory for brittle fracture.

KEY WORDS: ferritic stainless steels, molybdenum additions, titanium additions, nickel addition, interstitials, second-phase content, grain boundaries, fracture toughness, ductile-to-brittle transition temperature, Cottrell theory for brittle fracture

Ferritic stainless steels offer desirable properties for many applications. They have excellent resistance to stress corrosion cracking and good resistance to crevice and pitting corrosion. They may be cold-headed, machined, and plastically shaped with relative ease [1].[3] Their low thermal

---

[1]Professor, Department of Mechanical Engineering, University of Waterloo, Waterloo, Ont., Canada.

[2]Marketing Manager, Tubular Products, Research Center, Sandvik A. B., S-81101 Sandviken 1, Sweden.

[3]The italic numbers in brackets refer to the list of references appended to this paper.

expansivity is attractive in making joints with ceramic materials. Also, the greater thermal conductivity of these ferritic grades may be used to increase the efficiency of heat exchangers by about 10 percent.

The reduction in toughness which occurred in ferritic stainless steels when the chromium levels were increased above about 20 percent was initially connected with the presence of this element. Binder and Spendelow [2] and Hochman [3,4], however, showed that if the carbon and nitrogen contents could be significantly lowered by melting in vacuum, high room-temperature impact values of iron-chromium alloys containing as much as 38 percent chromium could be achieved. Recent investigations have emphasized the importance of low carbon and nitrogen levels in order to maintain good low-temperature ductility in high-chromium ferritic stainless steels [5–8]. A low interstitial content is also of great importance in reducing sensitization, which takes place in these alloys following high-temperature heat treatment [9–11]. Hence, there is general concern to maintain low interstitial levels in high-chromium ferritic stainless steels.

This present work was undertaken in an attempt to correlate the ductile-to-brittle transition temperature (DBTT) with interstitial content for various Fe-18Cr-2Mo and Fe-25Cr alloys and to determine the amounts of interstitial elements that may be tolerated to maintain a low DBTT and high toughness. Included in this work is an examination of the role of chromium and other substitutional alloying elements such as molybdenum, titanium, and nickel on the ductility and toughness of ferritic stainless steels. A mechanism responsible for relating the notched-bar impact test results with composition is also considered.

Materials and Testing Procedure

Several ferritic stainless steels based on Fe-25Cr or Fe-18Cr-2Mo were used in this investigation. In a few cases, substitutional elements such as molybdenum, nickel, and titanium were added to the Fe-25Cr steels and titanium to the Fe-18Cr-2Mo steels. The carbon and nitrogen (C + N) contents, together with the amounts of these substitutional alloys, when added, are given in Tables 1 and 2 for the Fe-25Cr and Fe-18Cr-2Mo steels, respectively.

Each steel was prepared by melting and casting under high vacuum, then warm-forging to 20 mm diameter and finally cold-drawing to 14.2 mm diameter. Heat treatments ranging between 850 and 1250°C for 30 min, followed by water-quenching, were carried out to provide a range of grain sizes (35 to 380 μm average diameter).

Full-sized Charpy notched impact specimens were prepared for each alloy and grain size. These impact tests were carried out at temperatures between −75 and 250°C, which allowed each respective DBTT and Charpy V-notch shelf energy (CVN) to be determined. The DBTT was defined as that

TABLE 1—Composition, grain size, and impact results of Fe-25Cr steels.

Alloy No.	Composition			Heat Treatment	Grain Size, μm	DBTT °C	CVN Shelf Energy, J
	C, %	N, %	Other, %				
58	0.006	0.048	...	1000°C WQ[a]	75	166	157
59	0.009	0.015	...	900°C WQ	40	87	231
59	0.009	0.015	...	1000°C WQ + 850°C WQ	120	114	245
59	0.009	0.015	...	1250°C WQ + 850°C WQ	350	120	216
64	0.011	0.090	...	1000°C WQ	75	147	147
65	0.021	0.018	...	900°C WQ	35	120	196
65	0.021	0.018	...	1000°C WQ + 850°C WQ	75	112	226
65	0.021	0.018	...	1250°C WQ + 850°C WQ	370	145	196
66	0.011	0.015	...	900°C WQ	60	125	196
66	0.011	0.015	...	1000°C WQ + 850°C WQ	100	98	196
66	0.011	0.015	...	1250°C WQ + 850°C WQ	325	116	196
12	0.011	0.013	...	900°C WQ	50	96	177
67	0.002	0.041	...	1000°C WQ + 850°C WQ	110	98	226
67	0.002	0.041	...	1250°C WQ + 850°C WQ	380	150	123
68	0.003	0.012	...	850°C WQ	35	-50	294
68	0.003	0.012	...	1000°C WQ	95	7	289
68	0.003	0.012	...	1000°C WQ + 850°C WQ	105	30	275
11	0.005	0.015	...	950°C WQ	70	38	206
2	0.004	0.002	...	850°C WQ	75	-54	289
69	0.030	0.022	...	1000°C WQ	35	150	157
13	0.012	0.015	0.07 Ti	900°C WQ	40	66	255
47	0.013	0.014	0.42 Ti	900°C WQ	59	80	255
19	0.013	0.014	3.62 Ni	900°C WQ	50	23	157
3	0.004	0.002	1.03 Mo	850°C WQ	80	-46	284
54	0.006	0.015	1.13 Mo	850°C WQ	50	105	235

[a] WQ = water quenched.

TABLE 2—*Composition, grain size, and impact results of Fe-18Cr-2Mo steels.*

Alloy No.	Composition			Heat Treatment	Grain Size, μm	DBTT, °C	CVN Shelf Energy, J
	C, %	N, %	Other, %				
41	0.002	0.001	. . .	850°C WQ[a]	36	−28	294
42	0.011	0.044	. . .	1000°C WQ	50	134	201
14	0.011	0.024	. . .	950°C WQ	45	100	177
49	0.025	0.015	. . .	1000°C WQ	65	140	147
56	0.009	0.011	. . .	1000°C WQ	75	75	255
149	0.005	0.010	. . .	1000°C WQ	70	60	275
43	0.013	0.014	0.66 Ti	1000°C WQ	80	83	284
79	0.029	0.023	0.15 Ti	1000°C WQ	50	119	235

[a]WQ = water quenched.

temperature corresponding to half the shelf height or energy (that is, 1/2 CVN). Tension specimens of 7 mm diameter and 50 mm gage length were machined from six of the Fe-25 Cr alloys and the tests were conducted at temperatures varying from −93 to 23°C in an Instron Universal Testing Machine using a crosshead speed of 0.2 mm/min.

Microstructural examination of the alloys was carried out on etched specimens in the optical microscope to determine the grain size. Transmission electron microscopy (TEM) was employed mainly to examine the grain boundary regions of the steels.

Results

Impact Tests Fe-25Cr Alloys

The results of notched-bar impact tests on the Fe-25Cr steels showed two important effects. First, the DBTT increased with increase in interstitial content and secondly the DBTT increased with grain size for any given alloy. Figure 1 gives the results of impact tests on specimens of Alloys 68, 67, 54, 13, 3, and 19. Impact test results for the full range of alloys with their various treatments are included in Table 1. In all cases, transgranular failures were observed.

It is obvious that, to make a valid comparison of the effect of interstitial content on the DBTT, the grain size must be held constant. Consequently, comparison of the DBTT for different (C + N) levels was made for a grain size of 55 ± 20 μm and the results are presented in Fig. 2. Although the general tendency, mentioned in the preceding, for the transition temperature to increase with total interstitial content is seen, it is apparent that for a (C + N) content of less than about 0.015 percent (150 ppm), the DBTT is low and constant at about −50°C. Exceeding this threshold results in a dramatic in-
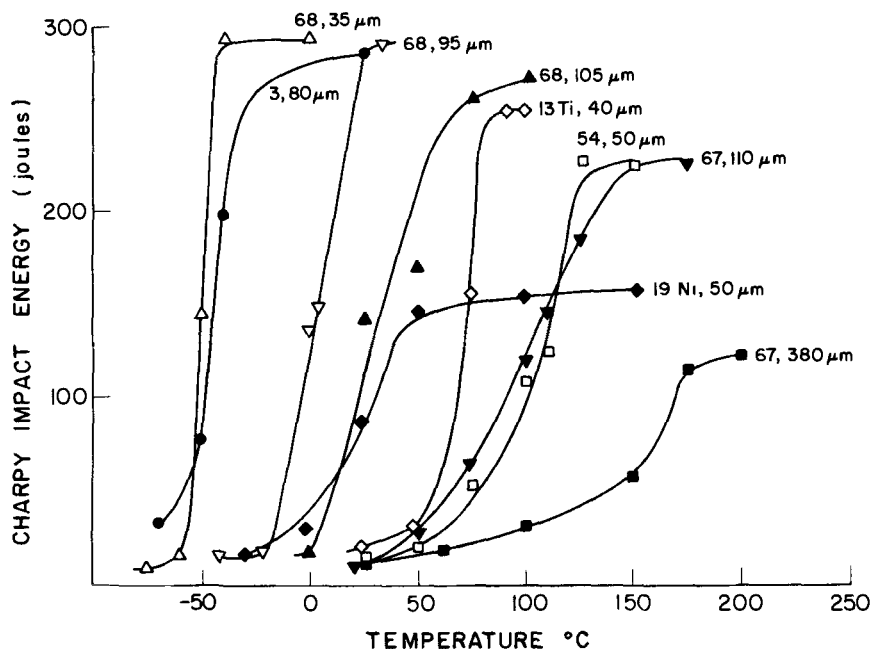
FIG. 1—*Impact energy curves for several Fe-25Cr ferritic stainless steels. The alloy number and grain size are given for each curve.*

crease in the DBTT. When the (C + N) content approaches about 0.05 percent (500 ppm), the DBTT is relatively constant, yet high ($\sim 160°$C). Considering the effect of alloying elements for a given (C + N) content, Fig. 2 indicates that titanium additions tended to slightly reduce the DBTT. Although only one nickel-containing ferritic stainless steel (Alloy 19) was investigated, the effect was to lower DBTT, whereas the presence of molybdenum appeared to have no effect.

Impact Tests of Fe-18Cr-2Mo Alloys

The results of notched-bar impact tests on Fe-18Cr-2Mo ferritic stainless steels with grain sizes ranging from 36 to 80 μm are given in Table 2 and also included in Fig. 2. Again, the same trend of increasing DBTT with (C + N) content is observed. In fact, the DBTT values were very similar to those of the Fe-25Cr ferritic stainless steels for a given (C + N) content. No apparent lower threshold interstitial level was seen, though this may be due to the relatively few low-interstitial-content steels investigated, in which case the results for the Fe-18Cr-2Mo steels follow the same curve as for the Fe-25Cr steels. However, the lower-chromium steels displayed no extra tolerance for
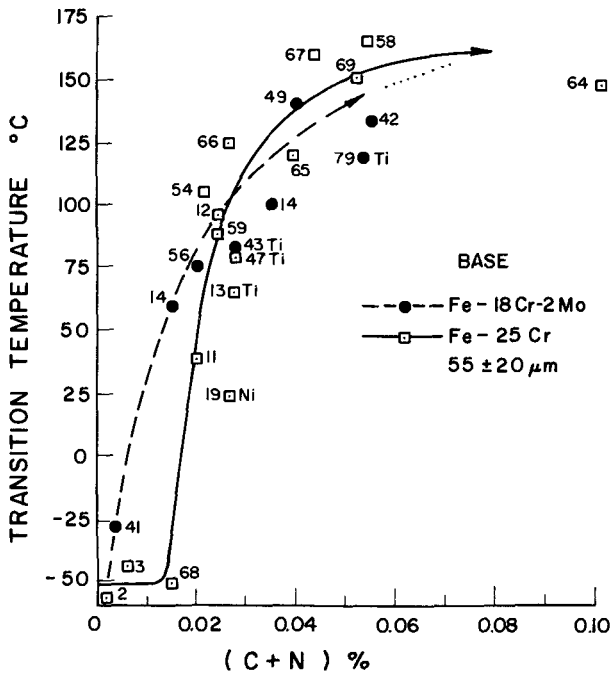
FIG. 2—*Plot of impact transition temperature against interstitial content for Fe-18Cr-2Mo and Fe-25Cr ferritic stainless steels with grain sizes within the range of 35 to 75 μm. The numbers given correspond to the alloy numbers.*

larger interstitial contents to maintain low DBTT values. Again the addition of titanium (Alloys 43 and 79) tended to lower the DBTT.

Tension Tests

No marked yield point behavior was observed in the tension tests and the 0.2 percent offset stress ($\sigma_{0.2}$) was used to indicate the onset of macroscopic yielding. Tests were conducted over a range of temperatures, varying from −93 to 23°C on Alloys 58, 59, 65, 66, 67, and 68, and it was found that the $\sigma_{0.2}$-values were independent of composition for any given testing temperature. Figure 3 shows the variation of $\sigma_{0.2}$ with temperature, which may be expressed in the form

$$\sigma_{0.2} = 666 \exp (-0.0027T) \text{ MPa}$$

where T is the test temperature (Kelvin).

Testing to failure at room temperature resulted in marked differences in the strain to fracture as seen in Table 3. The true strain to fracture decreased as the interstitial content of the alloy increased.
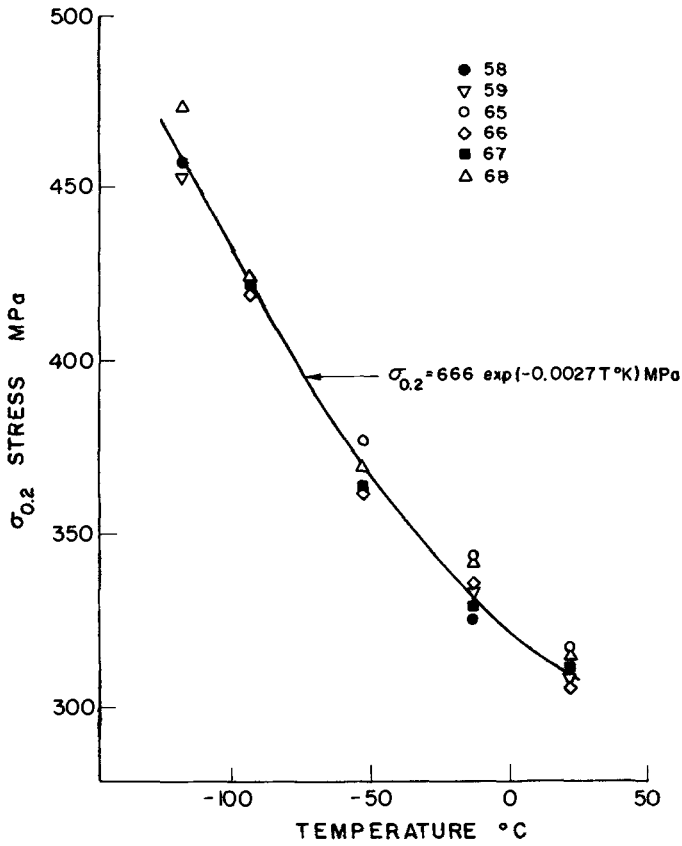
FIG. 3—*Variation of $\sigma_{0.2}$ with temperature for several Fe-25Cr ferritic stainless steels.*

Metallography

Transmission electron miscroscopy of thin foils and extraction replicas was carried out on specimens of the various Fe-25Cr alloys. Examination revealed the presence of fine films of second-phase particles at the grain boundaries. The extent and amount of these films increased with interstitial content and the temperature from which the specimen was quenched (hence grain size). Figure 4 (Alloy 68) shows a clean grain boundary representative of the low-interstitial-content alloys. Figure 5 (Alloy 67) is an extraction replica micrograph and shows the presence of grain boundary particles. This is representative of the higher-interstitial-content alloys. Electron diffraction studies indicated that such particles were mainly CrN or Cr_2N, although $M_{23}C_6$ was detected in Alloy 65.

TABLE 3—*Room-temperature tension properties of some Fe-25Cr alloys.*

Alloy	Heat Treatment (30 Min at Each Temperature)	Grain Size, μm	Ultimate Tensile Strength, MPa	True Fracture Stress, MPa	True Fracture Strain, ϵ_f $(=\ln A_o/A_f)^b$
58	1000°C WQ+[a] 850°C WQ	75	456	861	1.14
59	900°C WQ+ 850°C WQ	40	435	1027	1.40
65	900°C WQ+ 850°C WQ	35	451	1000	1.29
66	900°C WQ+ 850°C WQ	60	436	1002	1.36
67	1000°C WQ+ 850°C WQ	75	455	898	1.12
68	900°C WQ+ 850°C WQ	35	437	1165	1.70

[a]WQ = water quenched.
[b]A_o is original area and A_f is final area.

FIG. 4—*Electron transmission image of grain boundary in Alloy 68 (Fe-25Cr).* ×20000.
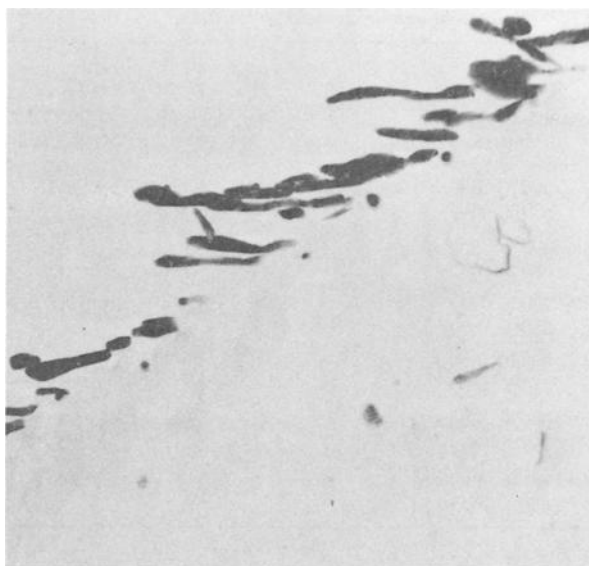
FIG. 5—*Extraction replica of particles at grain boundary in Alloy 67 (Fe-25Cr) ×5000.*

Discussion

Grain Size and Surface Energy Effects

In crystalline solids it is established that some plastic deformation precedes cleavage failure due to the movement of dislocations [12,13]. Such a movement can cause failure by building up stresses at obstacles such as grain boundaries [12,13], slipband intersections, [14,15] and twin intersections. Independent of the exact mechanism, the critical condition for crack nucleation at the yield stress ($\sigma_F = \sigma_y$) can be expressed by the Cottrell [14] equation

$$\sigma_y k_y d^{1/2} = C \mu\gamma \qquad (2)$$

where

C = constant related to stress state ($\sim 4/3$ for a notched specimen and 4 for a plain specimen),

γ = work done in forming a fracture surface (or the effective surface energy of the crack),

μ = shear modulus, and

σ_y, k_y = yield stress and Petch slope, respectively, related to grain size, d, by the Hall-Petch equation

$$\sigma_y = \sigma_o + k_y d^{-1/2} \tag{3}$$

in which σ_o is the friction stress. Substituting this Hall-Petch relationship, Eq 3, into Eq 2, the following Cottrell-Petch equation is obtained

$$(\sigma_o d^{1/2} + k_y) k_y = C \mu \gamma \tag{4}$$

At any test temperature there is only one grain size, d^*, for which Eq 4 holds. Equations 2 and 4 express the condition for plastically induced crack nucleation at a given temperature. Any factor that increases σ_o, k_y, or d increases the tendency for brittle fracture. In iron, a marked increase in σ_o with decreasing temperature is experienced. The parameter k_y may depend upon alloy content, test temperature, or heat treatment. Generally, k_y will increase with decrease in stacking fault energy, hence alloying. Long-range order accomplishes the same effect as low stacking fault energy in varying k_y [16].

Petch [17] considered that the major temperature-dependent term in Eq 4 was σ_o and could be expressed by

$$\sigma_o = B \exp(-\beta T) \tag{5}$$

where T is the absolute temperature and B and β are experimental constants.

Combining Eqs 4 and 5, a relation may be derived expressing the transition temperature (DBTT or T_c for short) at which the fracture stress (σ_F) and yield stress (σ_y) are equal for the grain size d^*. Thus

$$T_c = \frac{1}{\beta} \ln \{ B k_y d^{*1/2}/(C \mu \gamma - k_y^2) \} \tag{6}$$

For a given material, the relation between transition temperature and grain size may be reduced as follows

$$T_c = D + 1/\beta \ln d^{*1/2} \tag{6a}$$

where D is a constant $= 1/\beta \ln \{ B k_y/(C \mu \gamma - k_y^2) \}$. Equation 6a has been verified for several metals, including mild steel [17]. Thus it can be predicted from Eq 6a that the temperature at which brittle-to-ductile behavior occurs is decreased with smaller grain size. Figure 6 gives such a plot for the Fe-25Cr and Fe-18Cr-2Mo alloys investigated. Rather than just one straight line, however, several exist and for clarity two main groupings are shown. The lower one includes the low-interstitial-content alloys (0.005 carbon maximum and 0.015 nitrogen maximum), whereas the upper includes the remainder. In general, the tendency for the DBTT to increase linearly with $\ln d^{1/2}$ is quite marked. According to Eq 6a the slope ($1/\beta$) should be constant and this is the rationale for the lower curve being constructed with the same slope
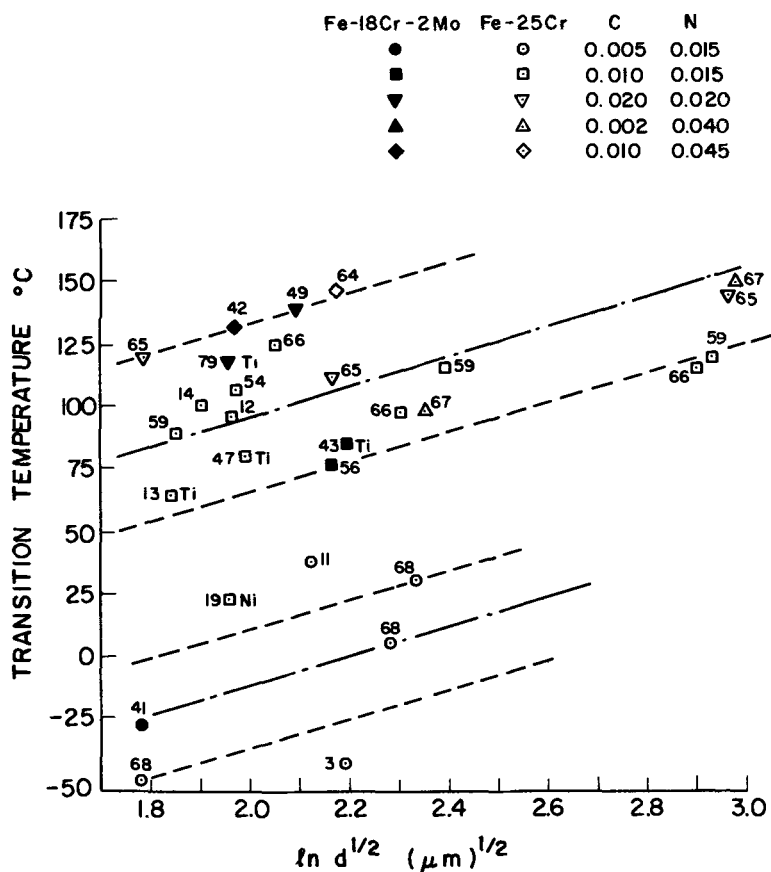
FIG. 6—*Plot of transition temperature versus* ln d$^{1/2}$*for Fe-18Cr-2Mo and Fe-25Cr ferritic stainless steels. The numbers given correspond to the alloy numbers.*

as the upper one. Also, for a constant grain size, the transition temperature will increase with increase in k_y and decrease in γ. Plumtree and Gullberg [*18*] showed that for water-quenched Fe-25Cr ferritic stainless steels the value of k_y was very small (∼5N/mm$^{3/2}$). In this present case, then, k_y may be neglected and the transition temperature for a constant grain size will be dependent upon surface energy. This term should be considered in greater detail since the influence of alloying elements on γ is more difficult to predict than the other terms given in Eqs 2 and 6. For fractures in which nucleation is the critical step, the appropriate value of γ is the true elastic surface energy. If solutes do not change the fracture mode from transgranular to intergranular cleavage, γ is not expected to be altered appreciably for dilute solute additions. For concentrated solutions, such as intermetallic com-

pounds, γ may be significantly increased. On the other hand, if solutes such as sulfur, antimony, phosphorus, or oxygen segregate to grain boundaries, a significant decrease in γ may be expected due to adsorption effects. Grain boundary films, as, for example, carbides in mild steels, produce similar results. In the present work, grain boundary particles were identified as mainly Cr_2N in the higher-interstitial-content alloys.

Figure 6 then should be regarded as a family of curves, all with the same slope and ascending in order of decreasing γ, which in turn would be dependent upon the amount of grain boundary particles present.

Amount of Second Phase

The amount of second-phase particles was found difficult to measure quantitatively by metallographic techniques due to the relatively small amount present in each alloy. However, when the yield strength is maintained constant, as in the present case, the particle content (V_f) may be related to the ductile fracture strain (ϵ_f) by an empirical relationship [19] based on the original work of Edelson and Baldwin [20]

$$V_f = \lambda/(\epsilon_f + \lambda) \tag{7}$$

where λ is a dimensionless constant for the particular alloy system. Thus when λ is small, V_f is directly related to $1/\epsilon_f$. The ductile fracture strains of some of the alloys investigated in the present study are given in Table 3 and it is apparent that, as the interstitial content of the alloy or the heat-treatment temperature (hence, grain size) increased, the fracture strain for the water-quenched specimens decreased, indicating the presence of a larger volume of second-phase particles and substantiating the metallographic observations. The term $1/\epsilon_f$ is plotted against (C + N) content in Fig. 7, which indicates an increasingly larger volume of second-phase particles with increasing interstitial content. Transferring this information to Fig. 2, the abscissa may be expressed as the volume fraction of second phase and the plot may be interpreted in terms of DBTT versus V_f. There is then a general tendency for the DBTT of either the Fe-25Cr or Fe-18Cr-2Mo steels to increase with the amount of second-phase present. When the amount is low, however, relatively small increases from these levels result in large increases in the DBTT, whereas when the second-phase content is high the DBTT is less sensitive to such changes.

Toughness

Besides the influence of interstitial or second-phase content on the transition temperature, it is worthwhile considering its effect on the Charpy V-notch shelf energy since this gives an indication of the amount of energy re-
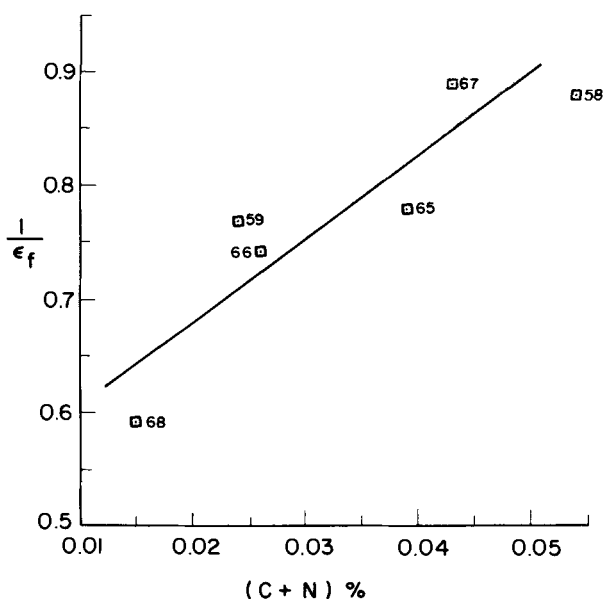
FIG. 7—*Variation of $1/\epsilon_f$ (or second phase amount—see Eq 7) with interstitial content.*

quired to cause ductile fracture. Recently Sailors and Corten [21] and Barsom [22] have suggested an empirical relationship between the plane-strain fracture toughness (K_{Ic}) and the Charpy V-notch shelf energy (CVN) for low-to-medium-strength (ferritic) steels in the transition temperature region as

$$K_{Ic}^2 = AE \text{ (CVN) [English units]} \qquad (8)$$

where A is a constant (in the range of 5 [22] to 8 [21]) and E is Young's modulus. Using this as a guide only, and choosing $A = 5$, the apparent K_{Ic} values for the present low-strength ferritic stainless steels may be approximated by

$$K_{Ic} = 11.56 \text{ (CVN)}^{1/2} \text{ [MPa } \sqrt{m}] \qquad (8a)$$

The Charpy V-notch shelf energy (CVN) and the apparent K_{Ic}, as given in Eq 8a, are plotted against the (C + N) content in Fig. 8. It is immediately apparent that below a (C + N) level of about 0.020 percent (200 ppm), the CVN (and K_{Ic}) values are constant and high. Once this threshold is exceeded, small increases in the (C + N) content cause the CVN values to decrease rapidly. Further increases in (C + N) content above about 0.050 percent (500 ppm) tend to have a small effect on reducing the CVN values. This figure includes both the Fe-25Cr and Fe-18Cr-2Mo steels investigated and it will be

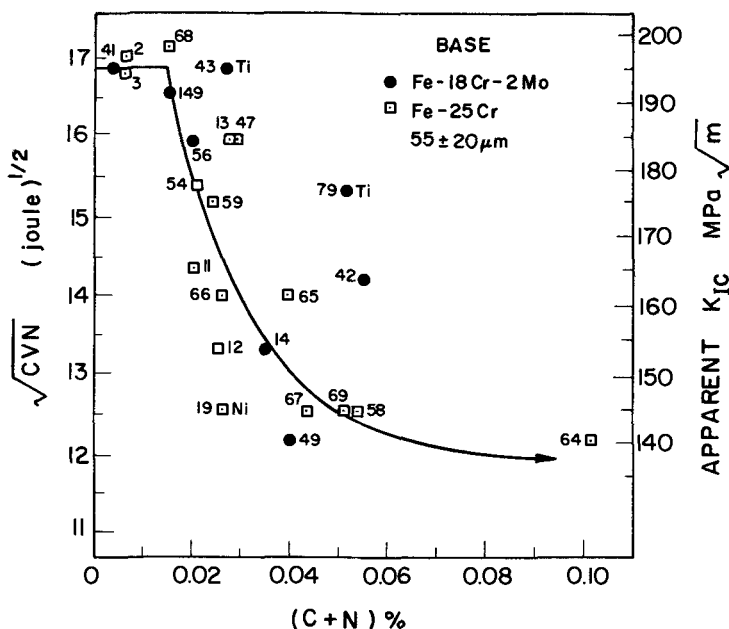FIG. 8—*Plot of* $\sqrt{CVN}$ *against interstitial content for Fe-18Cr-2Mo and Fe-25Cr ferritic stainless steels with grain sizes within the range of 35 and 75 μm. The numbers given correspond to the alloy numbers. The apparent* K_{Ic} *has been calculated according to Eq 8a.*

seen that the results of these two steels follow the same curve. Hence this plot gives very similar information to that of DBTT versus (C + N) content (Fig. 2). For a given (C + N) level, titanium additions of up to 0.66 percent tended to raise the shelf energy and apparent K_{Ic} values whereas an addition of 3.62 percent nickel to the Fe-25Cr alloy resulted in an opposite effect. Again, the addition of molybdenum to the Fe-25Cr steel appeared to have no effect since the observed CVN shelf energy for a given (C + N) content showed no deviation whatsoever from the composite curve shown in Fig. 8.

Alloy Content

Previous work on high-purity vacuum-melted ferritic stainless steels containing small amounts (less than 150 ppm) of (C + N) has shown that chromium additions of up to 30 percent appear to have a slightly beneficial effect by increasing the shelf energy and decreasing the DBTT [2]. Although very few alloys were prepared with such a low interstitial content, the results of the present work do not fully support this previous work. In fact, it would seem that changing the chromium from 18 to 25 percent has very little, if any, influence on either the shelf energy or the DBTT for this low (C + N)

level, or, for that matter, any (C + N) level investigated. Although chromium additions should produce solute hardening, some solution softening may occur at low temperatures [23]. Other workers have reported little influence on the yield stress [24–26], yet have found that the associated DBTT may either increase [24] or decrease [25,26]. Hence the effect of chromium on the DBTT or shelf energy appears to be in doubt presumably because it has no strong effect in itself and because its apparent effect is brought about by other additional elements, mainly interstitial carbon and nitrogen. Work by Binder and Spendelow [2] showed that as the chromium content increases the combined (C + N) level must decrease if the ferritic stainless steel is to maintain an impact strength of between 14 and 70 J at room temperature; in particular, the (C + N) content should not exceed 0.050 percent (500 ppm) for an Fe-18Cr alloy and 0.030 percent (300 ppm) for an Fe-25Cr alloy. The present results showed that a tolerance level of about 0.015 percent (150 ppm) (C + N) existed for both the Fe-25Cr and Fe-18Cr-2Mo steels with no higher tolerance level associated with the latter. On examination of the notched-bar impact test results, the following low-interstitial-content alloys exceeded an impact strength of 70 J at room temperature—Fe-25Cr: Alloys 19 (C + N = 0.027 percent), 11 (C + N = 0.020 percent), 68 (C + N = 0.015 percent), 3 (C + N = 0.006 percent), and 2 (C + N = 0.006 percent); Fe-18Cr-2Mo: Alloy 41 (C + N = 0.003 percent). However, the remainder possessed impact strength values in excess of 14 J at room temperature. Thus the hypothesis of Binder and Spendelow was difficult to apply to the present case.

Molybdenum additions of up to 1.13 percent in the Fe-25Cr steel appeared to have little effect on the DBTT or CVN shelf energy. Molybdenum may increase the friction stress at room temperature although it is known to be a solid solution softener in iron at lower temperatures [27]. Additions of up to 3 percent molybdenum appear to have a negligible effect on the ductility of iron-chromium alloys provided that no intermetallic phases are formed [14,28]. Hence, although having little effect on the DBTT or K_{Ic} values, additions of 2 percent molybdenum are considered to be beneficial since they provide increased corrosion resistance to a wide range of environments [14]. The presence of molybdenum may also reduce the tendency for secondary recrystallization to occur.

Titanium additions of up to 0.66 percent to both the Fe-25Cr and Fe-18Cr-2Mo steels tended to lower the DBTT and increase the CVN shelf energy when compared with alloys of similar (C + N) content containing no titanium. The results are restated in terms of the Ti/(C + N) ratios in Table 4. The first three alloys listed (Alloys 13, 47, and 43) have a constant (C + N) content of about 0.027 percent (270 ppm). On increasing the Ti/(C + N) ratio it would appear that the shelf energy (or K_{Ic}) is returned to the base level of 285 J (Alloy 68) when the Ti/(C + N) ratio approaches about 25:1. However, a corresponding improvement in DBTT was not observed. Alloy

TABLE 4—Effect of Ti/(C + N) ratio on impact results.

Alloy No.	Ti/(C + N) Ratio	DBTT, °C				CVN, J			
		Observed a	Predicted Without Titanium—Fig. 2 b	Base—Alloy 68 or 41 c	Improvement Expressed as % of Base, $(b-a/b-c) \times 100\%$	Observed d	Predicted Without Titanium—Fig. 8 e	Base—Alloy 68 or 41 f	Improvement Expressed as % of Base, $(d-e/f-e) \times 100\%$
13 (25Cr)	2.6:1	66	108	−50	26	255	203	285	63
47 (25Cr)	15.6:1	80	108	−50	18	255	203	285	63
43 (18Cr-2Mo)	24.4:1	83	105	−50	14	285	203	285	100
79 (18Cr-2Mo)	2.9:1	119	145	−50	13	234	156	285	60

79, containing a larger amount of interstitial carbon and nitrogen (520 ppm), displayed a similar improvement in shelf energy to Alloy 13 with approximately the same Ti/(C + N) ratio of 2.9:1. However, the former displayed less of an improvement in DBTT. These results agree with those of Wright [29] investigating a series of Fe-26Cr-1Mo ferritic stainless steels. He showed that the addition of titanium generally improved toughness (and also weldability) when the (C + N) level was in the range of 0.03 to 0.08 percent (300 to 800 ppm). Dundas [30] also investigated the influence of carbon, nitrogen, and titanium on the impact properties of high-purity Fe-17Cr and commercial-purity Fe-18Cr-Mo ferritic stainless steels. He showed that titanium additions improved the impact properties, although the DBTT or shelf energies were not returned to their respective levels associated with the high-purity specimens. The addition of titanium as a scavenging element to ferritic stainless steels containing higher carbon and nitrogen amounts may result in solid solution softening [31] where the solute elements form precipitates of nonhardening complexes with the carbon or nitrogen atoms [32]. The consequent nitrides or carbides are instrumental in initiating recrystallization as well as retarding grain growth; however, nitrides or carbides will reduce the γ-term in Eq 6 and the DBTT associated with low (C + N) content will not be attained.

The addition of 3.62 percent nickel to the Fe-25Cr ferritic stainless steel resulted in a decrease in the DBTT and also a decrease in the shelf energy (or K_{Ic}) value for the appropriate (C + N) content. The former effect may be again explained in terms of the Cottrell-Petch equation, Eq 6. Nickel additions are expected to reduce the amount of precipitation at the grain boundaries, thereby increasing the value of γ. This is achieved by trapping interstitial atoms in the lattice, distorted by pairs of the substitutional nickel atoms. It has been suggested that the interstitial atoms migrate preferentially to these locally strained sites [33]. Consequently the energy barrier for an interstitial atom leaving a nickel atom pair will be high. Experimental evidence for a decrease in the magnitude of dislocation locking due to the presence of nickel has been provided by a shift in the internal friction peak for carbon to lower temperatures [34] and a drop in peak height [25].

Conclusions

1. Within experimental error, notched-bar impact test results were very similar for water-quenched specimens of vacuum-melted Fe-18Cr-2Mo and Fe-25Cr ferritic stainless steels. Subsequent analysis was carried out regarding the two steels as having the same general properties.

2. The impact test results indicated that an increase in the amount of carbon and nitrogen caused an increase in the ductile-to-brittle transition temperature and a decrease in shelf energy. Below a (C + N) level of 0.015 percent (150 ppm), however, the transition temperature was constant and

low ($-50\,°C$) and the shelf energy was constant and high (equivalent to a K_{Ic} value of ~ 195 MPa$\sqrt{m}$).

3. The increase in transition temperature with interstitial content was related to an increase in the amount of second phase (mainly chromium nitride), particularly at the grain boundaries. It is suggested that this in-homogeneous distribution of second-phase particles lowers the effective surface energy of a crack, γ, promoting transgranular brittle fracture.

4. The increased brittleness with increase in second-phase content and grain size, d, may be explained in terms of the Cottrell relationship: $\sigma_y k_y d^{1/2} = C\mu\gamma$. A brittle condition is reached when the left-hand side of this equation exceeds the right. For constant σ_y and k_y values associated with the present water-quenched ferritic stainless steels, lower γ-values and larger grain sizes facilitate brittle fracture.

5. Titanium additions to the ferritic stainless steels tended to have a beneficial effect by lowering the transition temperature and raising the shelf energy. A Ti/(C + N) ratio of about 25:1 restored the shelf energy to that of the low-interstitial-content alloys [(C + N) ~ 0.015 percent]. A similar improvement in transition temperature was not observed.

6. The addition of nickel to one alloy caused the transition temperature to decrease. However, a decrease in the shelf energy was also observed when compared with alloys of similar interstitial content.

References

[1] Richmond, F. H., *Metal Progress*, Vol. 97, 1970, p. 103.
[2] Binder, W. O. and Spendelow, H. R., Jr., *Transactions* American Society for Metals, Vol. 43, 1951, p. 759.
[3] Hochman, J., Discussion of Ref 2, *Transactions*, American Society for Metals, Vol. 43, 1951, p. 773.
[4] Hochman, J., *Comptes Rendus Hebdomadaires des Séances de l'Académie des Sciences*, Vol. 226, 1948, p. 2150.
[5] Oppenheim, R. and Laddach, H., *Deutsche Edelstahl-Werke Technische Berichte*, Vol. 11, No. 2, 1971, p. 71.
[6] Semchyshen, M. and Bond, A. P., *Proceedings*, Symposium Towards Improved Ductility and Toughness, Kyoto, Japan, 1971, p. 235.
[7] Steigerwald, R. F., Dundas, H. J., Redmond, J. D., and Davison, R. M., *The Metallurgist and Materials Technologist*, Vol. 10, No. 4, 1978, p. 181.

[8] Plumtree, A. and Gullberg, R., J. *Testing and Evaluation*, Vol. 2, No. 5, 1974, p. 331.
[9] Hodges, R. J., *Corrosion*, Vol. 27, No. 3, 1971, p. 119.
[10] Hodges, R. J., *Corrosion*, Vol. 27, No. 3, 1971, p. 164.
[11] Demo, J. J., *Corrosion*, Vol. 27, No. 10, 1971, p. 531.
[12] Zener, C., *Fracturing of Metals*, American Society for Metals, Cleveland, Ohio, 1948, p. 246.
[13] Stroh, A. H., *Proceedings*, Royal Society (London), Vol. 223, Series A, 1954, p. 404.
[14] Cottrell, A. H., *Transactions*, Metallurgical Society of American Institute of Mining, Metallurgical, and Petroleum Engineers, Vol. 212, 1958, p. 192.
[15] Honda, R., *Journal of the Physical Society of Japan*, Vol. 16, 1961, p. 1309.
[16] Johnston, T. L., Davies, R. G., and Stoloff, N. S., *Philosophical Magazine*, Vol. 12, 1965, p. 305.
[17] Petch, N. J., *Fracture*, Wiley, New York, 1959, p. 305.
[18] Plumtree, A., and Gullberg, R., *Metallurgical Transactions*, Vol. 7A, 1976, p. 1451.
[19] Tetelman, A. S. and McEvily, A. J., Jr., *Fracture of Structual Materials*, Wiley, New York, 1967, p. 220.
[20] Edelson, B. and Baldwin, W., *Transactions*, American Society for Metals, Vol. 55, 1962, p. 230.
[21] Sailors, R. H. and Corten, T. H. in *Fracture Toughness, ASTM STP 514, Part II*, American Society for Testing and Materials, 1972, p. 164.
[22] Barsom, J. M., *Engineering Fracture Mechanics*, Vol. 7, 1975, p. 606.
[23] Spitzig, W. A, and Leslie, W. C., *Acta Metallurgica*, Vol. 19, 1971, p. 1143
[24] Rinebolt, J. A. and Harris, W. J., *Transactions*, American Society for Metals, Vol. 43, 1951, p. 1175.
[25] Stoloff, N. S., *Proceedings*, Fourth Annual Symposium on Materials Sciences, Plenum Press, New York, 1966, p. 197.
[26] Stoloff, N. S., *Proceedings*, Conference On Physical Basis of Yield and Fracture, Physical Society, London, 1966. p. 68.
[27] Takeuchi, J., Yoshida, H., and Taoka, T., *Proceedings*, International Conference of Strength of Metals and Alloys, Japan Institute of Metals, 1968, p. 715.
[28] Wilshaw, T. R. and Pratt, P. L., *Journal of the Mechanics and Physics of Solids*, Vol. 14, 1966, p. 7.
[29] Wright, R. N., *Welding Journal*, Vol. 50, No. 10, 1971, p. 434S.
[30] Dundas, H. J., Report No. RP-33-1968-4, Climax Molybdenum Co. of Michigan, July 1970.
[31] Urakami, A., *Proceedings*, Second International Conference on Materials Behavior, Kyoto, Japan, 1971.
[32] Ravi, K. V. and Gibala, R., *Acta Metallurgica*, Vol. 18, 1970, p. 623.
[33] Gladman, T. and Pickering F. B., *Journal of the Iron and Steel Institute*, Vol. 203, 1965, p. 1212.
[34] Jackson, J. K. and Winchell, P. G., *Transactions*, Metallurgical Society of American Institute of Mining. Metallurgical, and Petroleum Engineers, Vol. 230, 1964, p. 216.

DISCUSSION

T. G. Gooch[1] *(written discussion)*—The author's results are most interesting and of considerable practical import. However, I question his analysis of the role of grain boundary carbides in reducing toughness. This

[1]The Welding Institute, Abington Hall, Abington, Cambridge, U. K.

model is based on an intergranular phenomenon, yet brittle fracture of ferritic stainless steels is normally transgranular. The role of carbides is probably more subtle than reducing grain boundary energy; from analogous studies on plain ferritic steels, they may well act by initiating transgranular cleavage cracking.[2]

A. Plumtree and R. Gullberg (authors' closure)—All the fractures were transgranular. The brittle failures were typical cleavage fractures which occur in body-centered cubic (bcc) metals at low temperatures and high strain rates. An example of transgranular cleavage cracking below the DBTT in Alloy 67 (Fe-25Cr) is shown in Fig. 9.

The present model considers only the initiation of cleavage cracks. Crack nucleation occurs when the concentrated stresses at the tip of a blocked dislocation band equal the cohesive stress given by

$$(\tau_N - \tau_i)\, nb \simeq 2\, \gamma_T \qquad (9)$$

where

τ_N = shear stress for crack nucleation,
τ_i = friction shear stress,
n = number of dislocations in the pileup,
b = burgers vector, and
γ_T = true surface energy.

This equation indicates that a crack will form when the work done by the applied shear stress ($\tau_N\, nb$) in producing a displacement nb equals the combined work done in moving the dislocations against the friction stress ($\tau_i\, nb$) and the work done in creating the new fracture surfaces ($2\gamma_T$). In most metals where some relaxation occurs around the blocked dislocation band, the term γ (as in the present work) is used rather than γ_T. Grain boundaries, hard particles, inclusions, and, of course, grain boundary carbides act as barriers to dislocation motion, favoring crack initiation. When second phases are inhomogeneously distributed (such as grain boundary carbides) the value of γ is reduced. Subsequently the amount of work done in nucleating a crack decreases, as indicated by Eq 9. Transgranular cleavage cracks form more easily and the toughness is reduced, compared with those alloys where γ remains high due to homogeneous second-phase distribution.

C. R. Thomas[2] (written discussion)—While it is recognized that the volume fraction of precipitates does control impact toughness to a certain extent, the morphology and distribution of carbonitrides is surely of significant importance. Would the authors please comment?

[2]Smith, E. in *Proceedings*, Conference on Physical Basis of Yield and Fracture, Institution of Physics and Physical Society, Oxford, U. K., 1966.
[3]Cranfield Institute of Technology, Department of Materials, Cranfield, Bedford, U. K.
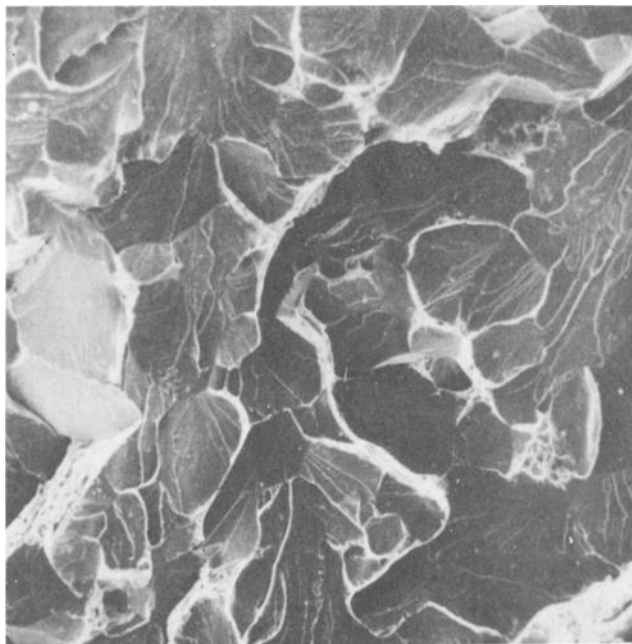
FIG. 9—*Transgranular brittle failure of Charpy impact specimen—Alloy 67. Original magnification ×100.*

A. Plumtree and R. Gullberg (authors' closure)—The distribution and morphology of the chromium nitrides and carbides will have a large effect on cleavage nucleation since the value of γ (see Eq 2 of the paper) for any particle-matrix orientation depends upon the size and shape of the particles. For a given volume fraction, γ will be high for a homogeneous distribution.

In a planar slip mode material such as the present Fe-Cr alloys, dislocations in a pileup at a particle may be able to activate sources above and below, especially when the particles are small and well distributed. In this case, the friction stress and hardness are raised, and γ remains high. When the same amount of second phase is segregated at the grain boundaries, crack nucleation is facilitated since these second-phase particles prevent much stress relaxation at the tip of the blocked slipband and the work done in crack nucleation is small (that is, γ decreases). When the thickness of the particles becomes large, a substantial part of the crack nucleates in this second-phase and γ is decreased further. Conversely, as the thickness is reduced, most of the nucleation takes place in the softer matrix, resulting in a larger value of γ.

It is apparent that a bcc alloy containing small homogeneously distributed second-phase particles will have a lower DBTT than the same alloy with
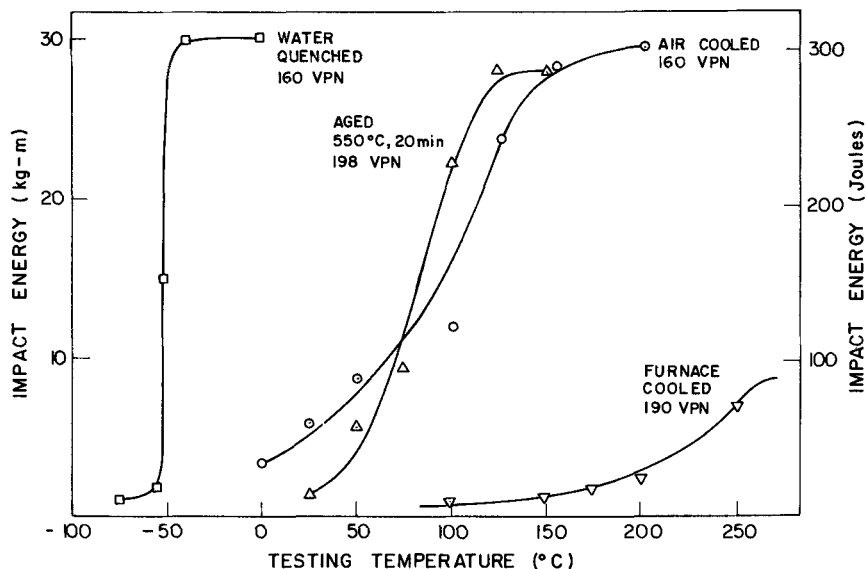
FIG. 10—*Impact energy curves for Charpy specimens prepared from vacuum-melted Fe-25Cr alloy (Alloy 68). Hardness is given for each heat treatment.*

grain boundary films. As these grain boundary films increase in thickness the DBTT will be expected to increase. This is seen to effect in Fig. 10. On aging the water-quenched Fe-25Cr alloy at 550°C for 20 min, the consequent form-ation of small, relatively well-distributed chromium nitrides or chromium carbonitrides or both results in an increase in DBTT from −50 to 80°C. A hardness of 198 VPN (compared with 160 VPN for the water-quenched alloy) indicates an increase in the lattice friction. On air-cooling the same alloy from 850°C, instead of quenching, the resulting DBTT is about 90°C, although the hardness is unaffected (160 VPN). In this case the second-phase is present at the grain boundaries in the form of films. If instead the alloy is air-cooled from 850°C, the grain boundary chromium nitrides become thick and the DBTT becomes very high (~ 225°C), yet the hardness of 190 VPN is very similar to that of the specimens quenched and aged at 550°C for 20 min. The microstructures of these alloys are considered in greater detail by Plum-tree and Gullberg (see Ref *18* of paper).

J. F. Grubb, [1] *R. N. Wright,* [1] *and P. Farrar, Jr.* [2]

Micromechanisms of Brittle Fracture in Titanium-Stabilized and α'-Embrittled Ferritic Stainless Steels

ABSTRACT: Fe-26Cr alloys, with and without titanium stabilization, have been studied in an effort to clarify the micromechanisms of brittle fracture in the presence of titanium stabilization and α'-precipitation (475°C embrittlement). Tension testing, Charpy testing and metallographic evaluations have been undertaken. Microscopic observations of electropolished strips pulled in the ductile-to-brittle transition temperature (DBTT) range have been made. Titanium stabilization can lead to DBTT increases in low carbon and nitrogen alloys and this embrittlement is associated with intergranular microcrack formation. Embrittlement due to α'-precipitation seems related to flow stress increase and the α'-precipitation is seen to bring about a gross change in slip character, leading to the development of relatively few, but extremely intense slipbands.

KEY WORDS: ferritic stainless steels, embrittlement, stabilization, tensile properties, toughness, interstitial, α'-phase, fracture mechanisms, fracture toughness

Ferritic stainless steels, due to their general corrosion resistance and excellent resistance to chloride-induced stress corrosion cracking, are increasingly being studied and applied. The potential cost reductions that go along with the elimination of nickel, manganese, and other austenite-stabilizing elements also ensure continuing metallurgical interest in ferritic stainless steel alloys. The use of these alloys has, however, historically been hindered by poor toughness, notch sensitivity, and susceptibility to embrittlement.

It had long been presumed that the lack of toughness exhibited by the high-chromium ferritic stainless steels was due to chromium, per se, until the works of Hochman [1] [3] and Binder and Spendelow [2] demonstrated

[1] Graduate student and associate professor, respectively, Materials and Engineering Department, Rensselaer Polytechnic Institute, Troy, N.Y. 12181.

[2] Associate engineer, IBM Corp., Burlington, Vt.

[3] The italic numbers in brackets refer to the list of references appended to this paper.

that good annealed ductility and toughness could be achieved through rigorous limitation of carbon and nitrogen (C + N) contents. More recently, Demo [3] demonstrated that even more drastic limits on (C + N) content were required for as-welded ductility and corrosion resistance. Within the past decade, advances in commercial steel melting and refining processes have made it possible to routinely produce alloys with the requisite low levels of (C + N). Thus, ferritic stainless steels of considerably improved toughness are now commercially available.

Wide variations in ductile-to-brittle transition temperature (DBTT) may be observed even in these modern, low (C + N) alloys, and two of the authors have recently completed a study of the dominant role of the (C + N) *state* in the varying micromechanisms of fracture in these steels [4]. This work relied heavily on microscopic observation of electropolished strips pulled in tension in the DBTT range. Such a technique may be usefully extended to additional fracture transition behavior in ferritic stainless steels. This paper reports two such evaluations, namely, studies of the respective roles of titanium "stabilization" and α'-embrittlement.

The high costs of reducing (C + N) levels in ferritic stainless steels have prompted alloy development involving titanium and columbium additions for the purpose of tying up or "stabilizing" (C + N) by forming compounds of greater stability than $Cr_{23}C_6$ and Cr_2N. While such alloying can have a quite positive effect on corrosion behavior, much optimism has been focused on fracture response.

The first such stabilization of high-chromium ferritic stainless steel was reported by Beckett and Franks [5] a decade before the role of (C + N) in promoting brittleness in these steels was demonstrated by Hochman [1]. These authors showed that titanium additions could substantially improve ductility. The effects of stabilization upon as-welded ductility have been reported by Demo [6,7], Semchyshen et al [8], Wright [9], and Pollard [10]. In general, it was shown that stabilization increases the interstitial element level compatible with good ductility. Stabilization improves the toughness of material quenched from high (>1000°C) temperature, and slightly improves the toughness of high interstitial annealed material. Wright [9] has shown, however, that titanium stabilization actually increases the DBTT of annealed low interstitial alloys. The effect of titanium additions on ferritic stainless steels continuously cooled from a high-temperature anneal was investigated by Pollard [10], who found that while titanium prevented embrittlement due to $Cr_2(C,N)$ precipitation, microcracks were initiated around titanium-nitride (TiN) particles during quenching. Thus, titanium stabilization may serve to induce the embrittlement it is designed to prevent. Pollard's work, however, was limited to continuous cooling followed by quenching, and fracture initiation was inferred from fracture surface observation. As one portion of this work, the behavior of a titanium-stabilized Fe-26Cr alloy was studied as a function of cooling rate and isothermal

annealing temperature. Selected conditions were then examined for fracture initiation mechanisms using the method of McMahon and Cohen [*11*].

One area in which interstitial element reduction is of little utility is the 475°C (885°F) embrittlement problem. Exposure of ferritic stainless steel at temperatures near 475°C for any appreciable period of time results in considerable loss of toughness and corrosion resistance. Investigators originally thought that this embrittlement was due to a precipitation process connected with the early stages of σ-phase formation [*12*]. It is now well established that 475°C embrittlement is a result of the precipitation of a chromium-rich body-centered-cubic phase, α', which forms due to a miscibility gap in the iron-chromium system [*13-17*]. This miscibility gap extends from about 10Cr to 90Cr. A spinodal exists within the miscibility gap [*18*]. Alpha-prime precipitation is thought to occur by nucleation and growth outside the spinodal and by spinodal decomposition within [*18-22*]. Evidence for nucleation-and-growth behavior has been presented for alloys containing as much as 23Cr [*15,18,21*], precipitation becoming more rapid with increased chromium content. Spinodal decomposition is probable for alloys of 29Cr or greater [*16,18,20,21*]. Embrittlement is associated with the earliest stage of α'-precipitation [*22*] and is accompanied by hardness and strength increases. Widespread twinning has been noted in connection with the deformation of α'-embrittled material [*14,15,23*].

The α'-precipitation may occur simultaneously with other embrittling reactions. In cold-worked materials, for instance, σ-phase may be precipitated along with α' [*13*]. More importantly, chromium carbide and chromium nitride precipitation occur readily at temperatures near 475°C, and embrittlement from this relatively rapid precipitation has often been mistaken for the early stages of the slower α'-precipitation embrittlement. The problem of distinguishing between carbonitride and α'-effects has been dealt with in detail by Plumtree and Gullberg [*24*].

Attempts to moderate 475°C embrittlement through alloying have been largely unsuccessful. In fact, nearly all impurities and alloying additions hasten α'-precipitation [*22,25,26,12*]. The effect of alloying additions has been ascribed to enhancement of α'-precipitation through chromium complex formation, to carbide and nitride precipitation, and to intensification of age-hardening through α'-lattice parameter mismatch increases [*26*]. Grain size refinement through titanium and columbium addition improves the ductility of α'-embrittled steel, even in the presence of the increased α'-precipitation and hardening associated with the alloying addition [*26*].

The cause of 475°C embrittlement may be related to the strengthening produced by α'-precipitation or to some intrinsic feature of the α-α' composite. Most past work has dealt with the phase transformation itself and little information exists concerning the micromechanics of fracture. Inhibition of slip is implicit in the observed strengthening and widespread

twinning. It has been observed that crack propagation is predominately by transgranular cleavage [15]. The mode of crack initiation, however, has been given little study.

In the second portion of this paper, the method of McMahon and Cohen [11] is applied to the study of α'-embrittled Fe-26Cr.

Materials and Procedure

Three 23-kg heats of low-residual-element Fe-26Cr were vacuum induction melted from electrolytic iron and chromium. The chemical analyses of these heats are given in Table 1. Processing involved hot rolling to 0.32 cm, annealing, cold rolling to 0.16 cm, annealing at 860°C for 4 min, and pickling. The pickled material was sawed into 11.5 by 1.3-cm blanks, with the long dimension of the blanks parallel to the strip rolling direction.

The blanks from Heats 1 and 2 were subjected to a variety of thermal cycles as shown in Table 2. All of these heat treatments included a preliminary 1290°C, 1-min anneal designed to produce a large, uniform grain size. Procedures A–D (Table 2) involved varied cooling rates from the solution anneal. The four cooling curves are shown in Fig. 1. The spray quenching was performed with a specially adapted Duffers Gleeble machine [27]. Procedures E–H simply involve appending an isothermal precipitation annealing cycle to the as-quenched condition produced by Procedure B. The blanks from Heat 3 were aged at 475°C for periods of 0, 6, 60, 600, and 6000 min, respectively. All heat treatments were performed in air. The heat-treated blanks were pickled by exposure to a 30 percent sulfuric acid solution for 2 min, followed by dipping in a 15 percent nitric-3 percent hydrofluoric acid solution at ~77°C.

The variously heat-treated materials were subjected to microstructural and mechanical characterization prior to the fracture mechanism study.

TABLE 1—*Chemical compositions of the experimental alloys (in weight percent, balance iron).*

Element	Heat 1	Heat 2	Heat 3
C	0.0030	0.031	0.0144
N	0.0052	0.022	0.0120
Cr	26.0	25.4	26.0
Ti	0.20	0.62	0.003
Mn	0.068	0.071	0.071
Si	0.17	0.18	0.19
Ni	0.010	0.010	0.010
Cu	0.010	0.010	0.010
P	0.008	0.002	0.006
S	0.005	0.007	0.006
O	0.0030	0.0070	0.0057

TABLE 2—*Heat treatments used to establish varied states of carbon and nitrogen.*

Procedure	Description
A	1290°C for 1 min; spray quench
B	1290°C for 1 min; iced-brine quench
C	1290°C for 1 min; air-cool
D	1290°C for 1 min; furnace-cool
E	1290°C for 1 min; iced-brine quench; 955°C for 10 min; iced-brine quench
F	1290°C for 1 min; iced-brine quench; 790°C for 10 min; iced-brine quench
G	1290°C for 1 min; iced-brine quench; 620°C for 10 min; iced-brine quench
H	1290°C for 1 min; iced-brine quench 540°C for 10 min; iced-brine quench

The microstructural characterization involved optical, scanning electron microscopy (SEM) and transmission electron microscopy (TEM). The mechanical characterization consisted of tension and subsize Charpy impact testing.

Normal metallographic specimen preparation included swabbing for 20 s in a "mixed acids" etch of 5-ml glacial acetic acid, 5-ml concentrated nitric acid, and 15-ml concentrated hydrochloric acid. The swabbing period was extended to 45 s in preparation for SEM study. TEM specimen preparation followed conventional procedures.

Mechanical characterization included tension and subsize Charpy V-notch impact testing. Room-temperature tension tests were performed at
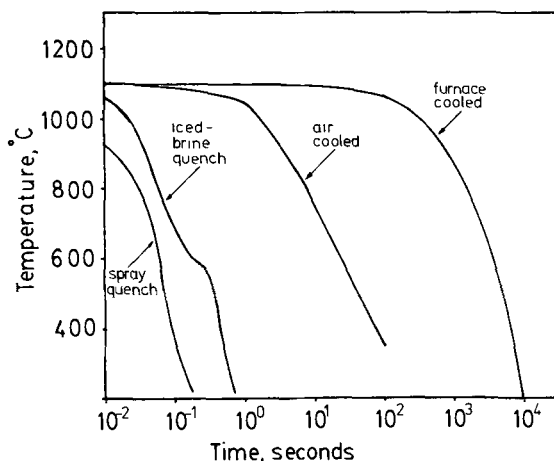

FIG. 1—*Near-surface cooling rates produced during specimen preparation.*

strain rates of 0.05 min^{-1} using an Instron machine. Duplicate tests were performed in accordance with ASTM Standard Methods of Tension Testing of Metallic Materials (E 8-78), except the gage length was three times the width rather than four times. The shorter gage section was necessary to insure a uniformly heat-treated test section on the spray-quenched specimens. Charpy testing was performed on a Physmet subsize impact testing machine in accordance with ASTM Standard Methods for Notched Bar Impact Testing of Metallic Materials (E 23-72), except that the specimen thickness was a nonstandard 0.155 cm. Charpy testing was undertaken throughout the range from −196 to +300°C using liquid nitrogen, 2-methyl-butane, ethanol, water, silicone oil, and fused bauxite as heat-transfer media. DBTT's were defined as the point where the energy absorbed was equal to one half of the upper-shelf energy. Approximately 10 tests were used to define the Charpy V-notch DBTT for each heat treatment.

Fracture initiation studies were performed using the approach of McMahon and Cohen [11]. Strip tensile specimens were ground and electropolished using a 70 percent methanol-30 percent nitric acid solution at −35°C for 1 to 2 min at 10 to 12 V and 0.4 A/cm². The electropolished specimens were then tension tested at temperatures in the DBTT range at the same strain rates used in the room-temperature tests. The DBTT for these tension test conditions (unnotched, slow strain rate) was considerably below that for the Charpy tests (notched, high strain rate) and was well below room temperature even for the 6000 min α'-embrittled material. Tension testing was performed on an Instron machine outfitted with a tension test fixture which could be immersed in a Dewar flask. Cooling media were selected from those used for the Charpy testing. After tension testing to fracture, the electropolished strip surfaces were examined by optical and SEM microscopy. The as-tested strip surfaces generally displayed gross strain markings (orange-peel effects, shear bands, etc.), slipbands, mechanical twinning, second-phase particles (but not α') and subcritical microcracks. The relationship of the microcracks to structural details allows direct inferences regarding the fracture mechanism.

Results

Microstructures

The microstructures of the titanium-stabilized Heats 1 and 2 are dominated by the presence of blocky intragranular titanium carbonitride particles. The results of optical metallography of Heats 1 and 2 are summarized in Table 3. Since all of these specimens were subjected to the 1290°C, 1-min solution anneal, all specimens within a given heat displayed a large

TABLE 3—*Summary of optical metallographic observations.*

Procedure	Observed Microstructure, Heat 1	Observed Microstructure, Heat 2
A	intragranular Ti(C,N) particles	large intragranular Ti(C,N) particles
B	intragranular Ti(C,N) particles	large intragranular Ti(C,N) particles
C	intragranular Ti(C,N) particles	large intragranular Ti(C,N) particles with grain boundary precipitates
D	intragranular Ti(C,N) particles with fine grain boundary precipitates and needle-like intragranular precipitates	large intragranular Ti(C,N) particles
E	intragranular Ti(C,N) particles	large intragranular Ti(C,N) particles with fine grain boundary precipitates
F	intragranular Ti(C,N) particles	large intragranular Ti(C,N) particles
G	intragranular Ti(C,N) particles with fine grain boundary precipitates	large intragranular Ti(C,N) particles with needle-like intragranular precipitates
H	intragranular Ti(C,N) particles with needle-like intragranular precipitates	large intragranular Ti(C,N) particles with needle-like intragranular precipitates

uniform grain size. The grain size was approximately 0.07 cm for Heat 1 and 0.04 cm for Heat 2. Water quenching from the solution annealing temperature essentially prevented carbide and nitride precipitation [except possibly on preexisting Ti(C,N) particles] in Heat 1, whereas only spray quenching seemed effective in preventing precipitation in the higher $(C + N)$ Heat 2. [In addition to having higher $(C + N)$ than Heat 1, Heat 2 has a lower ratio of titanium to combined $(C + N)$; the $Ti/(C + N)$ ratio is still higher than normally deemed necessary for $(C + N)$ control].

In Heat 1, even air cooling did not produce any real evidence of grain boundary carbide or nitride precipitation. Grain boundary precipitate was produced, however, by furnace cooling. This furnace cooling also resulted in precipitation of a fine needle-like intragranular phase. The results of 10-min isothermal precipitation annealing can be summarized as follows:

1. Annealing above $\sim 750°C$ leads to no grain boundary carbide or nitride precipitation.

2. Annealing at 705 or 620°C produces grain boundary precipitation.

3. Annealing at 540°C produces needle-like intragranular precipitation. Representative micrographs of Heat 1 are shown in Fig. 2.

The variation in precipitate distribution for Heat 2 is very similar. In general, structures equivalent to Heat 1 can be produced in Heat 2 at shorter time or at higher temperatures. Grain boundary precipitates are now produced during the 955°C, 10-min isothermal anneal while needle-like intragranular precipitates now appear at 620°C. A representative micrograph for Heat 2 is shown in Fig. 3.

FIG. 2—Optical microstructures of Heat 1 material: (a) Solution annealed at 1290°C for 1 min and spray quenched (Procedure A); note precipitate-free grain boundaries; ×525. (b) Solution annealed at 1290°C for 1 min and iced-brine quenched (Procedure B); note precipitate-free grain boundaries; ×525. (c) Solution annealed at 1290°C for 1 min and furnace-cooled (Procedure D); note grain boundary and needle-like intragranular precipitate; ×525.
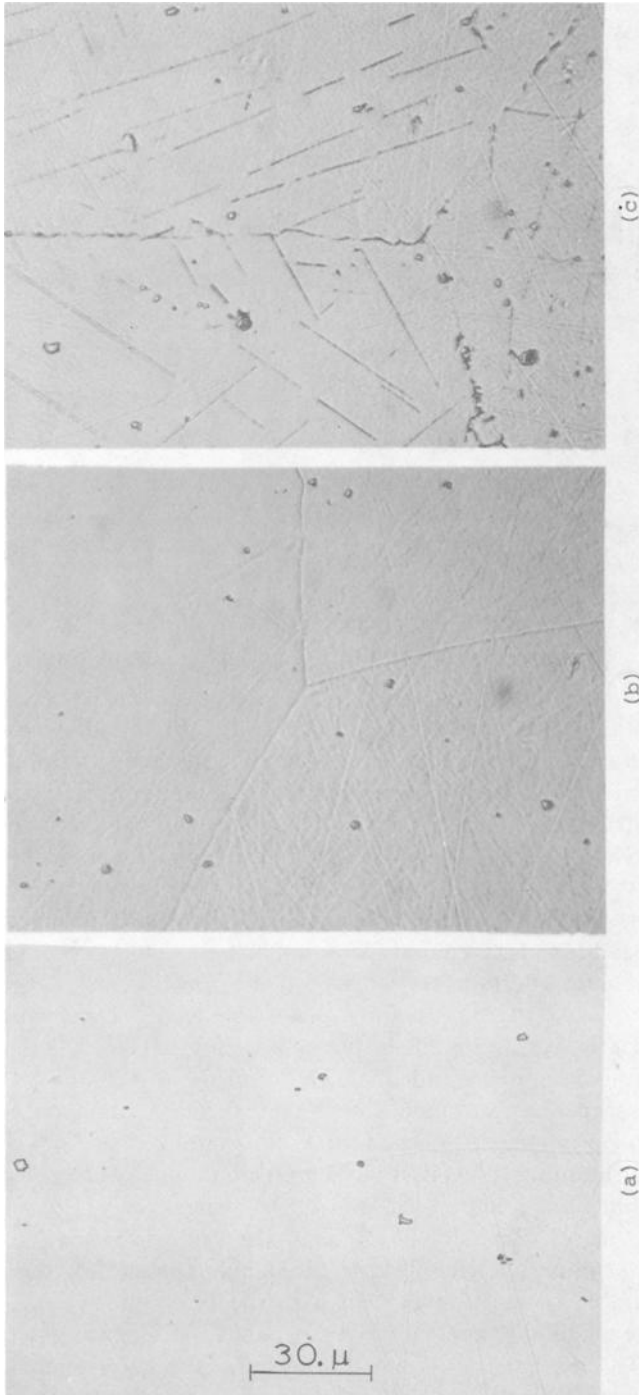
FIG. 3—*Optical microstructure of Heat 2 material: ×525. Solution annealed at 1290°C for 1 min and iced-brine quenched (Procedure B), note precipitate-free grain boundaries. Same magnification as in Fig. 2.*

The subject of phase identification in iron-chromium alloys has been dealt with in detail in previous work [4,10,16,24,28], and only limited precipitate identification was undertaken in the present study. In the *absence* of titanium, the nature of the precipitates can be summarized as follows. The carbide and nitride precipitates observed in high-chromium ferritic stainless steels are Cr_2N, $Cr_2(C,N)$, and $Cr_{23}C_6$, although one observer reported the presence of CrN [24]. $Cr_{23}C_6$ predominates with high carbon-to-nitrogen ratios while Cr_2N [or $Cr_2(C,N)$] predominates at low carbon-to-nitrogen ratios [10]. The needle-like intergranular precipitate which forms at low temperatures has been observed and identified by Lena and Hawkes [28] as Cr_2N. With titanium addition, (C + N) is tied up as Ti(C,N), largely in the molten steel. The Ti(C,N) is readily identifiable as a "blocky" precipitate, such as clearly seen in Fig. 3. Ratios of titanium to (C + N) of 10 or more are generally regarded as adequate to tie up the vast majority of the carbon and nitrogen. Even so, some (C + N) remains in solution and lower-temperature precipitation does occur in titanium-stabilized steels. There is no evidence that titanium is involved in such precipitation. Pollard observed *chromium* carbide precipitation on previously formed TiN [10]. In the present study, energy-dispersive X-ray analysis was performed on low-temperature precipitates. Generally the chromium content registered as roughly comparable to the iron content with the titanium level being at least an order of magnitude lower. By contrast, no chromium was detectable within blocky Ti(C,N) particles. Thus it seems that the lower-temperature precipitation is substantially that of *chromium* carbide and nitride. More-

over, it will be assumed that the observed lower-temperature precipitates are of approximately the same composition as those documented for unstabilized alloys.

None of the heat treatments used for Heats 1 and 2 are sufficient to produce α', σ, or χ-phase precipitation.

The microstructure of the Heat 3 material, annealed at 860°C, was, of course, quite different from those of Heats 1 and 2. The material had a fine, uniform, equiaxed grain size of 25 to 30 μm and contained intragranular precipitates which were presumably $Cr_2(C,N)$, Cr_2N, and $Cr_{23}N_6$ as discussed in the preceding. TEM observation revealed α'-precipitation in the material aged for 6000 min.

Mechanical Characterization

The results of room-temperature tension tests and Charpy V-notch impact tests for material from Heats 1, 2, and 3 are presented in Tables 4, 5, and 6, respectively.

The tensile strength variation in the Heat 1 material is minor. The ductilities are somewhat erratic. One of the two specimens for Condition B and both the Condition H specimens fractured in a brittle fashion after 8 to 12 percent strain. The fracture surfaces for Condition B displayed an area which appeared to be intergranular fracture while both Condition H specimens displayed classic transgranular cleavage fractures mixed with ductile tearing. The Charpy V-notch DBTT's ranged from -90 to $+70°C$ and indicate an increase in DBTT with extended lower-temperature exposure, either by furnace cooling (Condition B) or by isothermal annealing (Conditions G and H).

For Heat 2, there is a greater variation in strength levels; the highest strength is associated with spray quenching, furnace cooling, and low-temperature precipitation annealing. The low-temperature precipitation anneal is also associated with reduced ductility. Again, the highest DBTT

TABLE 4—*Results of mechanical characterization, Heat 1.*

Procedure	0.2% Offset Yield Strength, MPa	Ultimate Tensile Strength, MPa	Elongation in 1.9 cm, %	Charpy V-Notch DBTT, °C
A	300	410	41	-60
B	300	400	15	-90
C	270	370	40	-75
D	330	460	31	70
E	280	370	33	-60
F	290	380	29	-60
G	300	380	29	-45
H	300	340	10	-30

TABLE 5—*Results of mechanical characterization, Heat 2.*

Procedure	0.2% Offset Yield Strength, MPa	Ultimate Tensile Strength, MPa	Elongation in 1.9 cm, %	Charpy V-Notch DBTT, °C
A	390	510	27	10
B	280	460	37	0
C	340	460	35	40
D	330	480	37	100
E	280	430	38	0
F	300	440	38	5
G	380	510	20	75
H	360	430	16	45

TABLE 6—*Results of mechanical characterization, Heat 3.*

Procedure	0.2% Offset Yield Strength, MPa	Ultimate Tensile Strength, MPa	Elongation in 1.9 cm, %	Charpy V-Notch DBTT, °C
Annealed @ 860°C	260	390	41	−140
Aged 6 min @ 475°C	290	410	43	−135
Aged 60 min @ 475°C	280	420	38	−130
Aged 600 min @ 475°C	380	470	33	−45
Aged 6000 min @ 475°C	600	660	17	+80

values are associable with extended lower-temperature exposure. However, even the toughest conditions of this heat have higher DBTT's than all but the most severely embrittled of the Heat 1 materials.

For the Heat 3 material, there is a relatively uniform trend toward higher strength, lower ductility, and higher DBTT as the α'-precipitation period is increased.

Fracture Initiation Studies

The microstructural information and mechanical test results set forth in the foregoing, in conjunction with similar data obtained by the authors on unstabilized Fe-26Cr alloys [4], motivated studies of fracture initiation in specimens produced by iced-brine quenching 1290°C solution-annealed material from Heats 1 and 2, and in unaged and aged specimens from Heat 3. General observations follow.

For Heats 1 and 2 (Procedure B, iced-brine quenching) the as-electro-

polished surface revealed faint acicular surface features arranged in Widmanstatten pattern. This feature of the microstructure had not been brought out by the "mixed-acids" etch and is not to be compared with the needle-like nitride formations that emerge upon low-temperature exposure. The tension test DBTT range was −75°C, comparable to the Charpy test DBTT range for Heat 1 and some 75°C below that of Heat 2. When tested at the DBTT of ~ −75°C, these specimens deformed primarily by slip with no twinning observed. The faint Widmanstatten precipitates did not lie on the normal slip planes and did not seem to interfere with slip; neither did they appear to act as crack initiation points. Essentially all subcritical microcracks observed were of the intergranular type, as shown in Figs. 4 and 5. It can be seen in Fig. 5 that the grain boundary microcrack appears to originate at a nearby titanium carbonitride particle. Very few of the grain boundary microcracks, however, were associated with visible titanium carbonitride particles. These microcracks could, of course, be associated with subsurface titanium carbonitride particles. In any case the grain boundaries in these alloys appear to be susceptible to brittle fracture; this is very different from the behavior of unstabilized alloys where grain boundaries more typically serve as crack arrestors.

FIG. 4—*Optical micrograph of grain boundary fracture on the electropolished surface of a Heat 1 Condition B specimen tension tested at* −75°C (×500).
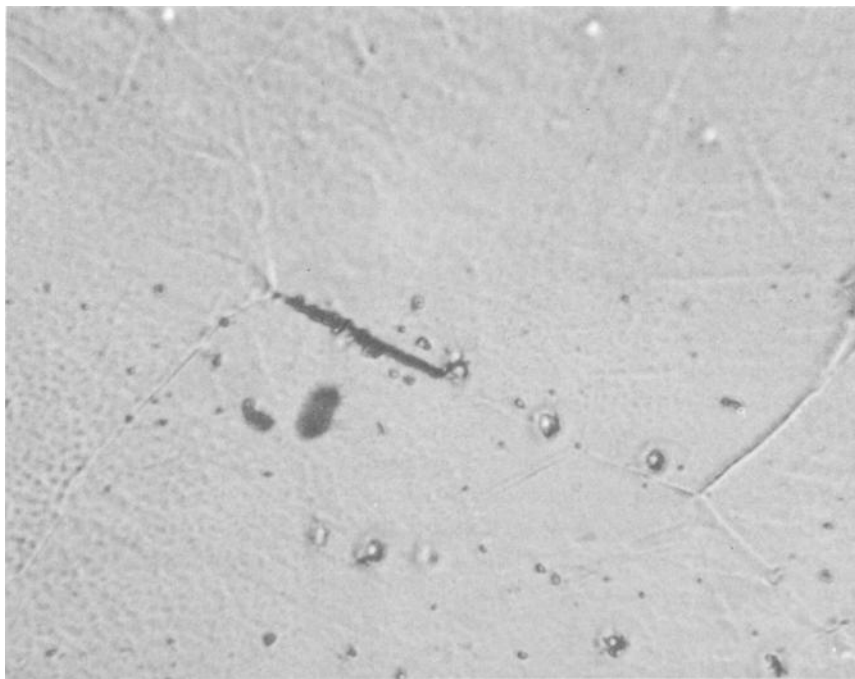
FIG. 5—*Optical micrograph of grain boundary fracture on the electropolished surface of a Heat 2 Condition B specimen tension tested at −80°C; note fractured titanium carbonitride at right end of microcrack (×1000).*

After preliminary testing to establish the approximate tension test DBTT range, electropolished specimens of Heat 3 material were tension tested at temperatures which resulted in cleavage fracture after strains of 0.12 to 0.21. These tension DBTT's ranged from −195 to −100°C, or 55 to 180 deg C below the Charpy V-notch DBTT's. The α′-embrittled specimens displayed the greatest sensitivity to the high strain rates and notch constraint of the Charpy impact test. Observations from the electropolished surfaces can be summarized as follows.

The 860°C annealed specimen tested at −195°C revealed transgranular microcracks which were often associated with carbide or nitride particles. These cracks were usually restricted to a single grain and appear to be simple cleavage cracks. An example of one such microcrack is shown in Fig. 6. When the test temperature was raised to −100°C, this material displayed numerous well-developed slipbands and cross slip, as shown in Fig. 7.

The specimens heat treated at 475°C for 6 and 60 min also displayed cleavage microcracks. As shown in Fig. 8, these were essentially undistin-
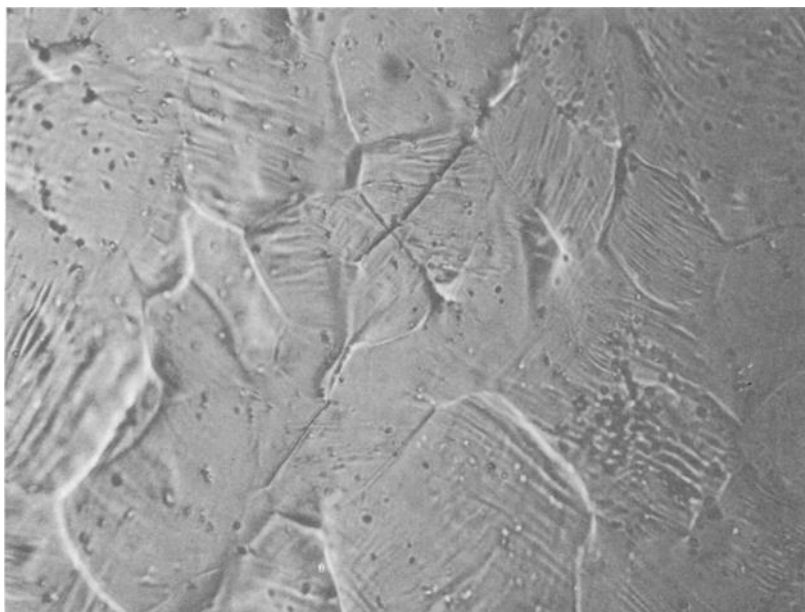
FIG. 6—*Light micrograph of a cleavage-type microcrack on the electropolished surface of an 860°C annealed specimen pulled at −195°C (×750).*
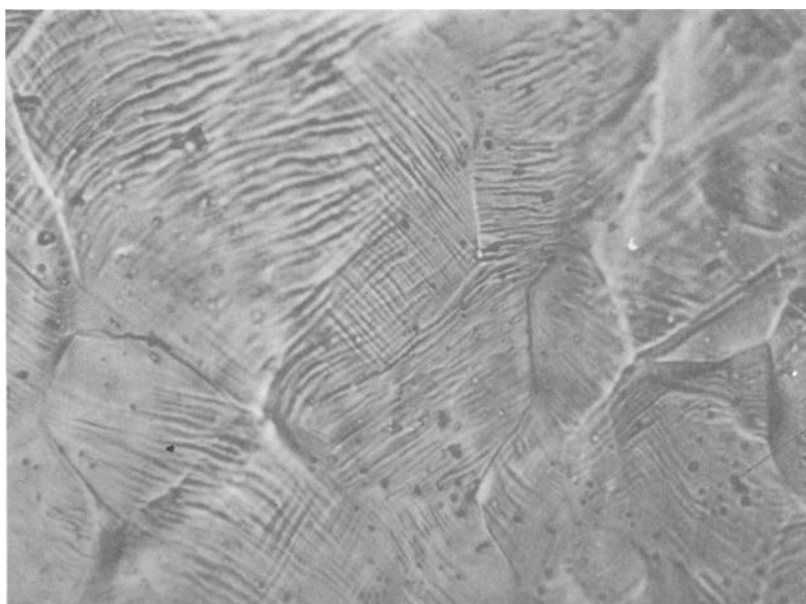

FIG. 7—*Light micrograph of slipbands on the electropolished surface of a specimen annealed at 860°C and pulled at −100°C to a strain of 0.23 (×750).*
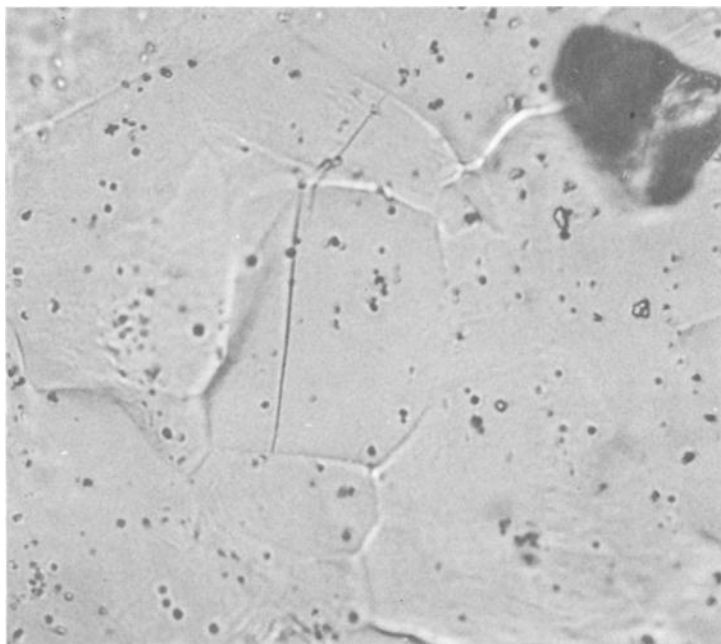
FIG. 8—*Light micrograph of cleavage-type microcracks on the electropolished surface of a specimen heat treated for 60 min at 475°C and pulled at −100°C (×1000).*

guishable in appearance from the microcracks in the unaged specimens. The slip character of the 6 and 60 min aged specimens was also very similar to that observed in the unaged material.

Subcritical microcracks were quite rare in the 600 and 6000 min aged specimens tested in the tension test DBTT range, in spite of extensive plastic deformation prior to cleavage. Evidence suggestive of cleavage or grain boundary microcracking was occasionally observed, but little role of the microstructure in crack initiation could be directly inferred. Rather it seems that the flow stress elevation of the α'-precipitation has led to fracture criterion satisfaction without the necessity of local stress-raising or strain-raising effects of, for example, carbides or nitrides.

The electropolished tension specimens from the 600 and 6000 min aged condition displayed a gross change in slip character, however. At the same −100°C test temperature as used for the unaged material shown in Fig. 7, the 6000 min aged material displayed relatively few, but quite intense slipbands as shown in Figs. 9 and 10. Despite the crack-like appearance of some of the intense slipbands, SEM observations have failed to reveal any cases of unambiguous slipband cracking.
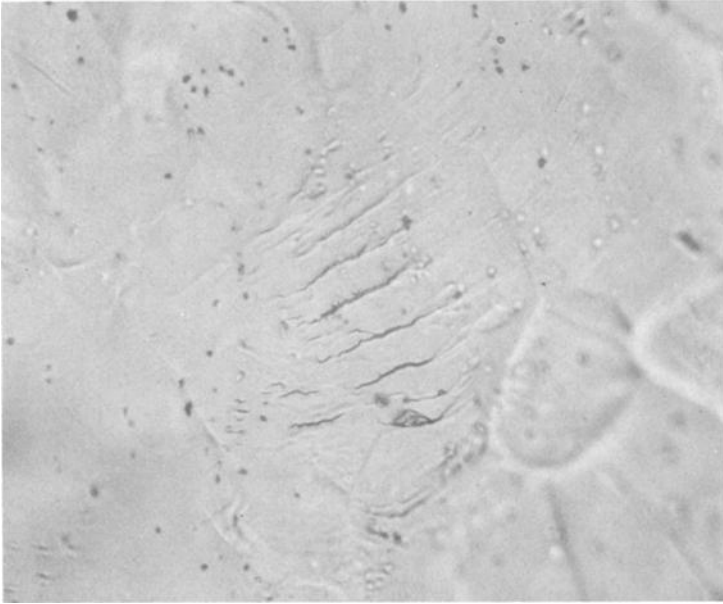
FIG. 9—*Light micrograph of slipbands on the electropolished surface of a specimen heat treated at 475°C for 6000 min and pulled at −100°C to a strain of 0.21 (×750).*

Discussion

The mechanical characterization makes the overall effects of titanium stabilization and α'-precipitation on the fracture transition quite clear. In Table 7, a comparison is made between DBTT data from the several heat treatments of Heats 1 and 2 and DBTT data from identical heat treatments on comparable heats which were not stabilized with titanium [4].

At the higher (C + N) level (Heats 2 and II), the effect of titanium is invariably to lower the DBTT (40 to 115 deg C), presumably by eliminating chromium carbide and nitride-related fracture initiation and greatly reducing the level of (C + N) in solution after rapid quenching. In conjunction, the strength elevation associated with rapid quenching and extended low-temperature exposure is greatly moderated by the titanium stabilization of the ≈550-ppm (C + N) level heats. Even so, the highest DBTT values are associated with extended low-temperature exposure, presumably reflecting the role of the needle-like precipitates in crack initiation [4].

In the case of the low (C + N) level (Heats 1 and I), the effect of titanium is quite different. For extended low-temperature exposure (Procedures D and H), the effect of titanium is beneficial and the DBTT is 20 to 30 deg C lower for the titanium-stabilized material. The crack initiation role of the
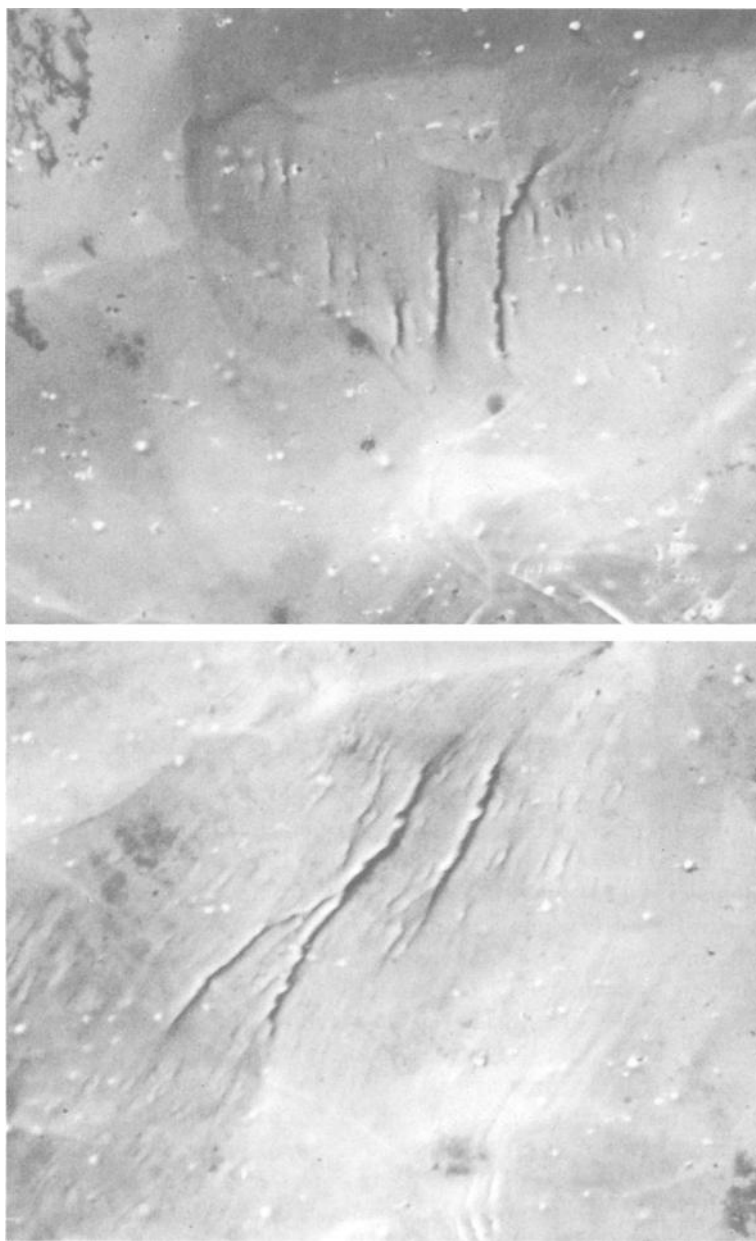
FIG. 10—*SEM micrographs of intense slipbands on the electropolished surface of a specimen heat treated for 6000 min at 475°C and pulled at −100°C (×2000).*

TABLE 7—*Comparison of subsize Charpy DBTT values for titanium-stabilized alloys of this study and comparable unstabilized alloys reported previously [4].*

Heat Treatment	Subsize Charpy DBTT Ranges, °C			
	Heat 1	Heat 2	Heat I[a]	Heat II[b]
A	−60	+10	−130	+75
B	−90	0	−130	+100
C	−75	+40	−100	+80
D	+70	+100	+90	+205
E	−60	0	−135	+115
F	−60	+5	−85	+50
G	−45	+75	−115	+115
H	−30	+45	0	+100

[a] Comparable to Heat 1, but without titanium [4].
[b] Comparable to Heat 2, but without titanium [4].

needle-like precipitates [4] is presumably mitigated, as in the high (C + N) case. In all other cases, however, the titanium-stabilized material has a decidedly higher DBTT (25 to 75 deg C) consistent with earlier work of one of the authors [9]. The beneficial role of titanium in preempting crack initiation from grain boundary chromium carbide and nitride precipitation [4] is somehow negated. In fact, for quenched conditions, where no carbide and nitride precipitation occurs anyway, the more purely negative effect of titanium is seen to raise the DBTT as much as 75 deg C.

The fracture initiation studies on iced-brine-quenched material provide some insight into the negative effect of titanium stabilization on DBTT. Work by Pollard has revealed microcrack initiation around Ti(C,N) particles during quenching [10]. Figure 5 suggests a role of Ti(C,N) particles as well. The striking feature of the subcritical flaws noted in the present work is, however, their *intergranular* nature.

Some intergranular microcrack formation has been noted in unstabilized alloys as well [4]. However, it is generally associated with fracturing of semi-continuous grain boundary carbides or with twin-grain boundary impingement. No grain boundary precipitates exist in this instance and twinning was not observed in these titanium-stabilized alloys. (It should be noted that Leslie and Sober observed that the addition of titanium had the effect of inhibiting twinning in low-carbon ferrite [29].

Intergranular embrittlement is often associated with the segregation of an impurity element to the grain boundary and it is conceivable that the embrittling effect of titanium is related to titanium segregation to the ferrite grain boundaries. Another possible explanation involves the interaction between titanium, carbon, and oxygen. It is well established that oxygen lowers the surface energy of iron [30] and that oxygen can produce inter-

granular embrittlement in iron [31,32]. Moreover, the intergranular embrittling effect of oxygen in iron can be mitigated by carbon [33,34]. This phenomenology has been discussed in some detail by Low [34]. If this behavior is relevant to iron-chromium alloys, it is quite possible that the high ratio of titanium to carbon and nitrogen in Heat 1 ($\approx$24 to 1) has so thoroughly gettered carbon that oxygen intergranular embrittlement is no longer suppressed. For iron, oxygen contents in the 20- to 160-ppm range will produce intergranular embrittlement if the available carbon is below 20 to 30 ppm. The carbon level in Heat 1 is only 30 ppm to start with. Of course, titanium and chromium are very active oxide formers and would tend to getter oxygen, and presumably would reduce oxygen in solution to very low levels. This gettering could inhibit the oxygen embrittlement just cited. Thermodynamic or analytic data needed to resolve this issue are, however, unavailable.

The relationships between tension test DBTT values and Charpy test DBTT values in this study are consistent with the previous observation that conditions with high transition temperatures display a greater sensitivity to test strain rate [4].

The embrittling effect of the flow stress increase associated with α'-precipitation can be readily understood using the approach of Cottrell [35], and extensive use of this model has been made in considering ferritic stainless steel fracture [4,24,36].

The change in slip character with α'-precipitation deserves careful consideration as a basis for considering alloying or process modifications or both which might reduce 475°C embrittlement. First of all, despite the accumulation of much plastic strain, well-defined slipbands are rare in Figs. 9 and 10 (as compared with the appearance of Fig. 7). This may simply result from the α'-precipitation generally being too finely dispersed to allow the repetitive, clustered slip necessary for band formation. On the other hand, the factors which inhibit band formation clearly break down in the regions of the intense bands. The concentrated slip of these regions reflects some form of microinstability. Perhaps the α' redissolves in the regions of the bands.

In any case, the development of slip in the α'-precipitated matrix surely controls the flow stress, and perhaps earlier development of the slipband microinstabilities would reduce embrittlement. Careful TEM evaluation will be necessary to achieve an understanding of any dislocation-precipitate structure interactions which lead to microinstability. Moreover, in studying this behavior in depth, the case of α'-precipitation through nucleation and growth should be evaluated separately from α'-precipitation through spinodal decomposition. The present subject alloy is, at 26 weight percent, midway between the clearly confirmed regions of nucleation-and-growth and spinodal decomposition. It was chosen in view of the commercial interest in 26Cr alloys and in view of the considerable literature extant on Fe-26Cr.

Summary

Microscopic observations of electropolished strips pulled in tension in the DBTT range have been made in an effort to clarify the micromechanisms of brittle fracture in titanium-stabilized and α'-embrittled Fe-26Cr alloys. Mechanical characterization makes it clear that at total (C + N) levels in the 550-ppm range the effect of titanium is to lower the DBTT through removal of (C + N). At total (C + N) levels of about 75 ppm, however, titanium lowers the DBTT for material which has undergone lengthy low-temperature heat treatment, but raises the DBTT in all other cases. This embrittling effect of titanium is associated with intergranular microcrack formation and may reflect embrittling titanium segregation to the grain boundary or oxygen intergranular embrittlement due to extensive carbon gettering. Microcrack development is rare in α'-embrittled material. It is likely that 475°C embrittlement is a result of the increased flow stress associated with the α'-precipitation. The α'-precipitation grossly alters slip character. The profuse, multiple slip normally observed is replaced by a relatively few, extremely intense slipbands, perhaps reflecting the development of microinstability in the α'-precipitated matrix.

Acknowledgment

References

[1] Hochman, J., *Comptes Rendus Hebdomodaires des Seances de l'Academie des Sciences,* Vol. 226, 1948, p. 2150.

[2] Binder, W. O. and Spendelow, H. R., Jr., *Transactions,* American Society for Metals, Vol. 43, 1951, p. 759.

[3] Demo, J. J., *Metallurgical Transactions,* Vol. 5, 1974, p. 2253.

[4] Grubb, J. F. and Wright, R. N., *Metallurgical Transactions,* Vol. 10A, 1979, p. 1247.

[5] Beckett, F. M. and Franks, R., *Transactions,* American Institute of Mining, Metallurgical, and Petroleum Engineers, Vol. 113, 1934, p. 126.

[6] Demo, J. J., "Ferritic Iron-Chromium Alloys," Canadian Patent No. 939,936, 15 Jan. 1974.

[7] Demo, J. J., "Ductile Chromium Containing Ferritic Alloy," Canadian Patent No. 952,741, 13 Aug. 1974.

[8] Semchyshen, M., Bond, A. P., and Dundas, H. J., *Proceedings,* Symposium Toward Improved Ductility and Toughness," Kyoto, Japan, 1971, p. 239.

[9] Wright, R. N., *Welding Journal Research Supplement,* Vol. 50, Oct. 1971, p. 434.

[10] Pollard, B., *Metals Technology,* Vol. 1, 1974, p. 31.

[11] McMahon, C. J., Jr. and Cohen, M., *Acta Metallurgica,* Vol. 13, 1965, p. 591.

[12] Heger, J. J., *Metal Progress,* Vol. 60, Aug. 1951, p. 55.

[13] Fisher, R. M., Dulis, E. J., and Carroll, K. G., *Journal of Metals, Transactions,* American Institute of Mining, Metallurgical, and Petroleum Engineers, Vol. 197, 1953, p. 690.

[14] Marcinkowski, M. J., Fisher, R. M., and Szirmae, A., *Transactions of the Metallurgical*

Society, American Institute of Mining, Metallurgical, and Petroleum Engineers, Vol. 230, 1964, p. 676.

[*15*] Blackburn, M. J. and Nutting, J., *Journal of the Iron and Steel Institute,* Vol. 202, 1964, p. 610.

[*16*] Lagneborg, R., *Transactions,* American Society for Metals, Vol. 60, 1967, p. 67.

[*17*] Williams, R. O., *Transactions of the Metallurgical Society,* American Institute of Mining, Metallurgical, and Petroleum Engineers, Vol. 212, 1958, p. 497.

[*18*] Chandra, D. and Schwartz, L. H., *Metallurgical Transactions,* Vol. 2, 1971, p. 511.

[*19*] Cahn, J. W., *Transactions of the Metallurgical Society,* American Institute of Mining, Metallurgical, and Petroleum Engineers, Vol. 242, 1968, p. 166.

[*20*] Vintoykin, Ye. Z., Dmitriejev, V. N., and Kolontson, V. Yu., *Fizika Metallov I Metallovedenie,* Vol. 29, 1970, p. 1257.

[*21*] DeNys, T. and Gielen, P. M., *Metallurgical Transactions,* Vol. 2, 1971, p. 1423.

[*22*] Grobner, P. J., *Metallurgical Transactions,* Vol. 4, 1973, p. 251.

[*23*] Nichol, T. J., *Metallurgical Transactions,* Vol. 8A, 1977, p. 229.

[*24*] Plumtree, A. and Gullberg, R., *Metallurgical Transactions,* Vol. 7A, 1976, p. 1451.

[*25*] Reidrich, G. and Loib, E., *Archiv feur das Eisenhuettenwesen,* Vol. 15, 1941–42, p. 175 (Brutcher Translation No. 1249).

[*26*] Courtnall, M. and Pickering, F. B., *Metal Science,* 1976, p. 273.

[*27*] Savage, W. F., *High Speed Testing,* Vol. III, Interscience Publishers, New York, 1962, p. 55.

[*28*] Lena, A. J. and Hawkes, M. F., *Journal of Metals, Transactions,* American Institute of Mining, Metallurgical, and Petroleum Engineers, Vol. 200, 1954, p. 607.

[*29*] Leslie, W. C. and Sober, R. J., *Transactions,* American Society for Metals, Vol. 60, 1967, p. 99.

[*30*] Hondros, E. D., *Acta Metallurgica,* Vol. 16, 1968, p. 1377.

[*31*] Rees, W. P. and Hopkins, B. E., *Journal of the Iron and Steel Institute,* Vol. 172, 1952, p. 403.

[*32*] Low, J. R. and Feustal, R. G., *Acta Metallurgica,* Vol. 1, 1953, p. 185.

[*33*] Honda, R. and Taga, H., *Metal Science Journal,* Vol. 2, 1968, p. 172.

[*34*] Low, J. R., Jr., *Transactions of the Metallurgical Society,* American Institute of Mining, Metallurgical, and Petroleum Engineers, Vol. 245, 1969, p. 2481.

[*35*] Cottrell, A. H., *Transactions of the Metallurgical Society,* American Institute of Mining, Metallurgical, and Petroleum Engineers, Vol. 212, 1958, p. 192.

[*36*] Plumtree, A. and Gullberg, R., *Journal of Testing and Evaluation,* Vol. 2, No. 5, 1974, p. 331.

S. Saito,[1] *H. Tokuno,*[1] *M. Shimura,*[1] *E. Tanaka,*[1] *Y. Kataura,*[1]
and T. Ototani[2]

On the Embrittlement and Toughness of High-Purity Fe-30Cr-2Mo Alloy

ABSTRACT: Experiments were conducted to explain unexpected embrittlement phenomena encountered in fabricating a high-purity Fe-30Cr-2Mo alloy. By means of a hydrostatic tension test with a Bridgman-type specimen it was found that the fracture behavior of the alloy is highly dependent on stress state. Under conditions of low triaxial stress, the alloy displays excellent ductility. Under conditions of high triaxial stress, however, it shows less strain to fracture and a transition from ductile to cleavage fracture. The toughness of the Fe-30Cr-2Mo alloy can be significantly improved by thermo-mechanical processing.

KEY WORDS: ferritic stainless steels, workability, hydrostatic tension tests, ductile-brittle transition, thermomechanical processing, fracture toughness

The Fe-30Cr-2Mo alloy is a high-purity stainless steel produced by vacuum induction melting with relatively pure raw materials. Deoxidation using both aluminum and calcium is required in the melting to get low oxygen content and to decrease the interstitial elements, carbon plus nitrogen, to below 120 ppm. A duplex process combining an electric furnace melting with vacuum oxygen decarburization (VOD) practice, that is, the so-called "Strong Stirring VOD" process [1],[3] has been established commercially to produce the high-purity Fe-26Cr-1Mo and Fe-30Cr-2Mo alloys. The Fe-30Cr-2Mo alloy has superior resistance to stress corrosion cracking and to pitting and crevice corrosion in chloride-containing environments [2,3]. The alloy is becoming

[1]Graduate student, research engineer, associate professor, professor, and assistant professor, respectively, The Research Institute for Iron, Steel and Other Metals, Tohoku University, Katahira 2-1-1, 980 Sendai, Japan.
[2]President, Metal Research Corp., Kawai Bld., Nihonbashi honmachi 4-1-5, Chyuo-ku, 103 Tokyo, Japan.
[3]The italic numbers in brackets refer to the list of references appended to this paper.

77

more and more acceptable as a new material for the chemical process industry. One for example, in an acetic acid plant, is a rectifying tower made of 6-mm-thick plate of the Fe-30Cr-2Mo alloy which is giving satisfactory service. Important problems still to be solved are the toughness and the as-welded ductility and formability of thicker sheet. The object of the present work is to study the embrittlement phenomena in deformation processing, the effect of thermomechancial treatment on toughness, and the fracture behavior in the multiaxial state of stress.

Unexpected Embrittlement Phenomena Encountered During Deformation Processing

The ductility of the alloy is very high in unidirectional mechanical testing [4]. It is also readily fabricated and easily cold-formed into shapes. For example, the hot-rolled plate 6 mm thick can be rolled at room temperature to foil of 0.006 mm thickness without intermediate annealing. At the beginning, however, unexpected embrittlement was encountered in mill processing. Some examples follow.

Example 1: Hair Cracks in Forged Billet

A 500-kg ingot (260 mm diameter, 600 mm height) was forged to a billet 35 mm thick in the temperature range 750 to 1000°C and cooled in air. Hair cracks were found in the cross section of the billet by dye check. The micromechanism of the hair crack formation was cleavage fracture. The cause seemed to be interaction between residual stress in the billet and 475°C embrittlement induced during the cooling process.

Example 2: Ring-Shaped Failure During Pipe Drawing

A pipe, extruded at 1000°C with glass lubricant and water quenched, was drawn at room temperature without a plug from a 43-mm outer diameter to 40 mm diameter. Ring-shaped circumferential cracks were found on the surface of the pipe. The micromechanism of failure in this case also was cleavage fracture.

Example 3: Penny-Shaped Central Bursting During Rod Drawing [5]

A rod was annealed at 1000°C, water quenched, and then drawn from 26.5 to 23.0 mm diameter at room temperature. Scattered internal cracks were detected by gamma-ray inspection. The cracks, however, were different in shape and fracture mechanism from the usual type of central bursting that occurs during conventional rod drawing. The cracks were not chevron-shaped but penny-shaped and also the micromechanism was not ductile (or

dimple) fracture but cleavage fracture. Moreover, a number of deformation twins were observed in the vicinity of the cracks. The conclusions based on analysis [5] are as follows: (1) The cracks are formed by cleavage fracture at the centerline of the billet, caused by the stresses operating during drawing; (2) in a drawing operation the hydrostatic stress components are primarily tensile stresses, according to slipline field analysis, and damage by a critical tensile stress is most severe along the centerline despite the small amount of deformation and strain-hardening involved in the drawing; and (3) the crack grows in a direction perpendicular to the highest tensile stress in a discontinuous cleavage manner to form the penny shape.

Example 4: Internal Cracking During Rolling of Thick Plate

When a thick plate (thickness 32 mm) annealed at 1000°C and water quenched was rolled at room temperature to a thickness of 26 mm in three passes, cavity-like flaws were found in the central part of the plate. They were oriented in the direction of rolling and connected partially to each other to form so-called "crocodile-like" cracking. In this case, the fracture mechanism of cracking was mainly cleavage in the direction perpendicular to the plate surface. Numerous deformation twins were observed in the vicinity of the cracks. In this specific case cracking occurred during rolling. There was, however, another instance in which no cracking occurred in rolling but where evidence of cracking was found later on the fracture surface of a Charpy impact specimen taken from the plate.

These processing difficulties were overcome by improvements in cooling rate, composition, distribution of carbides, heat treatment, deformation schedule, etc. The common features of cracking in the aforementioned cases were as follows:

1. Fracture occurred under the complex state of stress.
2. Micromechanism of fracture was cleavage.
3. Numerous deformation twins were observed in the vicinity of the cracks.
4. Fracture occurred at relatively small amount of deformation.
5. Fracture occurred in a coarse-grained structure.

It is suggested that the five features seem to be closely connected with the workability of the alloy in the bulk deformation process and with ductile-brittle transition phenomena in the alloy.

Fracture Behavior Under Hydrostatic Tensile Stress and Its Value as a Measure of Workability and Toughness

In describing the mechanism of failure of metals in forming operations, it is necessary to consider both the stress state and the mechanism of failure in relation to the microstructure. Several criteria of internal fracture are based

on the effect of hydrostatic pressure in suppressing ductile fracture and of tensile stresses in promoting fracture [6]. To date, however, little data are available on this aspect, although some valuable progress has been made in the discussion of the influence of hydrostatic pressure on the strain to failure resulting from void nucleation and growth [7,8]. It is also reported that cleavage fracture is influenced by pressure at the location of grain boundary crossing [9]. Therefore, experimental studies of the influence of negative pressure (hydrostatic tension) on microscopic processes of fracture were carried out with Fe-30Cr-2Mo alloy.

Experimental Procedure

A 1000-kg (1 ton) heat was produced by vacuum induction melting using high-purity charge materials. The ingot was forged to slabs 35 mm thick and 110 mm wide. The chemical composition is given in Table 1. Bridgman-type specimens machined from the slabs were used in order to investigate the effect of hydrostatic tension on fracture behavior of the alloy. In his pioneering study [10] on the effect of pressure on fracture, Bridgman obtained, for a given longitudinal profile radius of curvature on the neck of a round bar, an approximate solution for the distribution of stresses and plastic strain across the plane of the neck at the smallest cross section. The stress distribution is shown in Fig. 1. Direct comparison of the extension of the Bridgman analysis for the distribution of negative pressure with the results of recent numerical computations [11] demonstrate that this solution is rather good near the neck. Therefore, the necked region of a bar with its distribution of plastic strains and negative pressure along the axis is a convenient plastic flow field for experimental studies of fracture behavior of the alloy. In round bar with initially machined grooves, however, the axial plastic strain increments may no longer be uniform along the plane of the neck, as is predicated by the Bridgman solution, making that solution no longer valid [12]. The departure from a condition of uniaxial strain in bars with initially machined longitudinal profile is a result of a departure of the machined profile from the natural neck geometry.

So, in the first stage of the experiment, a number of natural profiles of necks were carefully measured on a steel bar. From such measurements it was determined that the natural neck profile can be described with a high degree of accuracy by the empirical equation developed by Dondik [13]. Bridgman-type specimens with a natural necking profile after the Dondik

TABLE 1—*Chemical composition of test material.*

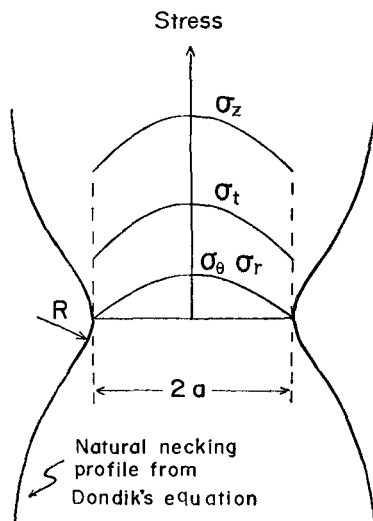| C	Si	Mn	P	S	Ni	Cr	Mo	Al	O	N	Nb
0.002	0.14	0.05	0.02	0.01	0.17	30.3	1.9	0.11	0.002	0.006	0.10

Stress

FIG. 1—*Illustration of the Bridgman-type specimen with natural necking profile and distribution of longitudinal stress component, σ_z, hydrostatic tensile stress (negative pressure) component, σ_t, radial stress component, σ_r, and circumferential stress component, σ_θ, at the narrowest cross section. R is the minimum longitudinal (profile) radius of curvature at the neck, and a is the radius of the narrowest portion of the neck.*

equation were machined using a numerically controlled lathe, as shown in Fig. 2.

The diameter of the narrowest portion of the neck of the specimen was 16 mm, and the minimum longitudinal radius of curvature at the neck was 3 ~ 45 mm. The grain size of this material after annealing at 1000°C was ~ 500 μm. Tension tests were carried out at room temperature.

Tension Test Results

Figure 3 shows the results of the tension tests. The ordinate represents reduction of area, and the abscissa represents the mean value of maximum hydrostatic tensile component in the deformation process. The subscale refers to maximum tensile stress. As seen in this figure, the higher the hydrostatic tensile stress, the lower the fracture strain. The results of the same experiments with 0.45 and 0.25 percent carbon steel are also shown for comparison. The influence of the hydrostatic tension on the fracture behavior of the alloy is higher than that of carbon steels. While the fracture strain is very large in low triaxiality, it decreases abruptly as the value of hydrostatic tensile component increases. Also shown in the figure for comparison are test results of a specimen aged for 1 h at 475°C and of a prestrained specimen.
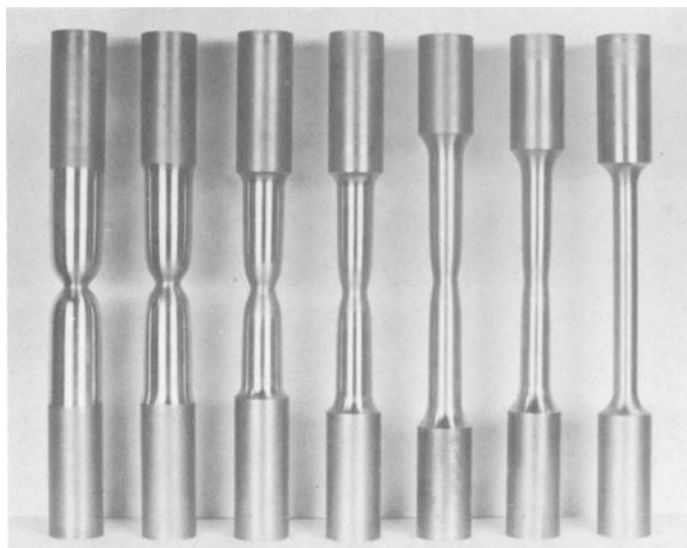
FIG. 2—*Bridgman-type specimens with the natural necking profile machined with numerically controlled lathe.*

Figure 3 also depicts the fracture modes. The open circle points denote overall fibrous fracture; the double circle points denote bimodal fracture, containing a fibrous region in the middle of the fracture surface surrounded by cleavage fracture. The crossed circles denote overall cleavage fracture.

It is noticeable that two types of transition from ductile to cleavage are involved in the process of fracture. The one is cleavage fracture as a function of negative pressure and the other is fibrous-cleavage transition in the growth of the crack. The fracture surface in the high hydrostatic tensile condition consists mostly of cleavage surface, while in the condition of low triaxiality it is fibrous. It is suggested that a ductile-to-brittle transition pressure (DBTP) (negative) may exist analogous to the ductile-to-brittle transition temperature (DBTT). The fracture surface shows bimodal fracture in the range of transition pressure. In this range, fibrous fracture initiates in the central part of the neck and propagates radially, as shown in Fig. 4. Figure 5 shows the transition phenomena from fibrous to cleavage failure as the crack grows.

Thermomechanical Processing for Improved Toughness

Several factors control the impact property of ferritic structural steels. The most important among these is grain size, since the decrease in grain size can raise both yield stress and notch ductility. It has been pointed out that
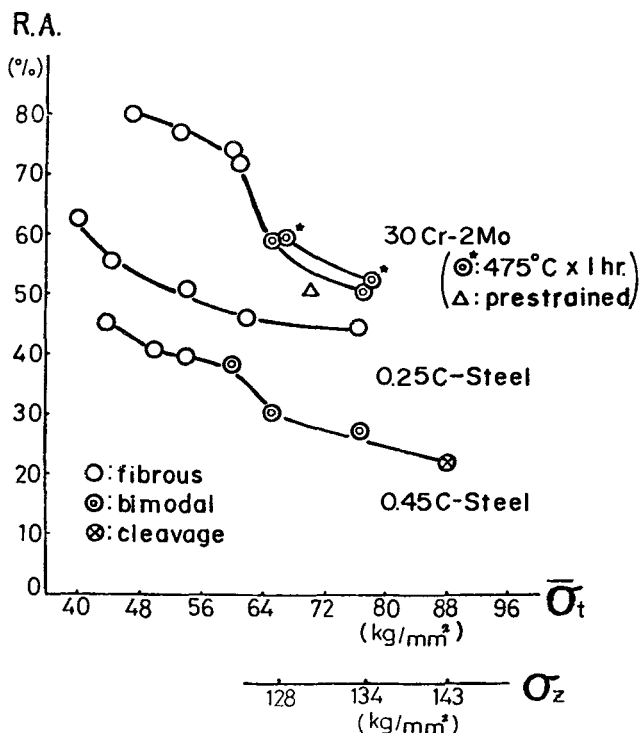
FIG. 3—*Influence of hydrostatic tensile stress on the fracture behavior of Fe-30Cr-2Mo alloy. The ordinate denotes reduction of area (or strain to fracture) and the abscissa denotes the mean value of maximum hydrostatic tensile component, $\bar{\sigma}_t$. The subscale denotes the value of maximum tensile stress component, σ_z.*

uniform recrystallization is a prerequisite for stable isotropic impact property of steel products—the finer the grain size, the higher the energy absorbed [14]. According to the data presented by Franson [15], however, hot-worked structure in high-purity Fe-26Cr-1Mo alloy is more resistant to recrystallization than cold-worked structure, so that annealing temperatures of 1600°F or higher are required to get full recrystallization of the hot-worked structure. The resultant grain size is therefore quite large. The Fe-30Cr-2Mo alloy also needs a high annealing temperature with an attendant coarse-grained structure and hence low impact properties. The DBTT of thick plates is easily affected by high-temperature annealing coupled with a slow cooling rate after hot-working. Currently, two methods are applied for grain refining: controlled rolling and heat treatment. Controlled rolling is the best option for grain refining. Rolling schedules can be established to produce varying degrees of grain refinement. This method is applicable to virtually all alloy combinations [16]. In general, the process for low-alloy carbon steels involves
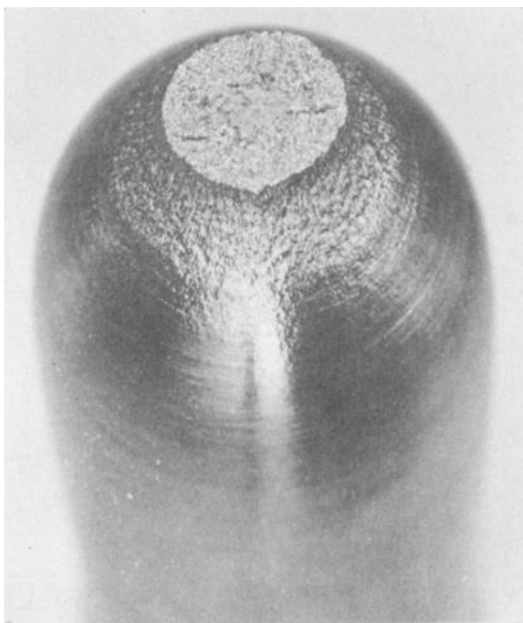
FIG. 4—*Light fractograph of Fe-30Cr-2Mo alloy: fracture surface of Bridgman-type specimen (radius at neck is 8 mm and minimum longitudinal radius of curvature at neck is 4.5 mm). It shows typical bimodal fracture.*

good control of the deformation schedule and temperature, especially during the final stage of rolling. And, the greater the reduction and the lower the temperature in the last pass, and the shorter the time taken for complete recrystallization, the finer the grain size. Post-rolling normalizing treatments are frequently given in order to improve the properties of rolled plate. The principles of recrystallization and inhibition of grain growth may be used in both the ferritic and austenitic conditions.

Experimental Procedure

Several labratory rolling experiments were conducted to examine the effect of different types of reduction schedule and of post-rolling heat treatments on ferrite grain size and on impact properties in the Fe-30Cr-2Mo alloy. Figure 6 shows the processes schematically. The initial flat thickness was 35 mm and the final thickness 7 mm. Individual processing steps were as follows:

1. One heat, one pass at 1000°C. Constant 5-mm-thickness draft per pass. Annealing at 1000°C for 5 min and water quenching.

2. Conventional continuous rolling. Constant 5-mm-thickness draft per pass. The finishing temperature was about 700°C.

    2a Annealing at 1000°C for 5 min and water quenching.

    2b Annealing at 850°C for 10 min, water quenching, subsequent annealing at 1000°C for 5 min, and water quenching.

3. Thermomechanical processing (TMP). Constant 5-mm-thickness draft per pass up to 12 mm thick, and then 5-mm-thickness draft in the last pass. The finishing temperature was approximately 600°C.

    3a Annealing at 850°C for 20 min and water quenching.

    3b Annealing at 850°C for 20 min, water quenching, subsequent annealing at 1000°C for 5 min, and water quenching.

A second set of experiments was conducted to examine the effect of the combination of warm rolling or cold rolling and the post-rolling heat treatment:

1. Constant 5-mm-thickness draft per pass to 16 mm thick. The finishing temperature was approximately 800°C. Subsequently, four passes with constant reduction to 7 mm thick at 400°C.

2. Constant 5-mm-thickness draft per pass to 16 mm thick, with a finishing temperature of approximately 800°C, followed by six passes with constant reduction to 7 mm thick at room temperature. Annealing at 720°C for 10 min, water quenching, annealing at 1000°C for 5 min, and water quenching.

The first heat treatment after hot-rolling was for activating a large number of potential nuclei for recrystallization. The second heat treatment was for softening. Charpy impact specimens 6 mm thick were cut in parallel to the rolling direction.

Results

Table 2 gives the processing conditions and the resulting grain sizes. A comparison of the results shows that there is a tendency toward finer grain sizes for schedules involving both hot-working at lower temperatures at the last pass and heat treatment for activating the nuclei for recrystallization prior to the final anneal.

The conventional hot rolling of the alloys results in a pancake structure of grain highly elongated in the rolling direction and with a moderately strong cube-on-edge texture. The elongated-grain boundaries and textures form continuous paths for easy fracture in the plane normal to the short transverse direction. Figure 7 shows the fracture surface of the specimen taken from the conventionally, continuously hot-rolled materials, impact fractured at −30°C. The surface shows a brittle cleavage fracture and delamination along the rolling direction. The upper-shelf energy level was low and ductile-brittle transition temperature was high in this case.
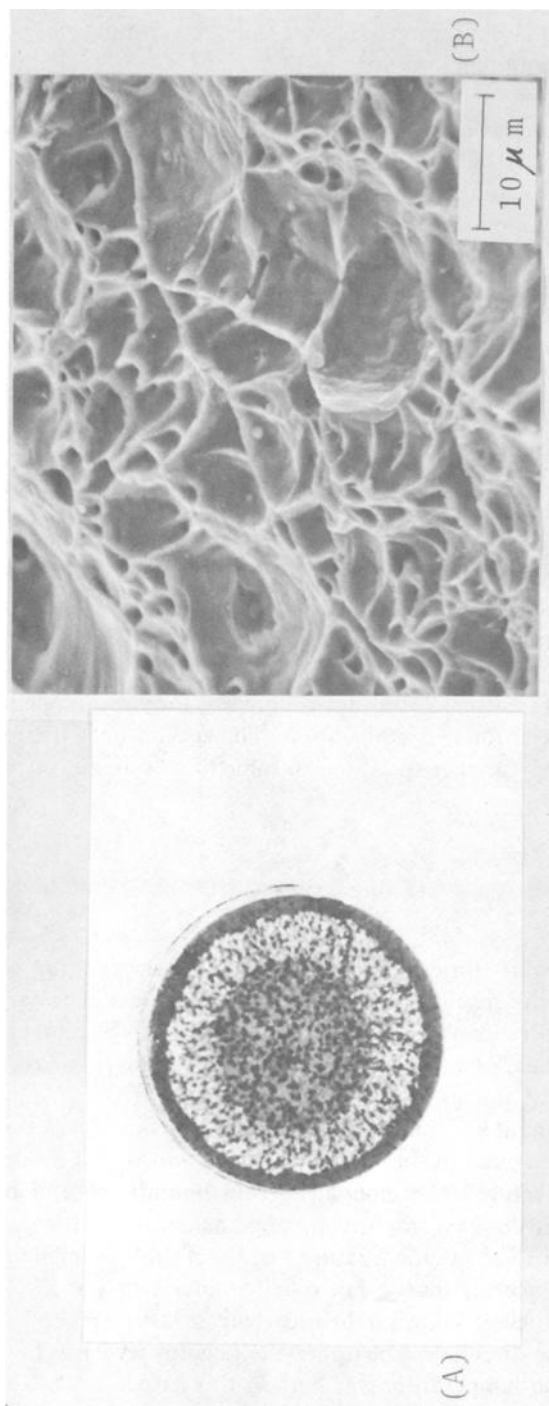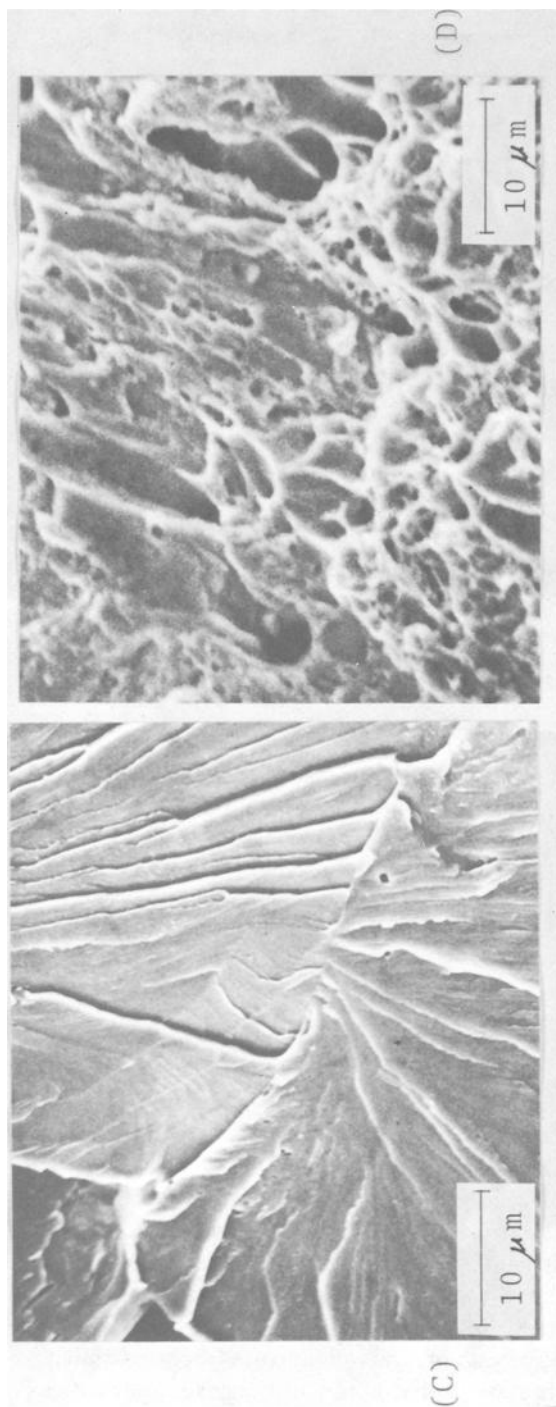
FIG. 5—*Light fractograph and SEM fractographs of Fe-30Cr-2Mo alloy, fractured by hydrostatic tension at room temperature. Typical bimodal fracture. ×4. (a) Light fractograph: fracture started at the center of the fibrous zone. The outer ring is the cleavage zone and the circumferential narrow zone is the shear-lip zone. (b) SEM fractograph: dimple fracture mode in the central, fibrous zone. (c) SEM fractograph: cleavage fracture mode in the outer zone. (d) SEM fractograph: shear mode dimple fracture in the circumferential zone.*

FIG. 6—*Schematic illustration of thermomechanical processing.*

TABLE 2—*Effect of processing condition on ferrite grain size.*

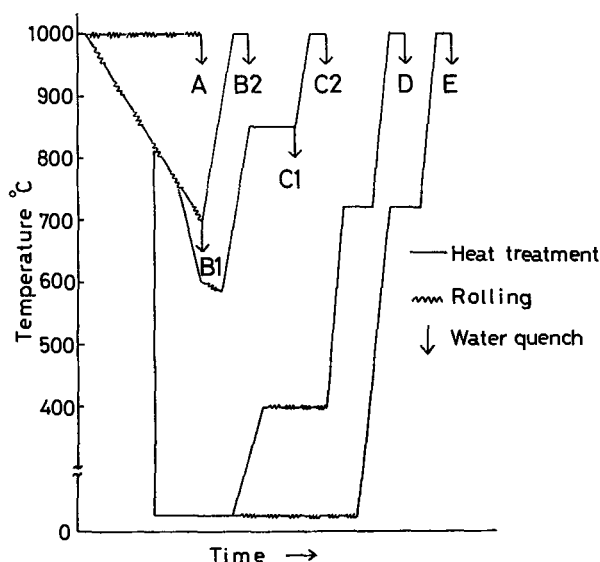| Processing	Temperature, °C			ASTM Grain size	Hardness, Hv
	Finishing	1st Anneal	2nd Anneal		
A	1000	...	1000	1 to 2	208
B1	700	...	1000	3 to 7	203
B2	700	850	1000	3 to 7	210
C1	620	850	...	8 to 9	208
C2	620	850	1000	7 to 6	212
D	400	720	1000	8	208
E	20	720	1000	8	232

The annealing of the conventional hot-rolled structure at 1000°C brings about very large grain size. The fracture mode of the Charpy impact specimens of the material annealed at 1000°C shows cleavage-type fracture at the lower-shelf energy level.

The fracture surface of the hydrostatic tension specimens shows some special features. A narrow irregular network was observed at the grain boundaries while the bulk of the surface is typical cleavage, as shown in Fig. 8. Figure 9 shows the enlarged grain boundary structure. It seems probable that this network, containing very fine, equiaxed dimples, was developed in the process of microligament fracture under the local, unidirectional tensile state in the vicinity of the grain boundaries [17].
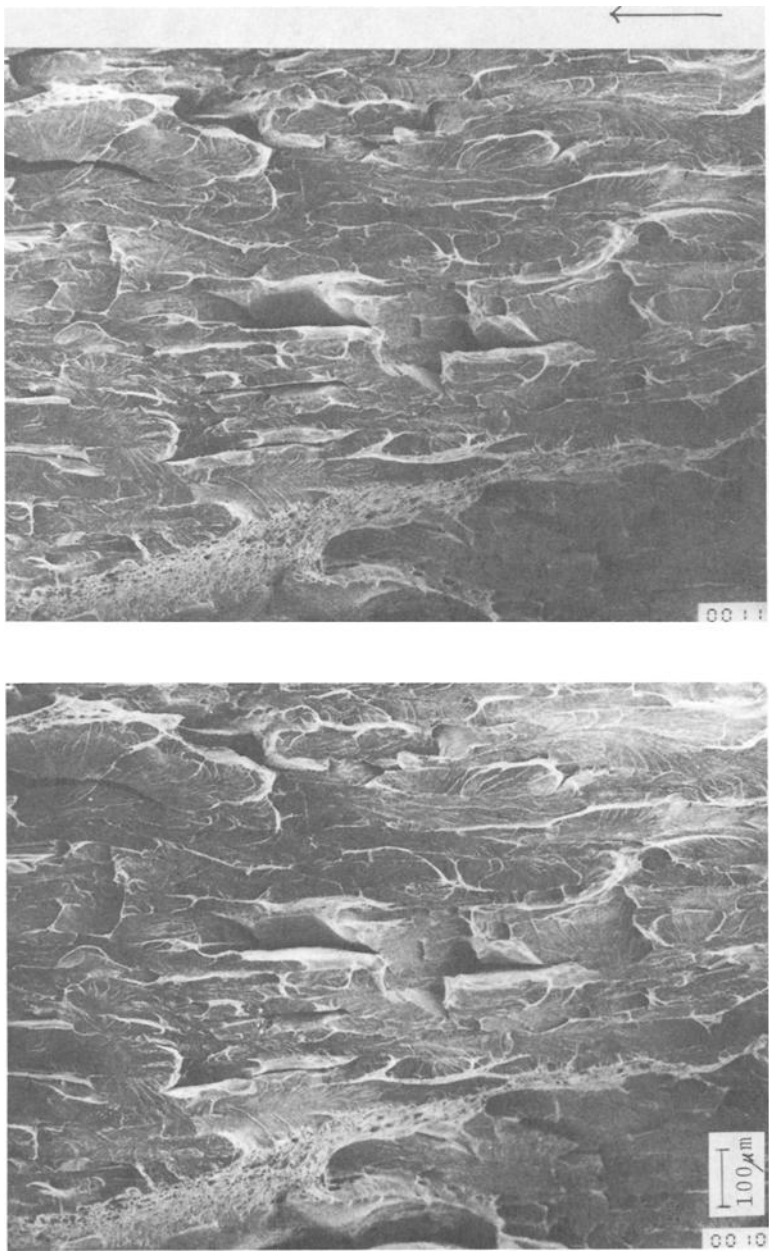
FIG. 7—SEM stereofractograph of Fe-30Cr-2Mo alloy, conventionally continuously hot-rolled, fractured by Charpy impact at −30°C. Arrow shows the rolling direction.
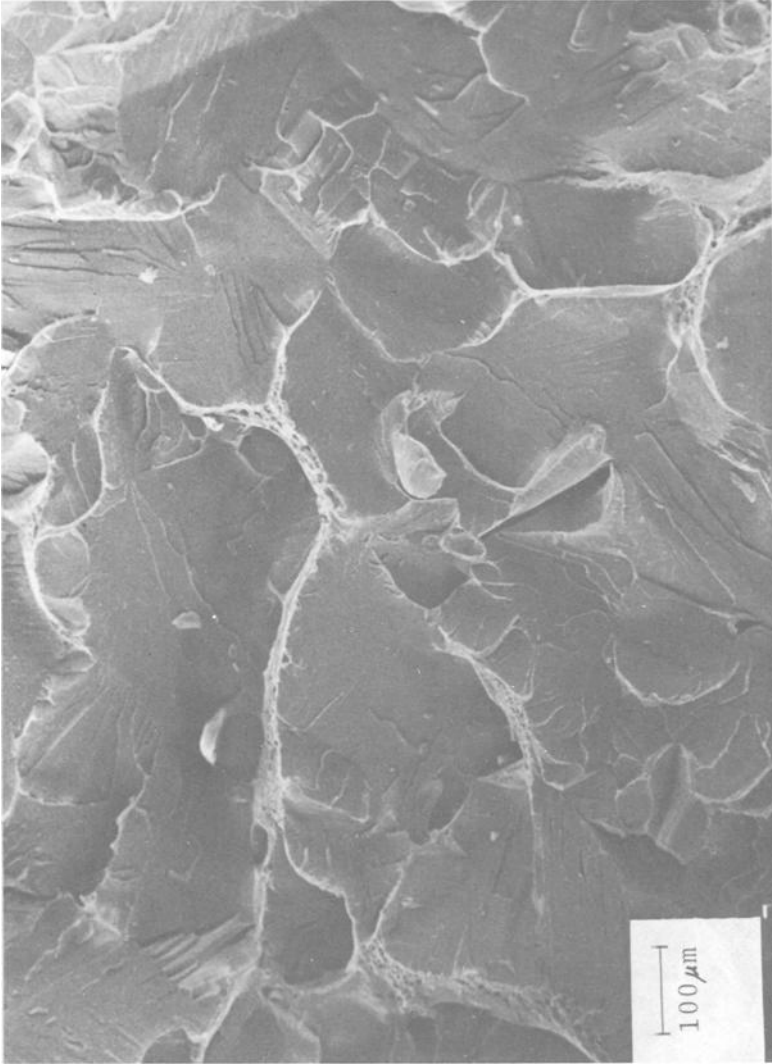
FIG. 8—SEM fractograph: network of dimple strips on the cleavage fracture surface. Fe-30Cr-2Mo alloy, conventionally continuously hot-rolled and annealed at 1000°C, fractured by Charpy impact at 0°C.

FIG. 9—SEM fractograph dimple strip formed by microligament fracture in the vicinity of grain boundary on the cleavage fracture surface. Fe-30Cr-2Mo alloy, conventionally continuously hot-rolled and annealed at 1000°C, fractured by Charpy impact at 0°C.
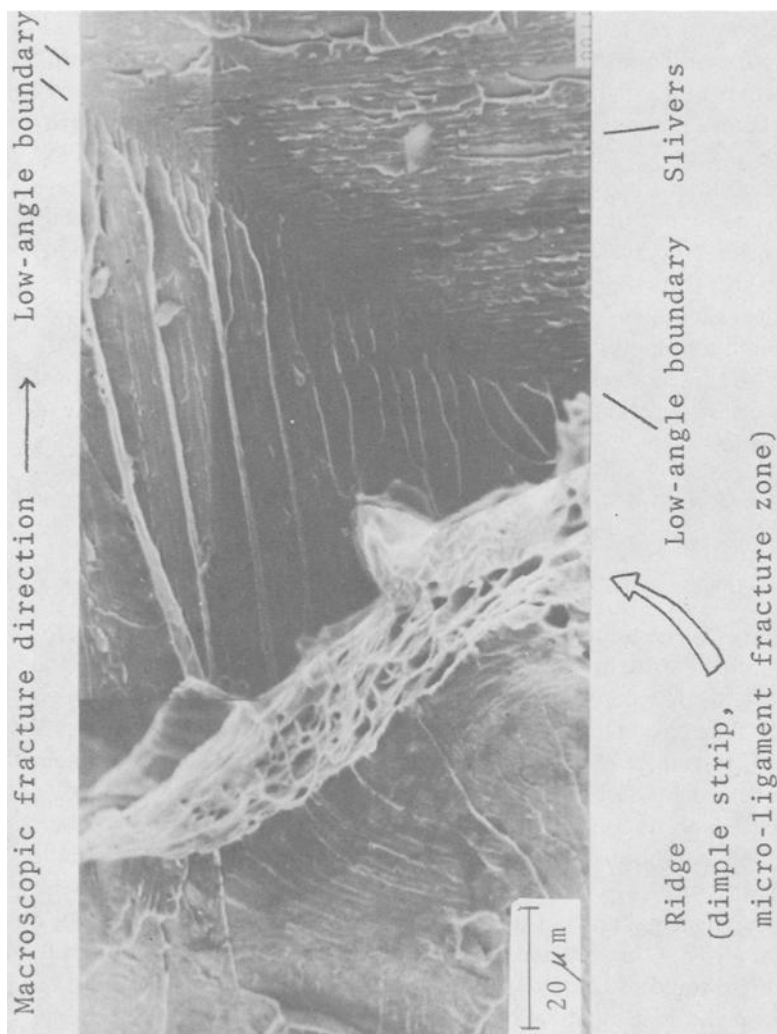
The impact energy absorbed by the conventionally hot-rolled materials and by the subsequently annealed materials is shown in Fig. 10. The levels of absorbed energy are low and the ductile-brittle temperature is near room temperature, in both cases. Figure 11 shows the impact energy absorbed in the materials made by TMP. The results show that an adequate combination of rolling passes and post-rolling normalization has a pronounced effect on the impact properties. The influence of the TMP on the shape and position of the impact transition curve is very marked. In a TM-treated plate, brittle fracture begins at a much lower temperature. The impact transition curve, however, shows a gradual decrease in a wide temperature range between brittle fracture and upper shelf. The controlled rolled high-strength low-alloy (HSLA) plate shows a pronounced tendency to splitting of the fracture planes. The cause of this splitting seems to be a weakening of the previously elongated grain boundaries due to precipitation [18]. In the case of the TM-treated Fe-30Cr-2Mo alloy, the influence of the previous grain boundaries, which are parallel to the plate surface, was recognized on the fracture surface, although a pronounced tendency to splitting could not be observed, as shown in Fig. 12. Good results were obtained in Processes D and E, as shown in Fig. 13. These processes are placing mill restrictions, however, because of too high loading.

Discussions

Fracture Behavior in the Hydrostatic Tensile State

The results of hydrostatic tension test with the Bridgman-type specimens of coarse-grained structure show that the fracture behavior of Fe-30Cr-2Mo alloy is more strongly dependent on the value of the hydrostatic tensile stress component than the plain carbon steels. While the fracture strain is very large in low triaxiality, it decreases abruptly as the value of hydrostatic tensile component increases. Under conditions of low triaxial stresses, the alloy displays excellent ductility. Under conditions of high triaxial stresses, however, the alloy shows less strain to fracture and a transition from ductile to cleavage fracture.

One of the principal aims of the investigation was to determine whether a "damage sensitivity" parameter could be assigned to the various materials studied which would indicate their propensity to the generation of damage, when deformed under identical processing conditions. The unexpected embrittlement phenomena, as mentioned previously, can be well explained qualitatively by the experimental results. The results suggest that to the left of the double circle points in Fig. 3, the state of stress is considered favorable for processing. The Cockcroft criterion [19] for workability, which suggests that fracture will occur when the tensile strain energy reaches a critical value, was applied with a high degree of success only in the range of fibrous frac-
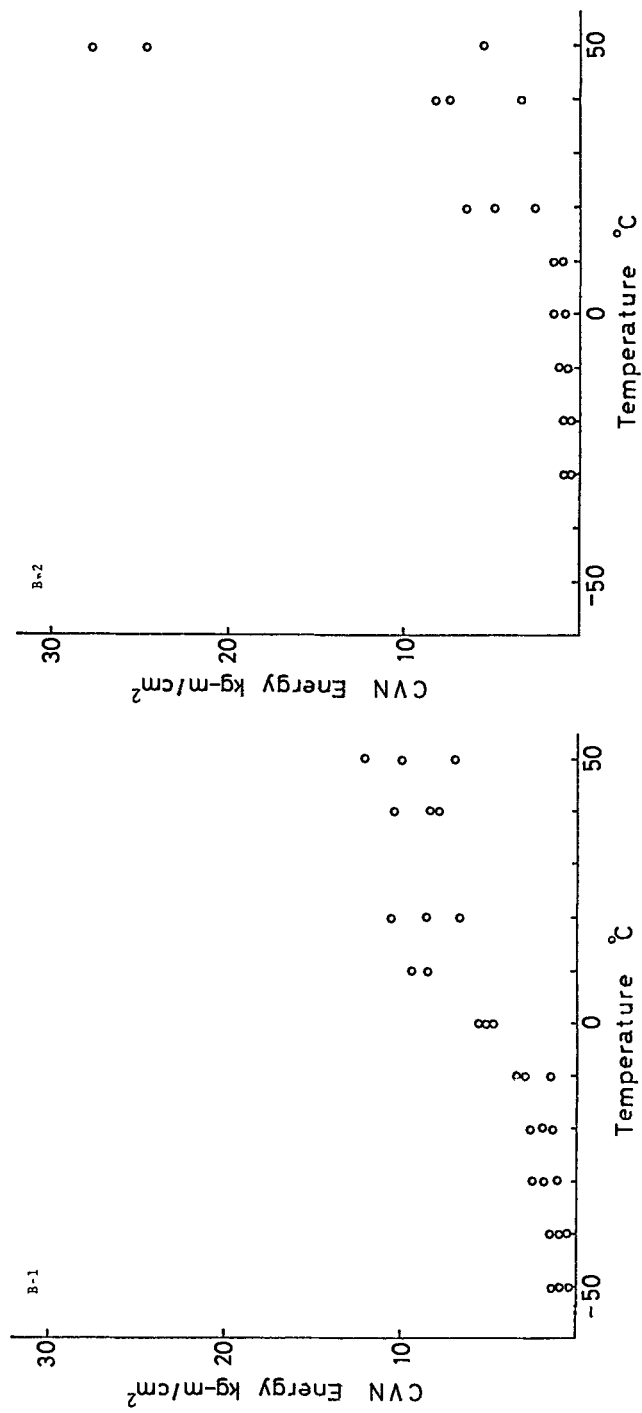
FIG. 10—*Effect of conventional processing on the impact resistance of 6-mm-thick Charpy V-notch specimens B-1 and B-2.*
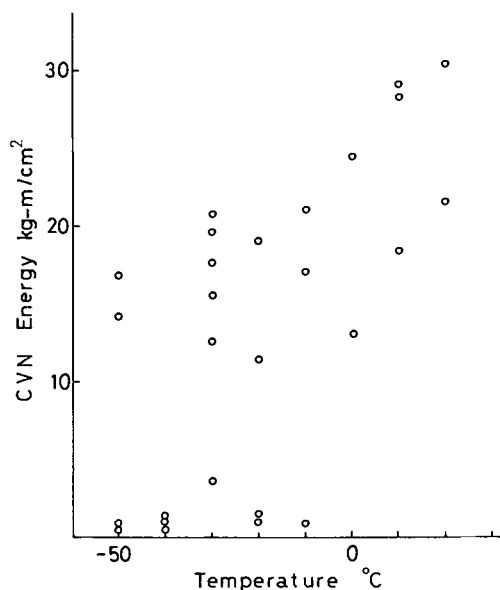
FIG. 11—*Effect of thermomechanical processing on the impact resistance of 6-mm-thick Charpy V-notch specimen C-1.*

ture, but not in the case of bimodal fracture. There was, however, a discrepancy between the values of hydrostatic component or maximum tensile stress component for cleavage fracture from the tests and the values estimated by the application of slipline field theory on the deformation processing [5].

The cause of this discrepancy is not clear from the results of the experiment. Many problems remaining unsolved; for example, strain dependency or history dependency of cleavage stress in the alloy, or slip-initiated cleavage and twin-initiated cleavage in the alloy, or both. Moreover, based on limited data, the specimen aged at 475°C for 1 h displayed a fracture strain equal to the unaged specimens, and there is no difference in the fracture surface. The room-temperature prestrained specimens displayed some resistance to bimodal fracture.

The two fracture modes, dimple and cleavage fracture appearing in the hydrostatic tension test, are expected to be influenced strongly by the microstructure. Consequently, if the hydrostatic tension testing is to be applied to the thermomechanically treated materials, the results will be rather interesting.

Thermomechanical Processing

Microstructure and impact property are closely related. The finer the grain size, the larger the impact-absorbed energy. However, the structure of the
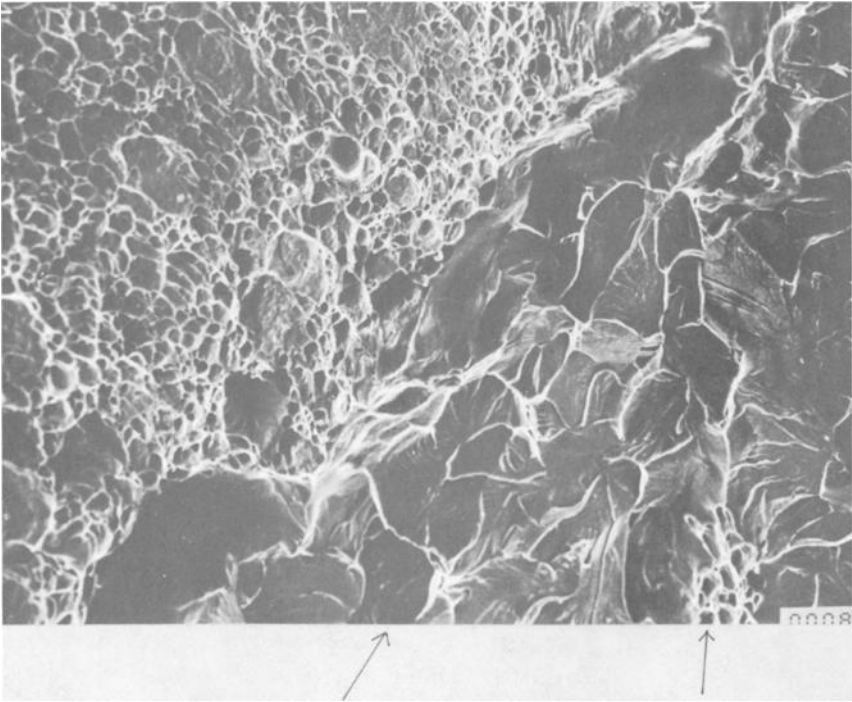
FIG. 12—*SEM fractograph of Fe-30Cr-2Mo alloy, thermomechanically processed, fractured by Charpy impact at* −50°C. *Arrows show previous grain boundaries. Scale mark shows 100* μm.

alloy after the usual hot-working practice is quite coarse [15], and this influences the impact strength, and especially the DBTT, of the thick plate. The experimental results on the thermomechanical processing for improvement of the impact properties showed that the fine-grained structure (~ ASTM No. 9) can be obtained, and consequently the impact property can be improved substantially.

Metallurgically, TMP is related to the effect of the microalloying elements. Small additions of columbium, for instance, are known to retard recrystallization and hence produce grain refinement.

Deformation Twinning

Generally, in cases where twinning is the operative mode of plastic deformation, twins may act as potent stress concentrators and provide nucleation of cracks. In this case, when the triaxiality is low and the tensile stress at the onset of twinning is insufficient to propagate the nuclei, the stress may be raised by increasing the applied load on the specimen [20] and, hence, the size of the plastic zone beneath a notch (or internal defect). When the triax-

FIG. 13—*Effect of thermomechanical processing on the impact resistance of 6-mm-thick Charpy V-notch specimens D and E.*

iality is high, on the other hand, the tensile stress below the notch as the twins are formed is more than sufficient to propagate immediately any cracks nucleated by the "burst" of twins, and final fracture is coincident with the onset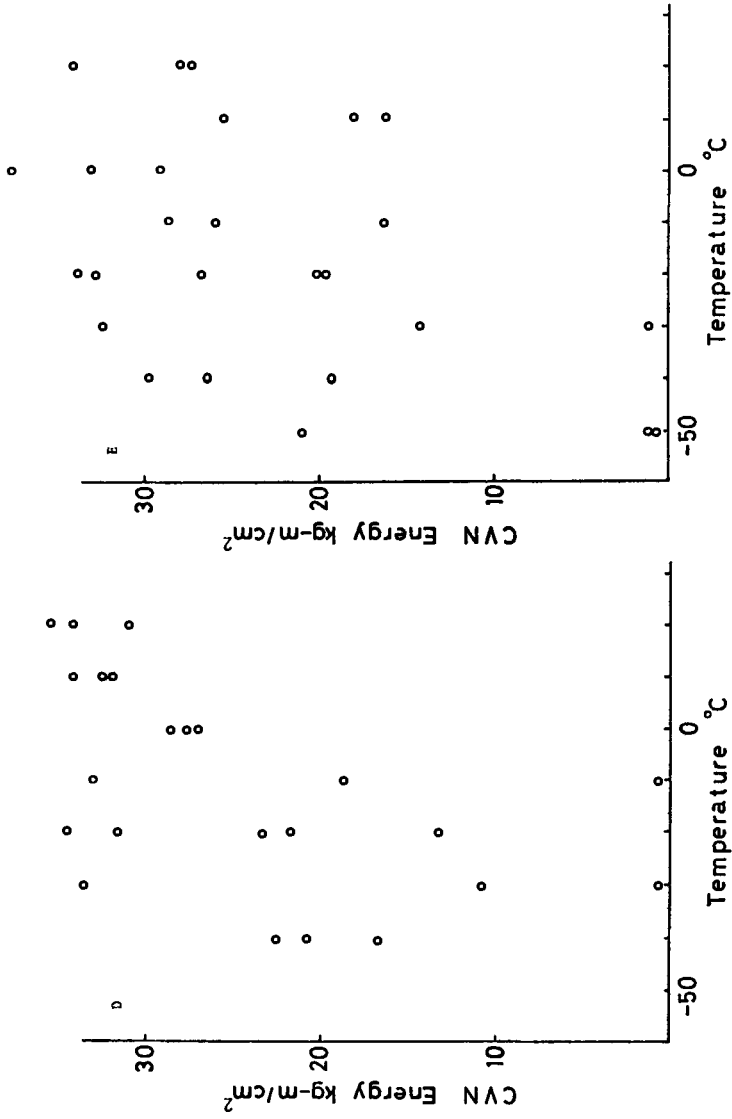 of twinning [20]. It is said that even coarse-grained mild steel twin-initiated fracture would not be anticipated at temperatures of about 150 K if the applied loading rate were equivalent to those normally obtained in standard fracture toughness testing [20]. In coarse-grained Fe-30Cr-2Mo alloy, however, twin-initiated fracture may be able to occur at room temperature, and twinning may be easily associated with propagating cracks, because very high strain rates are produced ahead of the accelerating crack tip. Twinning usually takes place in materials containing few mobile dislocation sources. Small amounts of prestrain at higher temperatures may therefore be effective in preventing twinning in the alloy. Grain refining is, of course, most effective in preventing twinning.

Summary

The Fe-30Cr-2Mo alloy displays excellent ductility in conventional mechanical testing. Several unexpected embrittlement phenomena were observed, however, in several deformation modes when the alloy had a coarse-grained structure or when it was in a complex state of stress. Experiments were conducted to explain the embrittlement phenomena by means of a hydrostatic tension test and to examine the effects of thermomechanical processing on the impact properties of the alloy.

The results of the tension test of the coarse-grained materials in the hydrostatic tensile state show that the fracture behavior of the alloy is highly dependent on the state of the stress. Under conditions of low triaxial stress, the alloy displays excellent ductility. Under conditions of high triaxial stress, however, it shows less strain to fracture and a transition from ductile to cleavage fracture.

Certain hot-working and annealing conditions are effective in improving the impact properties of the alloy.

The successful use of high-purity higher-chromium ferritic stainless steel requires extensive understanding of the fracture characteristics of the alloy. Special attention should be paid to the conditions of deformation processing of the alloy with a coarse-grained structure and the conditions of practical use of the thick plate. Producing a fine-grained structure is a most effective means of preventing the occurrence of embrittlement.

Acknowledgments

research. Experimental materials were kindly supplied by the Research Laboratory for Metals, Showa Denko Co. Ltd.

References

[1] Iwaoka, S., Kaito, H., Ohtani, T., Ōhashi, N., Takeda, M., and Kinoshita, N. in *Proceedings.* Stainless Steel '77, A Global Forum, Climax Molybdenum Co., Greenwich, Conn., 1977.

[2] Morimura, T., *Kinzoku,* Vol. 42, 1972, p. 130.

[3] Shimodaira, S., Saito, H., Morimura, T., and Hirano, T., presented at Japan Society of Corrosion Engineering, 12-14 May 1976.

[4] Ichikawa, K., *Kinzoku Zairyo,* Vol. 17, No. 6, 1977, p. 33.

[5] Shimura, M., *Transactions,* Japan Institute of Metals, Vol. 19, 1978, p. 589.

[6] Rogers, H. C. in *Proceedings.* The Metallurgical Society of the American Institute of Mining, Metallurgical, and Petroleum Engineers, 1971, p. 453.

[7] Rice, J. R. and Tracey, D. M., *Journal of the Mechanics and Physics of Solids,* Vol. 17, 1969, p. 201.

[8] Brown, L. M., *The Mechanics and Physics of Fracture.* Metal Society, London, 1976.

[9] Francois, D. in *Proceedings.* Fourth International Conference on Fracture, Vol. 1, 1977, p. 805.

[10] Bridgman, P. W., *Studies in Large Plastic Flow and Fracture.* McGreen Book Co., New York, 1952, p. 9.

[11] (a) Needleman, A., *Journal of the Mechanics and Physics of Solids,* Vol. 20, 1972, p. 111.
(b) Chen, W. H., *International Journal of Solids and Structures.* Vol. 7, 1971, p. 685.
(c) Norris, D. M. et al, *Journal of the Mechanics and Physics of Solids.* Vol. 26, 1978, p. 1.

[12] Clausing, D. P., *Journal of Materials.* Vol. 4, 1969, p. 566.

[13] Dondik, I. G., *Problemy Prochnosti.* No. 8, 1970, p. 54; also, *Strength of Materials.* 1972, p. 937.

[14] Matejka, W. A. and Knoth, R. J., *Journal of Testing and Evaluation.* Vol. 3, No. 3, 1975, p. 199.

[15] Franson, I. A., *Metallurgical Transactions.* Vol. 5, 1974, p. 2257.

[16] George, T. G., Bashford, G., and MacDonald, J. M., *Journal of the Australia Institute of Metals,* Vol. 16, 1971, p. 36.

[17] Shimura, M. and Tokuno, H., *Transactions,* Japan Institute Metals, to be published.

[18] Meyer, L. and de Boer, H., *Journal of Metals.* Vol. 29, 1977, p. 17.

[19] Cockcroft, M. G. and Latham, D. J., *Journal of the Institute of Metals,* Vol. 96, 1963, p. 33.

[20] Knott, J. F., *Fundamentals of Fracture Mechanics,* Butterworths, London, 1973, p. 198.

T. Nakazawa, [1] *S. Suzuki,* [1] *T. Sunami,* [1] *and Y. Sogō* [1]

Application of High-Purity Ferritic Stainless Steel Plates to Welded Structures

ABSTRACT: This investigation deals with the practical application of high-purity 18Cr-2Mo-Nb ferritic stainless steel plates 6, 12, and 25 mm thick to welded structures.

In the V-notch Charpy test, the ductile-to-brittle transition temperature is about $-30°C$. The fracture toughness, K_c, determined by the deep-notch test is 350 kgf/mm² · $\sqrt{mm}$ for 12-mm-thick plate at $-100°C$. In the ESSO test, which has a temperature gradient, the K_c-value obtained is more than 400 kgf/mm² · $\sqrt{mm}$ at 0°C.

The toughness of the gas tungsten-arc welded joints using 316 L (C < 0.02 percent) wire deteriorated to some extent, compared with that of the base metal. In the deep-notch test (notch position: fusion boundary, heat-affected zone), however, the K_c-value is more than 200 kgy/mm² · $\sqrt{mm}$ at 0°C.

It is generally recognized that the safety of a weldable structural steel can be secured if its weld zone has resistance to brittle fracture initiation and the base metal has brittle fracture arresting properties. It can be concluded, therefore, that in thicknesses up to 12 mm this material can be used for welded structures at service temperature above 0°C because of its excellent fracture toughness.

Since the toughness of 18Cr-2Mo-Nb deteriorates with aging above 300°C or in cold-working in excess of 10 percent, and even further deteriorates in strain-aging, these effects must be taken into account in its fabrication.

KEY WORDS: ferritic stainless steels, deep-notch test, ESSO test with temperature gradient, fracture toughness, welded joint, cold-work, aging, precipitation treatment

In recent years, significant progress has been made on the development and industrial application of high-purity ferritic stainless steels. Strictly speaking, however, many problems remain concerning the practical use of these high-purity steels in thick plate and welded structures. The major prob-

[1] Assistant to manager, engineering metallurgist, manager, and research supervisor, respectively, Yawata Works, Nippon Steel Corp., Kitakyushu, Japan.

lem that has prevented the utilization of plates for welded structures has been the decrease of toughness by welding.

Improvements in toughness which result from increasing the purity of ferritic stainless steels were pointed out by Binder [1][2] and Baerlecken et al [2]. And the effects of stabilizing elements on toughness were investigated by Semchyshen et al [3] and Jarleborg [4].

Based on these results, the authors have made a systematic study [5] of the relationships between the carbon and nitrogen contents of this steel and the stabilizing elements such as titanium and niobium, because they relate to the toughness and the intergranular corrosion resistance of welded joints. As a result, it was found that the toughness of welded joints is improved by the addition of niobium and is at an optimum level when the Nb/(C + N) is around 10. It was also recognized that the steel becomes immune to intergranular corrosion if its niobium content is 0.02 percent or higher at C + N ≤ 140 ppm.

Based on these results, we selected the following composition for plates applicable to welded structures: ≤ 140 ppm (C + N)−0.14Nb−19Cr−2Mo. This material has a corrosion resistance similar to that of Types 304 or 316 steels.

Successful production trials were carried out with this composition using the 54 431-kg (60 ton) vacuum oxygen decarburization (VOD) process. We succeeded in producing hot-rolled plates up to 12 mm thick. This paper discusses the applicability of the mill-produced plates to welded structures on the basis of the evaluation of the results of Charpy and wide-plate tests, and describes the effects of fabrication and service conditions on the steel properties.

Materials and Experimental Procedure

The materials used in this study were hot-rolled plates of 6, 12, and 25-mm thicknesses produced commercially. Chemical compositions are described in Table 1. Figure 1 illustrates the schematic flow diagram for the preparation of test specimens. The welded joint was prepared by gas tungsten-arc welding (GTAW) techniques using Type 316 L filler metal. Cold-working was induced by tensile strains of 5, 10, and 20 percent. Aging treatment was carried out at 300 ~ 550°C for 10 ~ 1000 h. As for strain-aging, specimens were strained to 10 percent in tension and then aged at 300 ~ 450°C for 300 h. After solid solution treatment (1250°C, 1 h; water-cooled), precipitation treatment was carried out at 400 ~ 1150°C for 2 h.

In order to study the fracture toughness of this steel, both Charpy and wide-plate tests were carried out. Since the brittle fracture characteristics of steels are evaluated normally in two different categories, that is, initiation of

---

[2]The italic numbers in brackets refer to the list of references appended to this paper.

TABLE 1—*Chemical composition (weight percent).*

C	Si	Mn	P	S	Cr	Mo	Nb	N
0.004	0 07	0.07	0.025	0.007	18.75	1 82	0.14	0.0085
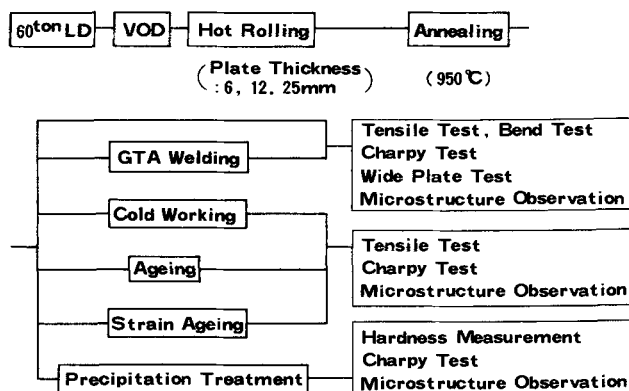
FIG. 1—*Flow diagram for the test procedure.*

brittle crack and propagation of brittle crack, the V- and U-notch Charpy tests and the deep-notch test [6] were conducted for the former and the press-notch Charpy test and the ESSO test with temperature gradient [7] for the latter.

Experimental Results and Discussion

Properties of Annealed Material

The microstructure of the steel annealed, shown in Fig. 2, consists of ferritic grains slightly extended in the rolling direction (a). Particles of about 0.1 μ in diameter were observed in the grains (b). These precipitated particles were identified as those of the Z-phrase (Cr_2-Nb_2-N_2) [8] and niobium carbonitride (carbon, nitrogen), indicating that both carbon and nitrogen were fixed by niobium.

The tension test results are given in Table 2. The proof stress and the tensile strength of the steel were slightly dependent upon the rolling direction, those in the rolling direction being smaller than those transverse to it. This test result may be attributed to the type of microstructure shown in Fig. 2a.

Figure 3 is a view of the bending tests, indicating that the steel is very ductile in this type of test.

Figure 4 provides the Charpy test results for specimens with a 2-mm V-notch (ASTM, E23, Type A), showing sharp ductile-to-brittle transition
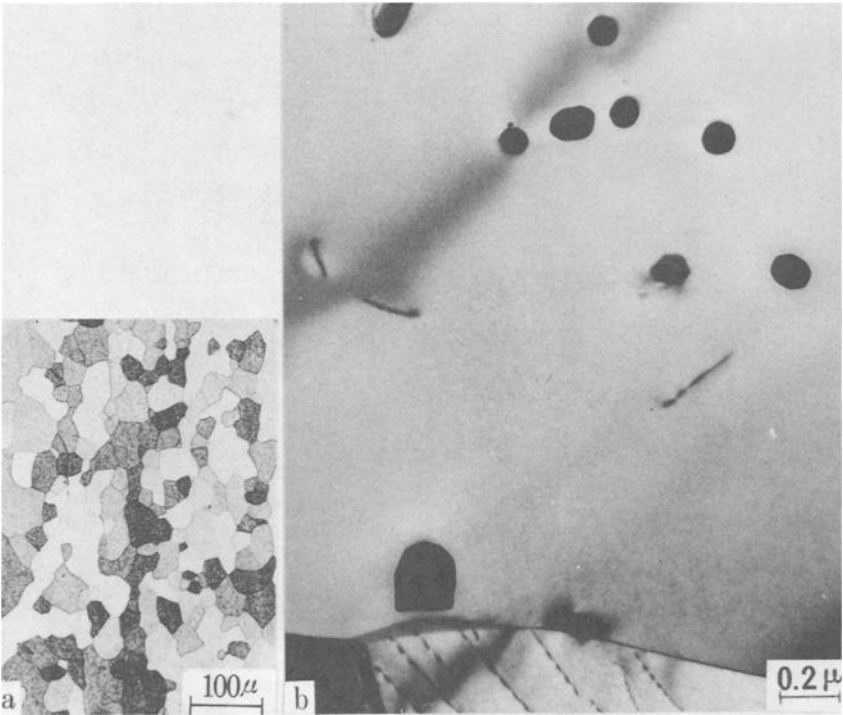
FIG. 2—Optical (a) and transmission electron (b) micrographs of annealed material.

TABLE 2—Tensile properties of base metal.

Plate	(1)	Tensile Tests (2)		
Thickness mm	Orientation	0.2%Proof Stress kgf/mm²	Tensile Strength kgf/mm²	Elongation %
6	L	32	47	33
	T	36	52	27
12	L	33	47	40
	T	34	50	37
12	L	31	47	42
	T	32	51	41
12	L	32	48	40
	T	34	51	41

Notes 1. L Parallel to the rolling direction.
          T Transverse to the rolling direction.
       2. Test Piece JISZ2201. No.13B tension test
          specimen with 50mm gauge length.
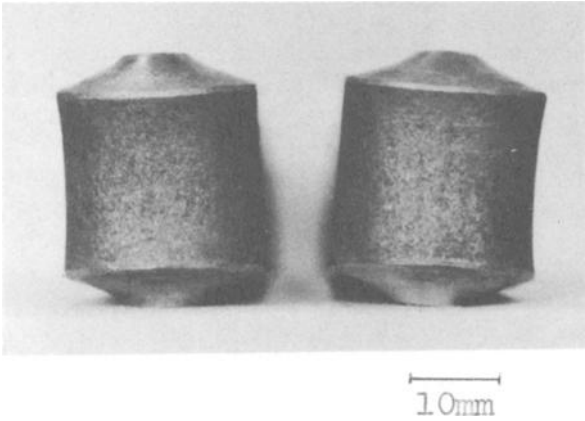
FIG. 3—*View of the bend-tested specimens.*
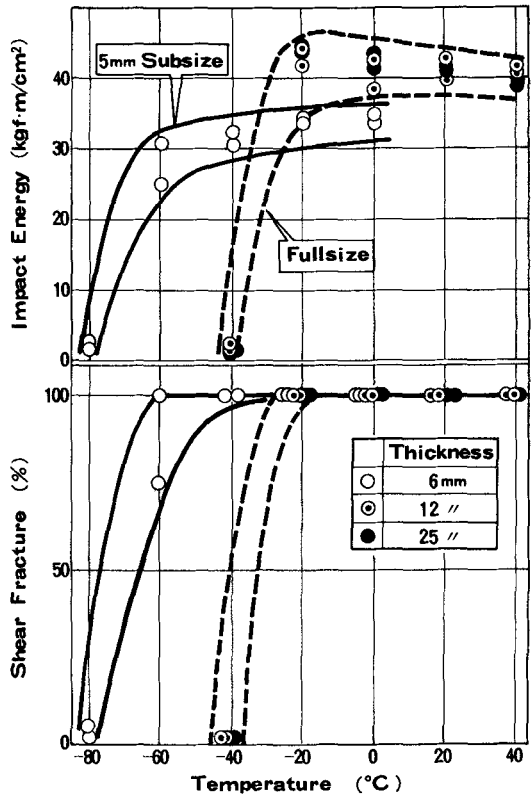
FIG. 4—*Transition curves for V-notch Charpy specimens of base metal.*

temperatures (DBTT's) for all the gages investigated. High impact absorbed energies—for example, 30 kgf·m/cm² at −60°C or higher for a plate thickness of 6 mm and 40 kgf·m/cm² above −20°C for plate thicknesses of 12 and 25 mm—were obtained. These high absorbed energies are probably due to the high purity of the steel [1]. The fractures observed within the brittle region were all of the cleavage type.

Test results for specimens with 2 mm deep and 5 mm deep U-notches are shown in Fig. 5. Both tests show a similar fracture transition temperature, which is about 20°C lower than that of V-notch tests.

Figure 6 shows the results of the deep-notch test [6]; the test specimen is also shown in Fig. 6. The fracture toughness value (K_c) is calculated from

$$K_c = \sqrt{\frac{2B}{\pi C} \tan \frac{\pi C}{2B}} \cdot \sigma \cdot \sqrt{\pi C}$$

where

B = half width of specimen,

FIG. 5—*Transition curves for full-size U-notch Charpy specimens of base metal* (L: *parallel to the rolling direction;* T: *transverse to the rolling direction*).
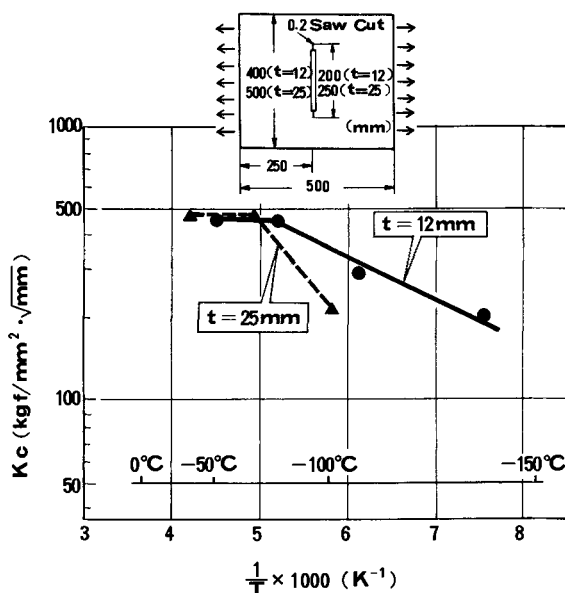
FIG. 6—K_c-value of base metal obtained by deep-notch test.

C = half length of notch, and
σ = mean stress.

Low-stress brittle fracture occurred only at temperatures below $-80°C$ for the 12-mm-thick specimens and below $-70°C$ for the 25-mm-thick specimens. The fracture toughness values (K_c values) obtained were 350 kgf/mm$^2 \cdot \sqrt{mm}$ for 12-mm-thick and 200 kgf/mm$^2 \cdot \sqrt{mm}$ for 25-mm-thick specimens, respectively, even at $-100°C$. The foregoing test results indicate that this steel in the annealed condition has a respectable resistance to brittle fracture initiation at 0°C.

Figure 7 shows the results of the press-notch Charpy test in the annealed condition. The DBTT in this test is slightly higher than in the V-notch Charpy test.

The results of the ESSO test with temperature gradient [7] are shown in Fig. 8. The test specimen is also shown in Fig. 8. The K_c-value is calculated from

$$K_c = \sqrt{\frac{2B}{\pi C} \tan \frac{\pi C}{2B}} \cdot \sigma \cdot \sqrt{\pi C}$$

where

B = width of specimen,

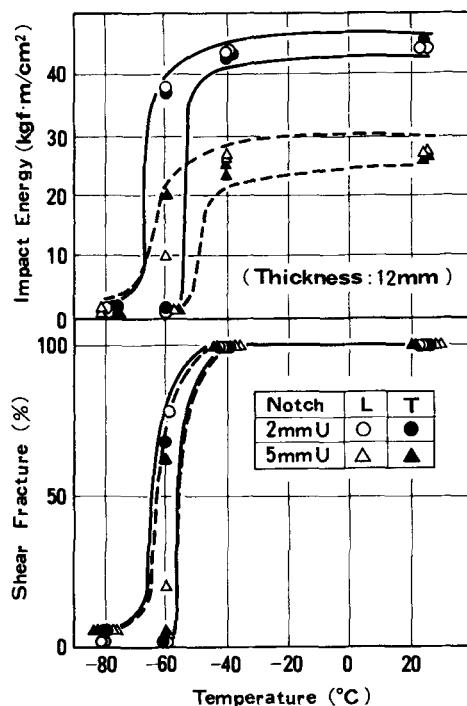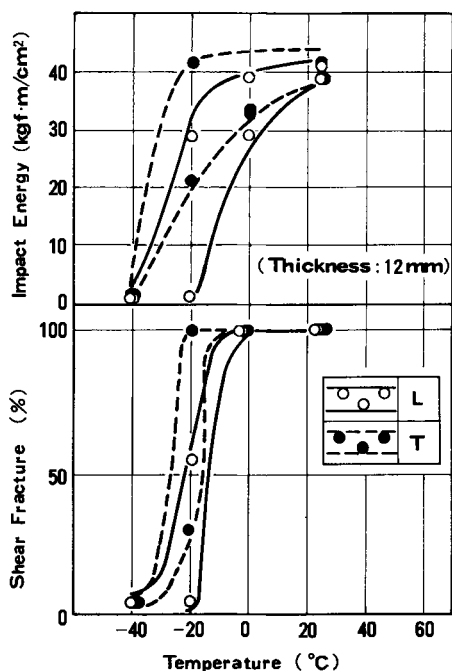FIG. 7—*Transition curves for full-size press-notch Charpy specimens of base metal* (L: *parallel to the rolling direction;* T: *transverse to the rolling direction*).

C = length of arrested crack, and
σ = applied stress.

The K_c-value somewhat decreased with the increase of plate thickness. The K_c-values were on the same level as the K_c values of JIS G 3126·SLA 33B (ASTM, A537, Class A) steels used for liquefied propane gas storage tanks. Further, when compared with the level required by WES 136 of the Japan Welding Engineering Society for A (arrest) use, which is calculated on the assumption of the existence of a crack 100 mm long and a design stress of 10.5 kgf/mm², the K_c value of this steel at 0°C was found to be high. Figure 9 shows a fracture surface of the tested specimens. Brittle fracture propagated with little shear lip on the plates of 12 and 25-mm thicknesses, and arrested at 0°C and −2°C, respectively. From the aforementioned observations, it is supposed that this steel, in the annealed condition, has good crack arresting properties for large brittle cracks at 0°C or higher.

Properties of Welded Joints

The GTAW joints were made using Type 316 L (C < 0.02 percent) welding wire under procedures given in Table 3.

Figure 10 shows transmission electron micrographs (TEM's) of the heat-
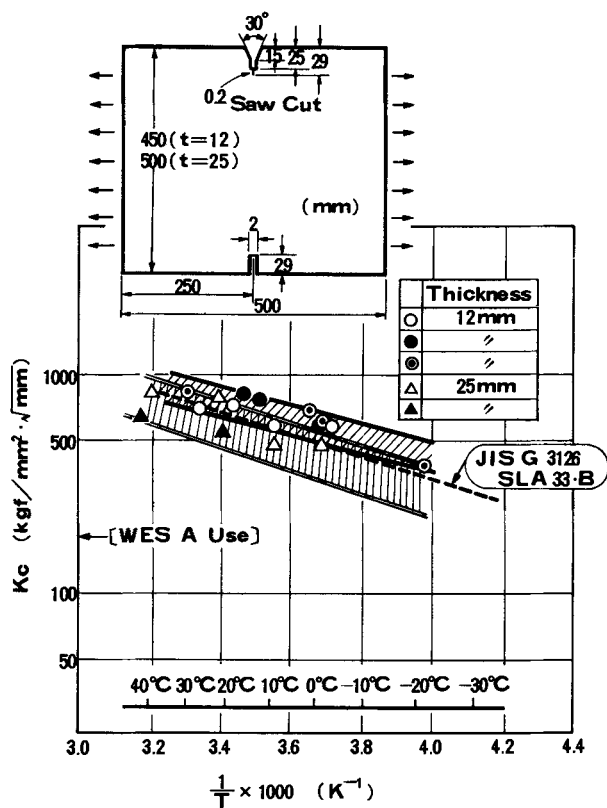
FIG. 8—K_c-value of base metal obtained by ESSO test with temperature gradient.

affected zone (HAZ). The particles of about 0.1 μ in diameter of the Z-phase and niobium carbonitride previously found in the annealed condition (Fig. 2) are not observed near the fusion boundary (a); instead, fine precipitates and an increase of dislocation density can be recognized. However, at a point 5 mm from the fusion boundary (b) the precipitate which appeared during annealing still remains and the dislocation density is significantly low. Hence, it can be considered that there occurred some microstructural changes such as an increase in the density of dislocations due to thermal stress and the taking in solution and reprecipitation of carbonitrides due to thermal cycle.

The results of the tension test, bending test, and Charpy test for the welded joints are given in Table 4. The tensile strength of welded joints was equal to that of the base metal. All the bend tests were free of cracks. The Charpy specimens were notched at the weld metal, fusion boundary, and HAZ. The DBTT of all specimens was lower than 0°C.

Figure 11 shows the results of the deep-notch test of the welded joints. As
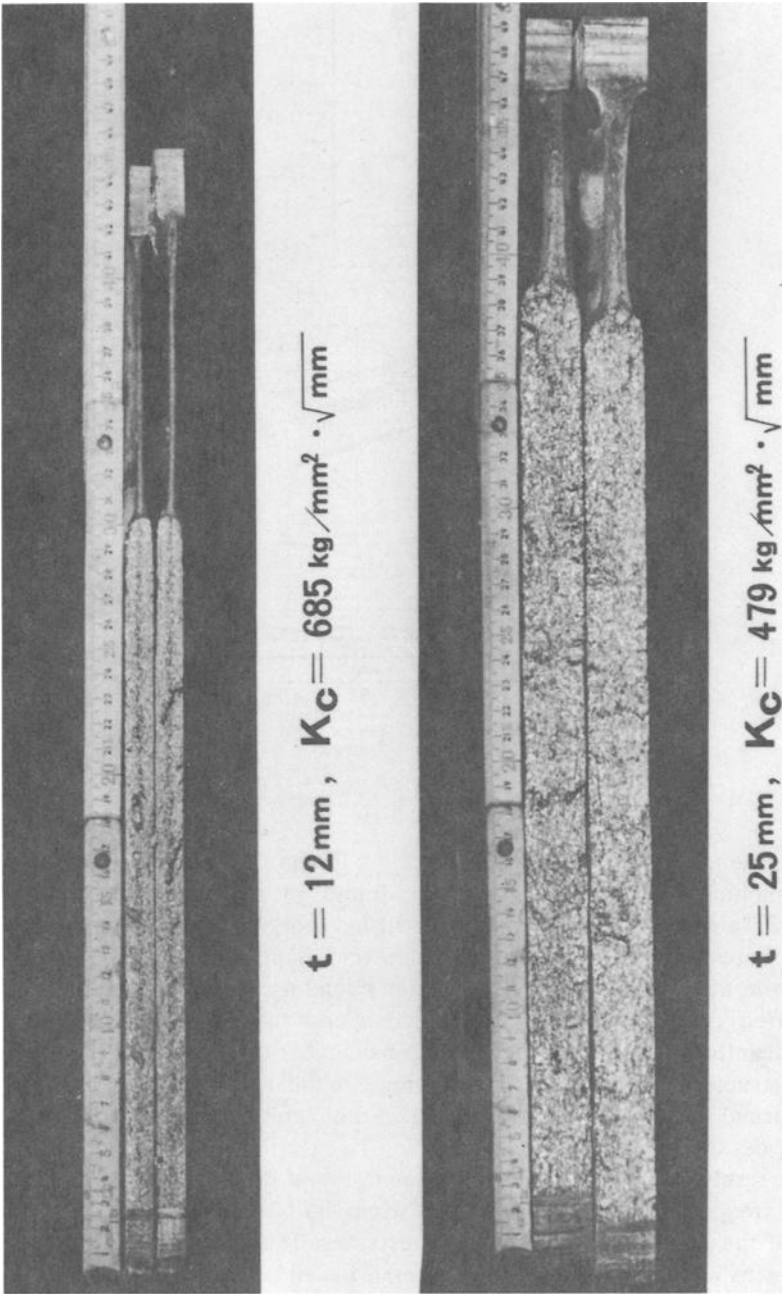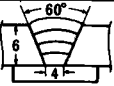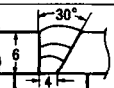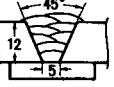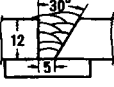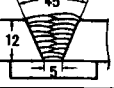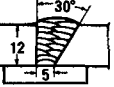
FIG. 9—Fracture appearance of the ESSO-tested specimens.

$t = 12 \text{ mm}, \; K_c = 685 \; kg/mm^2 \cdot \sqrt{mm}$

$t = 25 \text{ mm}, \; K_c = 479 \; kg/mm^2 \cdot \sqrt{mm}$

TABLE 3—*Welding procedure.*

Plate No.	Thickness (mm)	Welding Condition					Test
		Geometry (mm)	Current (A)	Voltage (V)	Speed (mm/min)	Interpass Temp. (°C)	
1	6	(60°, 6, 4)	250	13	100	100 ~150	Tensile Bend
		(30°, 6, 4)	″	″	″	″	Charpy Deep Notch
2,4	12	(45°, 12, 5)	250	13	100	100 ~150	Tensile Bend
		(30°, 12, 5)	″	″	″	″	Charpy Deep Notch
3	12	(45°, 12, 5)	150	12	100	100 ~150	Tensile Bend
		(30°, 12, 5)	″	″	″	″	Charpy Deep Notch

Welding Wire : 316UL, 1.6φ
Position   : Flat

shown in Fig. 11, specimens having the straight weld fusion boundary perpendicular to the plate surface were prepared, with the notch at the fusion boundary and in the HAZ 2 mm away from the fusion boundary. All the test results are plotted in Fig. 11. The K_c-values show a considerable amount of scatter. The K_c-value at the fusion boundary is somewhat higher than that in the HAZ. The K_c-value at 0°C, however, was over 200 kgf/mm$^2 \cdot \sqrt{\text{mm}}$. Compared with the K_c-value calculated on an assumption of the existence of a crack 100 mm long and a design stress of 10.5 kgf/mm^2, this value is still adequately high to withstand brittle fracture initiation. The K_c-value thus obtained is substantially lower, however, than that of the base metal shown in Fig. 6. The reduction in toughness is undoubtedly caused by the microstructural changes indicated in Fig. 10, namely, the change in the precipitation morphology of the carbonitrides and the increase in dislocation density.

As a general rule, the application of steels for welded structures is considered safe, on condition that the steel possesses resistance to brittle fracture initiation in welds and is able to arrest brittle fracture in base metal. As shown in Fig. 12, plates of this steel can be used safely for welded structures at 0°C or higher.
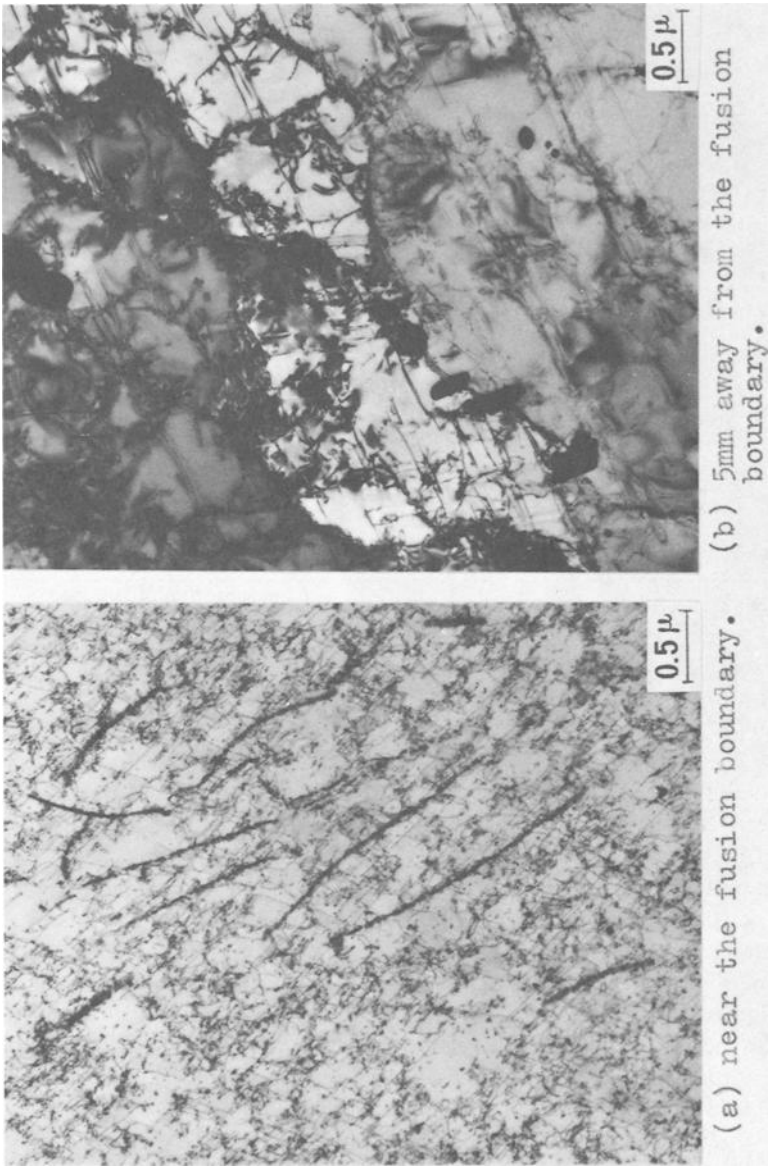
FIG. 10—Transmission electron micrographs of the heat-affected zone in butt welded joint.

TABLE 4—*Mechanical properties of welded joints.*

Plate No	Thickness (mm)	Tensile Test			Bend Test	Charpy Test Location of Notch (*)					
		TS (kgf/mm²)	Eℓ (%)	Break Position	Roller Bend Bend Radius 2t	D (°C) vTrE	(kgf·m/cm²) vE₀	A (°C) vTrE	(kgf·m/cm²) vE₀	B (°C) vTrE	(kgf·m/cm²) vE₀
1	6	49.7	20	Base Metal	Good	<−20	20	−60	28	−70	25
2	12	48.9	31	″	″	″	20	−17	21	−20	25
3	12	50.4	30	″	″	″	21	−10	22	−15	35
4	12	51.4	31	″	″	″	19	−16	19	−20	23

(*) Location of Notch   Weld Metal

2mm

B A D
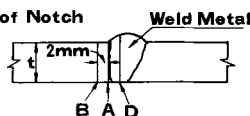
Effects of Cold-Working and Heat Treatment on Steel Properties

Effect of Cold-Working—The results of the tension test and the V-notch Charpy test on cold-worked specimens are summarized in Fig. 13. With the increase in the amount of tensile strain, the tensile strength and especially the proof stress increase while the ductility decreases.

The decrease of toughness is first observed at about a 10 percent strain. Close to about 20 percent strain, the DBTT rises to +20°C.

Effect of Aging—Shown in Fig. 14 is the behavior of change in tensile properties caused by aging. Practically no change was observed up to 400°C. The increase in strength and the decrease in ductility are shown when aging in the 450 to 500°C temperature range, with the maximum increase occurring at 475°C, where the tensile strength after aging for 1000 h attained 80 kgf/mm². Aging at 550°C, however, produced no changes in mechanical properties.

Figure 15 shows the effect of aging on the toughness of the steel. There is no change up to 350°C, even in 1000 h. At 400°C there is no change in toughness in 300 h, but in 1000 h the toughness shows some deterioration. The embrittlement is quite severe in the 450 to 500°C temperature range, with 475°C exposure being the most severe. In 1000 h at this temperature the DBTT is +180°C, an indication of typical 475°C embrittlement. Little change occurred at 550°C for 300 h, but slight deterioration was recognized at 1000 h.

Comparing the isostrength and the isotoughness curves in Figs. 14 and 15, it can be concluded that the effect of aging on tensile properties is quite similar to that on toughness.

The 475°C embrittlement of high-chromium steels has been widely studied [9,10] and is said to be caused by the precipitation of the chromium-rich α'-phase. A similar embrittlement was investigated by Grobner [11] on lower
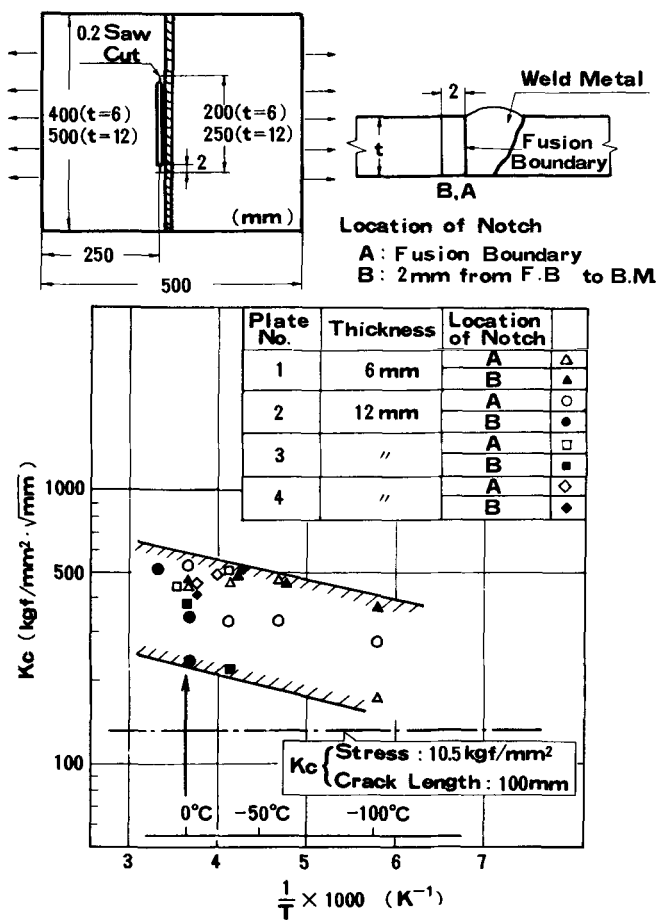
FIG. 11—K_c-value of welded joint obtained by Deep-Notch test.

chromium containing steels such as the 18Cr and 18Cr-2Mo steels. Accord-ing to Grobner, in the case of low-chromium steels the precipitation of the α'-phase takes place on dislocations rather than by spinodal decomposition. It was also reported by Grobner that embrittlement can also be casued by precipitation of carbonitrides on dislocations at 538°C.

Figure 16 shows the TEM's of specimens aged at 475 and 550°C. Com-pared with the annealed condition (Fig. 2), the TEM's show no definite change in their microstructure. The precipitation on the dislocations reported by Grobner or fine precipitation in the matrix are not observed. Such differences resulted from the following facts. These specimens were an-nealed at 950°C, a temperature at which sufficient recrystallization takes place such that they had a considerably lower dislocation density which

```
            ┌──────────────────────────────┐
            │   Steel  for  Welded  Structure   │
            └──────────────────────────────┘
         ┌───────────────────┐  ┌───────────────────────┐
         │ Resistance to brittle │  │ Resistance to propagation │
         │ fracture  initiation  │  │ of brittle fracture in    │
         │ in welds          │  │ base metal            │
         └───────────────────┘  └───────────────────────┘
─────────────────────[ This Steel  at  0 ℃ ]─────────────────────
         ┌───────────────────┐  ┌───────────────────────┐
         │ Deep Notch test of │  │ ESSO  test of base    │
         │ welded joints     │  │ metal                │
         │ K_c > 200 kgf/mm² √mm │  │ K_c > 400 kgf/mm² · √mm │
         └───────────────────┘  └───────────────────────┘
            ┌──────────────────────────────┐
            │ Applicable to Welded Structures │
            └──────────────────────────────┘
```
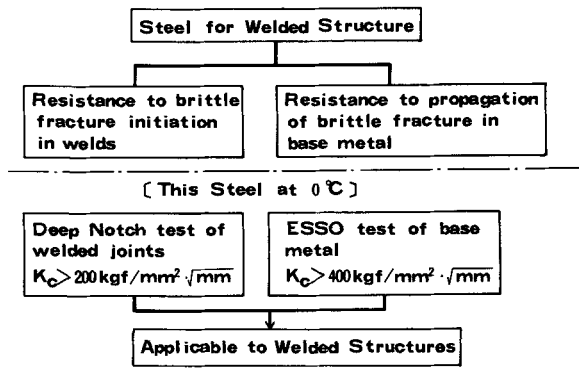
FIG. 12—*Application of steel plates for welded structures.*
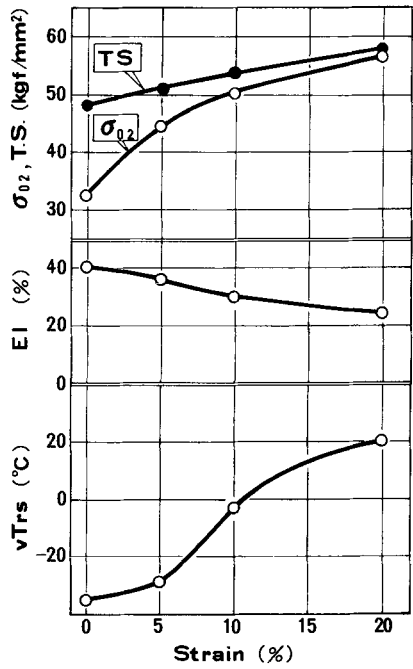
FIG. 13—*Effects of cold-working and room-temperature aging on the tensile and V-notch Charpy impact properties of base metal (vTrs: V-notch Charpy 50 percent shear fracture transition temperature).*
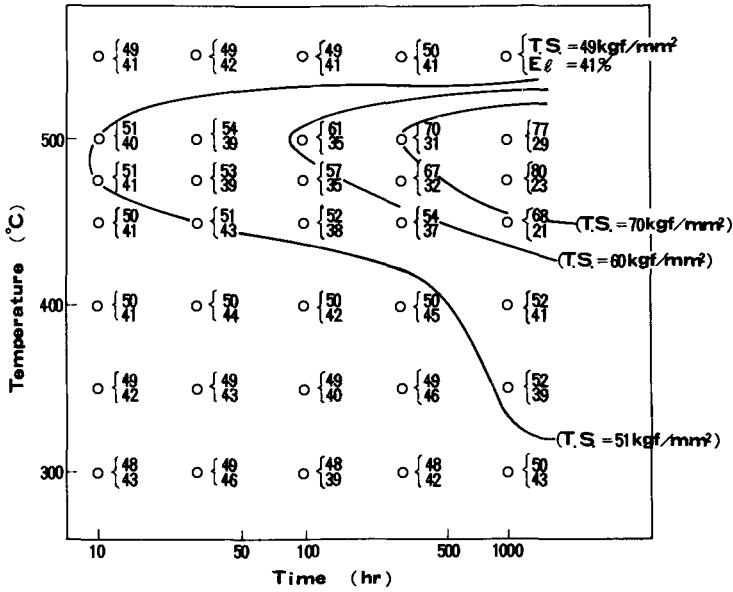
FIG. 14—*Effects of aging time and temperature on the tensile properties of base metal.*
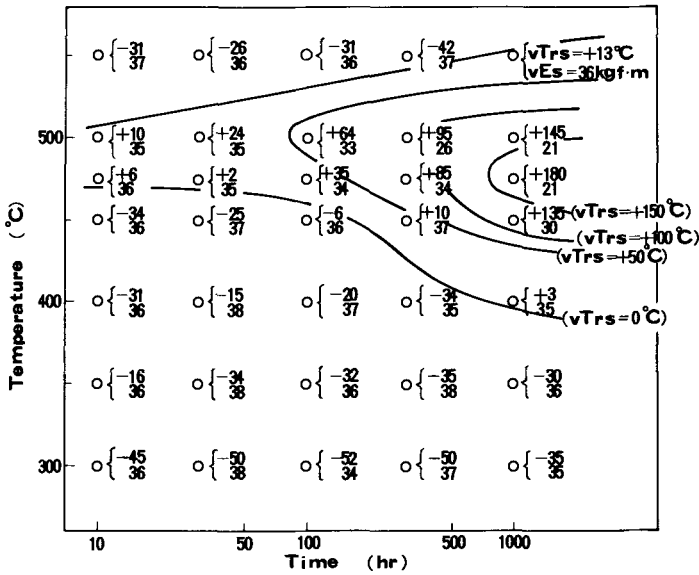
FIG. 15—*Effects of aging time and temperature on the V-notch Charpy impact properties of base metal.*
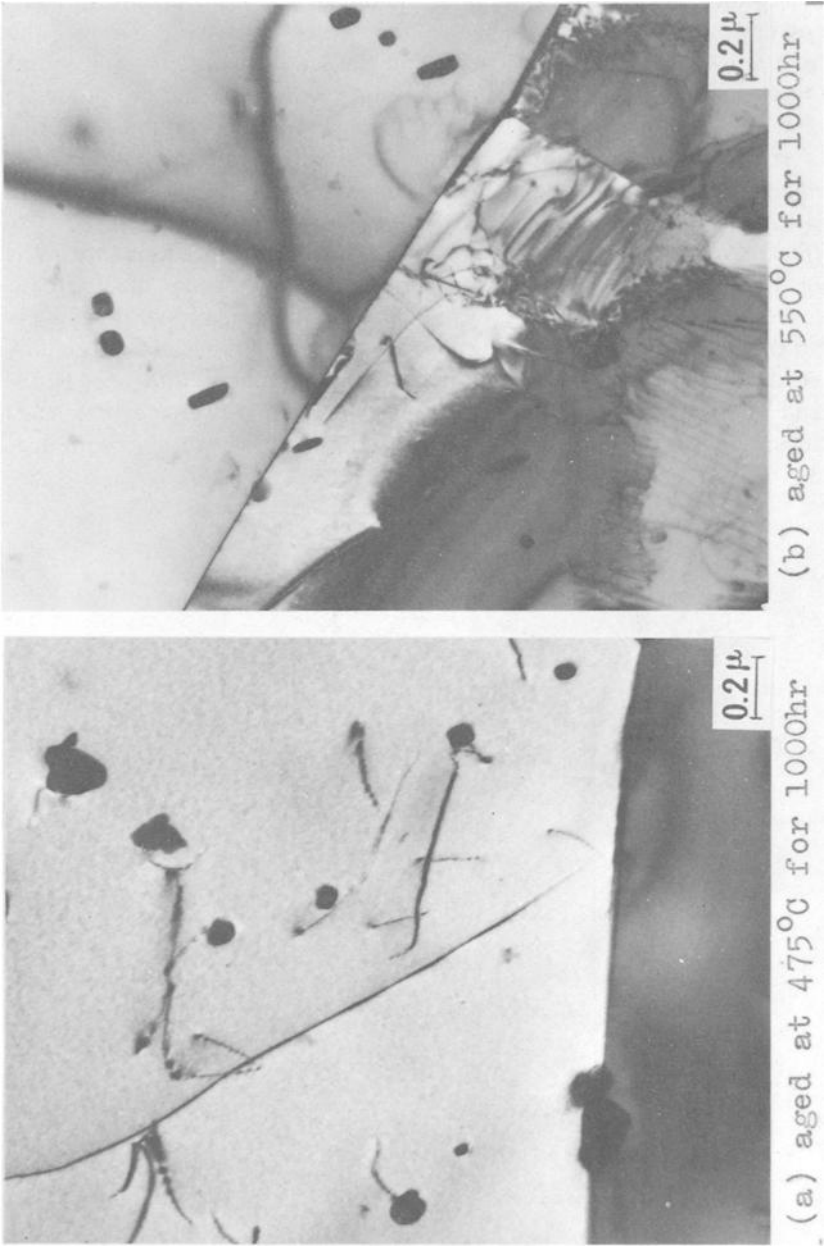
FIG. 16—*Transmission electron micrographs of aged specimens.*

would serve as precipitate nuclei. The carbon and nitrogen which are said to promote the precipitation of the α'-phase [11] were fixed by niobium. Also, we could not detect clearly the fine α'-phase by the transmission electron microscope because the difference in the lattice parameter between the α-phase and the α'-phase is so small and the scattering factor of iron and that of chromium are so similar that the contrast between the two phases is very low. In other words, since this steel, being a niobium-stabilized steel, it has a very low initial dislocation density. In addition, the α'-phase has not developed to a size detectable by the transmission electron microscope at the aging time of 1000 h.

Effect of Strain Aging—The test results of strain-aged specimens are given in Fig. 17 in comparison with the data obtained by aging alone. The increase in tensile strength and 0.2 percent proof strength produced by strain aging is higher than that produced by aging alone. The difference becomes more pronounced at higher aging temperatures. The toughness of the steel is decreased by strain aging, and the extent of deterioration is greater than that produced by aging alone. The higher the aging temperature, the more pro-
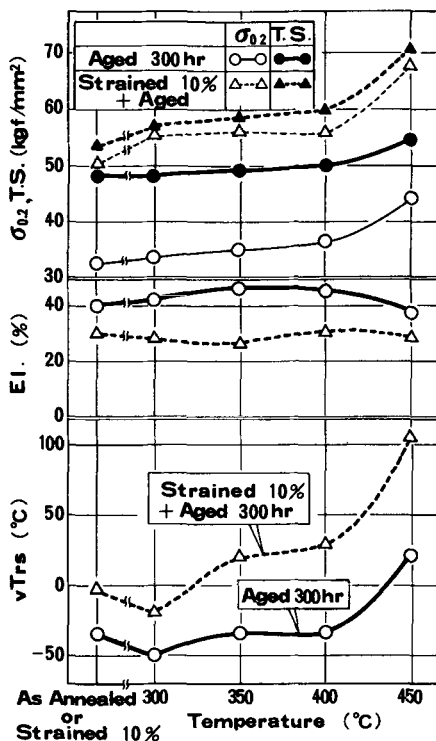
FIG. 17—*Effect of strain-aging on the tensile and V-notch Charpy impact properties of base metal.*

nounced this trend became. Thus, this steel is susceptible to strain-aging, a phenomenon explained by Grobner [11], who postulated that α' precipitates on dislocations.

Our data are, however, different from the results obtained by Grobner and Steigerwald [12], since they reported that up to 30 percent cold-work does not accelerate the 475°C embrittlement of 18Cr-2Mo steels stabilized with either niobium or titanium.

Effect of Precipitation Treatment—The results of hardness measurement and Charpy test of precipitation-treated specimens are shown in Fig. 18. The hardness increases substantially to about Hv 250 at temperatures between 550 and 600°C. The DBTT shows two peaks, at 550 and 950°C, while between these two it shows the best DBTT value of −35°C after a 750°C aging. Thus, at 550°C both hardening and embrittlement take place, while at 950°C the DBTT increases and the hardness decreases to a level lower than that of the solid solution state of the steel.

The effect of the heating time was studied at these three characteristic temperatures, that is, 550°C, at which both hardening and embrittlement occur; 750°C, at which toughness alone improves; and 950°C, at which only embrittlement occurs. Figure 19 shows the results of heating the specimens up to 100 h. Hardness slightly rose with time at 550°C, but toughness underwent little change. At 750°C, the change in hardness with holding time was negligible, while the toughness decreased substantially with longer time. At 950°C the hardness showed only a little change, but toughness deteriorated further with time. The analysis of electrolytically extracted residues was conducted for these test specimens. The results are shown in Fig. 20. Precipita-
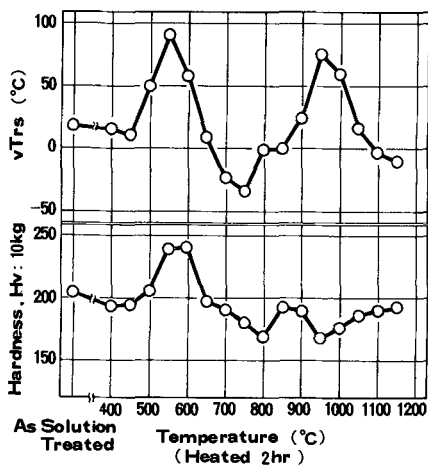
FIG. 18—*Effect of precipitation treatment on the V-notch Charpy impact property and hardness of base metal.*
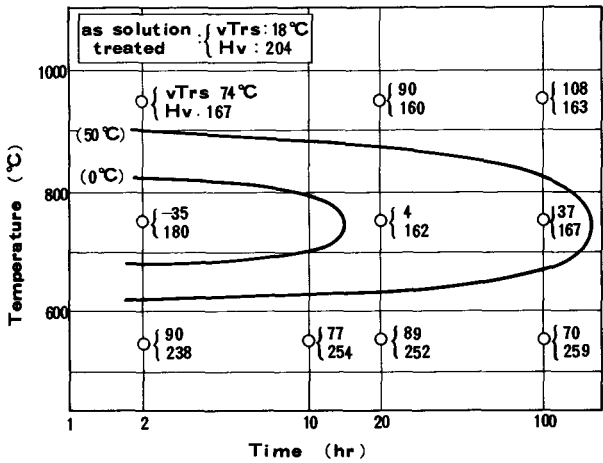
FIG. 19—*Effects of precipitation treatment on the V-notch Charpy impact property and hardness of base metal.*
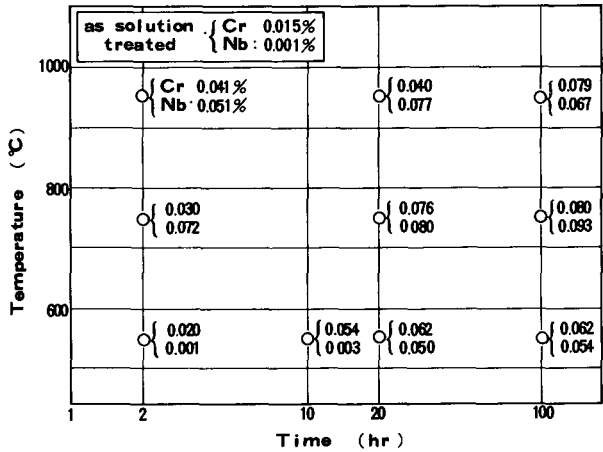
FIG. 20—*Effects of precipitation treatment on the amount of chromium and niobium in the electrolitically extracted residues base metal.*

tion of elements, mostly chromium, took place at the shorter time at 550°C, but in the longer times niobium began to precipitate. At 750 and 950°C, on the other hand, both niobium and chromium precipitated even in a short time. The Z-phase (Cr_2-Nb_2-N_2) and niobium carbonitride were identified by X-ray diffraction analysis of the residues precipitated at 750 and 950°C.

Figure 21 shows the TEM's of the steel under different heating conditions. Highly dense and homogeneous precipitation of very fine particles was seen
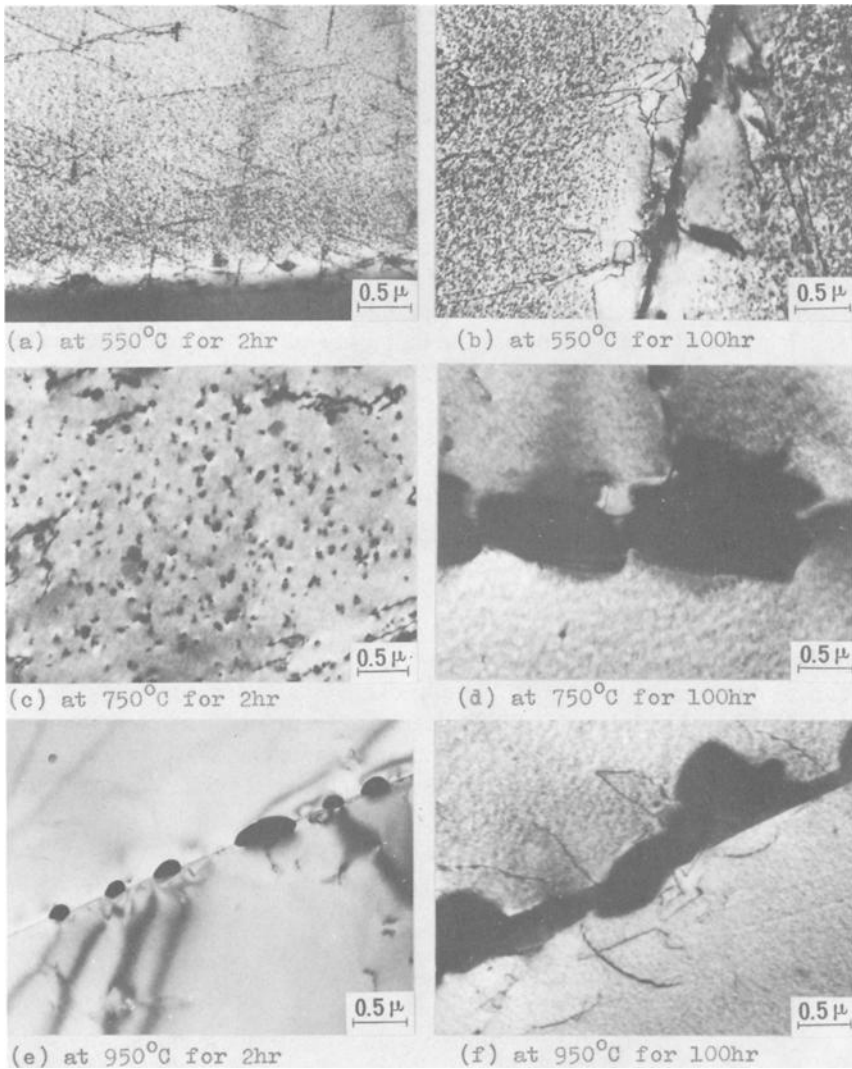
FIG. 21—*Transmission electron micrographs of specimens precipitation-treated after solution-treating at 1250°C for 1 h.*

at 550°C after 2 h of heating. When the heating time was extended to 100 h, the precipitated particles coalesced, and some coarse precipitates were found on the grain boundaries and on dislocations. No fine precipitates were found near these grain boundaries and dislocations. Such a precipitation-free zone is caused by solute atom depletion or vacancy depletion [13,14] near the grain boundary and dislocations. In this case it is not clear which factor is

dominant. While precipitates of approximately 200 Å in diameter were scattered homogeneously within the grains after 2 h at 750°C, coarse precipitates started to appear side by side on the grain boundaries in 100 h. The coarser precipitates were observed at the grain boundaries and within the grains at 950°C for 2 h. The grain boundary precipitates were closely aligned and after 100 h were further coarsened.

Based on the preceding observations, the changes in the mechanical properties of the solution-treated and aged alloy can be explained as follows. The hardening and embrittlement occurring at 550°C is caused by a fine precipitation which is not chromium-rich α' phase, since this temperature is well over the precipitation temperature range of the chromium-rich α'-phase [11]. It can also be assumed that the niobium and chromium carbonitrides precipitated at 750°C in short time (2 h) were too isolated to bring about precipitation hardening or to decrease the toughness. Therefore we assume that the improvement in toughness was caused by the decrease in the amount of carbon and nitrogen in solid solution. In contrast, either at 750°C in longer time or at 950°C, the toughness was deteriorated because the carbonitrides were considerably coarsened and were almost continuous at the grain boundaries, thus acting akin to a notch.

Fabrication of a Model Tank

The applicability of this steel to welded structures was confirmed by fabricating a model tank. The 200-mm-diameter nozzles were made out of welded 6-mm-thick plate. The spherical heads were made by cold-spinning 8-mm-thick plate, and the actual 1000-mm-diameter, 2000-mm-long tank also used 8-mm plate welded with Type 316L (C < 0.02 percent) wire. Figure 22 is an outside view of the model tank.

No problem was found by the X-ray test and by the hydraulic test (7 kgf/cm²), and thus the applicability of this steel to welded structures was demonstrated.

Conclusions

1. Based on the fracture toughness values of the base metal and weld zone, steel plates up to 12 mm thick can be used safely for welded structures at 0°C or higher.

2. The toughness of this steel decreased by cold-working. Some care therefore should be exercised when forming it by more than 10 percent.

3. This steel is susceptible to the 475°C embrittlement by aging. The increase in strength and the decrease in toughness concur around 475°C. Hence, the upper temperature limit for use of this steel should be about 300°C. In view of the strain-aging sensitivity of this steel strained plates should not be heated above 300°C.

4. After a solid-solution treatment and aging, this steel undergoes the

FIG. 22—*View of the model tank.*

following three property changes: (1) At an early stage of reheating, that is, at 550°C, hardening and embrittlement occur due to a dense precipitation of fine particles. (2) Heating at 750°C for a short time improves the toughness since both carbon and nitrogen are tied up by niobium. (3) Longer time exposure at 750 or 950°C produces precipitation of coarse particles and embrittlement. Because of these embrittling phenomena, any welding or fabrication which requires excessively large heat input should be avoided.

5. A model tank was successfully fabricated with this steel plate by welding with Type 316L (C < 0.02 percent) wire. Thus, the applicability of the steel to welded structures was well demonstrated.

References

[1] Binder, W. O. and Spendelow, H. R., *Transactions*, American Society for Metals, Vol. 43, 1951, p. 759.
[2] Baerlecken, E., Fisher, W.A., and Lorenz, K., *Stahl und Eisen*, Vol. 81, No. 12, 1961, p. 768.
[3] Semchyshen, M., Bond, A. P., and Dundas, H. J. in *Proceedings*, Symposium Toward Im-

proved Ductility and Toughness, Kyoto, Japan; Climax Molybdenum Co., Greenwich, Conn., 1971, p. 239.

[4] Jarleborg, O. H., Sawhill, J. M., and Steigerwald, R. F., *Stahl und Eisen*, Vol. 97, No. 1, 1977, p. 29.

[5] Abo, H., Nakazawa, T., Takemura, S., Onoyama, M., Ogawa, H., and Okada, H. in *Proceedings, Stainless Steel '77, A Global Forum*; Climax Molybdenum Co., Greenwich, Conn., 1977, p. 35.

[6] Ikeda, K., Akita, Y., and Kihara, H., *Welding Journal*, Vol. 46, No. 3, 1967, p. 133-s.

[7] Hall, W. J., Kihara, H., Soete, W., and Wells, A. A., *Brittle Fracture of Welded Plate*, Prentice-Hall, Englewood Cliffs, N.J., 1967, p. 290.

[8] Jack, D. H. and Jack, K. H., *Journal of the Iron and Steel Institute*, Vol. 210, 1972, p. 790.

[9] Marcinkowski, M. J., Fisher, R. M., and Szimae, A., *Transactions*, American Institute of Mining, Metallurgical, and Petroleum Engineers, Vol. 230, 1964, p. 676.

[10] Williams, R. O., *Transactions*, American Institute of Mining, Metallurgical, and Petroleum Engineers, Vol. 212, 1958, p. 497.

[11] Grobner, P. J., *Metallurgical Transactions*, Vol. 4, 1973, p. 251.

[12] Grobner, P. J. and Steigerwald, R. F., *Journal of Metals*, Vol. 29, No. 7, 1977, p. 17.

[13] Rosenbaum, H. S. and Turnbull, D., *Acta Metallurgica*, Vol. 6, 1958, p. 653.

[14] Rosenbaum, H. S. and Turnbull, D., *Acta Metallurgica*, Vol. 7, 1959, p. 664.

J. D. Redmond[1]

Toughness of 18Cr-2Mo Stainless Steel

ABSTRACT: The effect of residual and stabilizing elements on toughness has been investigated for a series of 18Cr-2Mo ferritic stainless steels which contained 0.015C and 0.015N. The residual elements varied were sulfur, manganese, and silicon. The stabilization variables were niobium, titanium, (Nb + Ti), and (Nb + Al).

The impact transition temperature was determined in the base metal and weld deposit for all steels. Crack opening displacement (COD) measurements were made on selected steels in the welded condition and a COD transition temperature was determined for these.

Over the ranges investigated, sulfur, manganese, and silicon had only minor effects on the base metal and welded impact toughness.

The best base metal impact toughness was achieved with a combination of (Nb + Al) stabilization. A niobium-stabilized steel to which 0.5 percent aluminum had been added exhibited a $FATT_{50}$ (fracture appearance transition temperature) of $-60°C$. Niobium stabilization and (Nb + Ti) stabilization gave transition temperatures intermediate between (Nb + Al) combination and titanium-stabilization.

The (Nb + Al) stabilizer combination also gave the best weld metal impact toughness with a $FATT_{50}$ of approximately 25°C; however, the steel had limited weld ductility. The niobium-stabilized steels had higher weld impact transition temperatures than the titanium-stabilized steel, with the mixed (Nb + Ti) combination being intermediate between them.

The (Nb + Ti) stabilized steel had the best COD fracture toughness and seems to be the best stabilizer choice for a combination of base metal and welded toughness and ductility.

KEY WORDS: ferritic stainless steels, 18Cr-2Mo stainless steel, impact toughness, crack opening displacement (cod), fracture toughness, transition temperature

Because of recent large-scale use of argon-oxygen decarburization and vacuum-oxygen decarburization, the low interstitial levels required for tough ferritic stainless steels have become economically possible. As a result, new compositions of iron-chromium-molybdenum and iron-chrom-

---

[1] Manager, Stainless Steel Development, Climax Molybdenum Co., Pittsburgh, Pa. 15222.

ium-molybdenum-nickel ferritic stainless steels have reached commer-
cialization. Among these, the 18Cr-2Mo steel has achieved the largest
production, with output coming from Japan, the United States, Europe,
and Australia. While known worldwide as "18Cr-2Mo," it is also fre-
quently called "Type 444" or simply "444" because it has been designated
S44400 under the new Unified Numbering System.

The fabrication and application of these steels inevitably require greater
understanding of the mechanical properties such as toughness and ductility.
The results presented here are a summary of a systematic study of the
effects of residual and stabilizing elements in 18Cr-2Mo stainless. The use
of stabilizers improves intergranular corrosion resistance by preventing
sensitization during welding. Good commercial melt practice typically
produces interstitial levels of approximately 0.015C and 0.015N; therefore,
these were chosen for the base composition of all the steels examined here.
Sulfur, manganese, and silicon were varied to explore their possible effect
on microhot-cracking. The amounts ranged from no deliberate addition to
amounts two to three times that normally found in commercial 18Cr-2Mo.
Other residual elements which were not varied (copper, nickel, and phos-
phorous) were added in amounts usually found in commercial heats. The
stabilizer element variables, namely, niobium, titanium, (Nb + Ti), and
(Nb + Al), spanned the range of commercial steels and also included some
experimental combinations.

Materials Preparation

Forty-nine 18Cr-2Mo ferritic stainless steel heats were vacuum induction
melted and cast under a one-half atmosphere of argon. The split-heat
technique was used to vary the residual and stabilizer elements to be
examined.

The ingots were forged to plates at 1200°C, hot-rolled at 1095°C, and
subsequently cold-rolled at 260 to 315°C to sheet approximately 3.2 mm
thick. The titanium-stabilized heats were recrystallized by heat treating
at 845°C for 5 min and water-quenching. The niobium-containing steels
had 5-min recrystallization temperatures between 980 and 1010°C. The
resulting microstructure was completely ferritic with carbonitrides scattered
throughout the matrix and with an average grain diameter of 20 to 50 μm
(ASTM Grain Size Nos. 5 to 8) determined in accordance with the ASTM
procedure for Estimating the Average Grain Size of Metals (E 112-74)
using the Single Circle (Hilliard) Procedure.

The chemical analyses of the steels are listed in Table 1. For some of the
alloy series where the stabilizer element is the variable, some of the steels
are understabilized. That is, the titanium content or niobium content or
both were less than that specified by the ASTM Specification for Heat-

Resisting Chromium and Chromium-Nickel Stainless Steel Plate, Sheet, and Strip for Fusion-Welded Unfired Pressure Vessels (A 240-75a), namely, (titanium, niobium) $\geq 4(C + N) + 0.20$. These steels have been included for completeness in assessing the effect of various stabilizer elements on toughness.

Experimental Procedures

Full-penetration gas-tungsten-arc bead-on-plate welds were made in the sheet perpendicular to the rolling direction at a speed of 635 mm/min. Prepurified argon was used in the torch, backup, and trailing shield. Quarter-size Charpy V-notch specimens were machined from the sheet in the base metal and welded conditions. The welded specimens were notched in the center of the fusion zone. Impact testing was conducted in accordance with the ASTM Methods and Definition for Mechanical Testing of Steel Products (A 370-76), and the fracture appearance transition temperature with 50 percent shear was determined.

The crack opening displacement (COD) specimens were also quarter-size Charpy specimens but without the V-notch. A 1-mm-deep (0.04 in.) notch was electrodischarge-machined at the center of the fusion zone. The notch was then extended an additional 1 to 2 mm by fatigue cracking. The total length of the precrack was determined after COD testing by fracturing the specimen and measuring the actual crack length. A three-point bend test fixture which satisfied the requirements of ASTM Plain-Strain Fracture Toughness of Metallic Materials (E 399-78) for fracture mechanics tests was used to determine the COD. The test procedure and calculations were patterned after those described by Barr et al [1].[2] The COD measurements were made over a range of temperatures to establish a COD transition temperature curve for the steels tested. For tests below room temperature, the bend test fixture was immersed in a tank containing solid carbon dioxide and methanol; above room temperature, heated silicone oil was used in the tank.

For general metallographic examination, the steels were mechanically polished and electrolytically etched in 50 percent aqueous nitric acid with the specimen as the cathode.

Bulk extraction residues were obtained from welds cut from some of the steels. The weld specimens were dissolved in an electrolyte of 10 percent hydrochloric acid in methanol with 1 percent tartaric acid at 200 to 300 mA at a potential of 2 to 3 V in a manner similar to that described by Donachie [2]. The residue was collected on a filter with a pore size of 0.20 μm, washed with methanol, and dried. X-ray diffraction traces were made on a

[2] The italic numbers in brackets refer to the list of references appended to this paper.

TABLE 1—*Chemical analyses of laboratory-produced 18Cr-2Mo ferritic stainless steels.*

Heat No.	Chemical Composition, weight %													
	Cr	Mo	C	N	O[a]	Mn	Si	S	P	Ni	Cu[b]	Al	Ti[b]	Nb
1581A	18.39	2.01	0.015	0.016	NA	0.007	0.07	0.004	0.002	0.052	NDA	0.018	NDA	0.39
B								0.010						
C								0.016						
D								0.031						
1629A	18.44	2.01	0.014	0.015	0.049	0.014	0.06	0.012	0.006	0.010	NDA	0.008	NDA	0.40
B			0.016	0.015		0.20								
C						0.40								
D						0.80								
1684A	17.63	2.10	0.014	0.017	0.028	0.42	0.15	0.010	0.015	0.22	0.09	0.024	0.26	0.03
B							0.34							
C							0.54							
D							0.96							
1686A	17.82	2.10	0.015	0.016		0.44	0.07	0.011	0.017	0.18	0.10	0.012	0.003	0.31
B							0.25							
C					0.018		0.44							
D					0.041		0.87							
1628A	18.35	2.02	0.018	0.017		0.46	0.48	0.012	0.020	0.15	0.10	0.015	0.01	0.10
B													0.13	
C					0.018								0.21	
D					0.041								0.29	
1503A	18.11	2.01	0.017	0.015	NA	0.45	0.54	0.014	0.026	0.20	0.10	0.026	0.007	0.22
B													0.11	
C													0.20	
D													0.31	
1504A	18.01	2.01	0.013	0.015	NA	0.45	0.52	0.012	0.019	0.21	0.10	0.024	0.01	0.33
B													0.11	
C													0.20	
D													0.29	

1505A	18.10	2.01	0.013	0.015	NA	0.45	0.53	0.012	0.016	0.20	0.10	0.025	0.01	0.44
B													0.12	
C													0.20	
D													0.31	
1682A	17.82	2.10	0.016	0.016	0.026	0.44	0.50	0.010	0.016	0.20	0.10	0.021	0.27	0.02
1772	17.95	2.08	0.016	0.015	0.023	0.44	0.43	0.009	0.016	0.20	0.09	0.019	0.10	0.28
1879A	18.20	1.98	0.016	0.020	0.029	0.39	0.37	0.010	0.013	0.20	0.08	0.041	0.006	0.16
B					0.025							0.33		
C					0.019							0.52		
1880A	18.16	1.98	0.015	0.021	0.033	0.39	0.40	0.011	0.011	0.20	0.08	0.014	0.006	0.22
B					0.024							0.28		
C					0.022							0.42		
1881A	18.24	2.01	0.015	0.021	0.029	0.38	0.37	0.010	0.012	0.19	0.08	0.43	0.006	0.32
B					0.022							0.33		
C					0.022							0.48		
20A	18.9	2.03	0.018	0.012	NA	0.45	0.53	0.010	0.021	0.28	0.11	0.04	0.34	
B													0.59	
C					NA							0.14	0.78	
22C	18.3	2.03	0.018	0.019	NA	0.43	0.48	0.013	0.018	0.28	0.11		0.37	0.26
1884A	18.18	1.99	0.016	0.018	0.034	0.45	0.40	0.009	0.012	0.20	0.08	0.052	<0.02	0.30
1972A	18.00	2.02	0.016	0.019	0.027	0.44	0.50	0.010	0.020	0.22	0.10	0.060	<0.01	0.35

[a] NA = not analyzed.
[b] NDA = no deliberate addition, not analyzed.

GE diffractometer equipped with a doubly bent graphite-crystal diffracted-beam monochrometer.

The Strauss test [ASTM Recommended Practices for Detecting Susceptibility to Intergranular Attack in Stainless Steels (A 262-75, Practice E)] was used to evaluate the effectiveness of mixed niobium plus titanium stabilization against intergranular corrosion. Duplicate weld sections were cut from selected steels, ground flush, polished through 600 grit paper, and degreased in hot trichlorethylene and a hot-water and detergent solution. The polished specimens were immersed for 24 h in a boiling aqueous solution of 16 percent sulfuric acid and 6 percent copper sulfate. The specimens were suspended in the solution in a vented 30-ml beaker containing 50 g of copper chips packed around them to insure good physical contact. After 24 h the specimens were bent through 180 deg with the weld at the apex of the bend. Because of their limited ductility, a modified Strauss test was used to evaluate the mixed niobium plus aluminum steels [*3*]. Polished, welded specimens were suspended in a boiling aqueous solution of 50 percent sulfuric acid and 6 percent copper sulfate. A 25-g piece of copper was also immersed in the test solution but not in contact with the specimen. After 120 h the specimens were examined metallographically for indications of intergranular corrosion and grain dropping.

Results

Residual Element Effects

The impact transition temperatures for the base metal and welded conditions are summarized in Table 2. For many of the steels, especially in the welded condition, 50 percent shear fracture appearance occurred over a range of temperatures due to experimental scatter. For this reason, a temperature interval has been listed rather than a single transition temperature.

Sulfur additions to the niobium-stabilized 18Cr-2Mo steel reduced the base metal impact toughness; the $FATT_{50}$ (fracture appearance transition temperature) rose from $-57°C$ at 0.004S to $-21°C$ at 0.031S. Weld metal impact toughness was not strongly affected by the sulfur content. Increasing sulfur contributed to more scatter but not to an absolute shift in the transition temperature. The $FATT_{50}$ of the welded specimens was approximately 50°C over the entire range of sulfur examined with the width of the scatter band increasing with increasing sulfur.

The addition of up to 0.80 manganese to a niobium-stabilized steel had little effect on the impact toughness of either the base metal or the weldment. The steel with no deliberate manganese addition (0.014Mn) had a sharply defined transition temperature in both the base metal and welded

condition. Manganese additions increased the amount of scatter especially after welding.

The effect of silicon on the impact toughness of 18Cr-2Mo steels with typical commercial purity levels is shown in Fig. 1. Silicon had a minor effect on impact toughness of the base metal regardless of whether niobium or titanium stabilization was used. The $FATT_{50}$ was $-40°C$ in a niobium stabilized steel with no deliberate silicon addition (0.07). Increasing the silicon content raised the transition temperature slightly and increased the amount of scatter, with most of the steels falling in a band from approximately -40 to $-22°C$. Titanium stabilization resulted in higher base metal impact transition temperatures; however, in all cases, the $FATT_{50}$ was below room temperature, with increasing silicon resulting in a small lowering of the transition temperature.

In the welded condition, silicon had essentially no effect on the impact toughness of the niobium-stabilized steels other than to increase the amount of scatter at intermediate silicon levels. Over the range of silicon typically found in commercial 18Cr-2Mo stainless steels (0.20 to 0.50), the impact transition temperatures were in a band from 52 to 82°C. For the welded titanium-stabilized materials, a minimum in the transition temperature occurred at 0.4 to 0.5 silicon. The welded titanium-stabilized steels exhibited better impact toughness than those with niobium stabilization although there was some overlap of impact transition temperatures. For the normal commercial range of silicon contents, the $FATT_{50}$ for the titanium-stabilized steels generally ranged from 32 to 57°C.

Niobium Plus Titanium Effects

The effect of combined niobium plus titanium stabilization on impact toughness is summarized in Fig 2. For the base metal specimens, increasing titanium resulted in continually increasing impact transition temperatures for the 0.10 and 0.22Nb steels. For the alloys with 0.34 and 0.44Nb, a maximum occurred in the $FATT_{50}$ of about 30°C at 0.20Ti. Further increases in titanium brought about an improvement in the toughness. When toughness was viewed as a function of niobium, the trend was less clear. The lowest transition temperatures occurred in the absence of titanium, as would be expected from the results in Fig. 1. At the 0.1, 0.2 and 0.3Ti levels, the transition temperatures fluctuated in an uneven fashion with increasing niobium and were generally within a band from -25 to $+25°C$. Heat-to-heat variations may well account for some of the variability. Similarly in the welded condition, there was no consistent trend with increasing niobium content. For the steels with 0.3Ti, there was a small but steady increase in transition temperature with increasing niobium. At the 0, 0.1,

TABLE 2—*Base metal and weld metal impact transition temperatures for 18Cr-2Mo ferritic stainless steel.*

Heat No.	Mn	Si	S	Al	Ti[a]	Nb	FATT$_{50}$, °C Base	FATT$_{50}$, °C Weld
1581A	0.007	0.07	0.004	0.018	NDA	0.39	−57	41 to 54
B	...	...	0.010	...	...	...	−34	27 to 49
C	...	...	0.016	...	...	...	−32	57 to 77
D	...	...	0.031	...	...	...	−21	27 to 66
1629A	0.014	0.06	0.012	0.008	NDA	0.40	−26	57
B	0.20	...	...	...	...	...	−41 to −29	46 to 63
C	0.40	...	...	...	...	...	−23 to −18	28 to 57
D	0.80	...	...	...	...	...	−43	43 to 57
1684A	0.42	0.15	0.010	0.024	0.26	0.03	0 to 17	52 to 61
B	...	0.34	...	...	...	...	−4 to 0	33 to 54
C	...	0.54	...	...	...	...	−7	33 to 53
D	...	0.96	...	...	...	...	2	53 to 66
1686A	0.44	0.07	0.011	0.012	0.003	0.31	−40	60 to 67
B	...	0.25	...	...	...	...	−37	42 to 44
C	...	0.44	...	...	...	...	−32 to −23	52 to 67
D	...	0.87	...	...	...	...	−32 to −23	66 to 79
1628A	0.46	0.48	0.012	0.015	0.01	0.10	−51	58
B	...	...	...	...	0.13	...	−4	21 to 43
C	...	...	...	...	0.21	...	+2	57 to 70
D	...	...	...	...	0.29	...	11	85
1503A	0.45	0.54	0.014	0.026	0.007	0.22	−68	27
B	...	...	...	...	0.11	...	−23 to 26	60
C	...	...	...	...	0.20	...	−4	91
D	...	...	...	...	0.31	...	17	99
1504A	0.45	0.52	0.012	0.024	0.01	0.34	−54	57
B	...	...	...	...	0.11	...	8	68
C	...	...	...	...	0.20	...	18 to 29	60
D	...	...	...	...	0.29	...	−21	104

	0.45	0.53	0.012	0.025	0.01	0.44		
1505A	0.45	0.53	0.012	0.025	0.01	0.44	−27	57 to 66
B	...	...	...	...	0.12	...	−21	27 to 38
C	...	...	...	...	0.20	...	23 to 29	93
D	...	...	...	...	0.31	...	4	104
1682A	0.44	0.50	0.010	0.021	0.27	0.02	3 to 10	52 to 57
1772	0.44	0.43	0.009	0.019	0.10	0.28	−14 to +1	86 to 92
1879A	0.39	0.37	0.010	0.041	0.006	0.16	−73 to −62	66 to 77
B	...	...	...	0.33	...	...	−48 to −34	−29 to −22
C	...	...	...	0.52	...	...	−73 to −62	−43 to −18
1880A	0.39	0.40	0.011	0.014	0.006	0.22	−52 to −43	10 to 16
B	...	...	...	0.28	...	...	−41 to −18	54 to 66
C	...	...	...	0.42	...	...	−34	−22 to −8
1881A	0.38	0.37	0.010	0.043	0.006	0.32	−22	66
B	...	...	...	0.33	...	...	−22 to −1	79 to 93
C	...	...	...	0.48	...	...	−59	10 to 38
20A	0.45	0.53	0.010	0.04	0.34	...	b	4[c]
B	...	...	...	...	0.59	...	b	32[c]
C	...	...	...	...	0.78	...	b	38[c]
22C	0.43	0.48	0.013	0.14	0.37	0.26	b	82[c]
1884A	0.45	0.40	0.009	0.052	<0.02	0.30	−43	64 to 82
1972A	0.44	0.50	0.010	0.060	<0.01	0.35	−12	60 to 71

[a] NDA = no deliberate addition, not analyzed.
[b] = Base metal transition temperature not determined.
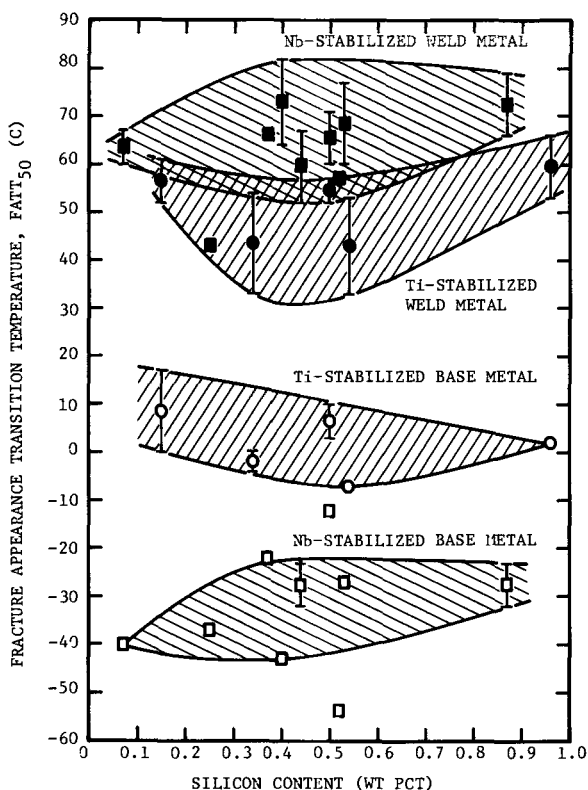[c] = 10.2 J energy absorption criterion, Ref 8.

FIG. 1—*Impact toughness of 18Cr-2Mo ferritic stainless steel as a function of silicon content. The limit bars indicate the temperature range over which 50 percent shear was observed. Quarter-size Charpy V-notch specimens.*

and 0.2Ti levels, the variability with increasing niobium did not follow a consistent pattern.

Based on expressions derived by Bond et al [4] to predict the minimum niobium or titanium content required to prevent sensitization during welding, four of the mixed niobium-plus-titanium steels were close to the minimum and therefore were subjected to the Strauss test (ASTM A 262-75, Practice E). They were the 0.10Nb steels with 0.01 and 0.13Ti and the 0.22Nb steels with 0.007 and 0.11Ti. Only the 0.10Nb-0.01Ti alloy failed; all the others contained sufficient stabilizer to prevent intergranular corrosion.

Niobium Plus Aluminum Effects

The effects of combined niobium plus aluminum stabilization on impact toughness are summarized in Fig. 3. In the base metal, a maximum in
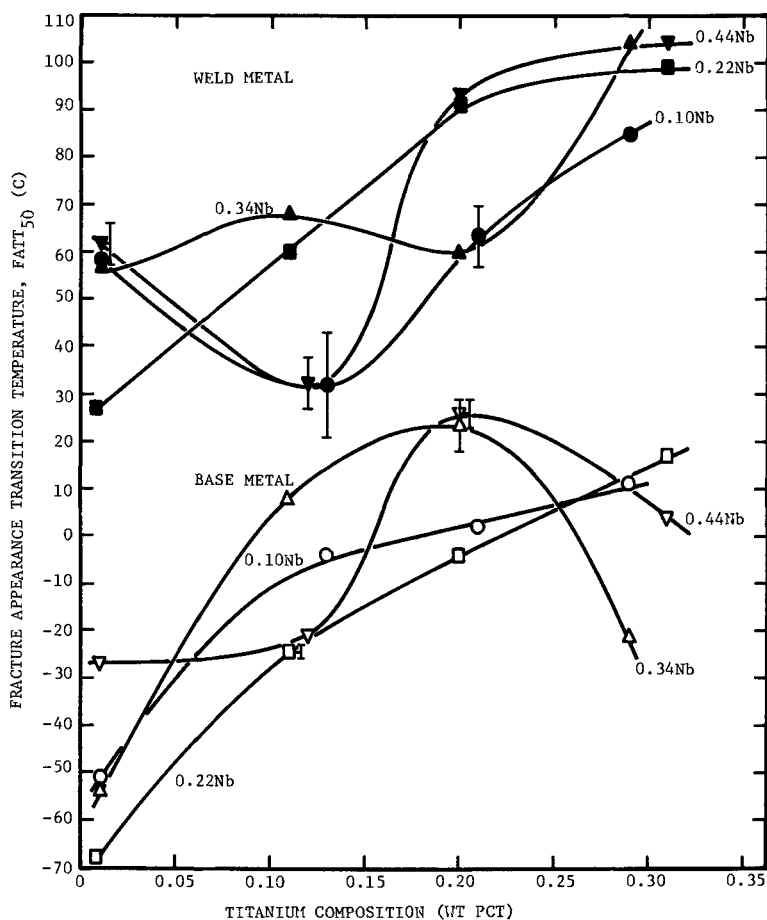
FIG. 2—*Impact toughness of 18Cr-2Mo ferritic stainless steel as a function of niobium and titanium content. Quarter-size Charpy V-notch specimens.*

transition temperature occurred at about 0.3Al for all three niobium levels tested. Further increases to approximately 0.5Al produced significant improvements in the toughness. Increasing the niobium level consistently increased the $FATT_{50}$ over the entire aluminum range examined. The 0.32Nb steels had the highest transition temperatures but still were lower than 0°C in all cases; for the 0.32Nb-0.48Al steel, the transition temperatures dropped to nearly −60°C. The weld metal impact toughness paralleled that of the base metal for the 0.22 and 0.32Nb steels. A maximum occurred in the transition temperature at about 0.3Al followed by a large drop in the transition temperature at about 0.5Al. The aluminum effect in the 0.16Nb steel was different, with increasing aluminum continuously
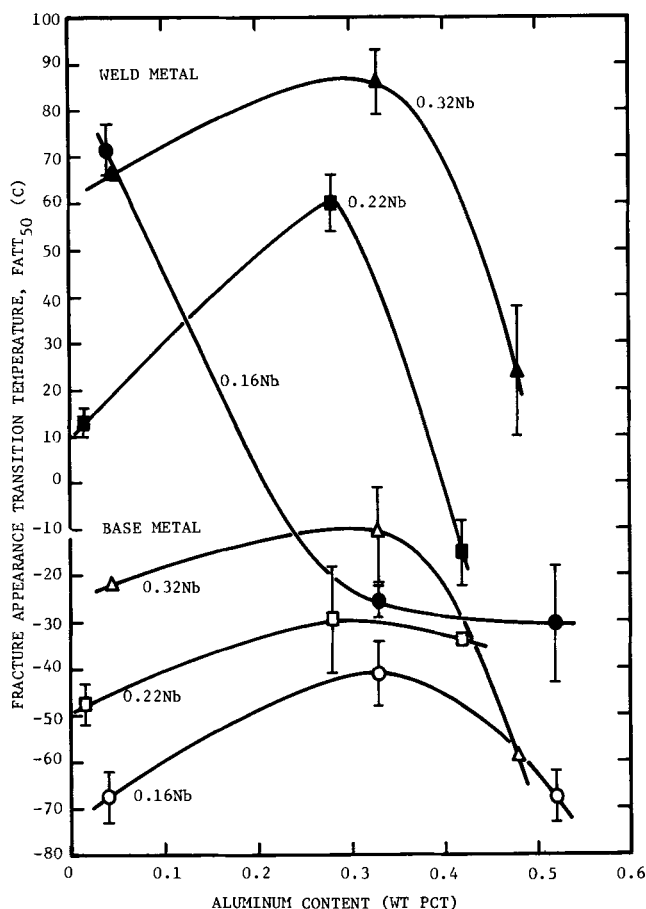
FIG. 3—*Impact toughness of 18Cr-2Mo ferritic stainless steel as a function of niobium and aluminum content. The limit bars indicate the temperature range over which 50 percent shear was observed. Quarter-size Charpy V-notch specimens.*

improving toughness. The weld metal impact transition temperature was approximately −30°C at the highest aluminum level.

The difference in the behavior of the 0.16Nb steel may be due to the interaction of niobium, aluminum, and the interstitial elements. Only the 0.32Nb steel passed the 50 percent Strauss test. Increasing aluminum improved intergranular corrosion resistance in the 0.16 and 0.22Nb steels, but even the highest aluminum levels examined failed to confer complete immunity to intergranular attack. The 0.16Nb steel with no deliberate aluminum addition went active during the 50 percent sulfuric acid copper sulfate test and catastrophic corrosion resulted. With the addition of 0.33Al, only a limited amount of grooving and grain dropping resulted. It

seems likely that aluminum combined with some of the interstitial atoms (probably nitrogen), thereby improving intergranular corrosion resistance. Lowering the uncombined interstitial content has been shown to improve impact toughness [5,6], and the formation of aluminum nitrides would provide a scavenging effect which could improve toughness by this mechanism.

COD Fracture Toughness

The weld metal COD fracture toughness measurements for three titanium-stabilized steels, one mixed niobium-titanium steel, and one mixed niobium-titanium-aluminum steel are summarized in Table 3. The test temperatures for which crack extension occurred by transgranular cleavage are indicated. The highest such temperature for each steel can be regarded as a type of transition temperature. For the 0.28Nb-0.10Ti steel, all the tests up

TABLE 3—*Cracking opening displacement test results for welded 18Cr-2Mo stainless steels with 0.030 (C + N).*

	Crack Opening Displacement and Stabilizer Content				
Test Temperature, °C	0.34Ti, mm	0.59Ti, mm	0.78Ti, mm	0.28Nb + 0.10Ti, mm	0.26Nb + 0.32Ti + 0.14Al, mm
−18	...	...	...	0.10[a]	...
−4	0.05[a]	...	...	0.41[a]	...
−4	...	...	...	0.05[a]	
10	0.05[a]	0.03[a]	...	0.13[a]	...
10	...	...	...	0.05[a]	...
16	...	...	...	0.64[a]	...
21	...	...	...	1.02[a]	...
22	0.91	0.86	0.03[a]	...	0.03[a]
22	...	0.10[a]	0.03[a]	...	0.05[a]
22	...	0.97	...	...	0.03[a]
22	...	0.81	...	...	...
23	...	...	...	0.66	...
23	...	...	...	0.89	...
24	0.08[a]	...	0.05[a]	...	...
38	0.10[a]	...	...	...	...
52	0.25[a]	...	0.05[a]	0.15[a]	0.10[a]
66	0.43	0.13[a]	...	...	...
79	...	...	0.13[a]	0.56	0.10[a]
79	...	...	...	...	0.25[a]
93	0.76	...	...	...	...
107	...	0.94	0.03[a]	...	0.51
121	...	...	...	...	0.56
135	...	1.19	0.76	...	...

[a] Crack extension occurred by transgranular cleavage.

to and including 21 °C resulted in crack extension by cleavage. The tests at 23 and 79 °C were ductile. The measurements at 16 and 21 °C resulted in a large amount of plastic deformation prior to brittle crack extension; in fact, the amount of ductility was similar to the specimens tested at 23 °C. The test at 52 °C gave apparently anomalous results in that ductile behavior would be expected; however, crack extension occurred by cleavage. The extent of ductile behavior and the similarity of COD values over the temperature interval 16 to 23 °C suggest that it is the COD transition temperature range for this steel. For all the other steels, the highest temperature with cleavage crack extension corresponds closely to significant increases in the critical COD values as shown by the COD transition temperature curves in Fig. 4.

The (Nb + Ti) mixed stabilizer exhibited better COD fracture toughness than any of the other steels. Increasing amounts of excess stabilizer adversely affected the fracture toughness; for example, increasing the titanium content resulted in low COD values (on the order of 0.1 mm) at increasing temperatures. That total excess stabilizer, rather than excess titanium only, is deleterious is indicated by the high COD curve for the steel containing (Nb + Ti + Al).

For the titanium-stabilized steels, the impact transition temperatures were lower than the COD transition temperatures with the difference between the two increasing with increasing stabilizer content. For the steel with (Nb + Ti + Al) mixed stabilization, the two transition temperatures were approximately the same. For the (0.28Nb + 0.10Ti) steel, the impact transition temperature was higher than the COD transition temperature. The same relative ordering of these two transition temperatures has been observed for high-purity, very low interstitial [0.007(C + N)] 18Cr-2Mo steels containing less than 0.45 niobium [7]. Apparently niobium and
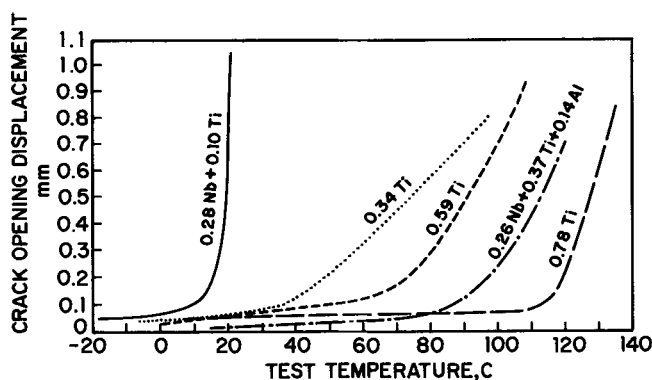

FIG. 4—*COD fracture toughness transition temperature curves for welded 18Cr-2Mo steels with a variation in stabilizing elements. Precracked quarter-size Charpy specimens.*

titanium have opposite effects on the relative ordering of the impact and COD transition temperatures, with the element in greatest quantity tending to dominate.

Microstructure

The choice of stabilizing element has been shown by Sawhill and Bond to strongly affect the weld microstructure of 18Cr-2Mo stainless steels [*8*]. For steels containing niobium as the sole stabilizing element, long columnar grains formed between the fusion line and the center of the weld. The weld centerline was continuous and very distinct. Niobium carbonitrides were distributed throughout as precipitate particles so small that their shape could not be resolved by optical microscopy. For the titanium-stabilized steels, the fusion zone contained primarily equiaxed grains and there was no centerline. The titanium carbonitrides were quite large and usually had a cubic morphology. Calmer and Grinder have demonstrated that titanium nitride particles form in the melt during the solidification of 18Cr-2Mo stainless steel [*9*]. It seems quite likely that titanium nitride particles act as nuclei for the formation of the ferrite grains, thereby producing the equiaxed microstructure.

The mixed (Nb + Ti) stabilized steels had weld microstructures which showed a titanium effect. The steels with no deliberate titanium additions displayed weld microstructures typical of niobium-stabilized steels. The smallest deliberate titanium addition (0.11) broke up the well-defined centerline by the formation of small equiaxed grains at the center of the fusion line. Further increases in the titanium content tended to cause a broadening of the band of equiaxed grains. The titanium nitride mechanism of microstructure alteration was supported by the X-ray diffraction results. The diffraction pattern of extracted residue from the niobium-stabilized steels matched that of the niobium carbide and probably was actually niobium carbonitride. The residues from the welds with deliberate titanium additions contained niobium carbide and titanium nitride. The stabilizing elements exhibited a very specific preference for each of the major interstitial elements.

The addition of aluminum to the mixed (Nb + Al) stabilized steels did not alter the weld microstructure from that typical of a niobium-stabilized weld. The welds were characterized by long columnar grains and a distinct weld centerline. In the absence of aluminum additions, the extraction residue from the welds gave the X-ray pattern for niobium carbide only. At the 0.3 and 0.5 aluminum levels, a weak pattern for aluminum nitride was also observed.

No microhot-cracking was observed in the welds of any of the steels evaluated, thus indicating a minimal effect of sulfur, manganese, and silicon, at least, over the ranges investigated.

Discussion

The steels in which sulfur and manganese were the variables contained no additions to simulate typical commercial-purity steels except carbon and nitrogen. All of the other steels discussed here were designed to have impurity levels one would expect in good commercial melt practice. Because of these differences, an absolute comparison of impact toughness results may not be appropriate. On the other hand, the trends induced by single-element variables are probably less sensitive to alloy purity. Of the residual elements examined, namely, sulfur, manganese, and silicon, none had a strong influence on base metal and weld metal impact toughness over the composition ranges studied. The effect of some residual elements of base metal toughness was investigated by Abo et al for a more highly alloyed ferritic stainless steel [10]. For an unstabilized 21Cr-1Mo steel with 0.002 to 0.005 carbon and 0.004 to 0.005 nitrogen, there was no effect with sulfur additions up to 0.037 percent and no manganese effect above 0.2, but increasing silicon did increase the impact transition temperature. The differences in the interstitial and stabilizer content make it difficult to extrapolate those results to the 18Cr-2Mo steels; nonetheless, they do in general support the indications of the modest influence of some of the residual elements unavoidably present in these steels.

While oxygen effects were not examined explicitly, the large number of heats does provide a means of assessing some effects. When titanium-stabilized heats are compared with niobium-stabilized steels, it is apparent that titanium is the more effective deoxidizing agent. When niobium stabilization is employed, the oxygen content is typically 270 to 41 ppm; for titanium stabilization or mixed (Nb + Ti) stabilization, the oxygen levels drops to 230 to 280 ppm. If oxygen levels of 400 ppm adversely affect toughness, that effect is more than offset by the beneficial influence of niobium stabilization because the niobium-stabilized steels consistently had lower base metal impact transition temperatures than the titanium-stabilized alloys (see Fig. 1). The well-known deoxidizing effect of silicon is shown in the two heats in which silicon was the chief variable. For both niobium and titanium stabilization, the oxygen content was lowered to about 180 ppm when the silicon levels approached 1 percent. The deoxidizing effect of deliberate aluminum additions seemed similar to the titanium effects. With aproximately 0.5 aluminum, the oxygen content was reduced to 190 to 220 ppm. Even though there were significant improvements in the base metal toughness by increasing from 0.3 to 0.5 aluminum, the corresponding reductions in oxygen content were minor. Abo et al have shown that significant improvements in the impact toughness of 25Cr-3Mo ferritic steels did not occur until the oxygen content was about 50 ppm [10]. A similar effect was noted by Hochmann in 25Cr steels [11]. It may well be that similar oxygen levels would be required in the 18Cr-2Mo steels before

any oxygen effect could be observed. That could account for the relative insensitivity of transition temperatures to changes in oxygen content on the order of 200 ppm in these steels.

Both Charpy impact tests and COD measurements offer some advantages as methods for evaluating toughness. The impact toughness test in relatively inexpensive both in terms of specimen preparation and actual conduct of the test; however, a fundamental interpretation of the results is lacking. The COD test is considerably more costly but fracture toughness is a fundamental material property. Furthermore, COD measurements can be used as a means of estimating resistance to fracture propagation because the critical COD can be related to critical defect size [*12,13*]. The COD fracture toughness test is performed at a substantially slower strain rate than the Charpy impact test. Because the slower strain rate more closely approximates the environment in which many of the materials are used, the COD transition temperature may be the more useful criterion for design specification. Because of the difference in cost of the two toughness tests, it would be desirable to use one as an estimator of the other. Unfortunately, niobium and titanium have opposing effects on the relative positions of the two transition temperatures, thereby making the impact transition temperature an unreliable indicator of the COD transition temperature.

Of the welded steels evaluated by COD testing, the mixed (Nb + Ti) stabilized alloy with a total stabilizer content close to the optimum amount had the best fracture toughness. The titanium-stabilized alloys had higher COD transition temperatures and were adversely affected by increasing amounts of excess stabilizer. The deleterious effect of excess stabilizer was also observed in the impact toughness test. For the (Nb + Ti) mixed stabilizer steels in the base metal condition and especially in the welded condition, increasing total stabilizer content correlated well with increasing impact transition temperature. Regardless of whether the impact toughness or the fracture toughness criterion is used, there is abundant evidence that best toughness will be achieved in 18Cr-2Mo ferritic stainless steel by minimizing the amount of stabilizer in excess of that required to prevent sensitization.

If toughness evaluation is based on the impact transition temperature criterion, the influence of the stabilizer element is much greater than that of any of the residual elements examined. If a single stabilizing element is used, niobium offers substantial improvements over titanium for base metal toughness. The (Nb + Ti) combination results were intermediate between these two single-stabilizer possibilities. The addition of 0.5Al to a steel already stabilized with 0.32Nb produced the best impact transition temperature, nearly −60°C. The failure of aluminum additions to prevent sensitization in alloys with lower niobium levels indicates that the aluminum does not readily combine with carbon. This is supported by the X-ray

observation of aluminum nitride. The heat of formation of aluminum nitride is nearly as large as that of titanium nitride, and aluminum nitride is noted for its stability [14]. As a result, the amount of interstitial nitrogen in the ferrite grains is probably quite low. This in turn could lead to lower dislocation activation energy and increasing dislocation mobility with a corresponding improvement in toughness. The amount of aluminum in the steels with the best impact toughness was far greater than the stoichrometric amount required to combine with all the nitrogen present. This indicates that aluminum may also play a solid solution role in improving toughness.

Weld metal impact toughness was less strongly affected by choice of stabilizer than the base metal toughness. In the case of a single stabilizer element, titanium resulted in lower transition temperatures than niobium but they overlapped from approximately 50 to 60°C. This differs somewhat from the results of Sawhill in which two split heats were examined—one niobium-stabilized, the other titanium-stabilized [8]. For those steels, the niobium-stabilized material had the lower impact transition temperature in both the base metal and welded conditions. While there is agreement on the base metal results, the larger number of steels studied here shows that titanium-stabilized 18Cr-2Mo has the lower weld metal impact transition temperature. A direct comparison of the results is complicated by the choice of different criteria for the transition temperature. In one case, fracture appearance with 50 percent shear was used while Sawhill used energy absorption of 10.2 J. Fracture appearance tends to be the more conservative measure and frequently results in a higher transition temperature than 10 J, for example, would give for the same steel. One variable influencing weld toughness is heat input; as a general rule, lower heat inputs produce tougher welds, all other things being equal. For the steels studied here, the heat inputs for the niobium- and titanium-stabilized steels were approximately equal. For the titanium-stabilized steels examined by Sawhill, the heat input was 30 to 50 percent greater than for similar steels studied here and this may have adversely affected the toughness of those steels. From Fig. 1 it is clear that there is sufficient heat-to-heat variation that the transition temperature is best characterized by a scatter band. Considering the larger specimen size examined here, the body of evidence shows that the titanium-stabilized weldments would be expected to have lower impact transition temperatures than otherwise comparable niobium-stabilized steels. Mixed niobium-titanium stabilization generally gave transition temperatures between the single stabilizer results. Mixed niobium-aluminum stabilization at the 0.5Al level resulted in the best weld metal impact toughness as discussed in the foregoing.

For many applications, toughness requirements must be combined with weld ductility. While the choice of stabilizer element has no effect on base metal ductility, it profoundly influences the ductility of weldments.

By means of Olsen cup tests, Sawhill demonstrated that the weld ductility of titanium-stabilized 18Cr-2Mo approaches that of the base metal; on the other hand, welds in niobium-stabilized steels have limited ductility and frequently fail in a brittle manner [8]. Similar tests were conducted on the steels discussed here with regard to toughness, and the detailed results will be reported elsewhere. It was found that titanium-stabilized and mixed niobium-titanium stabilized steels had excellent ductility. Niobium stabilization and niobium-aluminum stabilization resulted in more limited ductility. One distinguishing feature was the weld microstructure. When the fusion zone was characterized by long, columnar grains and a distinct weld centerline, the weld usually exhibited limited ductility and fractured by transgranular cleavage. There was evidence of microhot-cracking in some of these steels. Whenever there was sufficient titanium present to nucleate equiaxed grains at the center of the fusion zone and break up the distinct weld centerline, the ductility was greatly improved.

Because differing stabilizing elements have conflicting effects on toughness and ductility, the choice of the optimum stabilizer necessarily involves compromises. When base metal and weld metal toughness are considered along with base metal and weld metal ductility, the mixed niobium-titanium combination seems to be the best stabilizer choice for 18Cr-2Mo ferritic stainless steels, at least among those examined here. Continuing research may lead to choices which represent a better optimization of mechanical properties. The niobium-aluminum combination appears particularly promising with regard to excellent toughness; perhaps the addition of titanium or some other third stabilizing element will lead to the next level of improvement in these steels.

Summary

For a series of 18Cr-2Mo ferritic stainless steels with approximately 0.015C and 0.015N:

1. The residual elements manganese, silicon, and sulfur had only a minor influence on the base metal and weld metal impact toughness.

2. The base metal $FATT_{50}$ was below room temperature for all stabilizing elements examined.

3. The niobium-stabilized steels had better base metal impact toughness than titanium-stabilized steel, with mixed niobium-titanium stabilization producing results between the two.

4. The weldment impact transition temperature was better in the titanium-stabilized alloys than in the niobium-stabilized alloys, although some overlapping of the two occurred. Mixed niobium-titanium stabilization gave results between the extremes of the steels with a single stabilizer.

5. A niobium-stabilized steel to which 0.5Al had been added gave the

lowest impact transition temperatures in both the base metal and welded conditions but suffered from limited weld ductility.

6. Increasing total niobium and titanium content tended to increase the impact transition temperature.

7. Among the mixed (Nb + Ti) stabilized and titanium-stabilized steels examined, mixed (Nb + Ti) stabilization gave the best COD fracture toughness.

8. Mixed (Nb + Ti) stabilization in an amount close to the minimum required for stabilization produced the optimum combination of base metal and weld metal toughness and ductility.

References

[1] Barr, R. R., Elliott, D., Terry, P., and Walker, E. F., *Metal Construction,* Vol. 7, No. 12, Dec. 1975, p. 604.
[2] Donachie, M. J., Jr., and Kriege, O. H., *Journal of Materials,* Vol. 7, No. 3, 1972, p. 269.
[3] Streicher, M. A., *Corrosion,* Vol. 20, 1964, p. 57t.
[4] Bond, A. P., Dundas, H. J., and Lizlovs, E. A., "Stabilization of Ferritic Stainless Steels," Symposium on New Higher Chromium Ferritic Stainless Steels, ASTM National Meeting, Dec . 1973.
[5] Binder, W. O. and Spendelow, H. R., Jr., *Tranactions,* American Society for Metals, Vol. 43, 1951, p. 759.
[6] Semchyshen, M., Bond, A. P., and Dundas, H. J. in *Proceedings,* Symposium Toward Improved Ductility and Toughness, Kyoto, Japan, Oct. 1971, p. 239.
[7] Redmond, J. D., Climax Molybdenum Co., Mich., unpublished data, 1977.
[8] Sawhill, J. M., Jr., and Bond, A. P., *Welding Journal,* Vol. 55, No. 2, 1976, p. 33-s.
[9] Calmer, B. and Grinder, O., "On the Solidification of Low Interstitial Ferritic Chromium Steels," Report IM-1319, Swedish Institute for Metals Research, Stockholm, Sweden, 1978.
[10] Abo, H., Nakazawa, T., Takemura, S., Onogama, M., Ogawa, H., and Okada, H. in *Proceedings,* "Stainless Steel '77," sponsored by the Climax Molybdenum Co., London, England, 26-27 Sept. 1977, p. 35.
[11] Hochmann, J., *Transactions,* American Society for Metals, Vol. 43, 1951, p. 774.
[12] Dawes, M. G., *Welding Journal,* Vol. 55, No. 12, p. 1052.
[13] Serensen, S. V., *Automatic Welding,* Vol. 28, No. 2, 1975, p. 42.
[14] Goldschmidt, H. J., *Interstitial Alloys,* Plenum Press, New York, 1967, p. 218, 234-235.

DISCUSSION

C. R. Thomas[1] *(written discussion)*—The trends shown in quarter-size Charpy V-notch (CVN) tests are not the same as those for full-size tests. Would the author please comment on the results obtained with full-size 10 by 10-mm CVN specimens machined from 12-mm square bar? An analysis is given in Table 4.

[1] Cranfield Institute of Technology, Department of Materials, Cranfield, Bedford, U.K.

TABLE 4—*Analysis.*

Steel	C	N	O	Si	Mn	P	S	Cr	Mo	Ti	Al	Nb
Nb—stabilized	0.011	0.016	0.019	0.38	0.41	0.013	0.010	18.18	2.00	0.005	0.045	0.23
Ti—stabilized	0.013	0.020	0.020	0.36	0.40	0.013	0.018	18.18	2.00	0.31	0.065	0.025
Mixed A	0.012	0.020	0.019	0.39	0.40	0.013	0.010	18.18	1.99	0.21	0.037	0.12
Mixed B	0.011	0.016	0.022	0.38	0.41	0.013	0.010	18.18	2.00	0.24	0.044	0.22

Steel	$FATT_{50}$ (annealed)	$FATT_{50}$ (after weld simulation 1350°C peak temperature)
Nb—stabilized	−50°C	0°C
Ti—stabilized	+45°C	+115°C
Mixed A	−10°C	+30°C
Mixed B	+10°C	+50°C

J. D. Redmond (*author's closure*)—The quarter-size and full-size Charpy results for the base metal are in complete agreement; namely, niobium-stabilization produces the best impact toughness with mixed niobium-plus-titanium stabilization giving impact toughness between that of the niobium-stabilized and the titanium-stabilized alloys.

The conclusions with regard to the effect of stabilizer element on weld metal impact toughness presented in the paper are based on nine niobium-stabilized and five titanium-stabilized alloys. While there is scatter and some heat-to-heat variability, the titanium-stabilized steels consistently gave the better impact toughness. The weld simulation experiments of Mr. Thomas did not produce liquid metal and this could have resulted in a number of differences. The size and distribution of carbonitrides would be different and since the edges and corners of the titanium carbonitrides may act as fracture initiation sites, this could be a significant difference. The poor ductility of the niobium-stabilized steels suggests the possibility of microhot-cracking associated with the formation of a low-melting-point, niobium-containing, eutectic film. The formation of such a film with attendant hot cracks is more likely during actual welding than in a weld simulation.

J. R. Wood[1]

Effect of Residual Elements and Molybdenum Additions on Annealed and Welded Mechanical Properties of 18Cr Ferritic Stainless Steels

ABSTRACT: The annealed and welded mechanical properties of titanium-stabilized 18 percent chromium (18Cr) ferritic steels were studied as functions of molybdenum content (0, 1, and 2 percent) and residual levels. The residual elements carbon, nitrogen, manganese, silicon, nickel, copper, and molybdenum were evaluated at low levels typical of virgin-charge, vacuum melt practice and at moderate levels typical of electric-arc furnace melt practice. It was found that the residual elements manganese, silicon, nickel, and copper and excess titanium [defined as total titanium minus that necessary for stabilization of carbon plus nitrogen (C + N)] influenced annealed and welded tensile properties to the greater degree, whereas titanium, (C + N), and molybdenum additions of 1 and 2 percent were more influential on as-welded toughness. Impact transition temperatures of welds were lowered by as much as 100 deg F (55 deg C) in 18Cr alloys by decreasing residual, titanium, and (C + N) levels from typical to very low levels. Titanium was found to be the most potent solid solution strengthening element. Titanium was approximately twice as effective as molybdenum and slightly more effective than the combined effects of other substitutional residual elements. For light-gage applications such as sheet, strip, or welded tubing, a good combination of strength, ductility, and toughness was found with a low (C + N), low-titanium, low-residual analysis at all molybdenum levels studied. For heavier-gage applications such as plate or piping, where ductility and toughness are probably more sensitive to grain size and annealing and welding variables, it is also implied that a low-residual, low-titanium, low (C + N) analysis would be beneficial for a good combination of toughness and ductility.

KEY WORDS: ferritic stainless steels, residual elements, interstitial elements, tensile properties, ductility, toughness, fracture toughness

[1]Metallurgy manager, Ring Products, Standard Steel Division of Titanium Metals Corp. of America, Burnham, Pa. 17009.

Advancements in melting and refining technology such as vacuum induction melting, argon-oxygen decarburization, and vacuum and electron-beam refining have made possible the production of large tonnages of low carbon and nitrogen (C + N) stainless steels. One group of steels which benefits from lower (C + N) levels is the 18 percent chromium (18Cr) ferritic stainless steels. Binder and Spendelow [1][2] and Semchyshen et al [2] showed that 18Cr steels must contain below about 0.05 percent (C + N) to have good room-temperature toughness in the annealed condition. In the as-welded or high-temperature annealed condition the tolerance was lowered to 0.03 percent maximum (C + N) [2]. For 18Cr-2Mo steels, similarly low levels of (C + N) were preferred for adequate toughness and ductility [2].

Very low interstitial levels of (C + N) (0.01 percent total) are necessary for resistance to intergranular corrosion following welding or high-temperature annealing of both 18Cr and 18Cr-2Mo types [2,3]. Because such low levels are difficult to achieve economically, stabilization with titanium or niobium is preferred at moderately low levels of (C + N) (0.02 to 0.05 percent total), which renders the 18Cr and 18Cr-2Mo alloys resistant to intergranular corrosion [2,4,5]. Although titanium additions are beneficial for stabilization against high-temperature embrittlement or intergranular corrosion or both, excessive amounts can be detrimental to toughness and ductility [2,6] and internal cleanliness and surface appearance [7]. Therefore, it is desirable to lower the (C + N) in order to minimize the titanium addition required for stabilization.

In addition to the interstitial elements, other residual elements may have importance in regard to toughness and ductility of 18Cr ferritic steels. Wright [8] observed in 26Cr-1Mo alloys that, in addition to carbon, nitrogen, and titanium effects, certain levels of the residual elements phosphorus, sulfur, manganese, silicon, copper, and nickel adversely affected impact properties of welded and annealed material. Effects of these other residual elements on 18Cr ferritic stainless steels have not been clearly established.

This investigation studied the effects of the residual elements carbon, nitrogen, manganese, silicon, nickel, and copper on the mechanical properties and weldability of 18Cr, 18Cr-1Mo, and 18Cr-2Mo alloys. All heats were stabilized with titanium, aiming for a minimum titanium level of 0.2 + 4 (C + N) to prevent sensitization during welding and subsequent intergranular corrosion of welds. Two levels of interstitials were studied, one simulating typical electric-arc furnace purity level and the other a moderate-to-low level achievable by the vacuum melting and refining techniques previously mentioned. Because of increased attention to the use of 18Cr ferritic steels in welded tubing applications, the present study was aimed primarily at the effects of residual elements on the properties of light-gage

---

[2] The italic numbers in brackets refer to the list of references appended to this paper.

strip material in both annealed and welded conditions. However, the general effects studied would probably be applicable to heavier-gage applications such as plate and piping.

Experimental Procedure and Results

Processing

Nine laboratory heats were vacuum induction melted and cast into 102-mm (4 in.) square ingots weighing approximately 22.7 kg (50 lb) each. Heat chemistries are shown in Table 1. Heats A through E contained 18Cr, Heats F and G contained 18Cr-1Mo, and Heats H and I contained 18Cr-2Mo. All heats had titanium additions which ranged from 0.30 to 0.79 percent depending upon the (C + N) content. Heats A and B contained low levels of (C + N) and either low or high (normal levels expected with conventional electric-arc melting) levels of the residual elements manganese, silicon, nickel, molybdenum, and copper, respectively. Heats C and D contained higher levels of (C + N) with low and high residual elements, respectively. Heat E was similar to Heat A with the exception of the higher titanium addition, which was deliberately made to assess the effects of excess titanium on properties. Heats F and G and Heats H and I with molybdenum additions, respectively, contained low and high total residual elements including (C + N).

Ingots were hot-rolled from 1121°C (2050°F) to 3.2-mm (0.125 in.) strip, finishing at approximately 816°C (1500°F). Hot-rolled strip specimens were annealed at 899°C (1650°F), descaled, cold-rolled to 1.27-mm (0.050 in.), annealed at 899°C (1650°F) for 5 min, and pickled. Annealed microstructures for all heats showed a uniform grain size of about ASTM 6 to 7.

Welding and Mechanical Testing

Duplicate longitudinal and transverse tension specimens were tested at room temperature with the tensile properties given in Table 2. The variation in properties between test directions was no greater than the variation between duplicate specimens in the same direction; therefore, for convenience, the longitudinal and transverse properties were averaged. A plot of tensile properties versus residual levels is shown in Fig. 1. A plot of tensile properties versus molybdenum content is shown in Fig. 2.

Autogenous gas tungsten-arc welds are made in a single pass using argon as both shield and backup gas. Longitudinal tension specimens were prepared from the as-welded strip with the weld bead centered in the reduced section and lying parallel to the tensile axis. The weld metal constituted approximately one-half the cross-sectional area in the reduced section. Tension test results are given in Table 3.

TABLE 1—*Composition of alloys studied.*

Heat	Weight %									
	C	N	Mn	Si	Cr	Ni	Mo	Cu	Ti	Excess Ti[a]
A	0.018	0.006	0.09	0.06	18.48	0.01	0.01	0.01	0.34	0.25
B	0.028	0.005	0.46	0.45	18.18	0.12	0.18	0.16	0.33	0.20
C	0.055	0.006	0.08	0.05	18.42	0.01	0.01	0.01	0.77	0.53
D	0.062	0.004	0.46	0.46	18.08	0.13	0.17	0.16	0.78	0.52
E	0.022	0.004	0.08	0.13	18.35	0.02	0.01	0.01	0.77	0.67
F	0.018	0.018	0.10	0.08	18.06	0.06	0.99	0.05	0.28	0.15
G	0.057	0.020	0.43	0.45	18.01	0.17	1.00	0.18	0.57	0.27
H	0.010	0.009	0.03	0.07	18.06	0.03	2.06	0.01	0.30	0.23
I	0.050	0.010	0.48	0.48	18.06	0.15	2.08	0.25	0.79	0.56

[a] Excess Ti = Total % Ti − 4.0 times % C − 3.4 times % N.

TABLE 2—Annealed tensile properties.[a]

Heat	Description	Yield Strength, 0.2% Offset, MPa (ksi)	Tensile Strength, MPa (ksi)	Elongation % in 50.8 mm (2 in.)	Hardness, R_B
A	low Ti, low C, low residuals	222 (32.2)	408 (59.2)	35.6	65
B	low Ti, low C, high residuals	283 (41.1)	451 (65.4)	32.9	74
C	high Ti, high C, low residuals	239 (34.7)	425 (61.7)	33.5	68
D	high Ti, high C, high residuals	301 (43.7)	489 (71.0)	32.3	77
E	high Ti, low C, low residuals	260 (37.7)	441 (64.0)	32.8	71
F	low Ti, C and residuals—1Mo	253 (36.7)	430 (62.4)	35.2	71
G	high Ti, C and residuals—1Mo	308 (44.7)	479 (69.5)	32.4	78
H	low Ti, C and residuals—2Mo	309 (44.9)	482 (69.9)	33.5	78
I	high Ti, C and residuals—2Mo	370 (53.7)	537 (78.0)	31.0	85

[a] 1.27-mm (0.05 in.) strip, annealed at 899°C (1650°F) for 5 min and air-cooled; grain size of ASTM 6 to 7; average longitudinal and transverse test results.
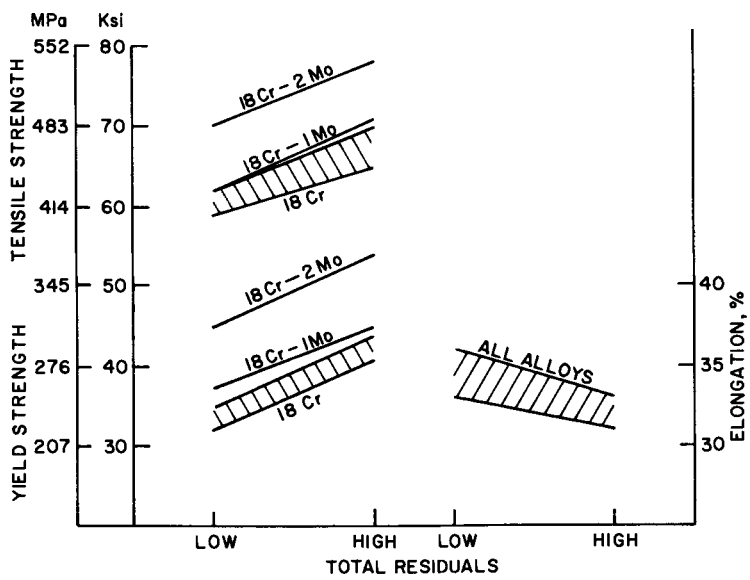
FIG. 1—*Tensile properties of 18Cr, 18Cr-1Mo, and Cr-2Mo compositions versus total residual level. Ranges for the 18Cr alloys encompass both high and low levels of titanium and carbon, whereas the end points for the 18Cr-1Mo and 18Cr-2Mo alloys contain only low or high levels of titanium and carbon.*
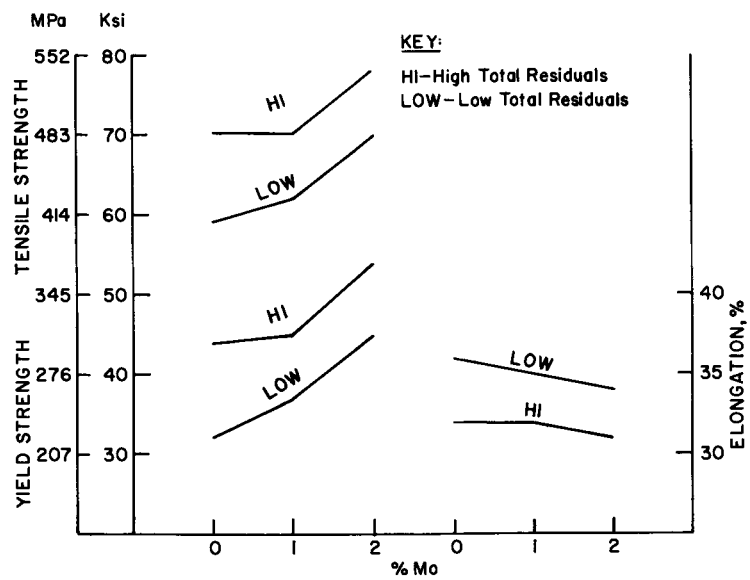
FIG. 2—*Tensile properties of 18Cr heats versus molybdenum level. Cold-rolled to 1.27 mm (0.05 in.) and annealed at (899°C) (1650°F).*

TABLE 3—As-welded tensile properties.[a]

Heat	Description	Yield Strength 0.2% Offset, MPa (ksi)	Tensile Strength, MPa (ksi)	Elongation, % in 50.8 mm (2 in.)	Weld Hardness, R_B
A	low Ti, low C, low residuals	285 (41.4)	426 (61.8)	37.0	79
B	low Ti, low C, high residuals	317 (46.0)	469 (68.1)	31.0	86
C	high Ti, high C, low residuals	281 (40.8)	462 (67.1)	35.0	84
D	high Ti, high C, high residuals	333 (48.4)	502 (72.9)	26.0	89
E	high Ti, low C, low residuals	297 (43.1)	457 (66.4)	30.5	81
F	low Ti, C and residuals—1Mo	308 (44.7)	455 (66.1)	32.5	81
G	high Ti, C and residuals—1Mo	339 (49.2)	508 (73.8)	29.0	85
H	low Ti, C and residuals—2Mo	336 (48.8)	495 (71.8)	32.0	86
I	high Ti, C and residuals—2Mo	386 (56.0)	553 (80.3)	26.5	89

[a] 1.27-mm (0.05 in.) strip; gas tungsten arc weld; average of two longitudinal test results with weld located in center of tension specimen parallel to tensile axis.

The longitudinal-weld tension tests are perhaps unusual in that they are not the customary transverse type of test in which the weld lies perpendicular to the tensile axis. It was believed that a transverse-weld tension test would give a determination of the strength of the weld only if the weld metal were more ductile or less strong than the base metal. Since the weld metal is generally stronger than the base metal, a transverse-weld specimen will usually break in the base metal without fully stressing the weld unless, of course, the weld is extremely brittle, in which case the weld will usually prematurely fracture after small strains. In order to more completely assess weld metal properties, a longitudinal-weld specimen was chosen so that both weld and heat-affected-zone (HAZ) strength and ductility could be measured along with the base metal.

Transverse subsize Charpy V-notch specimens were prepared from both annealed and as-welded strip. The notch was centered in the fusion zone for the as-welded specimens. Duplicate specimens were tested at temperatures ranging from −73°C (−100°F) to +38°C (+100°F) to obtain transition curves. The ductile-to-brittle transition temperature was defined as the temperature at which the energy absorbed dropped to one-half the average of the upper- and lower-shelf values. This energy level was about 8 to 9 J (6 to 7 ft-lb) for most of the 1.27-mm (0.050 in.) subsize specimens. A summary of the impact data is given in Table 4. Transition temperatures versus residual and molybdenum levels are shown in Fig. 3.

Bend test coupons 25.4 by 50.8 mm (1 by 2 in.) were prepared with the weld running both parallel and perpendicular to the bend axis. All welds were capable of bending 180 deg around a radius of one-half times the thickness with no signs of fusion or HAZ cracking when examined at an ×20 magnification.

Transverse microsections were prepared from the welds and examined at ×100. Representative photomicrographs of the welds are shown in Fig. 4

TABLE 4—*Annealed and welded impact properties.*[a]

| | | Impact Transition Temperatures, °C (°F) | |
| | | Annealed | Welded |
Heat	Description		
A	low Ti, low C, low residuals	−62 (−80)	−54 (−65)
B	low Ti, low C, high residuals	−62 (−80)	−48 (−55)
C	high Ti, high C, low residuals	−62 (−80)	−15 (+5)
D	high Ti, high C, high residuals	−46 (−50)	−29 (−20)
E	high Ti, low C, low residuals	−57 (−70)	+2 (+35)
F	low Ti, C and residuals—1 Mo	−60 (−75)	−46 (−50)
G	high Ti, C and residuals—1 Mo	−40 (−40)	−15 (+5)
H	low Ti, C and residuals—2 Mo	−65 (−85)	−49 (−55)
I	high Ti, C and residuals—2 Mo	−29 (−20)	+7 (+45)

[a]1.27-mm (0.05 in.) subsize CVN specimens; transverse specimens with notch parallel to rolling direction; notch located in center of weld.
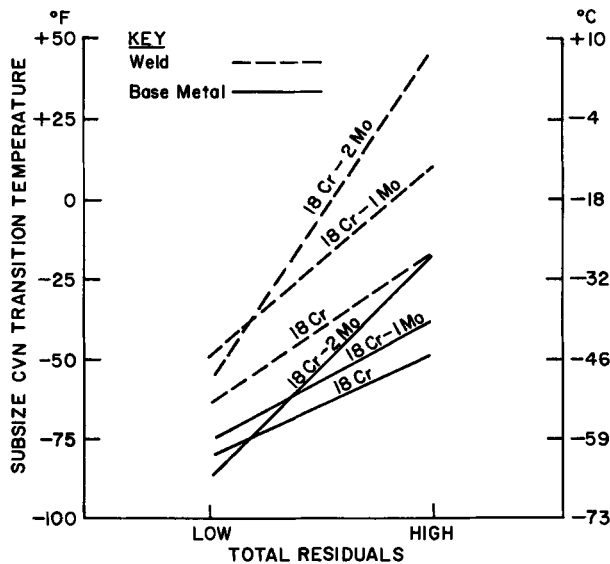
FIG. 3—*Impact transition temperatures of 18Cr, 18Cr-1Mo, and 18Cr-2Mo welds and base metal versus residual level. Subsize CVN test results.*

for Heats A through E. Heats F and G with 1Mo and Heats H and I with 2Mo showed weld structures very similar to Heats A and D at similar residual levels and therefore are not shown.

Corrosion Testing

Coupons 25.4 by 50.8 mm (1 by 2 in.) were prepared with machined edges from base metal and welded specimens with the weld lying in the long direction. Duplicate specimens in each condition were tested for susceptibility to intergranular corrosion in a boiling solution of copper-copper sulfate-sulfuric acid [ASTM Recommended Practices for Detecting Susceptibility to Intergranular Attack in Stainless Steels (A 262-68, Practice E)]. Samples were exposed for 24 h, bent 180 deg, and examined at an ×20 magnification for cracks. All heats passed this test.

Discussion

Tensile Properties

The annealed tensile properties in Table 2 and Fig. 1 show that, regardless of titanium and (C + N) content, Heats A and C with low residuals had considerably lower strength and hardness and slightly higher ductility
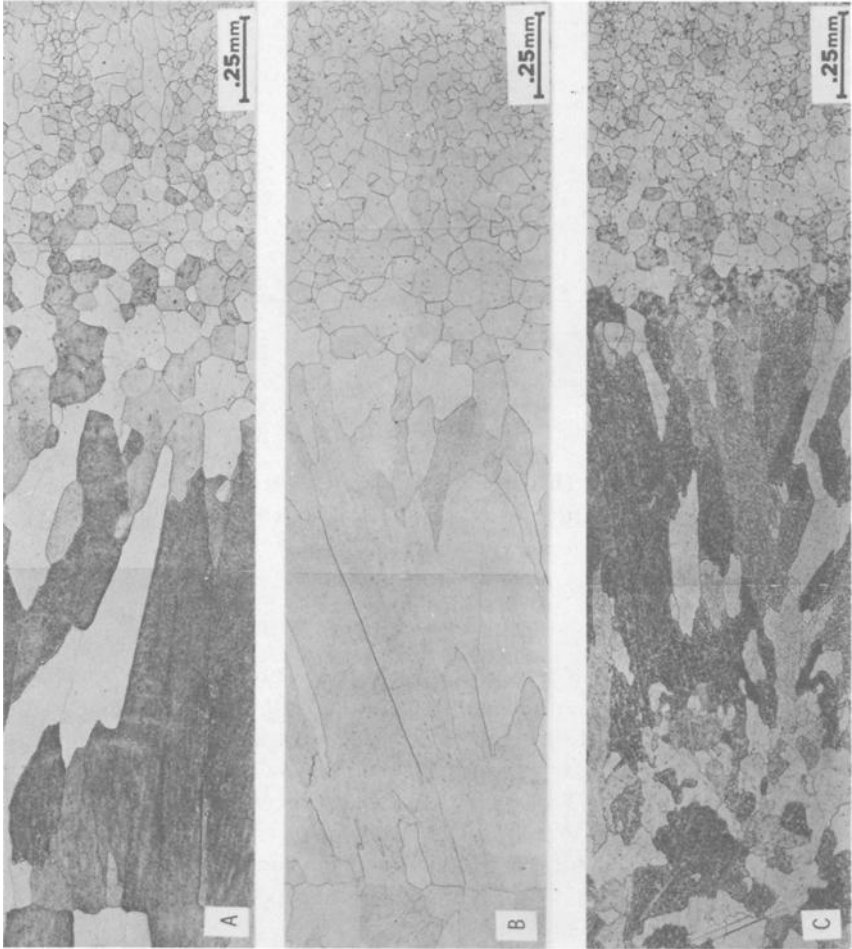
FIG. 4—Typical weld microstructures of 18Cr heats with various levels of residuals. (a) Heat A. low carbon. low titanium. low residuals; (b) Heat B: low carbon. low titanium, high residuals; (c) Heat C: high carbon, high titanium. low residuals; (d) Heat D: high carbon, high titanium. high residuals. (e) Heat E. low carbon, high titanium. low residuals. Magnification: ×100: Etchant: HCl-Picric.

than their high residual counterparts, Heats B and D, respectively. At comparable residual levels, there was a modest increase in strength and a slight decrease in ductility in going from low to high titanium and (C + N) levels (compare Heats A, C, and E with Heats B and D). After adjusting for small chromium differences, the strengthening effect on both yield and tensile strength due to residual elements was found to be about 66 MPa (9.5 ksi) per 1.0 percent total residuals (Mn + Si + Ni + Cu + Mo). The strengthening effect due to titanium was found to vary from about 61 MPa (8.9 ksi) per 1.0 percent excess titanium at low residual levels to about 88 MPa (12.8 ksi) per 1.0 percent excess titanium at high residual levels, where excess titanium was calculated as follows

$$\text{Excess Ti} = \text{total \%Ti} - 4.0 \text{ times \%C} - 3.4 \text{ times \%N}$$

Since carbon and nitrogen were presumably tied up as coarse Ti(C,N) particles in the fully annealed condition, it was assumed that neither (C + N) in solution nor the Ti(C,N) particles contributed to the strength of the alloys studied. Therefore, excess titanium in solid solution was used to measure the effects of high or low titanium and (C + N) levels. From the strengthening effects observed, it is seen that excess titanium as well as the other residuals were rather potent solid solution strengthening elements.

For the molybdenum-bearing alloys, it was observed that molybdenum was a moderate solid solution strengthening element with an average strengthening factor of about 41 MPa (6.0 ksi) per 1.0Mo addition. (Compare Heats A, F, and H with Heats D, G, and I.) The strengthening effect appeared to be more pronounced at the low residual level and in going from 1.0Mo to 2.0Mo as shown in Fig. 2. The separate effect of titanium could not be determined for the molybdenum-bearing alloys since high titanium heats also contained high residuals. However, the effect of total residuals (including excess titanium) on strength was found to be the same for the molybdenum-bearing heats as for the 18Cr alloys as indicated in Fig. 1.

Results of the present study can be compared with early work by Gensamer [9] on low-carbon ferritic steels which showed that the most potent strengthening elements in iron alloys were phosphorus, copper, silicon, and titanium, followed in decreasing order by aluminum, manganese, nickel, molybdenum, and chromium. It is noted that Gensamer's iron alloys contained alloying additions up to 4.0 percent, well in excess of the residual levels explored in this study. Furthermore, in the 18Cr alloys of the present study, the strengthening effect of residual elements would probably be diminished because of the additional solid solution strengthening effect already provided by the higher chromium content. The strengthening coefficients for alloying elements in Gensamer's iron alloys, which ranged

from about 124 MPa (18 ksi) per 1.0 percent addition of copper, silicon, or titanium to about 34 MPa (5.0 ksi) per 1.0 percent addition of manganese, nickel, molybdenum, or chromium, were found to be higher or equal to those of the present study.

Welded Properties

The effect of residual elements on welded tensile properties (see Table 3) followed the same pattern as the annealed material. The yield strengths were generally 21 to 62 MPa (3 to 9 ksi) higher and the tensile strengths about 14 to 41 MPa (2 to 6 ksi) higher for the welds compared with the annealed specimens. The weld hardnesses were also higher than the annealed material by as much as 14 points on the Rockwell B scale. The increases in strength and hardness tended to be more pronounced in the 18Cr alloys and less pronounced in the 18Cr-2Mo alloys. Weld ductility showed mixed behavior depending upon the particular residual level. For example, Heats A and C with low residuals showed a slight increase in tensile elongation after welding whereas Heats B and D with high residuals and Heat E with a high level of excess titanium showed a moderate decrease. All four molybdenum-bearing heats showed a decrease in weld ductility, with the high residual heats (Heats G and I) showing the greatest drop. It was observed that Heats D, G, and I with high titanium and high residuals including (C + N) showed the greatest drop in weld ductility for the alloys studied. Despite these differences in weld tensile ductility, it will be recalled that the bend ductility of welds was quite good, with all heats successfully passing 180-deg bend test at a radius of one-half times the thickness. Thus, reasonably good bend ductility was obtained at tensile elongations as low as 26 percent.

The increase in strength and hardness of the welded specimens was most likely the result of additional solid solution strengthening by the partial dissolution of Ti(C,N) inclusions in both fusion and HAZ's. Submicroscopic precipitation of Ti(C,N) particles during the rapid thermal cycle of welding may also have occurred in the welds to account for the higher strengths. Titanium carbonitride precipitates were observed by Sawhill and Bond [6] in 18Cr-2Mo titanium-stabilized welds. These were found to be more numerous and finer in the weld compared with the HAZ or base metal.

The ductility loss in the welds of the high residual heats may also have been related to the partial dissolution of Ti(C,N) inclusions or submicroscopic precipitation of titanium-rich particles or both. In this case, however, an interaction effect with other residual elements may have resulted since Heat C with low residuals was unaffected by higher titanium and (C + N) levels, whereas Heat D with high residuals was significantly affected. Excess titanium did not appear to be grossly detrimental to weld ductility since

Heat E with 0.67 percent excess titanium had reasonably good ductility when compared with the annealed material. Heat E contained low residuals, however, which apparently was desirable for good weld ductility.

Grain size variations were noted in the welded specimens as shown in Fig. 4. It was observed that high titanium and high (C + N) (Heats C and D) produced a generally finer and more equiaxed weld structure than low (C + N) (Heats A and B), which produced a columnar structure. Heats F and H with low titanium, low (C + N) and Heats G and I with high titanium, high (C + N) also formed a columnar weld structure, indicating that perhaps Ti(C,N) particles in the higher (C + N) heats served as nucleation sites for equiaxed grain development. This same effect was observed by Sawhill and Bond [6] on 18Cr-2Mo titanium-stabilized welds. The finer grain size in welds of the higher (C + N) heats may have also contributed to the higher strength in these alloys compared with the lower (C + N) heats. Therefore, high titanium and high (C + N) welded structures had the potential to be strengthened by (1) excess titanium in solution; (2) (C + N) in solution; (3) Ti(C,N) precipitation, and (4) smaller grain sizes.

Impact Properties

The impact data in Table 4 and in Fig. 3 indicate that weld toughness was affected to a large degree by increases in titanium and (C + N) and, to a lesser degree, by molybdenum level. The effects of other residual elements were negligible in the straight chromium alloys. In the molybdenum-bearing heats, the effects of other residuals and titanium and (C + N) could not be separated. At high levels, however, these elements together were detrimental to toughness, particularly in welds. Comparison of Heats A and B versus Heats C and D shows that, at comparable manganese, silicon, nickel, copper, and molybdenum residual levels, increasing titanium and (C + N) increased the weld transition temperature by 20 to 40 deg C (35 to 70 deg F). Heat E, with very high titanium, showed the highest weld transition temperature of the straight chromium alloys, indicating a high degree of sensitivity to excess titanium or precipitation of titanium-rich particles or to both. Interestingly, the alloy with the lowest as-welded tensile ductility (Heat D) was not the one with the lowest weld toughness (Heat E). Sawhill and Bond [6] in their 18Cr-2Mo weld study also did not find a direct correlation between weld toughness and ductility. They observed, however, that excess titanium decreased weld ductility in an Olsen cup test, but did not lower notch impact properties to any significant degree. Their results are directly opposite to the present study and may reflect the difference in residual levels or molybdenum levels or both between the two studies.

The molybdenum-bearing alloys showed an even greater increase in the

weld transition temperatures in going from low to high residuals or from low to high titanium or both. The weld transition temperatures also tended to increase in going from 0Mo to 2Mo at comparable residual levels (compare Heats A, F, and H with Heats D, G, and I). Heats G and I with high residuals also had the lowest tensile ductility, perhaps indicating a relationship between weld toughness and weld ductility. Heat I not only has the highest weld transition temperature but also the highest base metal transition temperature, indicating that high titanium or high residuals or both adversely affected the toughness of an alloy of the 18Cr-2Mo type. At low residual levels the molybdenum-bearing heats behaved quite similarly to the straight chromium alloys. The behavior at low residual levels agrees in part with work by Semchysen et al [2], who found that molybdenum additions up to about 3 percent in a high-purity 18Cr alloy with no titanium additions did not affect annealed impact properties. They did not study the effect of molybdenum levels on 18Cr alloys with titanium additions or high residual levels or both, so the high residual results of the present study cannot be confirmed. Nevertheless, it appears that the strengthening effect of molybdenum additions and other residual elements coupled with the embrittling effect of titanium and (C + N) is detrimental to as-welded impact properties and, to a lesser degree, to base metal toughness.

Corrosion Properties

Results of the acid copper sulfate test indicated immunity to intergranular corrosion for all heats in the as-welded condition. These results agree with other work [2,4,7] on 18Cr alloys which has shown that stabilization with titanium equal to 0.2 + 4(C + N) effectively prevents sensitization and intergranular corrosion of welds in this test so long as the titanium/carbon ratio is greater than about 11 to 1 [7] or a minimum titanium level of 0.30 percent is maintained [4]. All of the heats in the present study contained 0.30 percent minimum titanium in order to maintain a minimum titanium/carbon ratio of 10.0.

Summary and Conclusions

This study has shown that titanium, (C + N), residuals, and molybdenum additions significantly affect the mechanical properties of 18Cr ferritic stainless steels. The residual elements manganese, silicon, copper, and nickel, as well as titanium, influenced annealed and welded tensile properties to the greater degree, whereas titanium (C + N), and molybdenum were most influential on as-welded toughness. Titanium was the most potent solid solution strengthening element, followed by the other residuals combined, then molybdenum additions. For light-gage applications such as welded tubing, a good combination of strength, ductility and

toughness lies with a low (C + N), low-titanium, and low-residual analysis at all molybdenum levels studied. For heavier-gage applications such as plate or piping, where ductility and toughness are probably more sensitive to grain size, annealing, and welding variables, it is also implied that a low-residual, low (C + N), and low-titanium analysis would be beneficial for a good combination of toughness and ductility. The following conclusions were made from this study:

1. The strengthening effect of the combined residual elements (Mn + Si + Ni + Cu + Mo) and excess titanium on both yield and tensile strength was found to be approximately 69 MPa (10 ksi) per 1.0 percent total addition. The strengthening effect due to molybdenum additions was found to be approximately 41 MPa (6 ksi) per 1.0 percent addition.

2. The yield and tensile strengths of welds were approximately 14 to 62 MPa (2 to 9 ksi) higher and ductility up to 6 percent lower than comparable annealed base material.

3. Ductility and toughness of welds were influenced to a greater degree by the presence of residuals and molybdenum additions than those of annealed material. Poorest weld ductility was observed at high titanium, (C + N), and molybdenum levels with little effect from other residuals.

4. Impact transition temperatures of welds were lowered by as much as 55 deg C (100 deg F) in 18Cr-2Mo and 28 deg C (50 deg F) in 18Cr alloys by decreasing residual, titanium, and (C + N) levels from typical electric-arc furnace levels to very low levels achievable by vacuum melting or refining.

References

[1] Binder, W. O. and Spendelow, H. R., Jr., *Transactions*, American Society for Metals, Vol. 43, 1951, pp. 759-772.

[2] Semchysen, M., Bond, A. P., and Dundas, H. J. in *Proceedings*, Symposium Toward Improved Ductility and Toughness, Climax Molybdenum Co. (Japan) Ltd., Kyoto, Japan, 25-26 Oct. 1971, pp. 239-253.

[3] Bond, A. P., *Transactions of the Metallurgical Society*, American Institute of Mining, Metallurgical, and Petroleum Engineers, Vol. 245, 1969, pp. 2127-2734.

[4] Steigerwald, R. F. in *Proceedings*, "Corrosion '74" Conference, Chicago, Ill., 4-8 March 1974.

[5] Bond, A. P. and Lizlovs, E. A., *Journal of the Electrochemical Society*, Vol. 116, 1969, pp. 1305-1311.

[6] Sawhill, J. M., Jr. and Bond, A. P., *Welding Journal*, Vol. 55, 1976, pp. 33s-41s.

[7] Kaltenhauser, R. H., *Metals Engineering Quarterly*, May 1971, pp. 41-47.

[8] Wright, R. N., *Welding Journal*, Vol. 50, 1971, pp. 434s-440s.

[9] Gensamer, M., *Transactions*, American Society for Metals, Vol. 36, 1946, pp. 30-60.

[10] Lula, R. A., Lena, A. J., and Kiefer, G. C., *Transactions*, American Society for Metals, Vol. 46, 1954, pp. 197-230.

C. R. Thomas[1] and R. L. Apps[2]

Weld Heat-Affected Zone Properties in AISI 409 Ferritic Stainless Steel

ABSTRACT: Although welding of thin-gage ferritic stainless steels is well documented, little information is available on the response of thicker (4.5 to 12.0 mm) sections to welding. With increasing interest in the use of heavier gages, it has become necessary to rectify this gap in knowledge. The work reported herein was undertaken to examine the metallurgical response of titanium-stabilized 11.5Cr steels to welding in terms of heat-affected zone (HAZ) structure, mechanical properties, and corrosion behavior.

Welds were made in four heats of steel to determine the thermal cycles occuring in the weld HAZ and to examine structures and give a general indication of joint properties. In order to examine the characteristics of different regions in the HAZ, a thermal simulation technique was used to produce specimens for examination and testing which had undergone a thermal cycle appropriate to a specific part of the HAZ. Parent steel, weldments, and simulated specimens were examined by optical microscopy, hardness testing, notch impact testing, and corrosion testing.

Four distinct regions of the HAZ were distinguished, as the HAZ was traversed from the unaffected parent steel to the fusion boundary. The amount of martensite formed reached a maximum where the HAZ peak temperature was in the duplex $\alpha + \gamma$ range. Impact transition temperature increased as the grain size increased, and martensite appeared to have little effect. In direct HAZ tests the transition temperature increased by 30 to 70 deg C irrespective of arc energy. Corrosion resistance deteriorated as the martensite content increased. Variations in nickel, manganese, and titanium within the steels used gave only minor variations in HAZ structure and properties, and it is concluded that compositional variations within the AISI 409 specification are unlikely to give significant improvements in the weldability of these steels.

KEY WORDS: ferritic stainless steels, weldability, stabilization, thermal history, impact toughness, martensite formation, grain growth, heat affected zone, fracture toughness

It is widely recognized that AISI 409 and speciality varieties of this titanium-stabilized 11.5Cr steel represent a particularly useful material for

[1] Middelburg Steel and Alloys, Sandton, South Africa.
[2] Professor of Welding Technology, Cranfield Institute of Technology, Cranfield, Bedford, U. K.

automotive muffler and catalytic converter applications [1,2].[3] Additionally, there are many potential applications for a low-cost corrosion-resisting steel such as ocean containers and sugar refinery equipment [3-5]. Many of these applications would require the fabrication of steel thicker than the maximum 3 mm generally recommended [1,6] if weldment toughness is to be maintained. Thus improvement of toughness in welded 11.5Cr ferritic steel is a critical factor in extending the applications of this steel. Attempts to improve toughness in welded 11.5Cr steels have concentrated on careful control of chemical composition to achieve optimum ferrite-austenite ratio at hot-rolling temperatures and to avoid excess stabilizer. It is perhaps significant that newer varieties contain more nickel and manganese and less titanium than standard AISI 409 steels [6, 7].

In an attempt to improve our understanding of the response of thicker AISI 409 steels to welding, four commercially produced 6-mm-thick plates, typical of the compositional range produced by one steelmaker, have been subjected to welding and weld simulation thermal cycles and the variation in properties determined. The work is part of a larger program to identify the critical factors in specifying weldable ferritic stainless steels.

The steels represent the range of typical compositions produced by the steelmaker and also reflect slight differences in annealing. The steels were annealed in 27 215-kg (30 ton) batches in a gas-fired furnace with temperatures between 700 and 750°C for up to 6 h.

Experimental

Materials

The four steels were supplied in the hot-rolled and annealed condition, without descaling; compositions are given in Table 1 and mechanical properties in both the 33-mm-thick sheet bar stage and 6-mm-thick final plate stage (nonstandard specimen size) are listed in Table 2.

Welding and Weld HAZ Simulation

Initially gas tungsten-arc (GTA) remelt welds (Table 3) were made on 300 by 200-mm plate specimens in order to measure typical weld heat-affected zone (HAZ) thermal cycles. Subsequently, actual 300-mm-long multipass shielded metal-arc (SMA) and gas metal-arc (GMA) welds were made to join 300 by 100-mm plates using a 60-deg vee included angle, 1-mm root face, and 1.5-mm root gap with jigging to eliminate distortion. Welding procedures are given in Table 3.

From the GTA remelt welds a series of HAZ thermal cycles (Fig. 1) was

---

[3] The italic numbers in brackets refer to the list of references appended to this paper.

TABLE 1—Chemical composition of AISI 409 steels.

Steel	C	N	Mn	Si	S	Cr	Ni	Ti	Al	Ti/(C + N)
AISI Specification Maximum	0.08	...	1.00	1.00	0.045	10.5	0.5	6 × C	...	...
A	0.025	0.015	0.74	0.39	0.017	11.75	0.60	0.30	0.09	7.5
B	0.026	0.013	0.98	0.49	0.018	11.51	0.38	0.25	0.14	6.4
C	0.027	0.015	0.72	0.51	0.023	11.57	0.49	0.33	0.12	7.9
J	0.020	0.012	0.78	0.48	0.015	11.42	0.32	0.17	0.28	5.3

TABLE 2—Properties of AISI 409 steels.

Steel	Grain Size, µm	Tensile Properties						Charpy V-Notch Transition Temperature, °C			Corrosion Rate, mils/year
		0.2% Proof Strength, N/mm²		Tensile Strength, N/mm²		% Elongation $L_o = 5.65\sqrt{S_o}$	Hardness, HV 10	30J	GE[a]	Upper Shelf Energy (J)	
		Sheet Bar	6-mm Plate	Sheet Bar	6-mm Plate						
AISI Specification	...	240 min	...	480 min	...	25 min	150 HB max	...	...	...	...
A	40	326	353	446	480	32	157	−24	−9	80	86
B	43	364	341	462	474	27	155	20	12	55	97
C	51	319	367	510	502	33	159	4	8	70	61
J	37	330	326	426	454	30	147	29	25	70	81

[a] GE = graphical determination of transition temperature using absorbed energy.

selected as representative of parts of the HAZ with different metallographic structures or properties (see Table 4). These cycles were then used in a thermal simulator [8] to produce 60 by 10.5 by 6-mm specimens representative of specific regions in the HAZ for subsequent testing. In one case a theoretically predicted thermal cycle was used as no suitable cycle had been measured [9]. Some specimens were initially cycled to over 1300°C to give a coarse-grained HAZ structure and then cycled to about 720°C to simulate the effect of a second weld pass.

Testing and Metallographic Examination

It was decided to characterize the parent steel and both actual and simulated HAZ by optical metallography, macro and microhardness tests, tensile properties using 10 by 5-mm cross section test specimens, toughness properties using substandard 55 by 5 by 10-mm Charpy V-notch specimens (notched on the 5-mm face), and corrosion resistance. Metallurgical structures were examined on surfaces after polishing and etching with a mixture of 2 percent picric and 1 percent hydrochloric acids in methanol. Grain size was determined at a magnification of 100 by a linear intercept method [ASTM Estimating the Average Grain Size of Metals (E 112-77)]. Percentage martensite was also estimated and precipitate morphology and distribution recorded. Extensive examination of impact test fracture surfaces was carried out using a Cambridge 600 Stereoscan. Tension, hardness, and Charpy V-notch impact tests were made with standard equipment and techniques. The notch for the substandard Charpy V-notch tests was positioned 4.5 mm from the weld centerline. Initially it was considered that intergranular corrosion would be the main corrosion problem in welded AISI 409 steels, and tests according to the ASTM Recommended Practices for Detecting Susceptibility to Intergranular Attack in Stainless Steels (A 262-76, Practice E) were undertaken. It soon became apparent, however, that general corrosion was occurring and that a different test was required. Finally a boiling aqueous solution of 2 percent sulfuric acid plus 600-ppm Cu^{2+} was selected and weight loss measured after 6 h. This test allowed simple comparisons to be made readily, but it must be emphasized that the corrosive media have no practical significance.

For the corrosion tests, both welded and simulated specimens were machined to 20 by 8 by 3 mm, polished (to 600 grit), and degreased. After weighing, the specimens were placed in 750-ml Erlenmeyer flasks fitted with finger-type reflux condensers. After 6 h the specimens were cooled, dried, and reweighed, allowing a corrosion rate to be calculated.

Results

The four steels (Tables 1 and 2) had microstructures consisting of fine-

TABLE 3—*Welding procedures.*

Process	Steel Weld Identification	Pass No.	Electrode Diameter, mm	Current, A	Voltage, V	Welding Speed, mm/min	Arc Energy, kJ/mm
GTA[a] (remelt)	A. GTA1	.		160	22	171	1.235
GTA (remelt)	C. GTA2			120	23.5	353	0.460
SMA[b]	A-1	1	3.2	120	22	263	0.602
		2	5.0	145	24	235	0.888
		3	5.0	140	21.5	205	0.881
GMA[c]	A-2	1	3.2	120	23.5	147	1.151
		2	5.0	145	21.5	161	1.162
GMA	A-1	1		120	21.5	164	0.834
		2		150	19	223	0.807
GMA	A-2	1		150	20	221	0.855
		2	.	145	21	257	0.677
SMA	B-1	1	3.2	120	20	294	0.576
		2	3.2	125	23.5	141	1.277
		3	3.2	125	24.0	144	1.223
SMA	B-2	1	5.0	150	23.5	134	1.444
			3.2	120	21.5	216	0.783
GMA	B-1	1	.	150	20	196	0.918
		2	.	160	20	181	1.061
GMA	B-2	1	.	160	20	271	0.709
		2	.	160	22	156	1.231
SMA	C-1	1	5.0	150	21.5	228	0.868
		2	5.0	145	23.5	167	1.120
SMA	C-2	1	3.2	120	21.5	353	0.479
		2	5.0	150	21.5	146	1.325
		3	5.0	150	22.0	157	1.261
GMA	C-1	1	.	165	20	183	1.082
		2	.	120	22	188	0.843
GMA	C-2	1	.	145	20	157	1.108
		2	.	150	20	174	1.035
SMA	J-1	1	3.2	100	24	117	1.231
		2	5.0	135	25	286	0.708
SMA	J-2	1	3.2	100	24	145	0.993
		2	3.2	100	24	150	0.960
GMA	J-1	1	...	160	22	171	1.235
		2		145	22	346	0.553
GMA	J-2	1	+	155	22	169	1.211

[a] GTA = gas tungsten arc.
[b] SMA = shielded metal arc.
[c] GMA = gas metal arc.
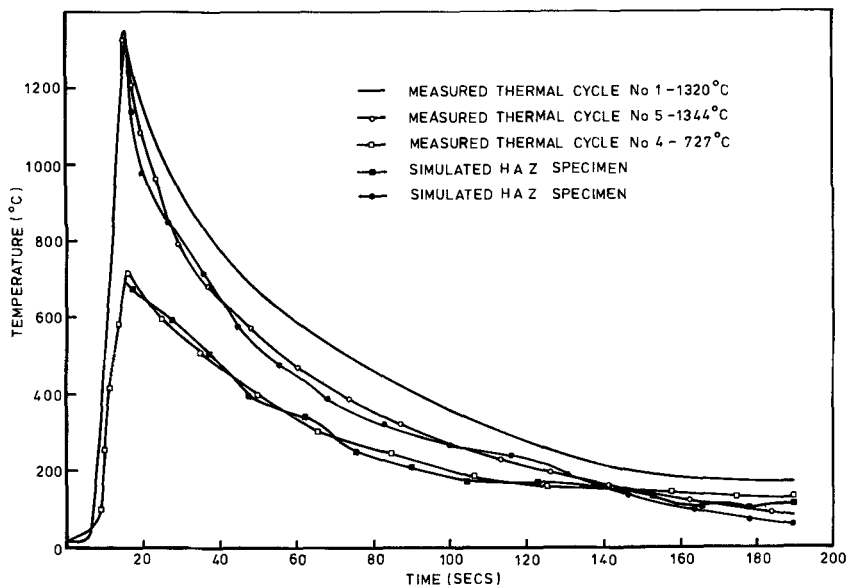
FIG. 1—*Typical measured (Welds A.GTA1 and C.GTA2) and simulated thermal cycles.*

grained partially recrystallized ferrite slightly elongated in the rolling direction, Fig. 2. Large cubic orange-colored titanium carbonitride precipitates were evenly distributed through the matrix, often associated with light-grey inclusions rich in sulfur, while numerous very fine precipitates occurred on the grain boundaries. These latter microdot precipitates were tentatively identified as Cr_2N and Cr_7C_3 [10]. The grain size hardness and strength varied from one cast to another but the greatest variation occurred in impact transition behavior, Table 2.

The weld HAZ formed by GTA remelt, SMA, and GMA welding exhibited a similar range of structures, that is

1. Coarse-grained close to the fusion boundary consisting of coarse ferrite, Fig. 3a.

2. Coarse-grained duplex region with somewhat smaller grain size than Structure 1 and martensite, mostly on grain boundaries (Fig. 4a).

3. Fine-grained duplex region with fine ferrite grains and a high proportion of inter and intragranular martensite Fig. 5a.

4. Untransformed HAZ distinguished by finer grain size and higher hardness than the parent steels.

The maximum grain size and properties of these welds are given in Table 5. The simulated HAZ specimens showed metallurgical structures similar to actual weld HAZ structures although the grain size appeared to

TABLE 4—Results of simulated HAZ tests.

Simulation	Steel	Grain Size, μm	Ferrite Hardness, HV 10	Martensite Volume, %	Martensite Hardness, HVO O35	Transition Temperature, °C			Corrosion Rate, mils/year
						30 J	GE[a]	Upper Shelf Energy (J)	
1. High arc energy 1320°C peak temperature	A	125	170	5 to 10	389	76	83	70	115
	B	132	184	5 to 10	364	75	86	45	137
	C	125	178	0 to 5	321	81	88	50	126
	J	154	159	0 to 5	354	78	88	75	99
2. High arc energy 1061°C peak temperature	A	59	161	10 to 15	305	40	45	50	281
	B	67	169	15 to 20	285	54	53	55	368
	C	85	158	10 to 15	291	42	63	80	279
	J	72	162	5 to 10	300	43	55	80	198
3. High arc energy 727°C peak temperature	A	36	164	0	…	86	89	45	128
	B	39	159	0	…	75	75	60	89
	C	36	152	0	…	84	79	40	113
	J	37	144	0	…	68	83	50	107
4. High arc energy 1 + 727°C peak temperature	A	137	174	5 to 10	286	71	92	40	227
	B	95	161	5 to 10	281	90	75	40	341
	C	111	158	0 to 5	295	67	112	45	190
	J	129	162	Trace	300	63	85	70	115
5. Low arc energy 1334°C peak temperature	A	123	187	15 to 20	432	86	85	30	435
	B	203	177	10 to 15	407	100+	124	30	277
	C	134	172	5 to 10	390	72	87	40	224
	J	113	196	5 to 10	482	80	88	35	250
6. Low arc energy 1035°C peak temperature	A	133	158	15 to 20	300	76	73	35	345
	B	95	165	10 to 15	315	100+	88	30	309
	C	128	181	5 to 10	325	80	74	40	262
	J	109	178	10 to 15	318	65	79	60	284
7. Low arc energy 911°C peak temperature	A	34	193	20 to 25	299	63	54	40	374
	B	28	166	10 to 15	286	64	64	40	291
	C	42	185	10 to 15	274	48	65	50	208
	J	39	174	10 to 15	265	32	49	60	244
8. Low arc energy 1 + 714°C peak temperature	A	181	154	15 to 20	350	76	62	35	362
	B	128	182	10 to 15	320	69	67	35	303
	C	154	163	5 to 10	339	80	75	40	178
	J	172	172	10 to 15	312	70	81	60	285

[a]GE = graphical determination of transition temperature using absorbed energy.
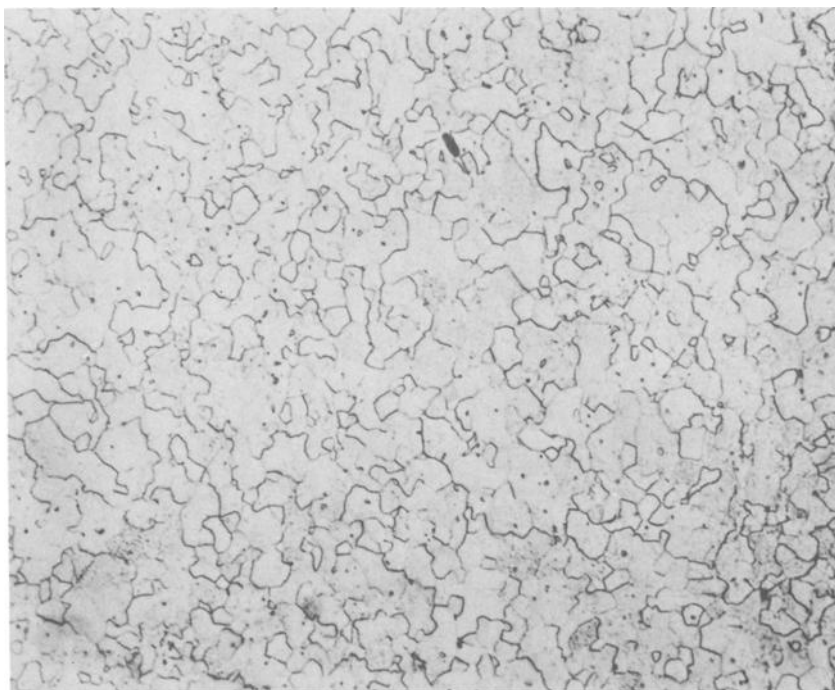
FIG. 2—*Typical microstructure of AISI 409 commercially produced 6-mm plate (Steel B)* (×100).

be larger (Figs. 3b, 4b, 5b). Grain size counts over several hundred grainings actually indicated that the average grain size in simulated specimens was no more than 15 to 20 percent greater than found in actual weld HAZ (compare Tables 4 and 5).

Typical impact transition curves obtained with HAZ simulated specimens are shown in Fig. 6 together with curves for one parent steel and two actual weld HAZ. Further results are given in Tables 4 and 5. It may be noted that welding results in a significant increase in transition temperature. The fracture surfaces of all the impact tests were examined under the scanning electron microscope (SEM). Above the transition temperature the fracture surfaces consisted of ductile dimples with sulfide and other inclusions at the base of the dimples. The cubic titanium (carbon, nitrogen) in the parent steels (Fig. 7a) was replaced in the weld and simulated HAZ samples by finer inclusions, mainly sulfides Fig. 7b. Below the transition temperature transcrystalline cleavage occurred in all cases although grain boundary precipitates were more evident in the weld HAZ and simulated specimens (Fig. 8).

Weight loss measurements from the corrosion tests are given in Tables 4
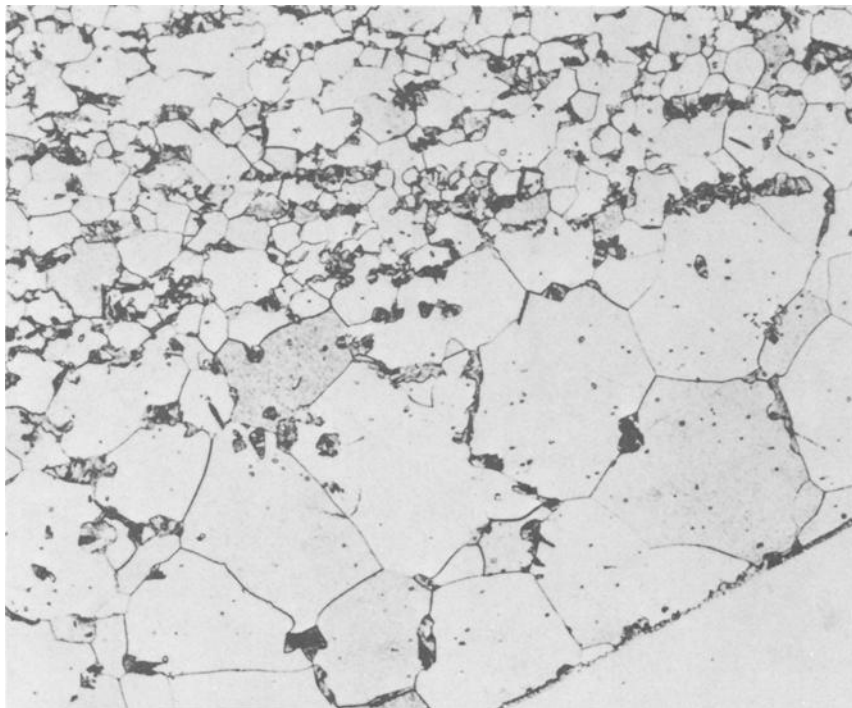
FIG. 3a—*Heat-affected zone in SMA weld B-2. Coarse-grain-size ferrite close to the fusion boundary, and fine-grained duplex ferrite/martensite in lower temperature region.*

and 5. It may be noted that the corrosion rate is directly related to the volume fraction of martensite in the metallurgical structure.

Discussion

The problems associated with the small size of an actual HAZ led to difficulties in distinguishing the relevance of the various metallurgical changes that occur on welding. Thermal simulation also poses many problems in that it is generally impossible to match both grain size and hardness to actual weld HAZ structures, but the technique does produce specimens of similar metallurgical structures with dimensions that are amenable to testing. As can be seen in Fig. 1, simulated cycles closely matched those measured in GTA remelt welds.

The four heats examined met the AISI 409 chemical composition specification, but were slightly harder than the maximum hardness permitted, possibly due to variations in the annealing temperature. Variations in
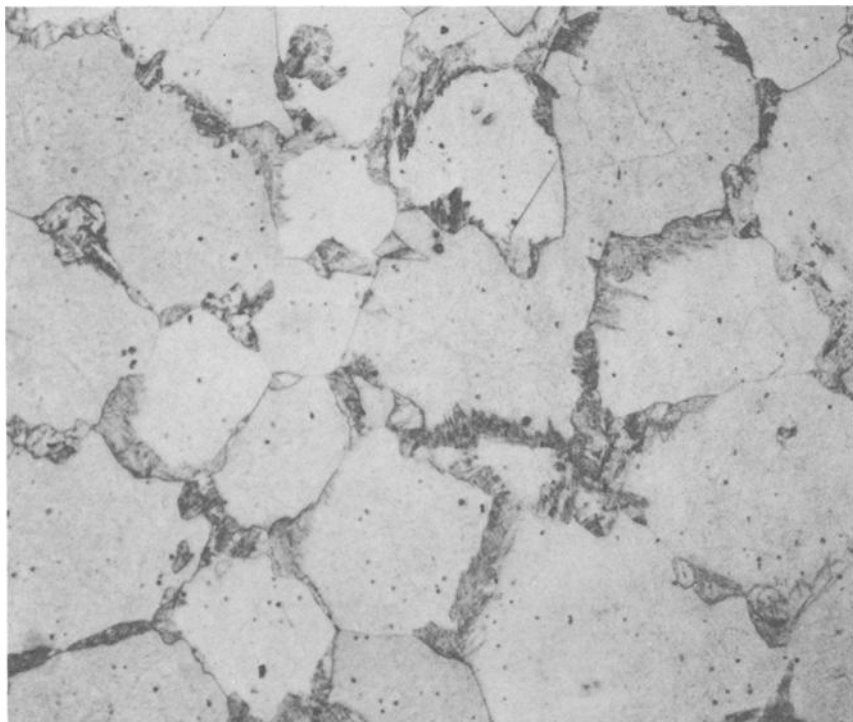
FIG. 3b—*Simulated HAZ microstructure. Steel B, Simulation 1, grain boundary martensite outlining coarse ferrite. HAZ microstructure GMA weld J-1 (×100).*

annealing time and temperature might also account for the significant differences in impact transition behavior of the four steels.

A major problem in the welding of thicker AISI 409 steel is the degradation of properties in the HAZ. Grain growth, which cannot be corrected by subsequent heat treatment, is the most damaging metallurgical change, but martensite formation is also significant. A redistribution of precipitates occurred within the HAZ, but the results obtained failed to indicate the significance of this change.

The predominant importance of grain size in influencing mechanical properties, particularly impact behavior, was shown by the continual increase in both ferrite hardness and transition temperature from the unaffected parent steel to the coarse-grained HAZ close to the fusion boundary, as indicated in simulated HAZ specimens. Thus there was a direct relation between impact properties and grain size. Martensite appeared to have less effect since the maximum martensite content occurred in the fine-
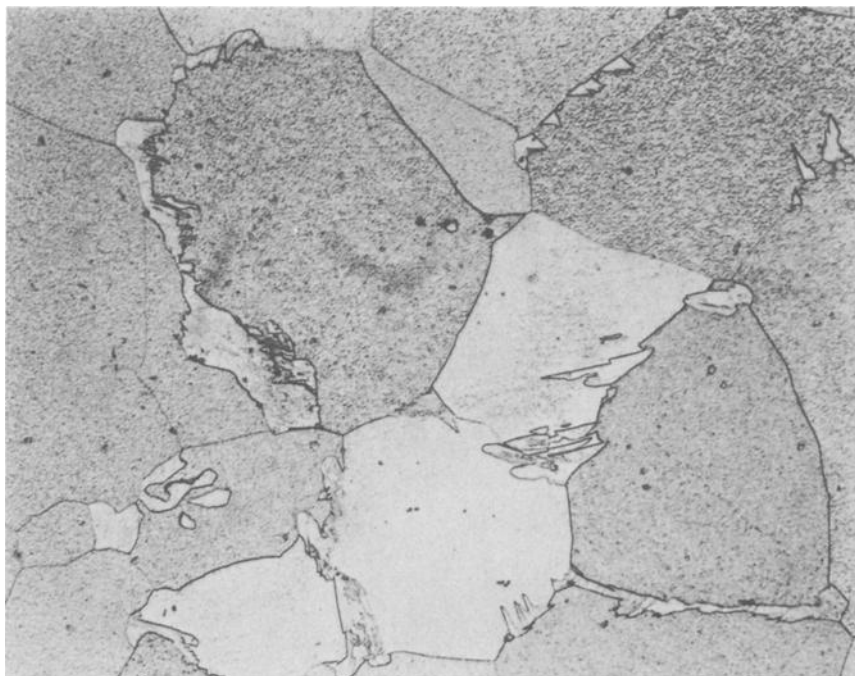
FIG. 4a—*Large-grain-size ferrite with limited quantity of martensite. HAZ microstructure GMA weld J-1 (×200).*

grained duplex region (about 1050°C peak temperature) while the impact transition temperature was highest in the coarse grained region.

The weld HAZ had markedly lower corrosion resistance than the parent metal. When the various regions at the HAZ were separated by the use of simulated specimens, the lowest corrosion resistance was found in the fine-grained duplex region, containing the highest martensite content. This confirmed qualitative observations of the actual weld HAZ. The lower corrosion resistance of the martensite was probably due to its higher carbon content, and the galvanic action between martensite and ferrite.

Improvements in the response to welding of AISI 409 steels must therefore concentrate on reducing grain growth and limiting martensite formation. Unfortunately, these requirements are mutually exclusive. Results indicate that grain growth can be reduced by increasing austenite-forming elements (nickel and manganese) and by reducing titanium contents, and this view is supported by a Japanese steelmaker [7]. This increase in austenite-forming elements has the effect of increasing the temperature stability of the duplex austenite/ferrite region as well as the proportion of austenite. Martensite formation can be reduced by increasing the titanium
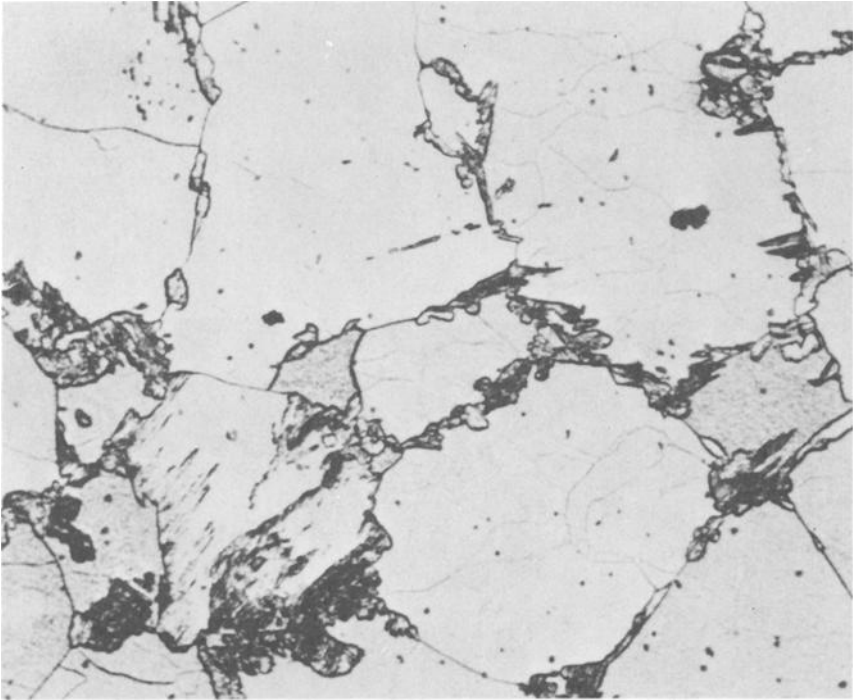
FIG. 4b—*Simulated HAZ microstructure, Steel J, Stimulation 2. Subgrain boundary precipitation of chromium carbonitrides outlining original grain boundaries (×200).*

content and employing lower carbon and nitrogen contents. However, improvements in the currently investigated steels were marginal.

Thus, within the AISI 409 specification, improvements in weldability and weld HAZ properties are almost impossible to achieve. This perhaps explains the efforts in developing proprietry grades of low-carbon chromium stainless steels in recent years.

The other major problem that has not been considered in the present work is that of filler compositions. Although some ferritic stainless steel-covered electrodes are available, the resultant weld deposits are low in ductility and austenitic stainless steel fillers are often recommended [11]. Such practices are often satisfactory but can lead to fusion line embrittlement.

Conclusions

1. The response of four heats of AISI 409 ferritic stainless steel to welding and simulated HAZ thermal cycles has been examined.

FIG. 5a—*HAZ microstructure in SMA B-2. Granular, blocky martensite and angular Widmanstatten intragranular martensite* (×300).
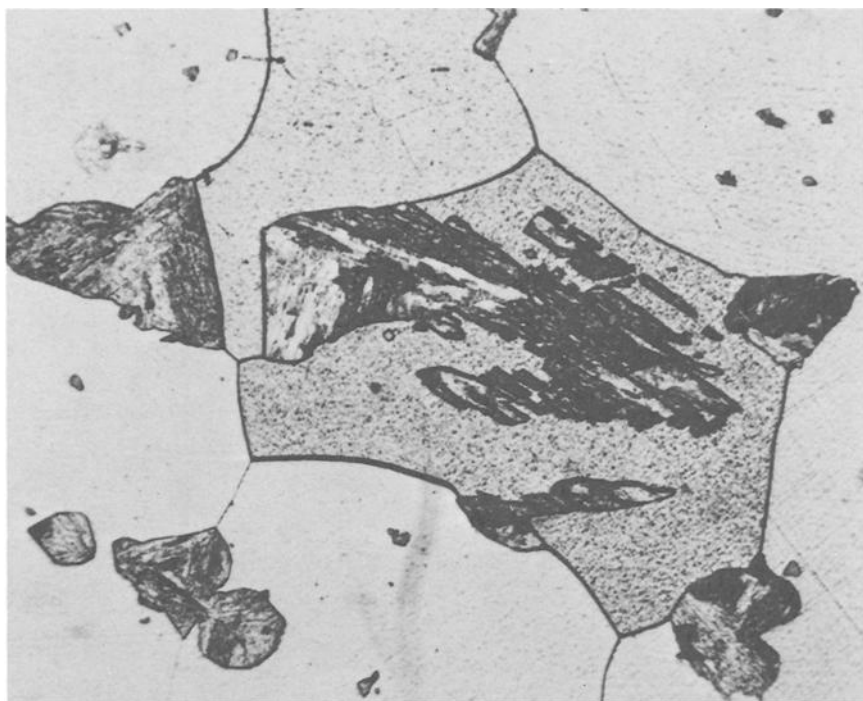
FIG. 5b—*Simulated HAZ microstructure. Steel C, Simulation 7 (×300).*

TABLE 5—Results of weld tests.

Steel Weld Identification	Process	Location of Failure[a]	Tensile Properties			Maximum HAZ Grain Size, ASTM No.	Transition Temperature, °C		Corrosion Rate, mils/year
			0.2% Proof Strength, N/mm²	Ultimate Tensile Strength, N/mm²	% Elongation, $L_o = 5.65\sqrt{S_o}$		30 J	GE[b]	
A-1	SMA	PM	334	452	30	2 to 3	74	61	183
A-2	SMA	PM	342	458	32	3	44	50	243
A-1	GMA	FB	170	230	12	2 to 3	..	..	186
A-2	GMA	FB	208	244	10	3	..	..	244
B-1	SMA	PM	360	470	34	2 to 1	44	48	177
B-2	SMA	PM	388	462	32	2 to 1	45	49	208
B-1	GMA	PM	370	468	32	3 to 2	52	53	165
B-2	GMA	PM	382	478	32	2 to 2	34	39	305
C-1	SMA	PM	330	510	28	3 to 2	31	44	195
C-2	SMA	PM/HAZ	398	544	24	2 to 1	57	64	318
C-1	GMA	FB	196	216	8	4 to 3	65	67	259
C-2	GMA	PM	324	522	28	2 to 1	36	30	342
J-1	SMA	PM	322	462	27	3 to 2	73	78	261
J-2	SMA	PM	343	481	30	2 to 1	63	55	179
J-1	GMA	PM	328	457	30	4 to 3	48	56	227
J-2	GMA	PM	331	473	27	4 to 3	57	66	356

[a]PM = parent metal.
 FB = fusion boundary.
HAZ = heat-affected zone.
[b]GE = graphical determination of transition temperature using absorbed energy.
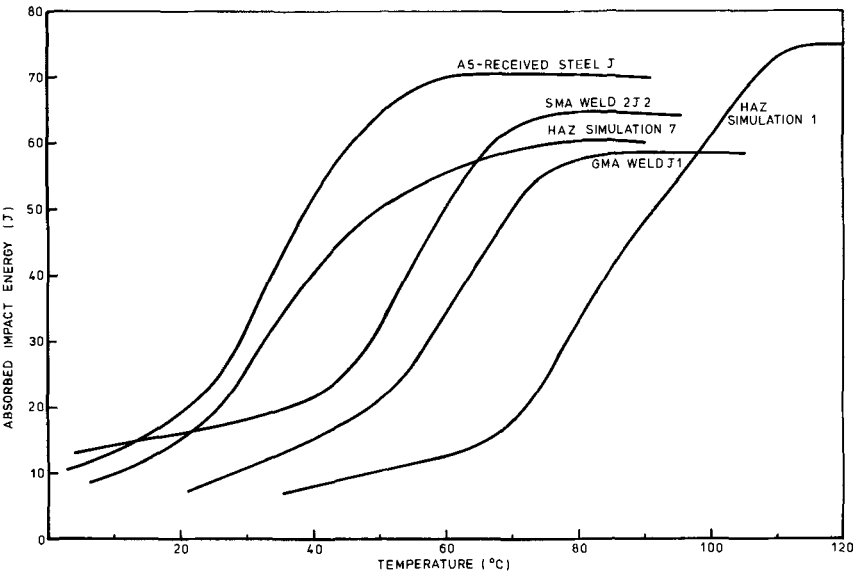
FIG. 6—*Impact transition curves for Steel J.*
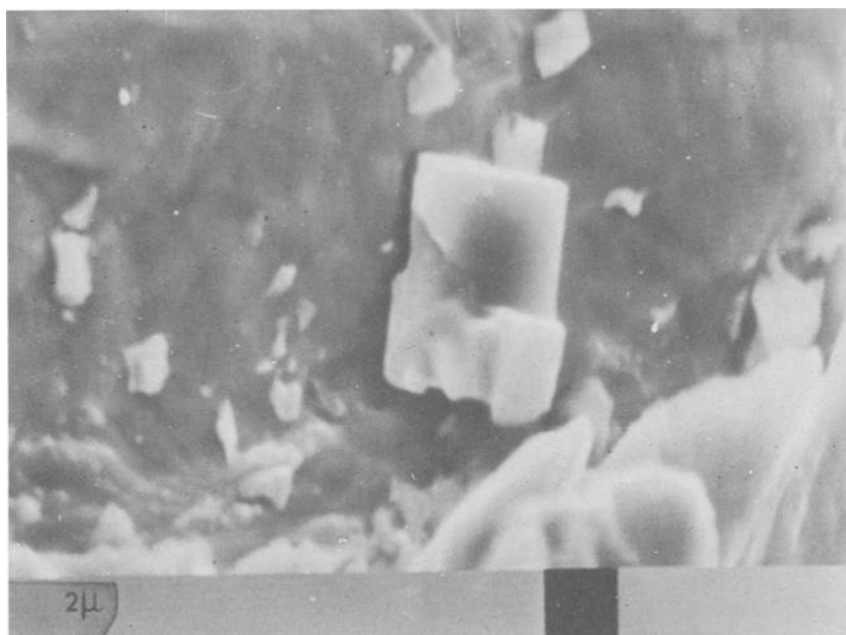
FIG. 7a—*Ductile fracture surfaces from impact tests. Cubic titanium carbonitride at base of ductile dimple. Steel C—as received.*
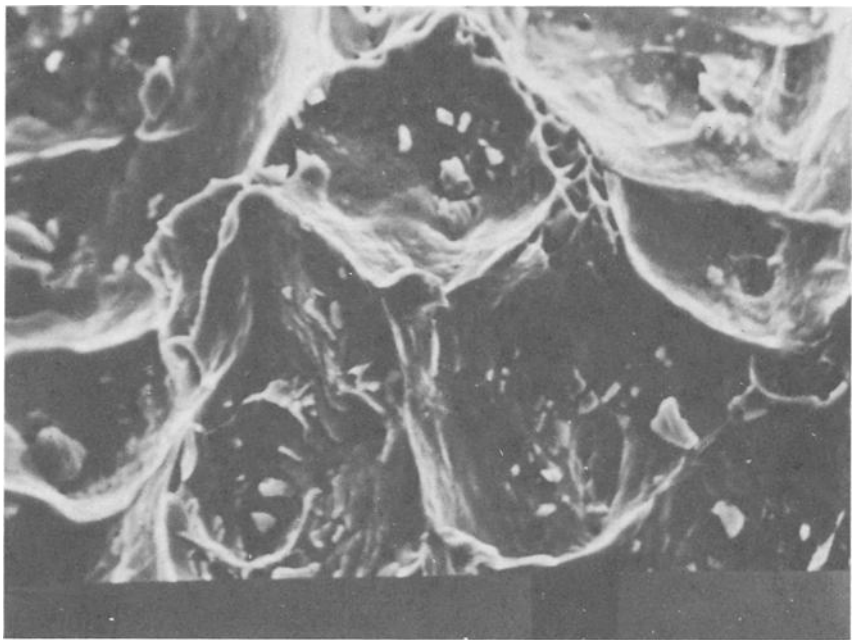
FIG. 7b—*Sulfide inclusions at the base of ductile dimples. Steel C—simulated HAZ No. 1.*
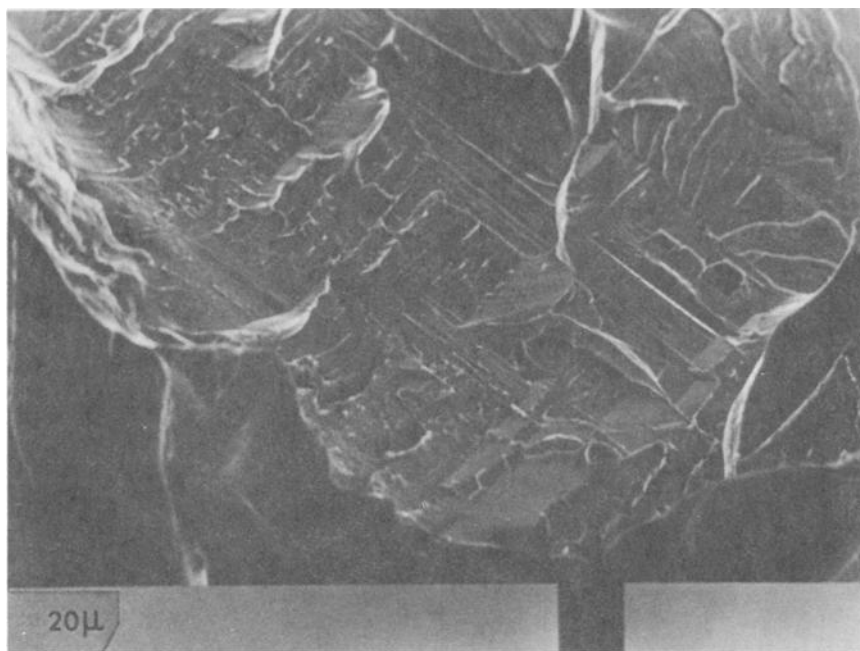
FIG. 8a—*Brittle fracture surfaces from impact tests. Transgranular cleavage fracture. Note crystallographic nature of cleavage facets. Steel A—as received.*
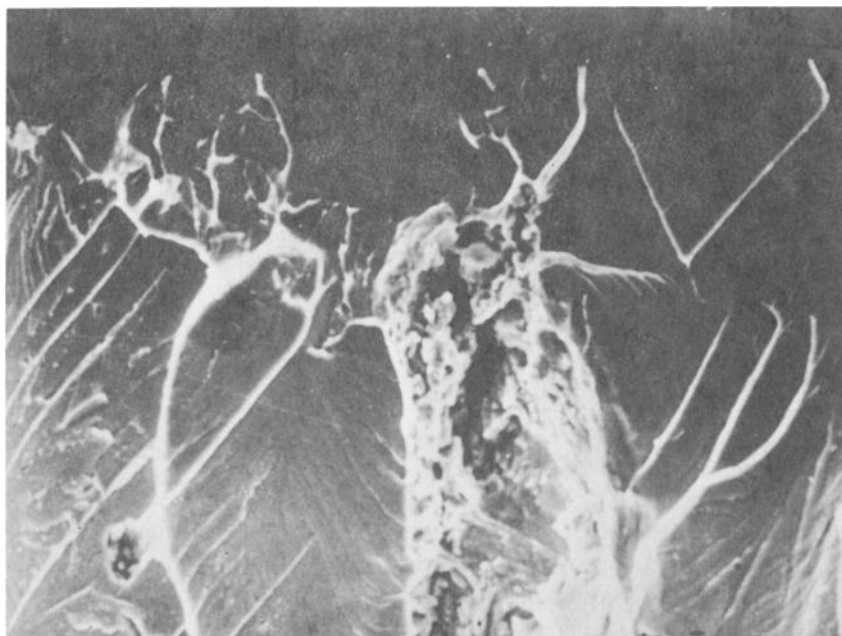
FIG. 8b—*Transgranular cleavage with sulfide-rich grain boundary precipitates.*

2. An increase in impact transition temperature of 30 to 70 deg C was noted for weld HAZ and simulated HAZ specimens, the increase being directly related to the peak temperature reached. A second weld pass or thermal cycle reduced the transition temperature somewhat.

3. Steel hardness increased by up to 30 percent on application of a thermal cycle, the increase being dependent upon peak temperature and rate of cooling.

4. HAZ thermal cycles resulted in significant grain growth, martensite formation, and precipitation of chromium-rich carbonitrides.

5. Use of higher nickel and manganese and reduced titanium restricted the grain growth marginally.

6. The amount of martensite formed was determined by the time spent in the duplex $\alpha + \gamma$ region, reaching a maximum at a peak temperature of 1050°C. Martensite hardness depended upon cooling rate and was reduced by a subsequent thermal cycle.

7. Corrosion resistance depended upon the amount of martensite formed by thermal cycling.

References

[1] Lula, R. A., *Metallurgical Progress*, July 1976, p. 24.

[2] Hooper, R. A. E., *Sheet Metal Industries*, Jan. 1978, p. 15.

[3] Kaltenhauser, R. H., *Metallurgical Engineering Quarterly*, May 1971, p. 41.

[4] "Heat Resisting Steel YUS 409D," Nippon Steel Corp., Japan, Sept. 1978.

[5] "Stainless Steel in Mining" in *Proceedings*, Conference, Southern Cross Steel Co., Johannesburg, South Africa, Aug. 1978.

[6] Miska, K. H., *Materials Engineering*, Vol. 85, No. 4, April 1977, p. 69.

[7] "An Introduction to NSS21-2 Stainless Steel," Nisshin Steel Co., Japan, Dec. 1972.

[8] Clifton, T. E. and George, M. J., College of Aeronautics, Cranfield, U. K., Mat. Note, Feb. 1968.

[9] Thomas, C. R. and Apps, R. L., to be published.

[10] Pickering, F. B., *International Metallurgical Review*, Vol. 21, Dec. 1976, p. 227.

[11] Castro, R. J. and de Cadenet, J. J. "Welding Metallurgy of Stainless and Heat Resisting Steels," Cambridge University Press, Cambridge, U. K., 1975.

DISCUSSION

J. P. Hoffman,[1] (*written discussion*)—Since February 1977 we have been producing commercially a modified 409 under the proprietary name 3CR12. Interstitial levels are kept low (total carbon plus nitrogen = 0.05 maximum) and, because titanium greatly in excess of that required for stabilization reduces toughness, a maximum titanium content is specified (0.30). Careful balancing of other elements like nickel, manganese, and silicon gives a steel with the following typical mechanical properties in the annealed condition (annealed at 700 to 720°C): Tensile strength (UTS), 460 MPa; 0.2 percent proof, 280 MPa; elongation, 30 percent; impact values for plate of 12.5-mm gage: 50 J at −10°C and 20 J at −30°C (full Charpy V-notch).

Welding tests show that the steel is not prone to excessive grain growth in HAZ provided heat input during welding is controlled. The low carbon martensite that forms during welding is tough and ductile. Half-size Charpy V-notch results with notch in HAZ: 8 J at −30°C.

Nil ductility tests (Pellini) on 19-mm material show low nil ductility transition, and fracture toughness tests (crack opening displacement) indicate that the steel has excellent resistance to crack propagation. Although the steel shows a lamellar mode of fracture (Charpy specimens), through-thickness tensiles on 19- and 25-mm plate give high reduction in area values (20 percent plus).

Typically the silicon content is approximately 0.4 percent, titanium 0.2 percent, carbon 0.025 percent, nitrogen 0.015 percent, manganese 0.80 percent, chromium 11.25 percent, nickel 0.4 percent minimum; sulfur and phosphorus are both about 0.015 percent. As sulfur is increased, the ductile-to-brittle transition temperature (DBTT) is increased.

High nickel 409 (stabilized) has a DBTT (at 30 J criterion) of approxi-

[1] Southern Cross Steel, Middelburg, Transvaal, South Africa.

mately −40°C compared with conventional UNS S40900, which is above room temperature. Other mechanical properties are also improved.

This modified 409 (3CR12) finds successful applications in the following areas: ore cars, chutes, expanded metal flooring, hoppers, tanks, abattoir trolleys, mobile garbage disposal units, sections of piping, etc.

T. G. Gooch[2] (*written discussion*)—1. I would endorse the view that martensite formation is not necessarily deleterious to toughness, as evidenced by the good behavior of a number of low-carbon fully martensitic stainless steels.

2. Differentiation in terms of ductility and toughness may be necessary between thick and thin material, with martensite being acceptable (or even beneficial) in, say, 6-mm steel, but fully ferritic stock being preferable for sheet products.

[2] The Welding Institute, Abington Hall, Abington, Cambridge, U. K.

H. E. Deverell[1]

Toughness Properties of Vacuum Induction Melted High-Chromium Ferritic Stainless Steels

ABSTRACT: Impact transition behavior of commercial heats of three low interstitial vacuum induction melted high-chromium ferritic stainless steels was studied as a function of gage. A 50 percent shear fracture ($FATT_{50}$) (fracture appearance transition temperature) of Charpy V-notch impact specimens was used as the transition criterion.

E-BRITE alloy, a 26Cr-1Mo alloy, was studied as formerly melted using electron beam refining and as currently melted by vacuum induction melting. With either melting, E-BRITE shows substantially lower impact transition at a given gage than a titanium-stabilized 26Cr-1Mo alloy made to conventional interstitial levels. Gage was observed to affect impact transition, with light gages showing lower $FATT_{50}$. Slow cooling from anneal is observed to substantially increase $FATT_{50}$ in comparison with water quenching. This effect is also seen in the heat-affected zone of welds. Using proper shielding and preparation, however, weld metal and base metal away from the weld show similar transition temperatures.

The other two alloys studied are high-purity materials containing 29Cr-4Mo and 29Cr-4Mo-2Ni, respectively. These are similar to E-BRITE alloy in impact behavior with the exceptions (1) that 2 percent nickel can lower water-quenched $FATT_{50}$, and (2) that these alloys are sensitive to precipitation of σ and χ phases.

Full-size (10 mm) impact specimens of each alloy can show $FATT_{50}$ below room temperature if satisfactorily heat-treated.

KEY WORDS: stainless steels, ferritic stainless steels, vacuum induction melting, 26Cr-1Mo, 29Cr-4Mo, 29Cr-4Mo-2Ni, gage, impact properties, toughness, Charpy V-notch, impact transition, fracture appearance transition temperature, fracture toughness

A purpose of this paper is to describe the toughness properties of three high-purity high-chromium ferritic steels which are presently produced in the United States by vacuum induction melting.

[1] Research specialist, Stainless and Alloy Metallurgy, Allegheny Ludlum Steel Corp., Research Center, Brackenridge, Pa. 15014.

One of these alloys is E-BRITE[2] alloy, a 26Cr-1Mo steel that was developed by Airco Vacuum Metals, a division of Airco, Inc. [1].[3] The chemical composition is given in Table 1. The alloy was initially produced by a process involving vacuum induction melting followed by electron beam refining and a form of continuous casting. In 1977 the rights to the alloy and accompanying trademark were purchased by Allegheny Ludlum Industries, Inc., and the process was changed to that of vacuum induction melting only, followed by pouring into conventional ingot molds. A secondary purpose of this paper is to compare the properties of the present product with those of the earlier product, since the processing practice is different from that used by Airco Vacuum Metals.

The other two alloys are 29Cr-4Mo (29-4) and 29Cr-4Mo-2Ni (29-4-2), both of which were developed and patented by Streicher of DuPont [2]. The compositions are shown in Table 1. These alloys were developed primarily for heat exchanger tubing that would resist crevice, pitting, and stress corrosion attack in particularly aggressive river waters.

Background

All three alloys must be melted to very low levels of carbon and nitrogen (C + N) to achieve the necessary as-welded mechanical properties and corrosion resistance. Vacuum induction melting is the only commercial method presently available in the United States to achieve the required low interstitial contents consistently. In addition, raw materials must be selected and controlled to obtain the necessary low nitrogen contents since this element is not readily removed during melting of large commercial heats. E-BRITE alloy is melted to 0.002 percent typical carbon and 0.010 percent typical nitrogen, but even at these low interstitial levels sensitization can occur in welds [3] unless care is taken to prevent it. Airco had controlled columbium to about 0.10 percent in the E-BRITE alloy for several years to improve toughness and prevent weld sensitization, presumably by removing some interstitials from solid solution. Allegheny Ludlum has continued this practice.

The 29Cr-4Mo and 29Cr-4Mo-2Ni alloys have somewhat higher tolerance for carbon and, particularly, for nitrogen [4,5]. A recent study of the 29Cr-4Mo alloy [4] showed that 250-ppm nitrogen did not cause weld sensitization at 42-ppm carbon. Weld sensitization did occur, however, at slightly higher interstitial levels of 45-ppm carbon and 265-ppm nitrogen. The study also indicated that carbon should be kept well under 100 ppm at any nitrogen level to avoid sensitization. Carbon contents between 50 and

---

[2] Registered trademark—Allegheny Ludlum Industries, Inc.
[3] The italic numbers in brackets refer to the list of references appended to this paper.

TABLE 1—Compositions of alloys.

	C	N	Cr	Mo	Ni	Mn	Si	(C + N)
E-BRITE								
type	0.010 max	0.015 max	25.0 / 27.5	0.75 / 1.50	0.50 max	0.40 max	0.40 max	... ...
range tested	0.0006 / 0.0030	0.003 / 0.017	...	...	...	...	...	0.005 / 0.019
AL-29-4								
type	0.010 max	0.020 max	28.0 / 30.0	3.5 / 4.2	0.15 max	0.30 max	0.20 max	0.025 max
range tested	0.002 / 0.007	0.005 / 0.019	...	...	...	...	...	0.007 / 0.025
AL-29-4-2								
type	0.010 max	0.020 max	28.0 / 30.0	3.5 / 4.2	2.0 / 2.5	0.30 max	0.20 max	0.025 max
range tested	0.002 / 0.006	0.005 / 0.016	...	...	...	...	...	0.007 / 0.019

100 ppm have not been thoroughly investigated. Present practice is to keep carbon below 50 ppm for this reason.

The levels of the interstitial elements, carbon and nitrogen, are important to the toughness as well as to the corrosion resistance of high-chromium ferritic alloys. Binder and Spendelow [6] and Baerlecken et al [7] established many years ago that these elements must be kept low to achieve good impact resistance in annealed and quenched ferritic stainless steels at ambient temperatures. Binder and Spendelow further showed that the tolerance for these elements decreased as chromium content increased—for example, from 375 ppm at 20 percent chromium to 200 ppm at 30 percent chromium. More recently Demo [8] has shown that the tolerance for interstitial elements is further restricted for the as-welded condition. Demo showed that to maintain good as-welded bend ductility at room temperature and intergranular corrosion resistance the interstitial elements must be kept below about 150 ppm at 25 percent chromium and 80 ppm at 30 percent chromium.

The room temperature toughness of ferritic stainless alloys is influenced by the rate at which they are cooled from elevated temperatures. For example, water-quenching from the annealing temperature consistently produces lower impact transition temperatures than does air-cooling in these alloys [9,10]. This cooling rate effect has been ascribed to either 475°C (885°F) embrittlement or precipitation of interstitial compounds. Recent unpublished data [11] show that there appears to be an incubation period of 1 to 10 h before exposures at 475°C (885°F) will produce embrittlement in these alloys, suggesting that the precipitation of interstitial compounds is responsible for the impairment in properties of air-cooled specimens.

Very slow cooling, however, or extended exposures at temperatures near 475°C (885°F) causes 475°C (885°F) embrittlement [9,10]. The 29Cr-4Mo and 29Cr-4Mo-2Ni alloys, but not E-BRITE alloy, are also readily susceptible to a high-temperature embrittlement caused by the precipitation of σ and χ phases. Embrittlement occurs most rapidly at about 750 to 800°C (1382 to 1472°F) and is more severe than that occurring at 475°C (885°F) [10]. The embrittling σ and χ phases persist to temperatures as high as 982°C (1800°F); therefore these alloys must be annealed at temperatures of about 1010°C (1850°F) minimum.

Another metallurgical variable that may affect impact transition temperature is the grain size. Little or no influence of grain size in the rather narrow range of ASTM No. 4.5 to No. 1 on impact transition temperatures was observed by Nichol [10] on the 29Cr-4Mo-2Ni alloy. Nichol also showed the relatively large influence on apparent transition temperatures of specimen thickness when reduced below the standard Charpy V-notch dimension. In the work reported herein, no attempt has been made to restrict grain size. In most observations, the anneal cycles used for 29Cr-4Mo and

29Cr-4Mo-2Ni produce a relatively large grain size compared with comparable E-BRITE products.

Typical mechanical properties of the alloys annealed and quenched are shown in Table 2. Figure 1, from a paper by Lula [12], provides impact transition data for a number of ferritic stainless steels over a range of gages. In this case, transition temperature is defined by absorption of 41 J (30 ft-lb) in tests at 5 mm (0.197 in.) or thicker. At lighter gages, half peak height was used. This recognizes again that low interstitials provide lower Charpy V-notch impact transition temperatures; however, not shown is the substantial variability possible in these materials from processing variations, such as cooling rates.

In the work reported here, the measure of impact transition temperature is 50 percent shear fracture in Charpy V-notch specimens.

Impact Toughness of E-BRITE

First discussed are the impact toughness properties of E-BRITE alloy, which appears to be the simplest metallurgically since it does not readily

TABLE 2—*Typical mechanical properties of the annealed and water-quenched alloys.*

Alloys	0.2% Offset Yield Strength, MPa (ksi)	Ultimate Tensile Strength, MPa (ksi)	% Elongation, 50.8-mm (2 in.) gage	Hardness, R_B
E-BRITE				
XM-27	379 (55)	503 (73)	37	84
AL-29-4	517 (75)	620 (90)	25	95
AL-29-4-2	586 (85)	655 (95)	22	95
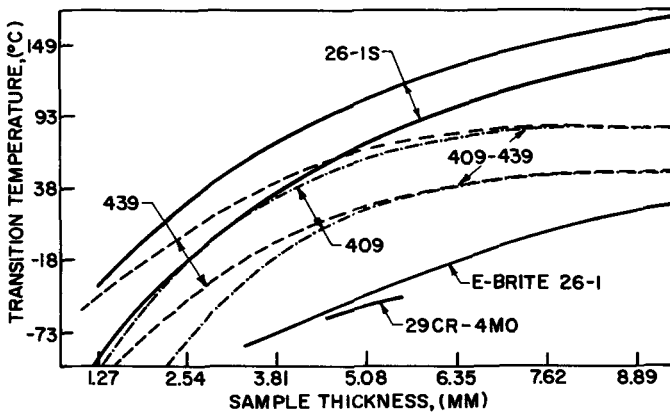
FIG. 1—*Impact transition as a function of section thickness for several alloys* [12].

form the embrittling σ or χ phases [*13*]. Figure 2 is a plot of FATT$_{50}$ (fracture appearance transition temperature) versus (C + N) contents for a large number of commercial heats. The data were obtained from 3.2 to 3.8-mm-thick (0.125 to 0.150 in.) hot-rolled band specimens that were annealed and water-quenched in our laboratory. They encompass late electron beam refined heats purchased as ingot or band from Airco and early vacuum induction heats made by Allegheny Ludlum. There is overlap in FATT$_{50}$ between heat sources, with, in this sampling at least, some lower values for the vacuum-induction-melted-only material. The Allegheny Ludlum melting encompasses a wide range of raw material selection with some early heats even above the 150-ppm-nitrogen maximum. Since then, raw material selection has been controlled to yield an average (C + N) value around 120 ppm.

Figure 3 summarizes FATT$_{50}$ determinations on laboratory annealed and water-quenched E-BRITE alloy as a function of gage for a number of commercial heats. The upper bound drawn on these data defines the capabilities of the material when water-quenched to minimize cooling rate effects. This upper bound defines a "capability curve," or the boundary of FATT$_{50}$ versus gage, which appears to be consistently achievable from commercial products. The shape of the curve is generally like that shown by Lula (Fig. 1) but at generally lower temperature levels than materials in his
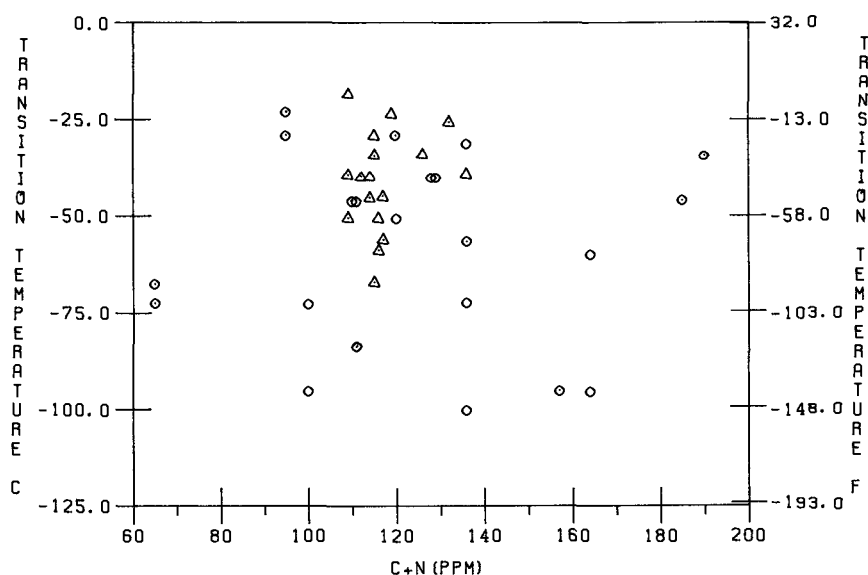
FIG. 2—*FATT$_{50}$ versus (C + N) for E-BRITE alloy commercial heats in 3.2 to 3.8-mm (0.125 to 0.150 in.) range. Material laboratory-annealed and quenched. Triangles: Airco heats; circles: Allegheny Ludlum heats.*
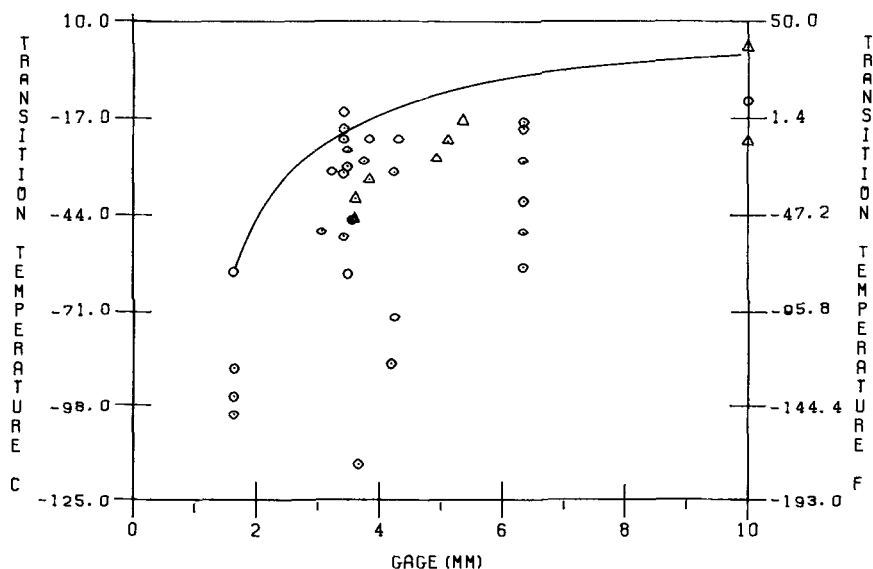
FIG. 3—*FATT$_{50}$ of E-BRITE alloy commercial heats as a function of section thickness. Materials laboratory-annealed and water-quenched. Triangles: Airco heats; circles: Allegheny Ludlum heats. Solid line denotes apparent material capability or "capability curve."*

figure, reflecting both the laboratory anneal and water-quench and the vacuum induction melting (C + N) levels. It should be noted that, at FATT$_{50}$ in laboratory-annealed and water-quenched specimens, average values of 68 to 83 J (50 to 60 ft-lb) are absorbed in the 4.76 to 6.35 mm (3/16 to 1/4 in.) thickness range and 150 to 175 J (110 to 130 ft-lb) in the full-size specimen, both considerably greater than the 41 J (30 ft-lb) transition measure used by Lula. Above FATT$_{50}$, E-BRITE alloy and also the 29-4 alloy will generally absorb about 325 J (240 ft-lb) in full-sized specimens. The nickel in 29Cr-4Mo-2Ni produces slightly lower upper-shelf energy compared with 29Cr-4Mo.

Slow cooling rates exert a significant detrimental effect on impact properties of these high-chromium alloys. Air-cooled FATT$_{50}$ was determined as a comparison for a number of the same heats used in the water-quenched series. These data are shown in Fig. 4. Air-cooling is observed to have the effect of increasing FATT$_{50}$ markedly. Neglecting the single very large difference in the figure, air-cooling increased observed FATT$_{50}$ by an average value of 35 deg C (63 deg F) with somewhat larger effects at heavier gages. Figure 5, showing full curves for water-quenched and air-cooled 6.35-mm (1/4 in.) specimens, shows also that the upper-shelf energy is somewhat lowered by air-cooling. In early experience with production of E-BRITE alloy, mill-produced material was compared with laboratory-anneal and water-quenched material. This comparison curve with data
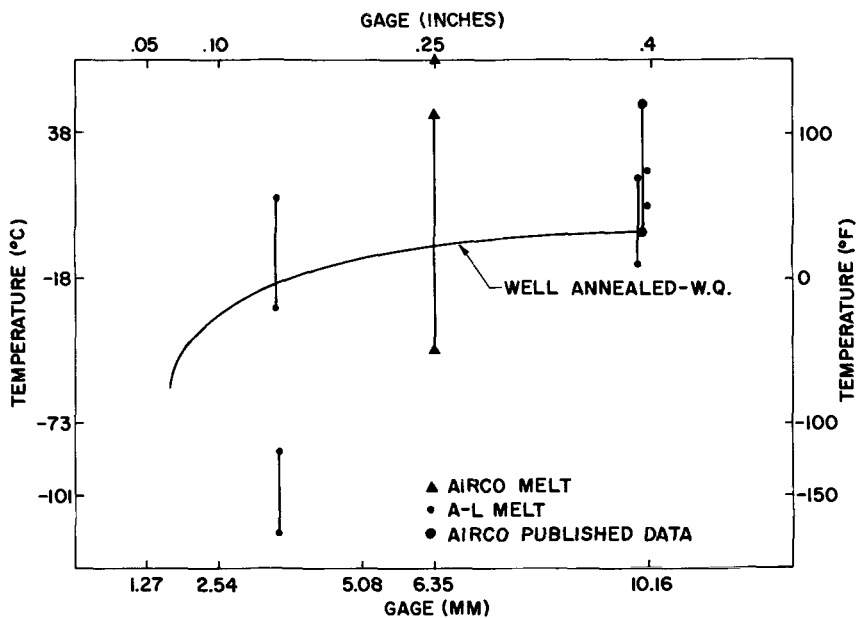
FIG. 4—*Effect of air-cooling versus water-quench on FATT$_{50}$ of E-BRITE alloy as a function of section thickness. Materials laboratory-annealed.*
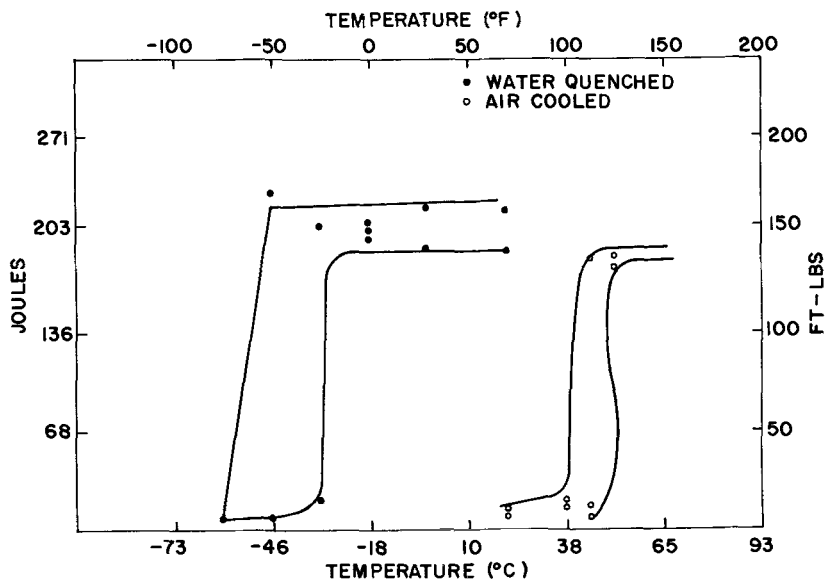
FIG. 5—*Full impact curves for 6.4-mm (0.25-in.) Allegheny Ludlum-melted E-BRITE alloy laboratory-annealed and air-cooled or water-quenched.*

from both Airco and Allegheny Ludlum melted materials, Fig. 6, shows
the virtual equivalence of laboratory water-quenched specimens and mill-
produced material at light gages. In thicker mill-produced plate, we ap-
parently observe cooling rate effects. This material, possibly 2.5 m (over
8 ft) wide by 6.2 m (over 20 ft) long, is sufficiently heavy gage that full size
Charpy V-notch specimens can be machined from it. Such plates, weighing
910 kg (2000 lb) or more, are quenched rapidly from the annealing temper-
ature. The results show that cooling rate effects on heavy-section plate
produce a product intermediate between small water-quenched and air-
cooled specimens annealed in the laboratory, but generally closer to the
water-quenched material. This demonstrates that care is required in the
controlling processing to get desired properties in mill product forms. These
results prove that properties are equivalent in laboratory-treated and mill-
treated material over all but the heaviest gage ranges and that both provide
very low impact transitions in comparison with a comparable alloy made
with air melt (C + N) levels.

Welding can alter properties by allowing pickup of carbon, nitrogen, or
oxygen, by changing grain size, and by cooling rate effects. Most of the
problems observed in E-BRITE alloy service, either mechanical or corro-
sion, have been caused by contaminated welds. Figure 7 provides full-range
curves from base, weld metal, and heat-affected zones (HAZ's) taken from
welds made using good shielding and preparation. The specimens were
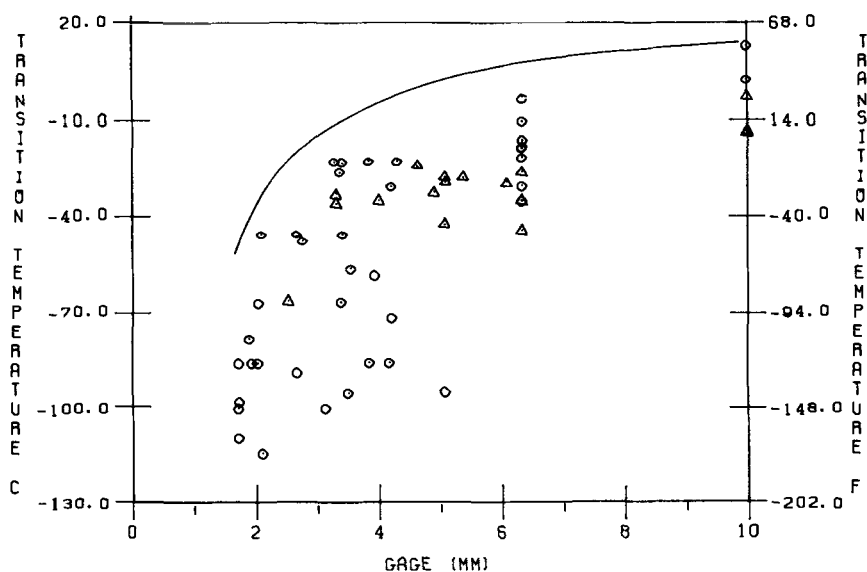
FIG. 6—*FATT$_{50}$ of mill-produced E-BRITE alloy as a function of section thickness.
Triangles: Airco heats; circles: Allegheny Ludlum heats.*
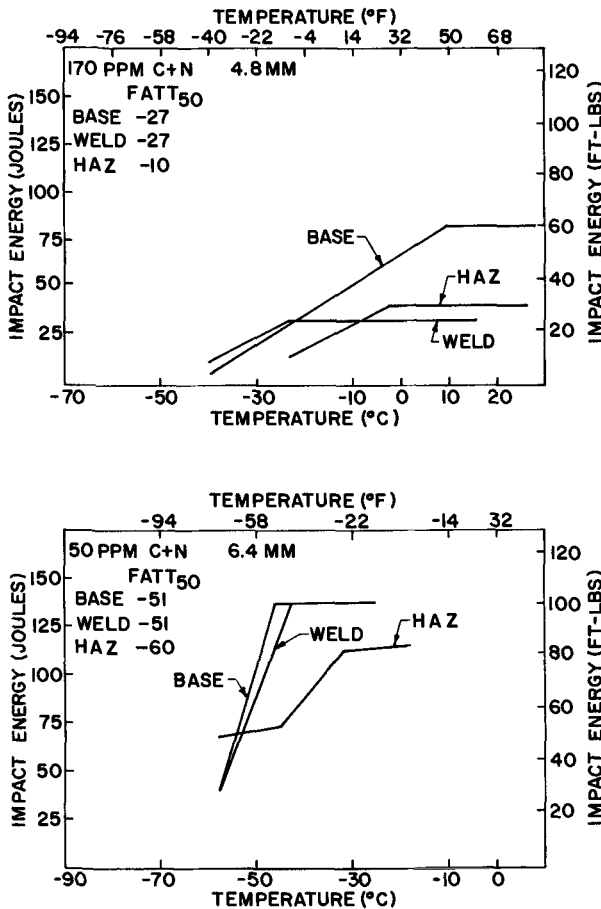
FIG. 7—*Full impact curves for base, weld metal, and heat-affected zone (HAZ) of two Allegheny Ludlum heats of E-BRITE alloy with different (C + N) levels and section thicknesses.*

taken from 6.4 mm (1/4 in.) for the 50-ppm (C + N) alloy and 4.8 mm (3/16 in.) for the 170-ppm alloy with bead-on-plate welds passed on surfaces aiming for 60 percent penetration in each of the two passes. With this technique, weld and base metal should have the same composition. This comparison is weld versus base metal versus HAZ. The apparent highest transition region in the material is in the HAZ, presumably from the thermal cycle undergone in welding. Tests to date have shown results typified by a schematic in Fig. 8 when shielding has been good.

So, in summary for E-BRITE alloy:

1. Low impact transition in a 26Cr steel as measured by $FATT_{50}$ is produced by low interstitials as was demonstrated long ago on laboratory heats.
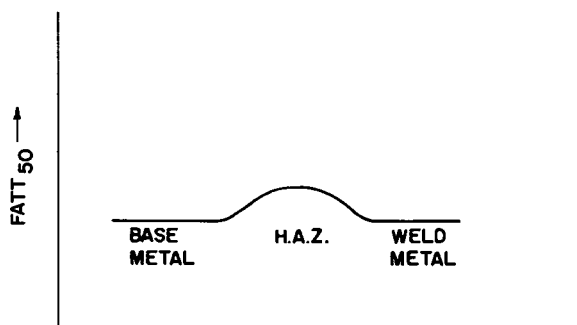
FIG. 8—*Schematic of base metal, weld, and HAZ FATT$_{50}$ for E-BRITE alloy welded with good shielding.*

These properties can be achieved on commercial heats.

2. There is a strong gage effect on transition temperature.

3. There is strong cooling rate effect on transition temperature. This effect is attributed to the precipitation of trace amounts of interstitial compounds.

4. There is a strong effect of contamination, should it occur, on weld metal transition temperature, though this is not demonstrated by data presented here.

5. When good shielding is used in fabrication, the HAZ shows slightly higher impact transition than the base metal away from the weld or the weld metal itself. This again is attributed to the precipitation of interstitial compounds, most likely chromium carbides and nitrides.

Impact Toughness of 29-4 and 29-4-2

We have treated the 29-4 alloys separately since they are more prone to precipitation of σ and χ phases. The 2Ni alloy is somewhat more sensitive to the formation of σ and χ phases than the low-nickel alloy. One reason for the nickel addition (29-4-2) is the improved corrosion resistance in some reducing media such as hydrochloric and sulfuric acids. The nickel addition also significantly improves impact transition temperatures provided that no σ or χ is precipitated during heat treatment.

The effects of reheating annealed and quenched specimens in certain temperature ranges which precipitate excess phases are shown in Fig. 9. AL-29-4, 1.6 mm (0.065 in.), initially observed to show a FATT$_{50}$ of $-55\,°C$ ($-65\,°F$), is observed to increase in two broad reheat temperature ranges, the upper as a result of σ and χ precipitation, the lower from $475\,°C$ ($885\,°F$) or interstitial compound precipitation or both. Figure 10 shows the same effects at full-thickness impact specimens for AL-29-4-2 initially showing FATT$_{50}$ at $-15\,°C$ ($+5\,°F$) and absorbing about 250 J (185 ft-lb) at room
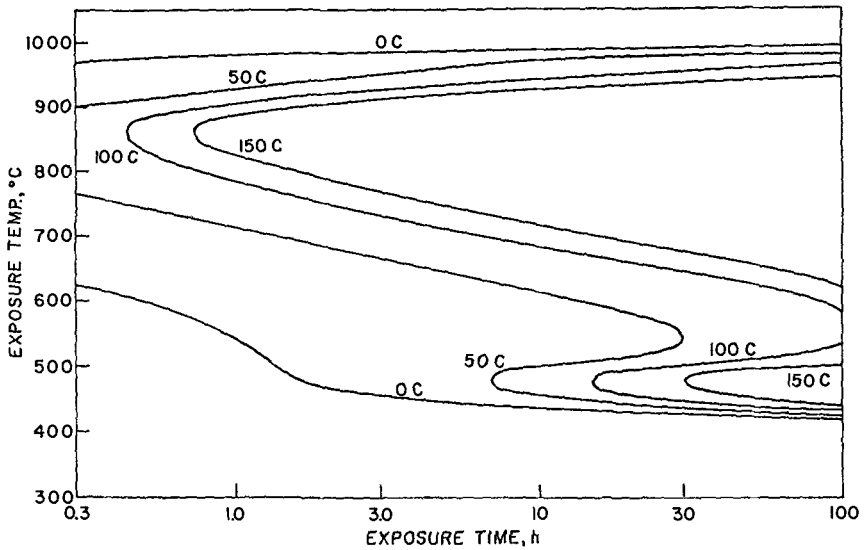
FIG. 9—*Temperature-time cycles to obtain indicated FATT$_{50}$ in 1.6-mm (0.065-in.) AL-29-4 commercial heat. Material initially laboratory-annealed and quenched to FATT$_{50}$ of −55°C (−65°F).*
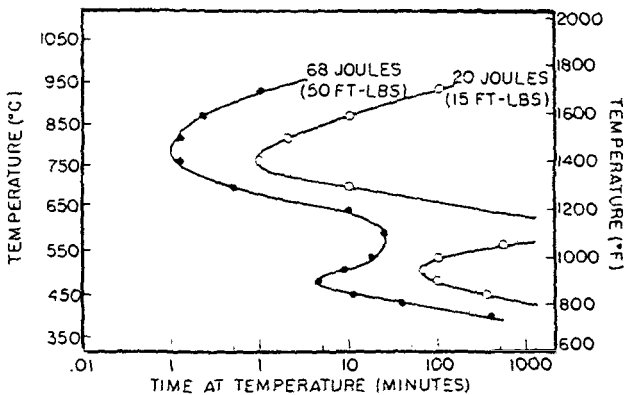
FIG. 10—*Temperature-time cycles to obtain indicated impact energy level in 10-mm (0.394-in.) AL-29-4-2 commercial heat at room temperature. Materials initially laboratory-annealed and quenched to about 250 J (185 ft-lb) at room temperature.*

temperature. Reheating degrades room temperature properties to the values shown through σ and χ or 475°C (885°F) or interstitial compound precipitation, or both, in the same temperature ranges as for AL-29-4. Figure 11 shows a comparison of Charpy V-notch impact energies of E-BRITE alloy, AL-29-4, and AL-29-4-2 alloys laboratory-annealed and water-quenched. As with E-BRITE alloy, but based upon a lesser quantity of test data,
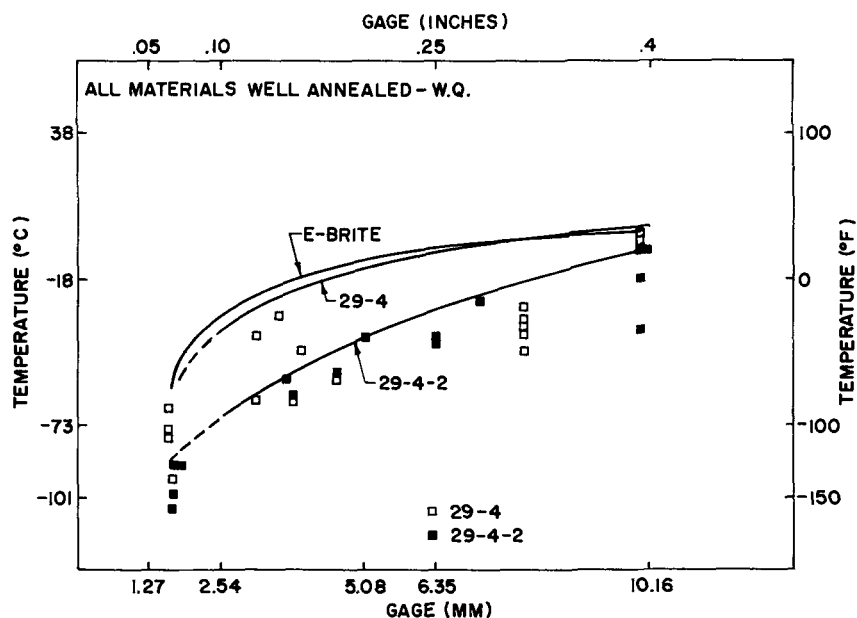
FIG. 11—*FATT_50 of commercial heats of AL-29-4 and AL-29-4-2 as a function of section thickness. Materials are laboratory-annealed and water-quenched. Solid lines denote apparent material capability or "capability curves."*

capability curves have been drawn. The effect of 2 percent nickel at the 29Cr-4Mo level is to lower the capability curve by 20 to 25 deg C (35 to 45 deg F) at lighter gages.

The same cooling rate effects are seen in the more complex alloys. Figure 12 shows air-cooled results for AL-29-4 and AL-29-4-2 compared with the capability curves. Both alloys have substantially higher $FATT_{50}$ temperatures when air-cooled rather than water-quenched and these are also higher than air-cooled E-BRITE alloy. There is a small difference between AL-29-4 and AL-29-4-2 when air-cooled. Figure 13 shows properties observed for mill-produced material.

Relatively few studies of weld metal toughness have been conducted. These are summarized in Fig. 14. The tests to date, which have used good shielding, show properties generally within the capability curves. It is again expected that the HAZ is the area having the highest impact transition temperatures; however, data have not been specifically determined to confirm this.

Discussion

These data show that 29Cr-4Mo alloys containing low interstitial levels can also be commercially produced with Charpy V-notch impact properties
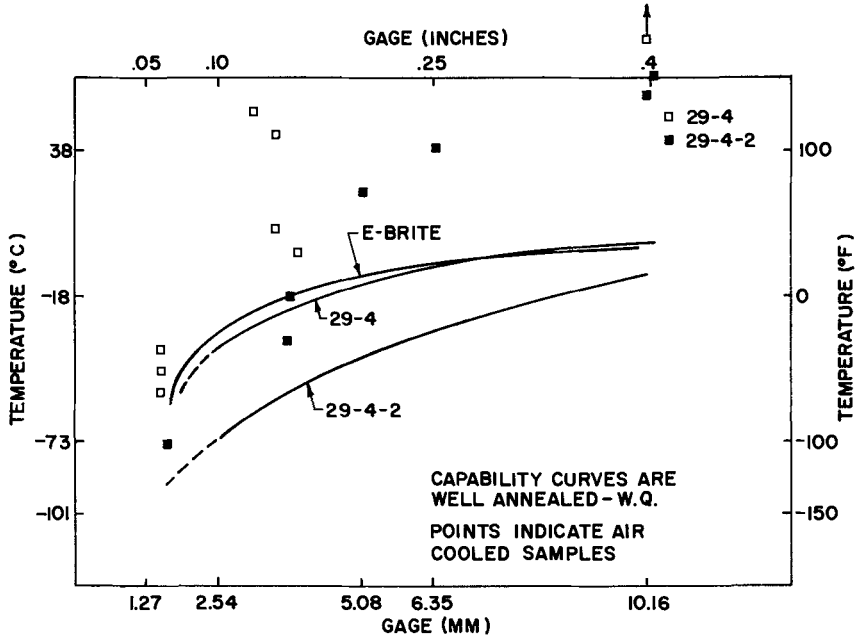
FIG. 12—*Effect of air-cooling on FATT$_{50}$ of AL-29-4 and AL-29-4-2 as a function of section thickness. Materials are laboratory-annealed.*
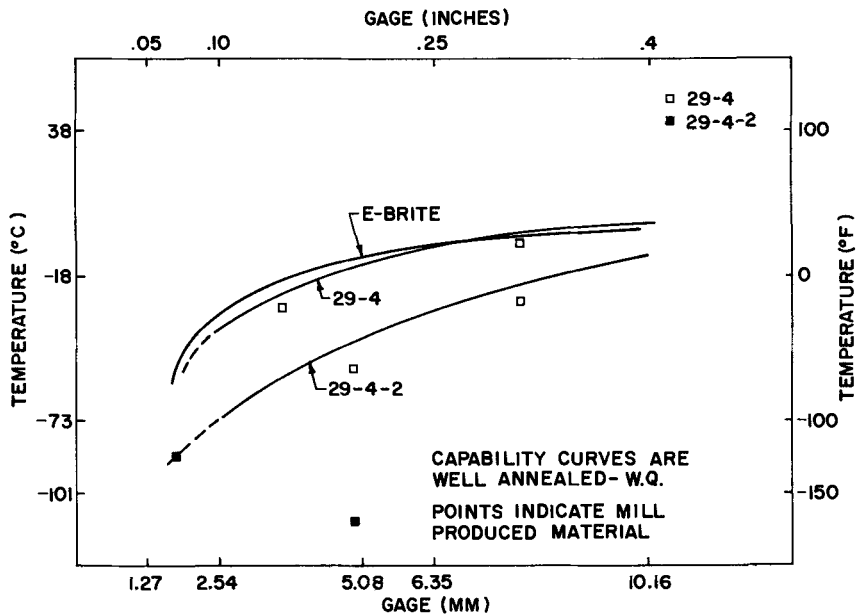
FIG. 13—*FATT$_{50}$ of mill-produced AL-29-4 and AL-29-4-2 as a function of section thickness.*
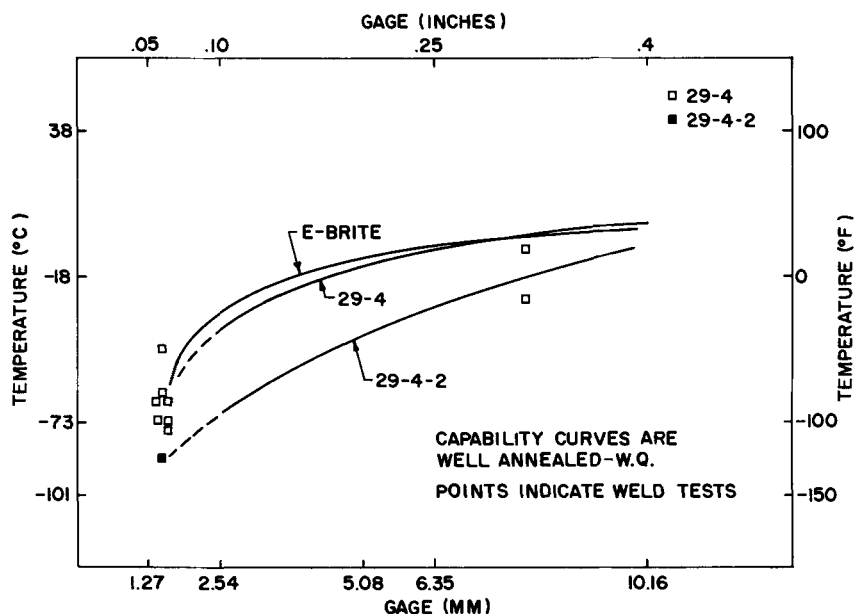
FIG. 14—*FATT₅₀ of AL-29-4 and AL-29-4-2 welds made using good shielding.*

comparable to the low interstitial E-BRITE alloy. The nickel addition provides some further decrease in Charpy V-notch transition temperatures on fast-cooled material. However, the beneficial effects of nickel are lost when the alloy cannot be rapidly cooled from its annealing temperature range, as in air-cooling in annealed specimens. Even with air-cooling, low interstitial levels still provide lower impact transition properties than air melt residuals, especially in heavier sections. When welded with good shielding, weld metal impact properties within the capability curves can be observed.

In all three alloys, full-thickness (10 mm) specimens were observed to show $FATT_{50}$ below room temperature when water-quenched from anneal.

Acknowledgments

The author thanks Dr. G. Aggen for his contributions to, and review of, this paper and Mrs. M. W. Guenther for preparation of the several drafts.

References

[1] U.S. Patents 3,723,101, March 27, 1973, and 3,807,991, April 30, 1974.
[2] U.S. Patents 3,929,473, Dec. 30, 1975; 3,832,174, Jan. 13, 1976; and 3,807,991, Jan. 13, 1976.
[3] Pinnow, K. E., Bressanelli, J. P., and Moskowitz, A., *Metals Engineering Quarterly.* Vol. 15, No. 3, Aug. 1975, p. 32.

[4] Nichol, T. J. and Davis, J. A. in *Intergranular Corrosion of Stainless Alloys. ASTM STP 656,* American Society for Testing and Materials, 1978, pp. 179–196.

[5] Streicher, M. A., *Corrosion.* Vol. 30, No. 3, 1974, p. 77.

[6] Binder, W. O. and Spendelow, H. R., *Transactions.* American Society for Metals, Vol. 43, 1951, pp. 759–772.

[7] Baerlecken, E., Fisher, W. A., and Lorenz, K., *Stahl und Eisen,* Vol. 81, No. 12, 1961, pp. 768–778.

[8] Demo, J. J., *Metallurgical Transactions.* Vol. 5, Nov. 1974, pp. 2254–2256.

[9] Franson, I. A., *Metallurgical Transactions.* Vol. 5, Nov. 1974, pp. 2257–2264.

[10] Nichol, T. J., *Metallurgical Transactions. A.* Feb. 1977, pp. 228–237.

[11] Nichol, T. J., Datta, A., and Aggen, G., "Embrittlement of Ferritic Stainless Steels," submitted to *Metallurgical Transactions, A.*

[12] Lula, R. A., *Metal Progress.* July 1976, pp. 24–29.

[13] Kies, F. K. and Schwartz, C. D., *Journal of Testing and Evaluation.* Vol. 2, No. 2, 1974, pp. 118–124.

DISCUSSION

T. G. Gooch[1] *(written discussion)*—Work at The Welding Institute using simulated and actual weld HAZ's on 26-1 material from 2.5 to 12.5-mm thickness has indicated some effect of grain size on toughness, whether determined by Charpy or crack opening displacement tests: coarser grain size tends to give higher transition temperatures. However, 26-1 plate material may have elongated grains. This has been found associated with poor toughness in the plane parallel to the plate surface.

H. E. Deverell (author's closure)—At and above about 4-mm thickness, due to the preparation technique used, elongated grains become more common, especially near center thickness. We have never attempted any short transverse tests but would expect these to exhibit increased transition temperatures as Mr. Gooch indicated.

C. R. Thomas[2] *(written discussion)*—It has been reported (for example, Jarleborg et al[3]) that the weld metal in 18Cr-2Mo-Nb stabilized steels consists of large epitaxial grains, but in titanium—or mixed—stabilized steels, the weld metal grain size is fine and equiaxed. Did the author note this epitaxial growth with 26Cr-1Mo and 29Cr-4Mo alloys? If so, were attempts made to change the weld metal structure by titanium stabilization, and with what effect?

H. E. Deverell (author's closure)—In the 26Cr-1Mo and 29Cr-4Mo alloys studied, the weld metal consisted of large epitaxial grains. We did not

[1] The Welding Institute, Abington Hall, Abington, Cambridge, U.K.

[2] Cranfield Institute of Technology, Department of Materials, Cranfield, Bedford, U.K.

[3] Jarleborg, O., Sawhill, J. M., Jr., and Steigerwald, R. F., *Stahl und Eisen.* Vol. 97, No. 1, 1977, pp. 29–38.

attempt to change the weld metal structure by titanium stabilization but have observed welds in a titanium-stabilized 26Cr-1Mo alloy made to conventional interstitial levels. In that alloy, a portion of the weld often remains as large expitaxial grains, with the center portion tending to finer, equiaxed grains.

B. Mintz[4] *(written discussion)*—The observation that there was little influence of grain size on impact behavior is somewhat surprising in light of the considerable amount of data that exist in the literature showing its importance. In steels containing free interstitials, a change of 1 $mm^{-1/2}$ in grain size has been shown to be accompanied generally by a change of ~10 deg C in transition temperatures.[5] Considerable variation in this vector for the influence of grain size on transition has been reported, however, the vectors quoted ranging from 6 to 25 deg $C/mm^{-1/2}$ (footnote 5). It is believed that the main source of this variability is the difficulty in isolating the influence of grain size from the other variables which affect impact behavior, namely, carbide thickness, precipitation hardening, and fissure formation. Thus, although fast cooling may result in finer grain sizes, it can also be accompanied by an increase in the hardness of the ferrite matrix.

Any improvement in impact behavior from refinement is then offset by the hardening of the ferrite. Coarse grain sizes are often achieved by slow cooling from the normalizing temperature and this results in coarse grain boundary carbides being formed which have an additional detrimental influence on impact behavior. In this case if the grain size is varied by altering the cooling rate, an abnormally high grain size vector could be obtained. Fissure formation, which is related to the presence of an elongated grain structure, relieves the triaxiality of the stress systems associated with a notch and gives rise to lower transition temperatures. Where such behavior is observed, and this is frequently so with the lower-chromium ferritic stainless steels, grain shape is likely to be more important than grain size. The more elongated the grains, the easier it is for fissure formation, resulting in lower transition temperatures. Mintz et al[6] have recently isolated the influence of grain size on impact behavior from all the aforementioned variables and, in these controlled experiments, vectors of 11 to 12 deg $C/mm^{-1/2}$ have been obtained. This work has also shown that generally the critical event in the fracture of steels is the propagation of a grain-size microcrack across the grain boundary, and this accounts for the importance of grain size in determining impact behavior. As the grain

[4] British Steel Corp., Scottish Laboratory, Meadow Road, Motherwell, Lanarkshire, U.K.

[5] Morrison, W. B. et al in *Proceedings*. British Steel Corp. Product Technology Conference on Controlled Processing of HSLA Steels, York University, York, U.K., 1976, Paper 1.

[6] Mintz, B. et al, private communication, British Steel Corp., Scottish Laboratory, Motherwell, Lanarkshire, U.K.

size dependence is linked to a Griffith crack criterion for failure, there should always be some grain size dependence even in the absence of interstitials. Work on interstitial-free iron alloys[7,8] has indeed given vectors of 6 to 12 deg $C/mm^{-1/2}$ for the influence of grain size on transition temperature, the average value being 9 deg $C/mm^{-1/2}$, which is very close to that obtained on interstitial-containing steels. It is therefore possible that the apparent absence of a grain size effect on impact behavior in your work could be due to it being obscured by the other variables detailed in this discussion.

H. E. Deverell (author's closure)—The observation that there was little influence of grain size on impact behavior is based on
  1. the full-range impact curves for base and weld metal shown for E-BRITE in Fig. 7, and
  2. the weld data points which are close to the capability curves (Fig. 14).
There are large epitaxial weld grains and finer equiaxed base metal grains. However, the choice of the customary transverse specimen with notch at the weld centerline may minimize any grain size effect. Similarly, cooling rate from weld was not controlled to give a comparable rate to base metal preparation.

Nichol [10] tested equiaxed material water-quenched after varied anneal cycles to reach the conclusion that the grain size effect is relatively small compared with the gage effect.

Therefore, we agree that additional experiments might isolate a grain size effect from the variability reported, as in the laboratory annealed and quenched data, but it was not attempted in this work.

[7]Leslie, W. C., *Metallurgical Transactions*, Vol. 2, 1971, p. 1989.
[8]Jin, S., Hwang, S. K., and Morris, J. W., *Metallurgical Transactions. A*, Vol. 6A, 1975, p. 1721.

N. Ohashi,[1] Y. Ono,[1] N. Kinoshita,[1] and K. Yoshioka[1]

Effects of Metallurgical and Mechanical Factors on Charpy Impact Toughness of Extra-Low Interstitial Ferritic Stainless Steels

ABSTRACT: The effects of precipitates, grain size, plate thickness, and notch sharpness on the Charpy impact toughness of extra-low interstitial 18Cr-2Mo, 26Cr-1Mo, and 29Cr-2Mo steels were investigated.

The steels exhibit good toughness in the solution-treated condition at 1000 to 1200°C and subsequently in the 2-mm V-notched condition. If the steels are subjected to fatigue cracks or brittle weld cracks, their transition temperatures increase and their shelf energies decrease.

When the steels are slowly cooled from the solution temperatures or reheated at intermediate temperatures, 700 to 900°C, after solution treatments, precipitation of second phases occurs, such as Laves phase in 18Cr-2Mo steel and sigma phase in 26Cr-1Mo and 29Cr-2Mo steels. The steels are embrittled by these precipitates and behave very similarly to the solution-treated specimens, having sharp notches such as fatigue cracks or brittle weld cracks.

A decrease in grain size or thickness is beneficial in lowering the transition temperatures of solution-treated and 2-mm V-notched specimens. This effect, however, decreases, when the specimens have brittle weld cracks.

These test results suggest that the solution-treated steels have good resistance to brittle fracture initiation and poor resistance to brittle crack propagation. Precipitation of second phases assists mainly crack initiation but also crack propagation to a lesser extent.

KEY WORDS: ferritic stainless steels, Laves phase, sigma phase, grain size, specimen size, notch sharpness, V-notch, fatigue notch, brittle weld crack notch, fracture toughness

[1] Assistant director and senior researchers, respectively, Research Laboratories, Kawasaki Steel Corp., Chiba 260, Japan.

In many studies devoted to improving the toughness of ferritic stainless steels, the effects of composition [1-9],[2] heat treatment [9-11], precipitates [2], 475°C holding [12,13], grain size [11], plate thickness [11,14], etc. have been extensively reviewed. From a practical point of view, studies on optimizing the manufacture of the plates [11], including welding [14], are of special interest. The general conclusion of these studies is that the toughness of the steels can be improved by reducing the contents of interstitial elements and oxygen to an extremely low level [1,9], by additions of proper contents of niobium [5,6], nickel [3,8] and aluminum [4], and by solution treatments at high temperatures [9].

Recent developments in steelmaking techniques [15] have made it possible for extra-low interstitial steels to be produced commercially without special facilities or refined raw materials. The practical application of these steels will be expanded in the near future as more data on their toughness and corrosion properties are accumulated.

The present investigation deals with the effect of some metallurgical and mechanical factors on the toughness of three kinds of superferritic stainless steels. These factors are precipitation of second phases, grain size, plate thickness, and notch sharpness.

Experimental Procedure

The steels used in the study were 18Cr-2Mo, 26Cr-1Mo, and 29Cr-2Mo. Their chemical compositions are given in Table 1. These steels are characterized by very low interstitials and the addition of niobium to avoid intergranular corrosion at the welds. They were melted in a modified vacuum oxygen decarburization (VOD) furnace of 50 metric tons capacity (strongly stirring-VOD process [15]). The 26Cr-1Mo steel was hot-rolled to 10-mm-thick and 4-mm-thick plates while the 18Cr-2Mo and 29Cr-2Mo steels were hot-rolled to 4-mm-thick plates by commercial production processes.

Experiments were divided into roughly two groups in order to find the effects of the metallurgical and mechanical factors. First, 2-mm V-notched Charpy impact tests were conducted using subsize specimens, 4 by 10 by 55 mm³, taken from solution-treated plate and also from embrittled plate; the longitudinal axis of the specimens was parallel to the rolling direction of the plates throughout the study. Solution heat treatments were done by heating the specimens at 1000, 1100 and 1200°C for 10 min and subsequent quenching in water. Heat treatments for embrittlement were performed by (1) reheating the solution-treated specimens at 700, 800, and 900°C and quenching in water; and (2) slow cooling the specimens from 1200°C to 700, 800, and 900°C and quenching in water. These heat treatment schedules are shown in Fig. 1. Changes in the microstructures

---

[2]The italic numbers in brackets refer to the list of references appended to this paper.

TABLE 1—Chemical compositions of steels used (weight percent).

Steel	C	Si	Mn	P	S	Cu	Nb	Cr	Mo	Ni	N	Al	O
18Cr-2Mo	0.0023	0.26	0.28	0.029	0.006	0.03	0.21	18.72	1.79	0.27	0.0039	0.008	0.0045
26Cr-1Mo	0.0022	0.33	0.08	0.018	0.004	0.02	0.17	25.88	1.20	0.16	0.0055	0.059	0.0027
29Cr-2Mo	0.0027	0.29	0.06	0.018	0.006	0.02	0.16	28.61	1.95	0.16	0.0070	0.098	0.0018
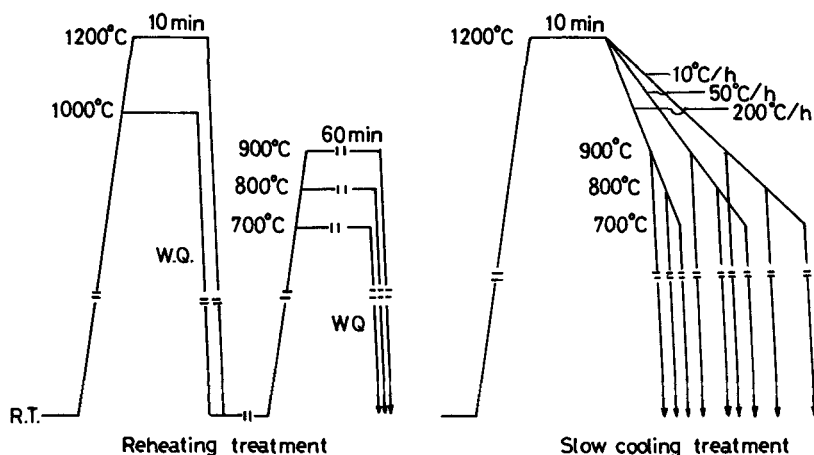
FIG. 1—*Schedules of heat treatments.*

of the specimens were observed through electron microscopy (Type JEPL-200, 200 kV), and the precipitates were identified by selected area transmission electron diffraction patterns. The foil specimens for the microscopic observation were prepared by "double jet" electrochemical polishing in a 10 percent perchloric acid plus 90 percent acetic acid solution at room temperature.

Subsequently, the effects of notch sharpness on Charpy impact toughness were evaluated using full-size specimens of 26Cr-1Mo steel, 10 by 10 by 55 mm^3, in the solution-treated (1020°C, 10 min, water-quenched) and embrittled (800°C, 60 min, water-quenched) conditions. Three types of notches were made in the cross-sections of the specimens: machined 2-mm V-notch, fatigue crack notch, and brittle weld crack notch. Fatigue cracks were introduced about 1.5 mm deep from the bottom of machined 2-mm V-notch under cyclic loads of 30 to 270 kgf for about 1.8×10^5 cycles. Brittle weld beads were made by electron beam welding after setting thin titanium and mild steel strips on the central part of the specimens, where natural brittle cracks were expected to be formed. The method of preparing specimens is illustrated in Fig. 2 and a typical cross section of a brittle weld bead is shown in Fig. 3. Both fatigue and brittle weld cracks were red-dyed prior to the impact tests to measure their depths on the fractured surfaces of the specimens.

The effect of grain size on the Charpy impact toughness was investigated using full-size and subsize 26Cr-1Mo steel specimens, provided with the usual 2-mm V-notch and brittle weld cracks. The grain size of the specimens was changed by heating at various temperatures between 1000 and 1200°C for 10 min and water-quenching. Before testing, all specimens were reheated at 1000°C for 10 min and quenched in water.
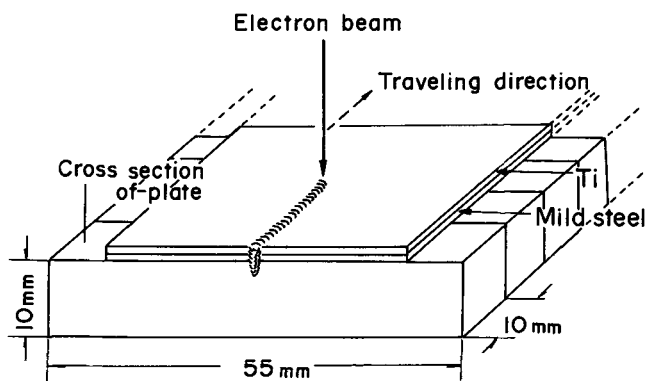
FIG. 2—*Preparation of the specimen having brittle weld crack.*

Results

Effect of Heat Treatments

The results of 2-mm V-notched Charpy impact tests on the solution-treated specimens are shown in Fig. 4. All specimens exhibit good toughness above −20°C. The 18Cr-2Mo steel treated at 1000°C is fully ductile even at −80°C. With increasing solution-treatment temperature, all steels tend to be brittle at low temperatures and this tendency is slightly stronger in the higher-chromium steels. It should be noted that the absorbed energies at low test temperatures are scattered at roughly two extremes, the entirely ductile and entirely brittle levels. Typical examples of the fracture surfaces of the two cases are shown in Fig. 5.

The results on the specimens reheated at 700 to 900°C after solution treatment at 1000°C are shown in Fig. 6. The 18Cr-2Mo steel is embrittled when reheated at 800 and 900°C, while the 29Cr-2Mo steel is only slightly embrittled by reheating at 800°C. The 26Cr-1Mo steel, however, shows no sign of embrittlement in the present reheating conditions. Results of the test on the specimens reheated at 700 to 900°C after solution treatment at 1200°C are also shown in Fig. 6. All specimens are brittle even at higher test temperatures and the scatter of absorbed energies at each test temperature becomes large.

Figure 7 shows the results for the specimens which were cooled from 1200°C to 900, 800, and 700°C with controlled cooling rates. All steels are clearly brittle even at high test temperatures and there is a tendency for embrittlement to be enhanced by lower cooling rates from the 1200°C anneal.

Figure 8 shows the transmission electron micrographs (TEM's) of the specimens solution-treated at 1200°C. No precipitates can be observed
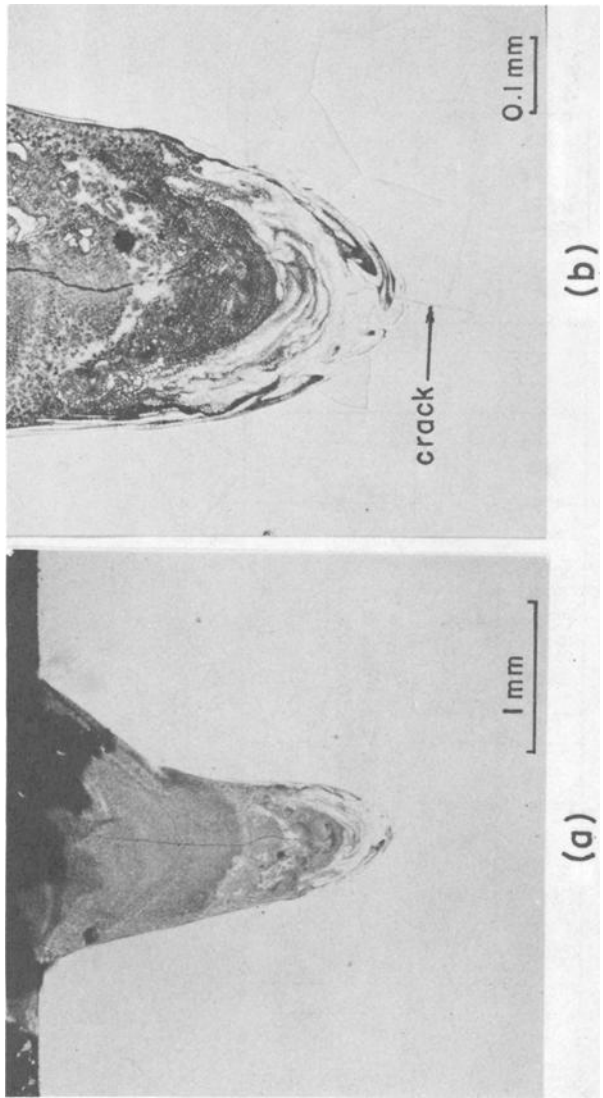
FIG. 3—Example of cross section of brittle weld bead on 26Cr-1Mo steel specimen. (a) cross section; (b) microstructure in the root of the bead, (a).
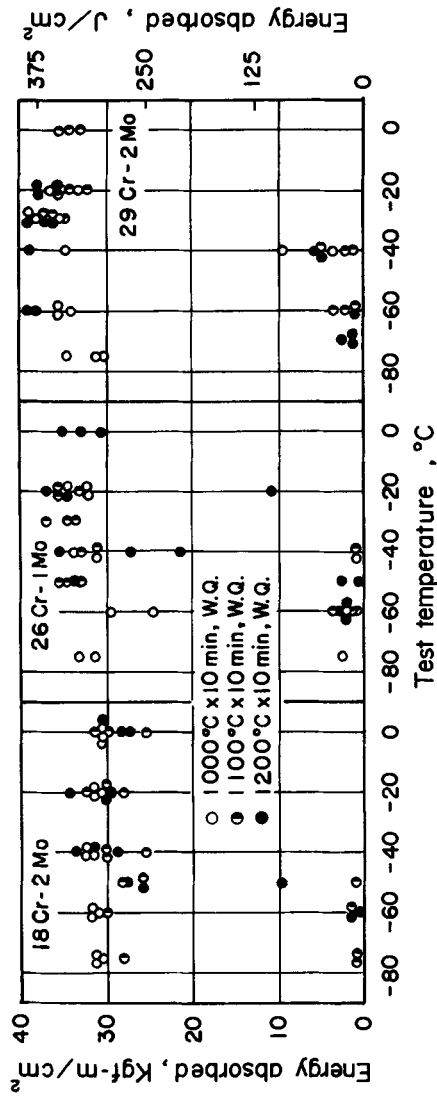
FIG. 4—*Charpy absorbed energy versus test temperature plots of solution-treated specimens (4 mm thick, 2-mm V-notch).*
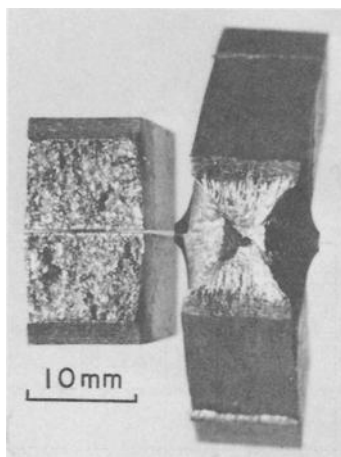
FIG. 5—*Typical examples of fracture surfaces of solution-treated and 2-mm V-notched 26Cr-1Mo steel specimens broken at −40°C.*

either at grain boundaries or within the grains. On the other hand, Fig. 9 shows the structures of the specimens embrittled by reheating at intermediate temperatures as shown in Fig. 6. Many precipitates are observed at the grain boundaries and within the grains. Electron diffraction patterns taken from the precipitates show the crystallographic structures characteristic in each steel: Laves phase [16] in 18Cr-2Mo steel and sigma phase [17] in 26Cr-1Mo and 29Cr-2Mo steels. Besides these phases, NbCrN [18] was detected by X-ray diffraction of extracted residues of 26Cr-1Mo and 29Cr-2Mo steels. The precipitates such as Laves and sigma phases are larger in size and are observed continually at grain boundaries in clearly embrittled specimens; for example, in 18Cr-2Mo and 29Cr-2Mo steels reheated at 800°C. In all other specimens embrittled by heat treatments, including slow cooling from 1200°C as shown in Fig. 7, similar precipitates are observed. No carbide can be detected by electron diffraction analysis in any steels, although it is suspected it precipitates as very fine particles in the specimens heated at intermediate temperatures.

Effect of Notch Sharpness

As indicated earlier, large scatter of Charpy absorbed energies was experienced, especially in the transition temperature range, for solution-treated "ductile" specimens. In order to clarify the effect of mechanical factors on this problem, three types of notches were made in full-size specimens of 26Cr-1Mo steel as described in the section on experimental procedure.
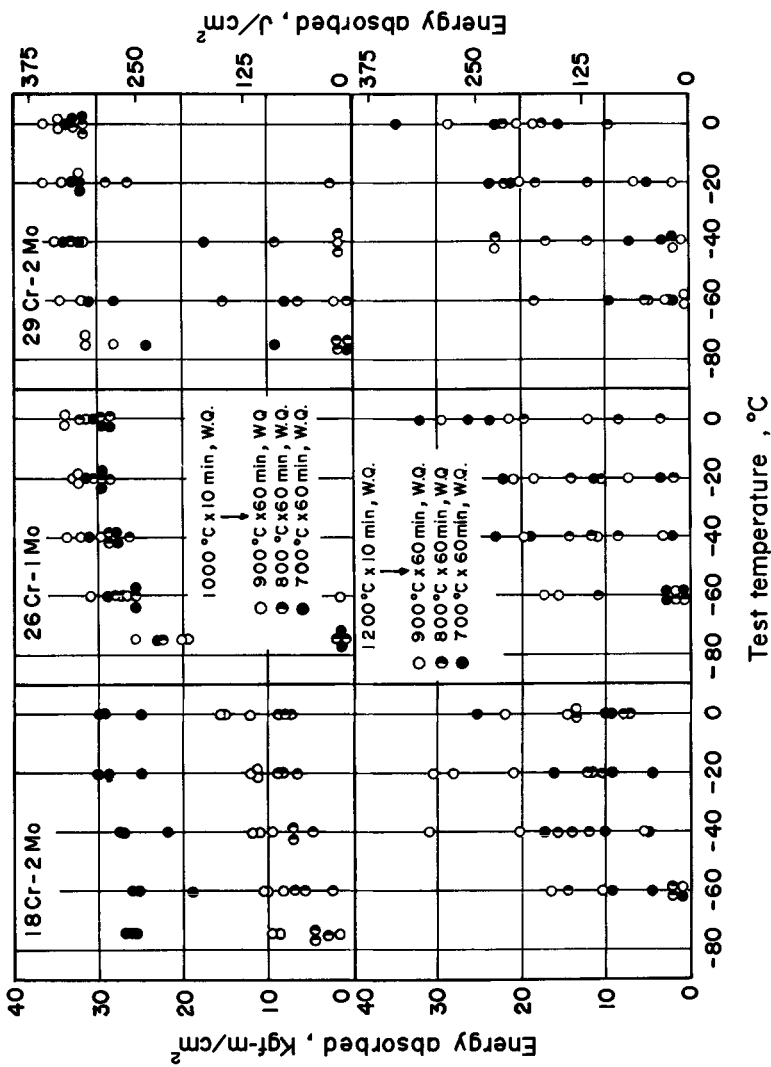
FIG. 6—Charpy absorbed energy versus test temperature plots of specimens reheated after solution treatment at 1000 and 1200°C (4 mm thick, 2-mm V-notch).
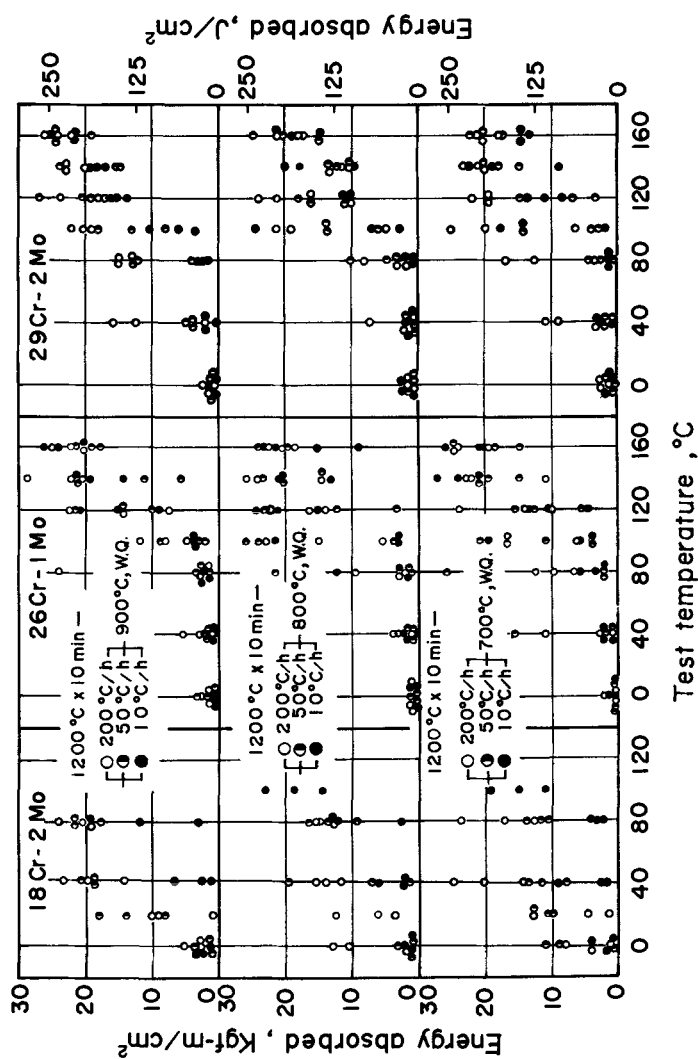
FIG. 7—Charpy absorbed energy versus test temperature plots of specimens slowly cooled from 1200°C (4 mm thick, 2-mm V-notch).
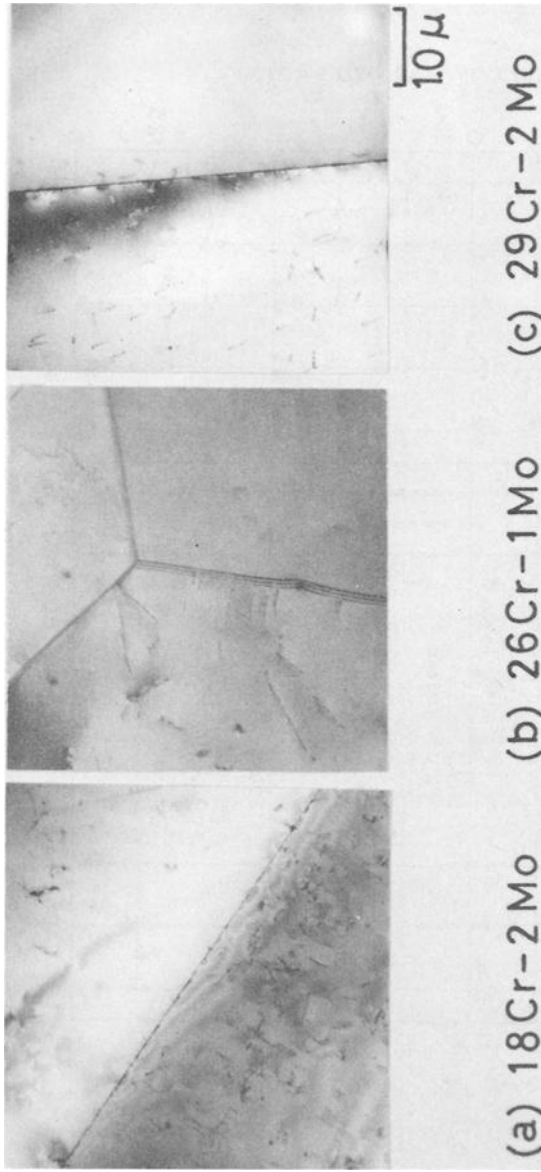
FIG. 8—*Transmission electron micrographs of specimens solution treated at 1200°C.*
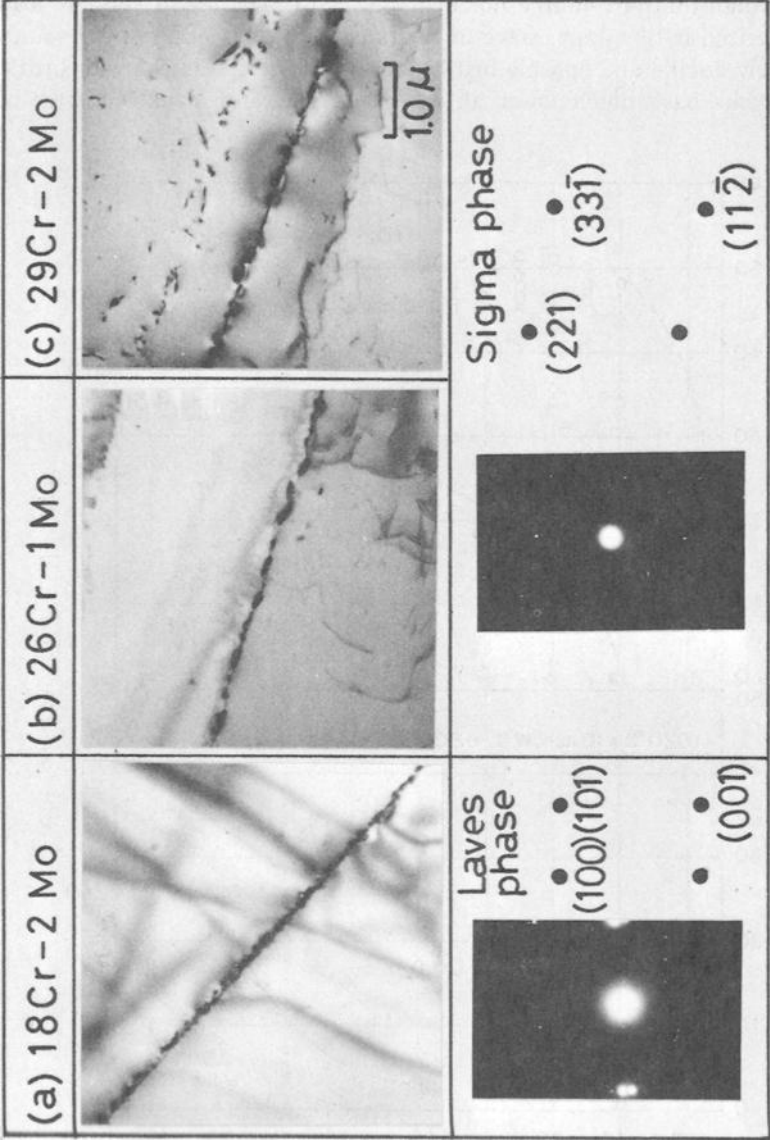
FIG. 9—*Transmission electron micrographs of embrittled specimens and electron diffraction patterns of precipitates.*

The effects of notch sharpness are shown in Fig. 10. In the solution-treated specimens, very large scatter of absorbed energies is observed in the 2-mm V-notched specimens. In the fatigue-cracked specimens, the absorbed energy versus temperature shows a wide scatter, but is slightly smaller than that of 2-mm V-notched specimens. The test results are also characterized by the appearance of intermediate values between the values of entirely ductile and entirely brittle fractures. The specimens with brittle weld cracks have much lower absorbed energies and smaller scatter of
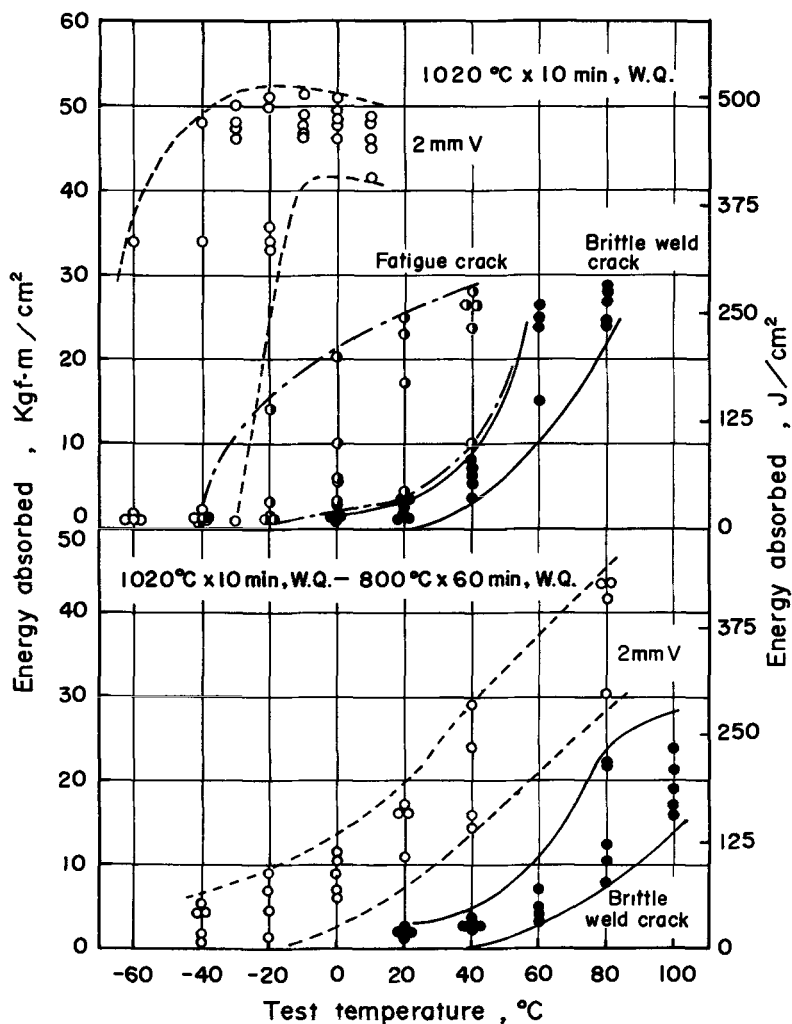
FIG. 10—Effects of notch sharpness on Charpy impact toughness of 26Cr-1Mo steel specimens solution treated at 1020°C or embrittled at 800°C for 1 h (10 mm thick).

data than fatigue-notched specimens, and the transition temperature shifts to a higher temperature, about 50°C.

The absorbed energy transitions of the specimens which were embrittled at 800°C and 2-mm V-notched or brittle welded are more sluggish than those of the as-solution-treated specimens. The embrittled and 2-mm V-notched specimens behave like as-solution-treated and fatigue-notched specimens. The embrittled and brittle welded specimens exhibit the smallest absorbed energies and the highest transition temperature among all the specimens tested.

Effect of Grain Size

Figures 11 and 12 show, respectively, the results of Charpy tests on solution-treated 4-mm-thick and 10-mm-thick 26Cr-1Mo steel plates whose grain sizes were varied in the range 0.03 to 1.6 mm by changing the heating temperature as described previously.

In both subsize and full-size 2-mm V-notched specimens, the energy transition temperature is raised with increasing grain size, while the shelf energy is almost independent of grain size in each specimen size. Comparing specimens of nearly the same grain size as shown in Figs. 11 and 12, the transition temperature is lower in the subsize specimens than in full-size ones. A very large scatter of data is observed, especially in the coarse-grained specimens.

On the other hand, in both subsize and full-size specimens having brittle welded cracks, the transition temperatures are higher than those of the 2-mm V-notched specimens. The grain size dependency of shelf energy and transition temperature in brittle welded specimens is very small, but is still observed. The transition temperatures of brittle welded specimens are about 30°C for subsize specimens and about 50°C for full-size ones. This again shows the effect of specimen size on the toughness of embrittled specimens. Examples of fracture surfaces of full-size specimens having brittle weld cracks are shown in Fig. 13. From the latent natural crack in brittle weld bead, brittle fracture is generated and changed into ductile fracture, which continues to the edge of the specimens. Scatter of the absorbed energies at each test temperature in Figs. 11 and 12 is caused mainly by the variation of the depth of the propagating brittle fracture.

Discussion

The results of this study of the effect of metallurgical factors on the Charpy impact toughness of ferritic stainless steels agree with the work of other investigators [9–11].

In a solution-treated condition, low-interstitial, high chromium and molybdenum bearing steels exhibit good toughness even at low tempera-
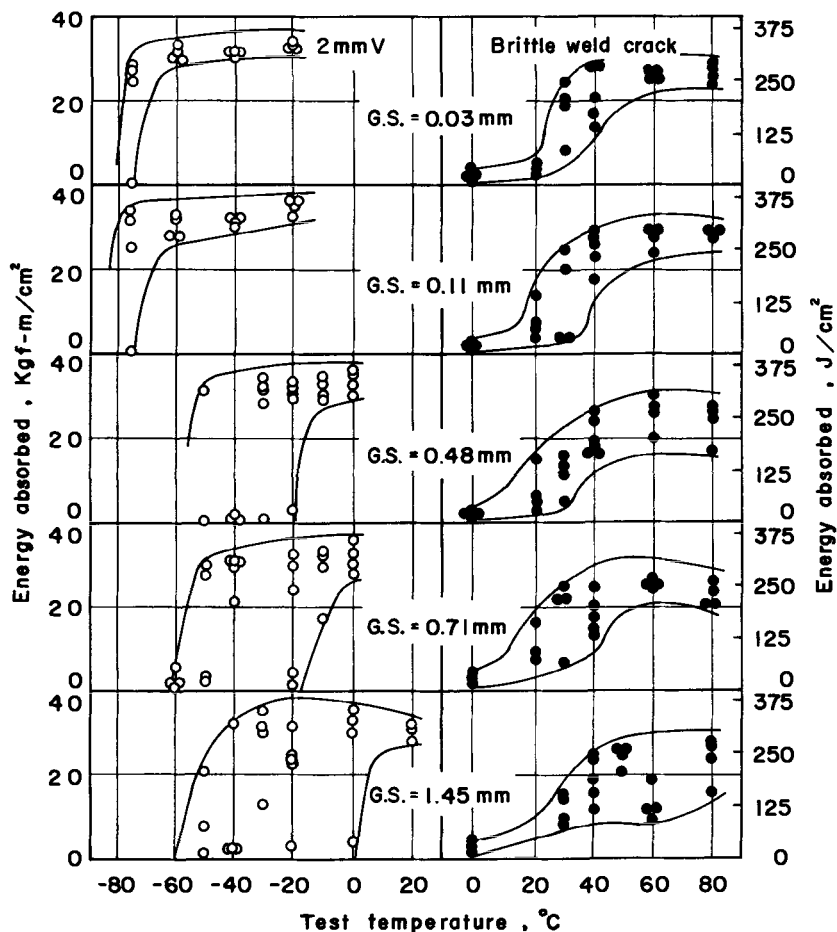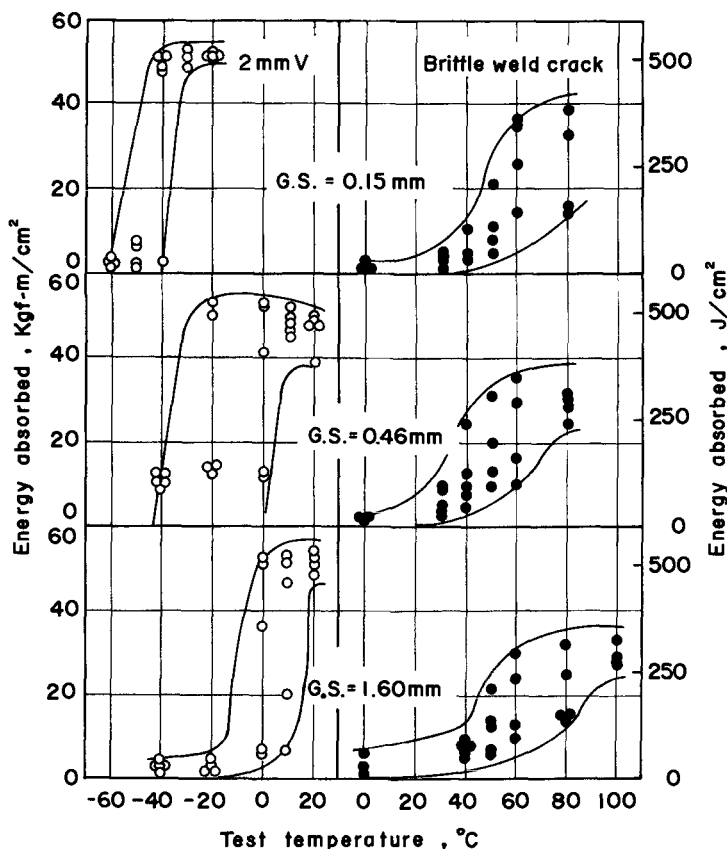
FIG. 11—*Effects of notch sharpness and grain size on Charpy impact toughness of the 4-mm-thick plate of 26Cr-1Mo steel solution treated at 1000°C.*

tures. A comparison of data in Figs. 4 and 10 showing the results of Charpy impact tests of the 26Cr-1Mo steel indicates a difference in toughness due to the difference in thickness of specimens. This well-known fact [9] is attributed to the difference in a mechanical factor—restriction of strain—during impact deformation of the specimens. In these figures, the solution-treated and V-notched specimens show the bimodal distribution of absorbed energies over a wide transition temperature range. At these temperatures fracture occurs either by entirely ductile or entirely brittle means as seen in Fig. 5. This phenomenon makes the transition range very broad. As shown in Fig. 10, some fatigue-cracked specimens exhibit intermediate absorbed energies in the transition temperature

FIG. 12—*Effects of notch sharpness and grain size on Charpy impact toughness of the 10-mm-thick plate of 26Cr-1Mo steel solution treated at 1000°C.*

range and a fracture surface of one of these specimens is shown in the center of Fig. 14. The fracture surface of the specimen is divided clearly into two areas, one entirely ductile and one entirely brittle.

On the other hand, fatigued notch or brittle weld cracks bring out lower absorbed energies and higher transition temperatures. In these cases, fracture starts in a brittle manner, consuming small amounts of absorbed energy, and subsequently changes into a ductile fracture. The path length of brittle fracture is dependent on the temperature and specimen size as well as the grain size, and consequently this determines the level of total absorbed energy.

The facts just mentioned suggest that resistance to fracture initiation during dynamic loading is quite high in these types of steels in the solution-treated condition and in the presence of blunt notches. If a brittle crack
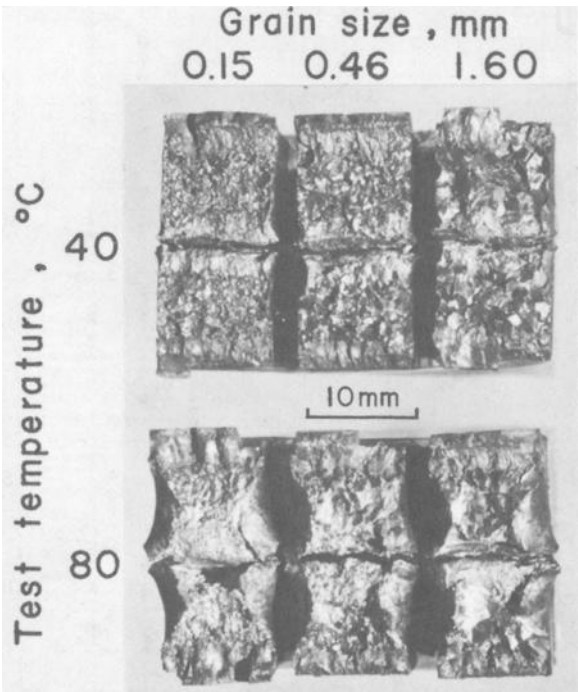
FIG. 13—Examples of fracture surfaces of the specimens having brittle weld cracks of 26Cr-1Mo steel whose grain sizes are 0.15 mm to 1.6 mm (test temperatures: 40 and 80°C).
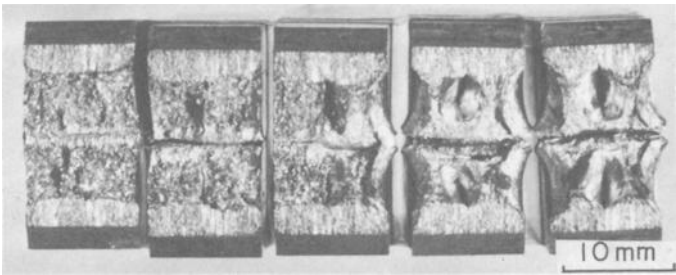
FIG. 14—Example of particular fracture surface of the specimen which was solution-treated, fatigue cracked, and tested at the transition temperature range (26Cr-1Mo). The particular fracture surface is on the specimen in the center.

is present, however, it can easily propagate in a brittle fashion and produces low absorbed energy. Although the factors which influence the incidental initiation of brittle fracture in the solution-treated and bluntly notched specimens have not been clarified yet, it is suspected that the crystallographic orientation of the grains at the root of the notch is important, especially in coarse-grained specimens.

V-notched specimens embrittled by the precipitation of Laves or sigma phase show toughness behavior very similar to that of the solution-treated and sharply notched specimens. This shows that the precipitates assist greatly in the initiation of brittle cracks at the time of dynamic loading. In Fig. 10, however, the embrittled and weld-cracked specimens show a lower toughness than the solution-treated and weld-cracked ones, and this indicates the adverse effect of precipitates on the resistance to brittle crack propagation.

In Figs. 11 and 12, which show the brittle-to-ductile transition of solution-treated 26Cr-1Mo steel, the effect of grain size is noticeable in the V-notched specimens but slight in the specimens with brittle weld cracks. This indicates that coarse grains tend to promote crack initiation even in the blunt-notched specimens; in other words, the grain size effect contributes mainly in the resistance to initiation of brittle fracture and only slightly to the propagation of brittle fracture.

The results obtained in this investigation indicate the importance of preventing brittle crack initiation and brittle fracture in these types of ferritic stainless steels. From this point of view a fracture mechanics approach is suggested to evaluate the practical application of these steels, especially those involving welding. The addition of nickel is proposed as a method of improving the toughness of the steels [3,8]. To apply this method, however, more information on the corrosion properties, especially on the stress corrosion behavior under various environmental conditions, should be acquired.

Conclusion

The effects of some metallurgical and mechanical factors on the Charpy impact toughness of extra-low interstitial 18Cr-2Mo, 26Cr-1Mo, and 29Cr-2Mo steels have been investigated. The results obtained are as follows.

1. The steels have good toughness in the as-solution-treated and bluntly notched conditions. There is, however, a large scatter of the data resulting in a wide range of transition temperature.

2. When the steels are embrittled by precipitation of second phases—for example, Laves or sigma phases in the present case—they behave very similarly to the solution-treated specimens having sharp notches such as fatigue cracks or brittle weld cracks. In these cases, Charpy impact

energies decrease and the transition temperatures increase with little scatter in the data points.

3. Small grain size or thin gage lowers the transition temperature of solution-treated and bluntly notched specimens. This beneficial effect decreases in the specimens having brittle weld cracks.

4. These test results suggest that the solution-treated steels exhibit good resistance to the initiation of brittle cracks, but relatively low resistance to crack propagation. Precipitation of second phase assists crack initiation mainly, but also crack propagation to a lesser extent.

References

[1] Semchyshen, M., Bond, A. P., and Dundas, H. J. in *Proceedings, Symposium Toward Improved Ductility and Toughness*, sponsored by Climax Molybdenum Co., Kyoto, Japan, 25–26 Oct. 1971, p. 239.

[2] Brandis, H., Kiesheyer, H., and Lennartz, G., *Archiv fur das Eisenhüttenwesen*, Vol. 46, 1975, p. 799.

[3] Brandis, H., Kiesheyer, H., Küppers, W., and Oppenheim, R., *TEW-Technische Berichten*, Vol. 2, No. 1, 1976, p. 3.

[4] Colombie, M., Condylis, A., Desestret, A., Grand, R., and Mayoud, R., *Revue de Metallurgie*, Vol. 70, 1973, p. 947.

[5] Jarleborg, O. H., Sawhill, J. M., and Steigerwald, R. F., *Stahl und Eisen*, Vol. 97, 1977, p. 29.

[6] Steigerwald, R. F., Dundas, H. J., Redmond, J. D., and Davison, R. M. in *Proceedings, Stainless Steel '77*, sponsored by Climax Molybdenum Co., London, England, 26–27 Sept. 1977, p. 57.

[7] Pollard, B., *Metals Technology*, Vol. 1, 1974, p. 32.

[8] Nakano, K., Kanao, M., and Hoshino, A., *Tetsu to Hagane*. Vol. 62, 1976, p. 1219.

[9] Abo, H., Nakazawa, T., Takemura, S., Onoyama, M., Ogawa, H., and Okada, H. in *Proceedings, Stainless Steel '77*, sponsored by Climax Molybdenum Co., London, England, 26–27 Sept. 1977, p. 35.

[10] Oppenheim, R. in *Proceedings, Stainless Steel '77*, sponsored by Climax Molybdenum Co., London, England, 26–27 Sept. 1977, p. 121.

[11] Nichol, T. J., *Metallurgical Transactions*, Vol. 8A, 1977, p. 229.

[12] Jacobsson, P., Bergström, Y., and Aronsson, B., *Metallurgical Transactions*, Vol. 6A, 1975, p. 1577.

[13] Grobner, P. J., *Metallurgical Transactions*, Vol. 4, 1973, p. 251.

[14] Matejka, W. A. and Knoth, J., *Journal of Testing and Evaluation*, Vol. 3, No. 3, 1975, p. 199.

[15] Iwaoka, S., Kaito, H., Ohtani, T., Ohashi, N., Takeda, M., and Kinoshita, N. in *Proceedings, Stainless Steel '77*, sponsored by Climax Molybdenum Co., London, England, 26–27, Sept. 1977, p. 139.

[16] Vowles, M. D. J. and West, D. R. F., *Journal of the Iron and Steel Institute*, Vol. 211, 1973, p. 147.

[17] Duwez, P. and Baen, S. R. in *Symposium on the Nature, Occurrence, and Effects of Sigma Phase, ASTM STP 110*, American Society for Testing and Materials, 1951, p. 48.

[18] Jack, D. H. and Jack, K. H., *Journal of the Iron and Steel Institute*, Vol. 210, 1972, p. 790.

K. F. Krysiak[1]

Weldability of the New Generation of Ferritic Stainless Steels—Update

ABSTRACT: The 26Cr-1Mo alloys stabilized with titanium and the 29Cr-4Mo alloys have many potential applications in the chemical process industries. There is particular concern about the effect of interstitial content and the titanium addition on weldability, weld fracture toughness, and ductility.

This paper discusses the weldability of the new titanium-stabilized 26Cr-1Mo and 29Cr-4Mo (26-1 and 29-4) alloys in various commercially available thicknesses [3.276 to 3.81 mm] (0.129 to 0.150 in.), using matching and dissimilar filler metals, and compares the ductility and impact toughness of these materials with those of E-BRITE 26-1 (a high-purity ferritic stainless steel). Both the gas tungsten-arc and shielded metal-arc welding processes were used.

Welds were evaluated on the basis of tensile, bend, Charpy V-notch impact properties, and weld metal interstitial content (carbon, nitrogen, and oxygen).

Sound welds were made in titanium-stabilized 26Cr-1Mo and 29Cr-4Mo alloys. It was concluded that welding procedures that optimize gas shielding must be used. Routine gas tungsten-arc welding procedures are not adequate. Because of the high ductile-to-brittle transition temperature and low notch toughness observed in the gas tungsten-arc welds, this procedure is not recommended for fabrication of chemical process equipment from the stabilized ferritic stainless steels in the thicknesses studied. It was found that the welds made with high-purity filler metal were superior to those made with the titanium-stabilized filler metal.

The fracture behavior and notch toughness of the shielded metal-arc welds made with Hastelloy C-276, Hastelloy G, and Haynes 25 were satisfactory, and these procedures can be used for fabrication of chemical process equipment.

KEY WORDS: ferritic stainless steels, weldability, weld impact toughness, weld ductility, weld lateral expansion, titanium stabilization, dissimilar filler metals, interstitials (purity), ductile-to-brittle transition temperature, welding procedures, fracture toughness

[1]Senior engineering specialist, Materials Engineering Section, Hercules Incorporated, Wilmington, Del. 19899.

Several years ago a high-purity 26Cr-1Mo single-phase ferritic stainless steel—E-BRITE 26-1[2]—was developed. This material had superior resistance to general corrosion, pitting, and crevice attack compared with austenitic stainless steels such as AISI Type 316. It also was virtually immune to intergranular corrosion and chloride stress corrosion cracking. The 26Cr-1Mo alloy also was reported to be readily weldable and able to be fabricated into a wide range of chemical equipment. It offered an economical advantage over competitive alloys, including titanium, high-nickel alloys and austenitic stainless steels.

Interest in this alloy developed quickly. Numerous applications were found and, before long, E-BRITE was being used successfully in several corrosive environments at Hercules plants. There were some failures and it was concluded that the weldability of this alloy needed to be investigated in some depth. It also became apparent that various equipment fabricators were not aware of the unique welding requirements of this new alloy.

An early study by Dorschu [1][3] gave some insight into the weldability of E-BRITE. At Hercules, an investigation to develop the necessary procedures to produce consistently strong, ductile, and corrosion-resistant weldments was initiated. Much information was gained concerning this alloy system, and techniques to minimize welding problems were developed. The results of this study were presented at Corrosion/75, the National Association of Corrosion Engineers (NACE) conference [2].

More recently, Allegheny Ludlum produced a 26Cr-1Mo alloy stabilized with titanium—26-1S (developed by Du Pont)—and Crucible Steel produced a similar 26Cr-1Mo + Ti alloy. Both of these alloys had mechanical and corrosion properties similar to E-BRITE except in strongly oxidizing environments. In addition, Allegheny Ludlum produced a 29Cr-4Mo alloy (29-4) of fairly high purity (but not quite as pure as E-BRITE) with improved mechanical properties and corrosion resistance.

These newer alloys had many potential applications in the chemical process industries, but weldability in actual vessel fabrication was questioned.

There was particular concern about the effect of the titanium addition on weld fracture toughness and ductility. A study by Wright [3] suggested that the addition of titanium would improve the toughness and weldability of 26Cr-1Mo ferritic stainless steels when the total carbon and nitrogen (C + N) level was 300 to 850 ppm. Therefore, an investigation was started at Hercules to develop welding parameters and techniques to make good, sound, tough corrosion-resistant weldments.

This paper discusses the weldability of the new titanium-stabilized 26-1 and 29-4 alloys in various commercially available thicknesses and compares

the ductility and impact toughness of these materials with those of E-BRITE 26-1.

Experimental Procedure

Material

The chemical composition of the titanium-stabilized 26-1 and 29-4 alloys used in this program is given in Table 1. In addition to the matching compositions, E-BRITE 26-1 filler metal (high purity) was also included to show the effect of interstitials on weld properties. Three high-alloy, covered electrodes were also evaluated. These electrodes, namely, Hastelloy[4] G, Hastelloy C-276, and Haynes[4] 25, were selected because of their good weldability, excellent corrosion resistance, and freedom from ductile-to-brittle transition behavior.

Lowrie [4] showed that dissimilar filler metals could be used to join E-BRITE 26-1 to other alloys successfully, but they were not recommended for corrosion service. This investigation examined additional filler metals to join E-BRITE and other ferritic stainless steels in various combinations.

To show the effect of interstitial content on weld metal toughness and ductility, E-BRITE 26-1 was welded with Allegheny 26-1S filler metal (Allegheny 26-1S base metal was welded with E-BRITE filler metal) [2].

Material thickness varied as follows:

Base metal: 26-1S, 3.3 mm (0.129 in.); 26-1Ti, 3.7 mm (0.145 in.); and
              29-4, 3.8 mm (0.150 in.)

Filler metal: E-BRITE 26-1, 2.4 mm (0.093 in.); 26-1S, 1.6 mm (0.062
              in.); 26-1 Ti, 1.1 mm and 2.4 mm (0.045 in. and 0.093 in.)

Joint Preparation

Cleanliness is essential when welding these new ferritic stainless steels. During fabrication, contaminants such as cutting lubricants, oils, grease, marking crayons, inks, paints, as well as dust, dirt, and moisture must be scrupulously removed from the joint surface prior to the start of welding. Many of these materials contain sulfur, lead, and other low-melting substances which will cause embrittlement of the weld joint and loss of corrosion resistance.

After machining, all weld joints were solvent-degreased on both sides for a distance of 5.1 cm. (2 in.) from the edges to be joined. It is important that the solvent used not leave a residue which would contaminate the weld. Care should be taken when wiping the joint surfaces. Lint-free cloths should be used to avoid leaving contaminated residues behind.

---

[4]Registered trademark of Cabot Corp.

TABLE 1—Composition of base metal[a] and filler metals—percent.

Element	Allegheny Ludlum 26-1S Plate Heat No. 448440	Allegheny Ludlum 26-1S Filler Wire Heat No. 440286	Crucible Steel 26-1Ti Plate Heat No. 633058	Crucible Steel 26-1Ti Filler Wire Heat No. 121218	Allegheny Ludlum 29-4 Plate Heat No. 281632	E-BRITE 26-1 Filler Wire Heat No. 538	Dissimilar Filler Metals Covered Welding Electrodes Hastelloy Alloy G	Hastelloy Alloy C-276	Haynes Alloy 25
C	0.030	0.033	0.02	0.01	0.004	0.0019	0.05 max	0.02 max	0.05 to 0.15
Mn	0.30	0.14	0.27	0.47	0.10	0.01	1 to 2	1.00 max	1.00 to 2.00
Si	0.20	0.20	0.43	0.32	0.05	0.22	1.0 max	0.05 max	1.00 max
P	0.025	0.020	0.030	0.025	0.013	0.018	0.04 max	0.03 max	0.03 max
S	0.012	0.010	0.008	0.007	0.013	0.012	0.03 max	0.03 max	0.030 max
Ni	...	0.25	0.25	0.28	0.12	0.10	balance	balance	9.00 to 11.00
Cr	26.00	25.72	25.60	29.75	29.3	26.56	21 to 23.5	14.5 to 16.50	19.00 to 21.00
Mo	0.97	1.0	0.09	0.90	3.95	1.04	5.5 to 7.5	15.00 to 17.00	...
Ti	0.33	0.94	0.42	0.45	...	...	...	...	...
Al	0.021	0.06	...	...	...	...	...	...	...
Cu	...	0.05	...	...	0.10	0.01	1.5 to 2.5	...	...
N	0.019	0.01	...	...	0.010	0.0021	...	...	...
Cb + Ta	...	...	...	...	...	...	1.75 to 2.5	...	...
Fe	balance	balance	balance	balance	balance	balance	18 to 21	4.00 to 7.00	3.0 max
Co	...	...	...	...	...	...	2.5 max	2.50 max	balance
W	...	...	...	...	...	...	1.0 max	3.00 to 4.50	14.00 to 16.00

[a] Supplier analyses.

Depending on metal thickness, the joint designs shown in Fig. 1 are generally used when gas tungsten-arc welding (GTAW) or shielded metal-arc welding (SMAW).

Manual Gas Tungsten-Arc Welding Process

This is an inert-gas shielded process and is used because it offers the advantages of good weld quality and good control of the weld puddle to achieve full weld penetration. The disadvantages are that it is a slow process, puts in considerable heat to the base metal, and a backing gas must be used to protect the underside of the weld.

The welder must be careful to maintain a high degree of cleanliness. For example, the filler wire should be removed from the container only for immediate use. Handling of the wire must be minimized to avoid pickup of moisture or dirt. If surface contamination is suspected, a clean cloth soaked in solvent should be used to clean the filler wire.

It is essential that the proper equipment be used. Most important is a large torch nozzle with a gas lens such as a Linde HW-18; see Fig. 2. This torch has been adapted to many different power supplies. The large-diameter gas cup [19-mm (3/4 in.) inside diameter] provides greater gas coverage and, therefore, requires higher argon gas flow rates. If a gas lens, which provides smooth laminar flow, is not used, turbulent flow occurs and air is entrained in the gas shield, causing weld contamination with resultant embrittlement and loss of corrosion resistance.

Maintaining a good gas shield is essential to making tough, ductile, corrosion-resistant weldments. Weld beads that are grey or black are contaminated and very brittle. Weld beads that are bright and shiny are best, while variations of light yellow to light blue are generally considered acceptable. Backing gas is recommended for the entire joint.

If necessary, gas shielding can be optimized with the addition of a trailing gas shield or similar modifications.
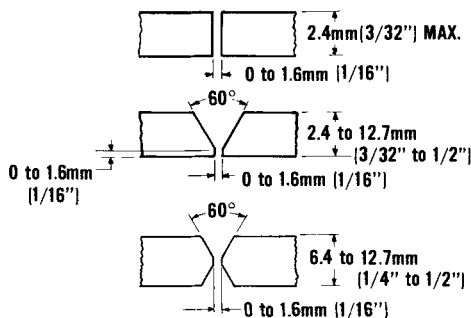
FIG. 1—*Standard weld joint design.*
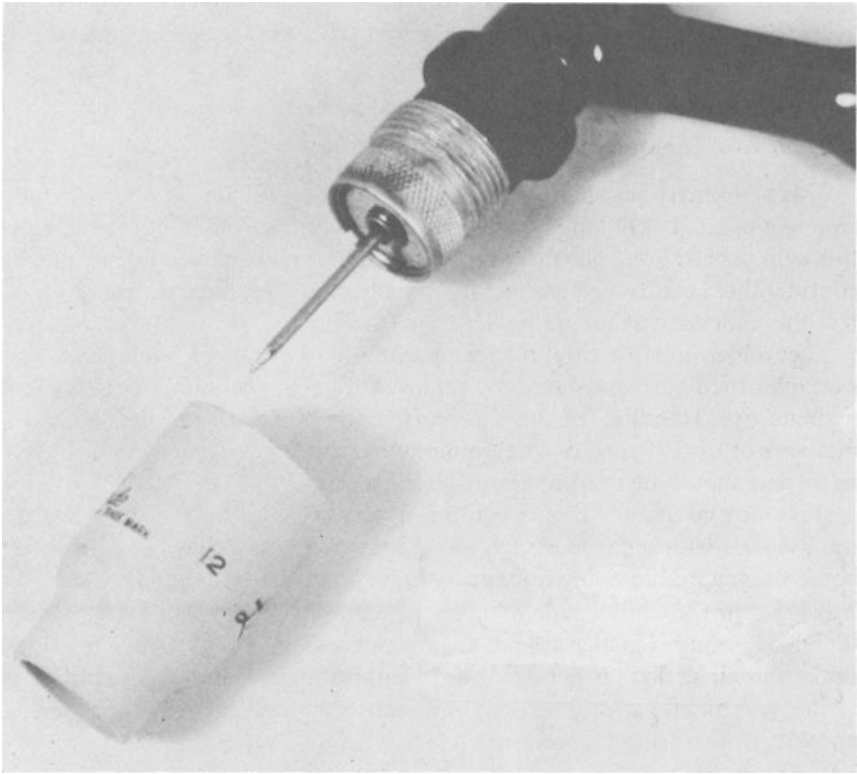
FIG. 2—*Recommended GTA welding torch with gas lens device. The gas cup has a 19-mm (3/4 in.) inside diameter.*

Two areas of a weld bead (especially in tack welds) that are particularly susceptible to cracking are the beginning and the end. Susceptibility to cracking is greatly reduced by using a rheostat current control device. The arc should always be initiated at the bevel of the joint and not on the adjacent base metal. As the arc is advanced into the root of the weld joint, current is steadily increased until a stable weld puddle is established, giving full penetration and sidewall wetting. When extinguishing the arc, the reverse procedure is done. This technique is shown for a tack weld in Fig. 3.

When welding, the two most important things to remember are (1) to keep the molten tip of the filler rod in the shielding gas envelope, and (2) after the arc has been extinguished, to hold the torch at this point until the weld bead has dropped below red heat while maintaining a post-purge. If these vital steps are ignored, contamination from the surrounding air will result and the weld will lose ductility and corrosion resistance.

Typical welding conditions that were used in this investigation are given in Table 2.
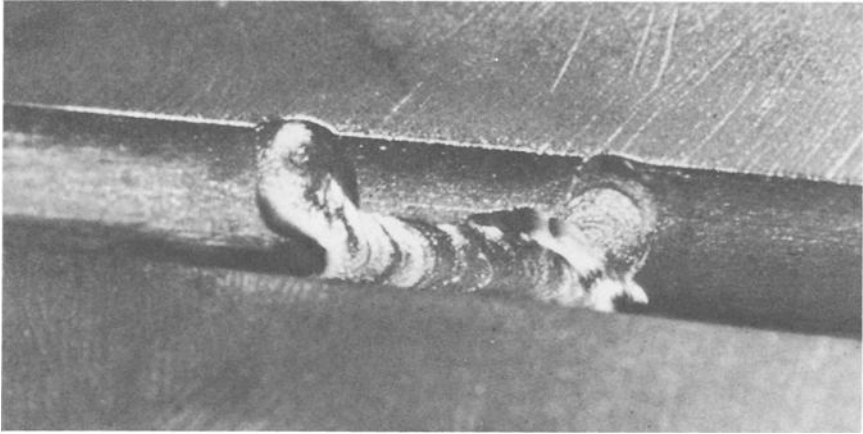
FIG. 3—*Recommended starting and stopping techniques.*

TABLE 2—*Typical gas tungsten-arc welding condition.*

Electrode	W-2% Thoria
Electrode diameter	4-mm (5/32 in.)
Current type	direct current straight polarity
Electrode tip angle	60 deg
Electrode extension	7.9 to 11.1 mm (5/16 to 7/16 in.)
Nozzle diameter ID	19 mm (3/4 in.)
Welding wire diameter	3.2 mm (0.125 in.)
Welding current	90 to 155 A
Torch shielding gas flow rate	1.7 mm^3/h (60 ft^3/h)
Backing gas flow rate	0.6 to 0.7 m^3/h (20 to 25 ft^3/h)
Travel speed	7.6 mm/min (3 in./min)
Preheat	none
Interpass	366 to 394 K (200 to 250°F)

Shielded Metal-Arc Welding Process

Dissimilar filler metals are of great interest because certain high-nickel and cobalt-base alloys have shown high degrees of corrosion resistance in field tests. In addition, there are many dissimilar metal joints in pressure vessels and little is known about the weldability of these joint combinations. These welds are complex because the degree of restraint can be considerable where there are large variations in section size.

Base metal preparations and joint design are the same as for GTAW. Electrodes must be kept clean and dry at all times. Electrode storage ovens are essential. Welding techniques, however, are different. Care must be taken to achieve sidewall fusion. Shrinkage stresses tend to be greater and distortion can be a problem. Furthermore, there is the problem of removing the slag on

top of the weld bead, which might be difficult, particularly in the groove of the weld joint.

To enhance weld soundness, a reverse restrike procedure was used. In this case, the arc was restruck at the leading edge of the crater and carried back to the extreme rear of the crater at a normal drag speed. The direction was then reversed and the weld continued.

Typical welding conditions used for this phase of the study are given in Table 3.

Weld Evaluation

The following test program was used to evaluate the weldments. Some test weldments were limited in size and thus it was not always possible to obtain a complete set of test specimens.

Tension Test—Where possible, two transverse flat plate-type specimens were removed from each test plate. The strength levels, tensile ductility, and fracture locations were recorded and compared with annealed parent material.

Transverse Bend Test—Two root and two face bends were tested using a $2t$-radius mandrel. This test is a good indicator of weld ductility. Poor welds or contaminated welds generally do not pass this test. This is especially true of the new family of ferritic stainless steels. Weld bend tests are mandatory when qualifying a welder to the ASME Boiler and Pressure Vessel Code.

Charpy V-Notch Impact Test—Impact information is especially important because ferritic stainless steels are subject to ductile-to-brittle transition behavior. Impact energy levels are dependent on notch configuration, specimen configuration, and strain rate. The ductile-to-brittle transition temperature (DBTT) is of critical importance when designing and building safe pressure vessels. The most common method used to determine impact energy is the Charpy V-Notch test. The lateral expansion of the fracture specimens was also measured.

Depending on whether weld-metal or heat-affected zone (HAZ) data are

TABLE 3—*Typical shielded metal-arc welding conditions.*

Current type:	direct current straight polarity
Preheat:	none
Interpass:	366 to 394 K (200 to 250°F)

Electrode Size, mm (in.)	Current, A	V	Travel Speed, cm/min (in./min)
2.4 (3/32)	65 to 75	22 to 26	10.2 (4)
3.2 (1/8)	80 to 125	22 to 26	15.2 (6)

required, specimen orientation would be as shown in Fig. 4. Eight specimens were removed from each weld joint.

Because of the metal thickness, subsize test specimens were tested with the notch centered in the weld perpendicular to the plane of the sheet. Although the impact specimens were subsize in the thickness dimension [2.5 mm (0.099 in.)], the width dimension of the Charpy bar in the plane of the sheet had the same dimension as a standard Charpy specimen.

Determination of Interstitial Content—Because of the degrading effect of carbon, nitrogen, and oxygen on the mechanical and corrosion properties of ferritic stainless steels in general, the materials used in this study were analyzed using vacuum fusion techniques to determine an interstitial profile of these elements. The filler wire specimens were etched prior to analysis to remove any surface contamination. Thus the data are representative of the core wire condition.

Results

Tensile Properties of Weldments

Tension test results for GTAW and SMAW specimens are given in Table
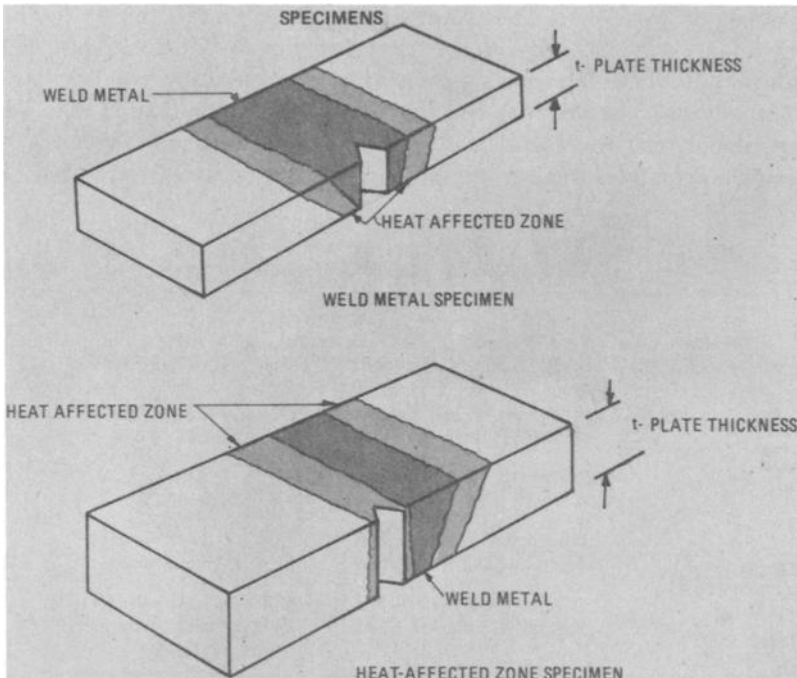
FIG. 4—*Location and orientation of weld-metal and heat-affected zone Charpy V-notched impact specimens.*

4. The ruptured specimens were examined and the fracture type and location recorded.

The GTAW specimens were characterized by rather inconsistent behavior and showed relatively poor tensile ductility.

Much better and more consistent properties were achieved with the SMAW test specimens. Tensile ductility was also considerably improved. All the specimens fractured in a ductile manner in the base metal except one of the specimens that was welded with Haynes 25. In that case, fracture was partially in the weld (ductile) and partially in the HAZ (brittle).

Bend Test—GTAW

As-welded GTAW bend test results are summarized in Table 5. All specimens were taken transverse to the weld and were bent using a 2*t*-radius mandrel.

Clearly the best bend performance was that of the Allegheny 26-1S base metal welded with the high-purity E-BRITE 26-1 filler metal.

Bend Test—SMAW

As-welded SMAW bend test results are summarized in Table 6. Best bend performance was achieved with Hastelloy C-276 metal and 26-1S base metal. Both root and both face bend specimens were successfully bent 180 deg.

Actually 26-1S welded with Haynes 25 bent better than it appears in Table 6. Although one *root* bend was shown to have bent only 130 deg, the specimen actually shifted in the die and fracture occurred in the HAZ ap-

TABLE 4—*Tensile properties of weldments.*[a]

Welding Process	Base Material and Weld Filler	Ultimate Tensile Strength		Fracture Location and Type
		MPa	(ksi)	
GTAW	Allegheny 26-1S	538	(78.0)	base metal (D)
	E-BRITE filler	414	(60.0)	base metal (B)
	Allegheny 26-1S	420	(61.0)	weld (B)
	26-1S filler	228	(33.3)	weld (B)
SMAW	Allegheny 26-1S	570	(81.6)	base metal (D)
	Hastelloy C-276	570	(81.6)	base metal (D)
	Allegheny 26-1S	552	(80.0)	base metal (D)
	Haynes 25 Filler	545	(79.0)	weld–base metal (D) (B)

NOTE: D = ductile shear fracture.
            B = brittle cleavage fracture.
[a]Test results are for the as-welded condition.

TABLE 5—*As-welded 2t bend test results—GTAW.*

Base Metal	Filler Metal	Bend Apex Location	Bend Angle[a] deg	Fracture Type and Location
Allegheny 26-1S	E-BRITE 26-1	root	180	DNF
			180	DNF
		face	180	DNF
			85	FL-weld-HAZ (B)
Allegheny 26-1S	Allegheny 26-1S	root	45	weld (B)
			85	weld (B)
		face	180	DNF
			180	DNF
Crucible 26-1Ti	Crucible 26-1Ti	root	60	weld (B)
		face	180	DNF
Allegheny 29-4	Allegheny 29-4	root	160	weld (D)
		face	35	HAZ (B)

NOTE: FL = fusion line.
HAZ = heat-affected zone.
B = brittle cleavage fracture.
D = ductile shear fracture.
DNF = did not fracture.
[a] A bend angle less than 180 deg is not acceptable.

TABLE 6—*As-welded 2t bend test results—SMAW.*

Base Metal	Filler Metal	Bend Apex Location	Bend Angle[a] deg	Fracture Type and Location
Allegheny 26-1S	Hastelloy C-276	root	180	DNF
			180	DNF
		face	180	DNF
			180	DNF
Allegheny 26-1S	Haynes 25	root	180	DNF
			130	HAZ (D)
		face	180	DNF
			150	HAZ (B)
Crucible 26-1Ti	Hastelloy G	root	90	HAZ (B)
		face	145	HAZ (B)

NOTE: FL = fusion line.
B = brittle cleavage fracture.
D = ductile shear fracture.
DNF = did not fracture.
[a] A bend angle less than 180 deg is not acceptable.

proximately 6.4 mm (1/4 in.) away from the weld fusion line.

It is worth noting that the bend performance of the SMAW welds was better than the GTAW welds. Furthermore, there were no SMAW weld failures. Fracture in every case occurred in the HAZ of the base metal.

Charpy V-Notch Impact Test

The impact test results for the base plate, GTAW, and SMAW material are shown in Figs 5, 6, and 7, respectively.

The energy absorption curve for the base materials, shown in Fig. 5, does not show any measurable improvement in impact toughness for the higher-purity 29-4 alloy. The lateral expansion curve, however, does reflect the benefit of higher purity.

In Fig. 6, the effect of purity is clearly seen. Note the very sharp drop in the energy absorption and lateral expansion curves. An improvement in impact
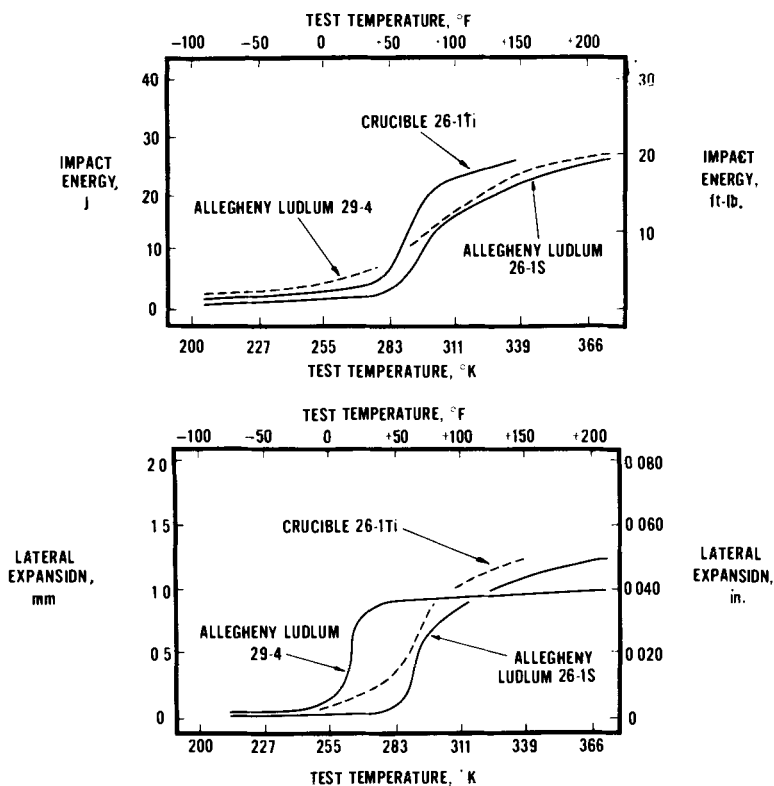
FIG. 5—*Results of Charpy V-notch impact test base material.*
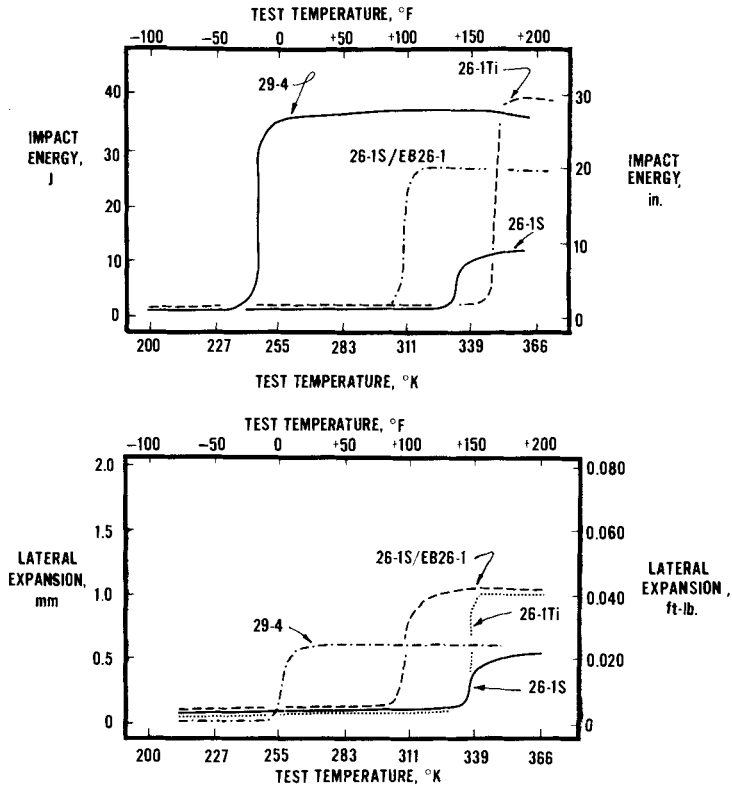
FIG. 6—*Results of weld metal Charpy V-notch impact test gas tungsten-arc welded.*

toughness is evident when the 26-1S grade, stabilized with titanium, is gas tungsten-arc welded with the high-purity E-BRITE 26-1 filler metal. A further improvement in toughness is noted when a high-purity alloy like 29-4 is welded with a matching filler.

The results of the SMAW specimens, illustrated in Fig. 7, were as expected since the weld metals do not display the ductile-to-brittle behavior characteristics of the ferritics.

The DBTT's for the ferritic base metals and weld metals studied in this part of the program are summarized in Table 7. Because of the very sharp drop in impact energy absorbed, the transition temperature is most meaningful and therefore has been selected as that point where fracture is 100 percent ductile shear. The better performance of the higher-purity grades is apparent. Similar results were obtained in the previous weldability study [2]. In that investigation, the DBTT for 6.4-mm (1/4 in.) E-BRITE 26-1 plate welds was 239 K (−30°F).
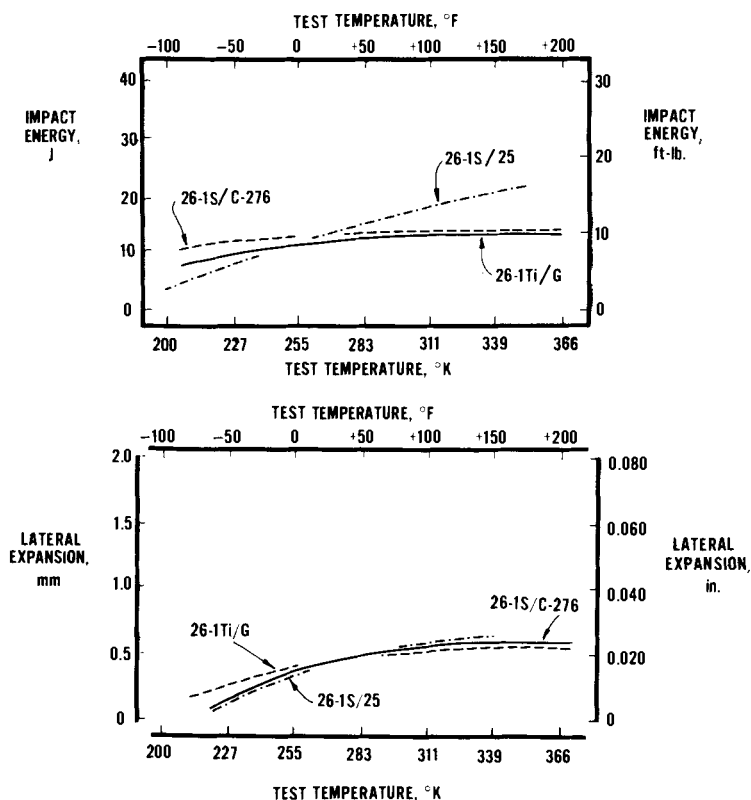
FIG. 7—*Results of weld metal Charpy V-notch impact test shielded metal-arc welded.*

TABLE 7—*Ductile-to-brittle transition temperature (DBTT) as determined from Charpy V-notch impact test.*

Base Metal	DBTT		Shear Fracture, %
	K	°F	
Allegheny 26-1S	372	210	100
Crucible 26-1Ti	>339	>150	60
Allegheny 29-4	>372	>210	80
Weld Metal—GTAW			
Allegheny 26-1S	>372	>210	90
Allegheny 26-1S @ E-BRITE 26-1 filler	311	100	100
Crucible 26-1Ti	>344	>160	60
Allegheny 29-4	258	5	100

Interstitial Content

The results of carbon, nitrogen, and oxygen analyses are presented in Tables 8, 9, and 10. The results for the E-BRITE materials used in the earlier study [2], but not reported at that time, are also included. Results show that there was little change in overall carbon and nitrogen levels after welding.

Discussion

The 26-1 titanium-stabilized alloys have been considered readily weldable using standard GTAW practices in contrast to the more elaborate procedures required to weld the high-purity E-BRITE 26-1 alloy. Thus, the

TABLE 8—*Interstitial content of base metal, ppm.*

	C	N	O	C + N
E-BRITE 26-1 [6.4 mm (0.250 in.)]	12	84	54	96
Allegheny Ludlum 26-1S [3.3 mm (0.129 in.)]	359	137	44	496
Crucible 26-1Ti [3.7 mm (0.145 in.)]	136	174	34	310
Allegheny Ludlum 29-4 [3.8 mm (0.150 in.)]	18	113	21	131

NOTE: ppm denotes parts per million.

TABLE 9—*Interstitial content of bare wire filler metals, ppm.*

	C	N	O	C + N[a]
E-BRITE 26-1 [2.4 mm (0.093 in.)]	19	21	53	40
E-BRITE 26-1 [3.2 mm (0.125 in.)]	13	49	58	62
Allegheny Ludlum 26-1S [1.6 mm (0.062 in.)]	348	129	34	477
Allegheny Ludlum 29-4 [1.6 mm (0.062 in.)]	24	254	46	278
Crucible 26-1Ti [2.4 mm (0.093 in.)]	99	141	31	240
Crucible 26-1Ti [1.1 mm (0.045 in.)]	106	142	40	248

[a]All wire specimens etched to remove surface contamination. These data are therefore representative of the core wire condition.
NOTE: ppm denotes parts per million.

TABLE 10—*Interstitial content of weld metal, ppm.*

	C	N	O	C + N
E-BRITE 26-1 welded with E-BRITE 26-1	10	85	65	95
E-BRITE 26-1 welded with Allegheny 26-1S	183	114	56	297
Allegheny 26-1S welded with Allegheny 26-1	352	149	68	501
Allegheny 26-1S welded with E-BRITE 26-1	127	102	66	229
Crucible 26-1Ti welded with Crucible 26-1Ti	126	162	45	288
Allegheny 29-4 welded with Allegheny 29-4	20	123	36	143

NOTE: ppm denotes parts per million.

stabilized grades would be less expensive to weld. Wright [3] showed, however, that while good weld ductility was dependent on a balance between the titanium and the (C + N) levels, the DBTT for titanium-stabilized weld metals was increased by either an increase in titanium or interstitial levels. Therefore the need to use exacting welding procedures to weld the stabilized grades is clear.

The published welding procedures for the titanium-stabilized grades were developed using thin-gage material and automatic processes with welds made autogenously (without the addition of filler metal). The usefulness of this type of data is limited. Fabrication of chemical process equipment requires that a substantial portion of the welding be done using manual techniques with the addition of filler metal. Weld contamination and pickup of (C + N + O) as well as improper welding techniques become perhaps the most important factors responsible for unsatisfactory welds.

In this study, the procedures necessary to weld the high-purity E-BRITE 26-1 alloy were found to also be necessary to successfully weld the stabilized 26-1S and 26-1 titanium alloys. Specifically, gas shielding was optimized and a high level of cleanliness to minimize weld contamination was maintained. The importance of these aspects cannot be overemphasized.

Tension Test Behavior

The results of the tension tests presented in Table 4 show that the SMAW properties are more consistent than those obtained by GTAW. An important factor may be the total heat input to the base metal and underlying weld beads. The manual GTAW process is characterized by a slower travel speed and therefore the heat input is greater than for the SMAW process.

The very low elongation and reduction in area of two of the GTAW specimens and the brittle cleavage failure indicate that the material was below or near its DBTT for this test method. Note that the DBTT for ferritic stainless steels is dependent on strain rate.

Overall ductility was lower than expected. The reason for this may be related to the relatively high levels of carbon, nitrogen, and titanim in the 26-1S alloy.

Consistent tensile properties were achieved using Hastelloy C-276 and Haynes 25 welding electrodes. Fracture essentially occurred in the base material and was generally ductile. Both electrodes have excellent operability.

Bend Ductility

The GTAW bend test results given in Table 5 are not consistent, with the possible exception of the 26-1S material that was welded with the high-purity E-BRITE 26-1 alloy. In that case, three out of four U-bends satisfactorily

bent 180 deg. The stabilized U-bend material all failed by brittle cleavage. It is apparent that the high-purity E-BRITE filler metal contributed to the improved bend ductility. The reason for the poor bend ductility of the 29-4 alloy is not known.

Considerably improved bend ductility was achieved by using SMAW techniques. In those cases where the U-bend specimens failed, fracture occurred in the HAZ of the base metal. Because of the higher work-hardening rates and higher strength levels of these dissimilar filler metals, difficulties were experienced in making the tests. The specimens tended to shift in the die, resulting in a stress concentration effect at the fusion line or in the HAZ. This resulted in premature failure several times. Longitudinal weld specimens eliminate the stress concentration effect and more realistically evaluate the quality of a dissimilar weld joint. Because of limited base metal specimens, however, the transverse test had to be used. It is expected that the covered electrodes tested in this program would pass the longitudinal bend test.

Charpy V-Notch Impact Behavior

Impact toughness was determined using energy absorption and lateral expansion criteria. Energy absorption values give an indication of the notch toughness and are a measure of the dynamic strength of the material and its ability to deform. The lateral expansion gives an indication of the ability of the material to flow.

The reason for the anomalous behavior of the 29-4 base material (see Fig. 5) is not known at this time. The lateral expansion does show the superiority of the high-purity 29-4 alloy over the two titanium-stabilized 26-1 alloys.

The impact behavior of the ferritic stainless steels is known to be related to purity. Matejka and Knoth [5] showed that for the high-purity materials, the lower the carbon and nitrogen, the better the notch toughness and the lower the DBTT. Wright [3] similarly showed that the DBTT for titanium-stabilized alloys would increase from either an increase in titanium or interstitial levels (C + N).

On the basis of the weld metal interstitial levels, 26-1S alloy welded with E-BRITE 26-1 should have a lower DBTT than either of the titanium-stabilized grades welded with matching filler metals. Weld metal interstitial analyses for the 29-4 alloy (see Table 10) indicate that it should have the lowest DBTT of the alloys studied. The results in Fig. 6 show this to be the case.

The exact DBTT's for 100 percent shear fracture were not determined; however, the percent shear fracture is shown for the highest temperature that was tested. Note in Fig. 6 the shape of the curves for the base metal versus the weldments. The weldments exhibit a very sharp drop in toughness compared

with the base metal. For this reason, 100 percent ductile shear fracture is a safe criterion to use for determining the DBTT.

The GTAW impact toughness results show that although the stabilized grades were welded with matching fillers without formation of cracks or other defects, weld properties (such as notch toughness and ductility) were not adequate for the fabrication of chemical process equipment. The data show that when stabilized 26-1 alloys are to be welded in the thickness range examined in this study, high-purity E-BRITE or a high-alloy filler metal should be used.

The advantages of using Hastelloy C-276, Hastelloy G, or Haynes 25 welding electrodes (SMAW) for joining the ferritic stainless steels are that these filler metals (1) do not exhibit the DBTT behavior of the ferritic materials, (2) are welded more easily and quickly, and (3) have good corrosion resistance. Another benefit is less heat input into the base metal. Excessive heat input leads to grain growth which degrades weld properties. The choice of which electrode to use will depend upon the application.

The results of this study suggest caution when using stabilized materials that have a high DBTT like those given in Table 7. During the fabrication of equipment, notches such as grind marks, arc strikes, and weld reinforcement are particularly harmful and can lead to premature brittle fracture. This is especially critical during hydrotest when the use of cold water can place the vessel or piping system in a temperature range below the DBTT for the alloy. Brittle fracture under these conditions is likely. Therefore, to bring the alloy into a safe ductile DBTT range, only heated water should be used when hydrotesting.

Conclusions

1. Sound welds have been made in titanium-stabilized 26Cr-1Mo [3.3 to 3.7 mm (0.129 to 0.145 in.) thick] and 29Cr-4Mo [3.8 mm (0.150 in.) thick] alloys.

2. Welding procedures that optimize gas shielding and cleanliness to avoid pickup of (C + N + O) must be used. Routine GTAW and SMAW techniques are not adequate.

3. Because of the high DBTT and low notch toughness observed in the GTAW welds, this weld procedure is not recommended for fabrication of chemical process equipment from these stabilized ferritic stainless steels. It should be noted, however, that the welds made with high-purity filler metal were superior to those made with the stabilized filler metal.

4. The fracture behavior and notch toughness of the SMAW welds made with Hastelloy C-276, Haynes 25, and Hastelloy G filler metal were satisfactory, and these procedures can be used for the fabrication of chemical process equipment.

Acknowledgments

References

[1] Dorshu, K. E., *Welding Journal,* Sept. 1971.
[2] Krysiak, K. F. in *Proceedings,* National Association of Corrosion Engineers, "Corrosion/75" Symposium, Toronto, Ont., Canada, 1975.
[3] Wright, Roger N., *Welding Journal,* Oct. 1971, pp. 434s-440s.
[4] Lowrie, R., *Welding Journal,* Nov. 1973, pp. 500s-506s.
[5] Matejka, W. A. and Knoth, R. J., *Journal of Testing and Evaluation,* May 1975, p. 199.
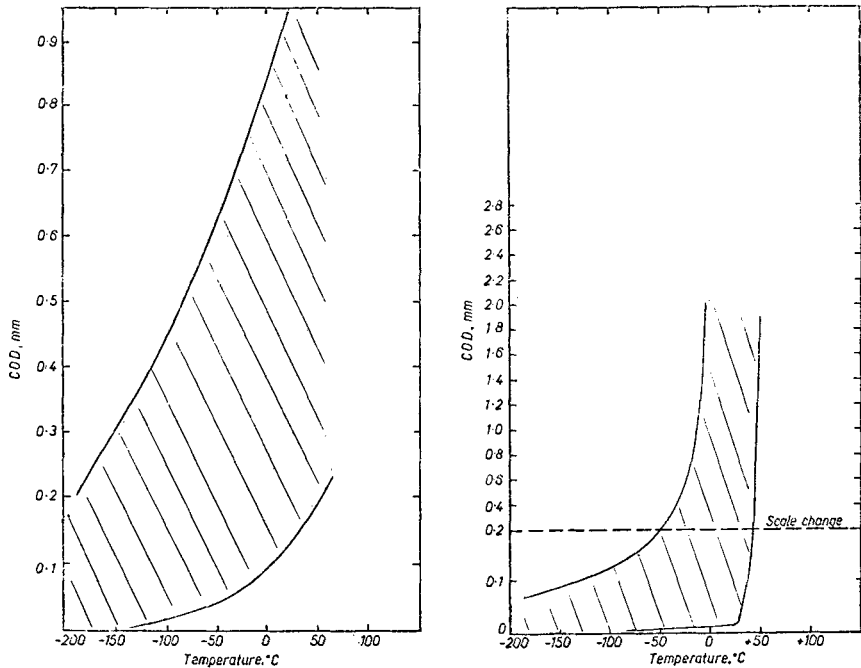
FIG. 8—*COD results for (left) arc weld HAZ's in plate ferritic/austenitic steels; and (right) arc weld HAZ's in ELI steel.*

DISCUSSION

T. G. Gooch[1] (written discussion)—Work at The Welding Institute has supported the view that ELI steels can show poor HAZ toughness at room temperature. Figure 8 shows envelopes of crack opening displacement (COD) results obtained for a range of duplex ferritic/austenitic steels and for $26 = 1$ materials. The data relate to HAZ's in 10 to 13-mm plate butt welds, made using the SMA, SAW, GTA, GMA, and electron beam processes, and were obtained from full thickness specimens. At room temperature, COD levels for the ELI alloy may be as low as 0.02 mm whereas the duplex alloys gave maximum-load COD values of 0.12 mm and above.[2]

[1]The Welding Institute, Abington Hall, Abington, Cambridge, U. K.
[2]Honeycombe, J. and Gooch T. G. in *Proceedings*, Conference on Trends in Steels and Consumables for Welding, The Welding Institute, London, Nov. 1978.

L. A. Scribner[1]

Evaluation of High-Purity 26Cr-1Mo Ferritic Stainless Steel Welds by Burst Tests

ABSTRACT: The objective of the testing program was to evaluate the toughness of the welds in high-purity 26Cr-1Mo ferritic stainless steel. The method used to determine the toughness was by bursting heavy-walled pipe. The burst specimens incorporated a longitudinal through-thickness weld that contained a machined notch part way through the wall thickness. A burst test specimen geometry was developed which tested the weld, heat-affected zone (HAZ), and base metal at the same time. Successful welding was done using the gas tungsten-arc welding (GTAW) method and an argon purge. The results of the investigation showed that the 26Cr-1Mo weld deposit and HAZ were brittle at room temperature. The welds were then made of a root pass of 26Cr-1Mo followed by filler passes of Hastelloy C-276 and a postweld heat treatment. The results of the composite welded specimens showed that the weld was now tough, because of the Hastelloy C-276, while the HAZ had a ductile-to-brittle transition temperature between room temperature and 65°C (150°F). The specimens were evaluated by visual characterization of the fracture appearance.

KEY WORDS: ferritic stainless steels, gas tungsten-arc welding, welding electrodes, brittle fracturing, burst tests, evaluation, impact tests, pipe, toughness, fracture (materials), fracture toughness

There are many processes in the petrochemical industry where the use of 26Cr-1Mo stainless steel is desirable from a corrosion standpoint. This alloy is essentially immune to stress corrosion cracking in fresh water and has excellent resistance to many corrosives such as hot organic acids, caustic, and alkaline amines. The recognized brittleness of the ferritic

[1] Senior engineer, Union Carbide Corp., Engineering Department, South Charleston, W. Va. 25303.

stainless steels, such as high-purity 26Cr-1Mo (E-BRITE 26-1 developed by Airco, Inc.) in the welded condition, made it imperative that an acceptable welding and postweld heat treating procedure be developed. This investigation was undertaken to determine the factors required to make an acceptable weld which would be both ductile and at the same time have corrosion resistance equal to the base metal.

Inasmuch as we were evaluating pipe material, the welds in the 26Cr-1Mo stainless steel were evaluated by burst tests in order to duplicate the operating stress condition, as opposed to impact tests, which establish notch toughness on an indirect basis that bears little relationship to service stresses. Impact test specimens test only a small portion of a metal whereas burst tests involve the testing of the material in a much larger specimen.

Experimental Procedure

Two different sizes of seamless pipe were used for specimens. Two heats of nominal pipe size (NPS) 1½ Schedule 160 pipe and one heat of redraw stock measuring 50.8-mm (2 in.) outside diameter by 4.7-mm (0.187 in.) wall were evaluated. Chemical analyses, mechanical properties, and corrosion test results of the heats are listed in Table 1. The material was produced by Airco Vacuum Metals, a division of Airco, Inc., by vacuum induction melting followed by electron beam refining. Approximately 300-mm (1 ft) lengths of the pipe were used as test specimens.

The test specimens for the base metal were notched approximately 76 mm (3 in.) long from the outside surface with a Charpy V-notch cutter and to a depth to leave 2.28-mm (0.090 in.) wall thickness under the notch.

There were two types of welded specimens as shown in Fig. 1. In the first style (Type A), the specimens were prepared by machining through the wall thickness with a 60-deg cutter for the full length of the specimen and then filling the groove with weld metal. The Charpy V-notch could then be located in either the heat-affected zone (HAZ) or the weld metal.

In the second style (Type B), the longitudinal groove was machined through the wall thickness but only for a distance of 178 mm (7 in.) from one end. The groove was filled with weld metal and then the Charpy V-notch was located in the HAZ. In the Type B specimen, the base metal, the weld, and the HAZ could be tested on a single specimen because the crack could propagate into either the HAZ or weld at one end of the Charpy V-notch or into the base metal at the other end of the Charpy V-notch. When the test required a postweld heat treatment, it was put into a preheated 980°C (1800°F) furnace, held at temperature for 20 min and water-quenching upon removal from the furnace.

After heat treatment, steel plugs were welded into the ends of the specimens, which then were pressurized to failure. Both the pressurizing fluid

TABLE 1—*Cr26-1Mo material for burst tests.*

	Heat X	Heat Y	Heat Z
	Seamless Redraw Stock 50.8-mm OD by 4.7-mm Wall, Babcock and Wilcox Heat No. B-79A2	Seamless NPS[a] 1½ Schedule 160 Pipe, Babcock and Wilcox Heat No. 0625A	Seamless NPS 1½ Schedule 160 pipe, Babcock and Wilcox Heat No. 0626A
COMPOSITION			
C	0.001	0.004	0.004
Mn	0.01	0.04	0.03
S	0.012	0.013	0.013
P	0.011	0.014	0.014
Si	0.22	0.22	0.21
Cr	26.44	26.29	26.20
Ni	0.08	0.13	0.14
Mo	1.01	0.94	0.90
Cu	—	0.02	0.02
N_2	0.010	0.010	0.014
MECHANICAL PROPERTIES			
UTS[b]	483.1 MPa (70 070 psi)	496.0 MPa (71 950 psi)	496.1 MPa (71 960 psi)
YS[c]	353.8 MPa (51 320 psi)	362.6 MPa (52 600 psi)	361.7 MPa (52 570 psi)
elongation, 50.8-mm gage	57%	55%	58%
CORROSION TEST			
ASTM A-262, Practice B (ferric sulfate-sulfuric acid) max rate 0.05 mm/month (0.0020 in./month)	...	0.046 mm/month (0.0018 in./month)	0.048 mm/month (0.0019 in./month)

[a] NPS = Nominal Pipe Size
[b] UTS = ultimate tensile strength.
[c] YS = yield strength.

and the fluid in the temperature bath were 50 percent inhibited ethylene glycol. A sketch of the test apparatus is shown in Fig. 2.

During burst testing, approximately 10 percent of the volume of the tubular specimens were filled with air. It was felt that the inclusion of air in the test specimen would be helpful in that the energy stored in the compressed gas would help to propagate a brittle fracture.

The type of fracture was easily evaluated by visual examination of the appearance of the fracture faces. A tough or ductile fracture was gray-looking and featureless whereas the fracture faces in a brittle crack were shiny and faceted.

TYPE "A" SPECIMEN
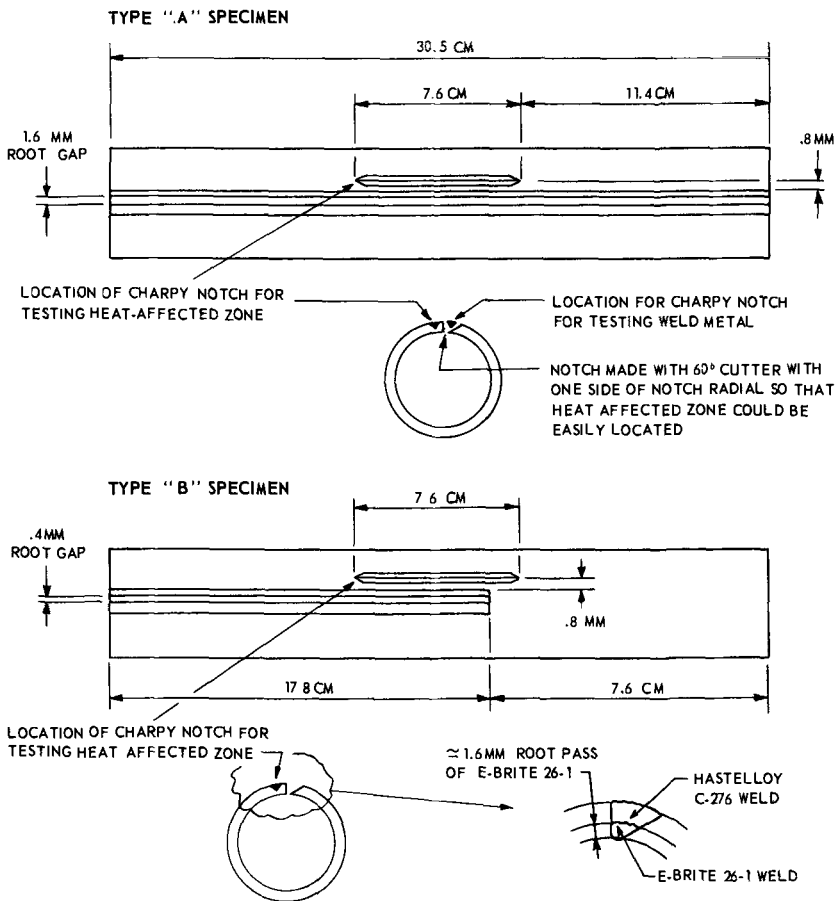
FIG. 1—*Burst test specimens.*

Results

Base Metal Specimens

The results of all of the burst tests are given in Table 2. The data for the base metal burst tests are shown graphically in Fig. 3. The data are depicted in the format typically used for Charpy impact tests. Because there was no easy method to measure the energy absorbed by the burst test specimen during failure, the energy axis was relabeled to show the type of fracture. A ductile fracture is indicative of a metal with high impact toughness whereas a brittle material would be indicative of a metal with low impact toughness. The results of the burst test specimens made from unwelded material revealed that Heat X had an apparent ductile-to-brittle
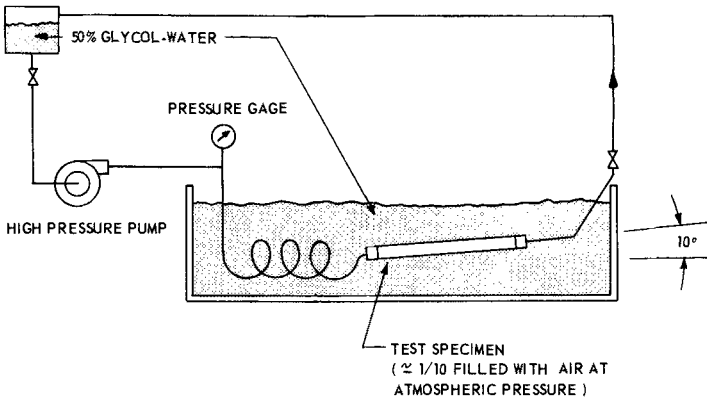
FIG. 2—*Burst testing apparatus.*

transition temperature (DBTT) between -18 and $-45\,^{\circ}$C (0 and $-50\,^{\circ}$F), Heat Y a DBTT of $0\,^{\circ}$C ($32\,^{\circ}$F), and Heat Z a DBTT between -18 and $-43\,^{\circ}$C (0 and $-45\,^{\circ}$F). In all instances of brittle fracture, the specimens exhibited some bulging ductility under the notch before failure. The brittle cracks ran in a longitudinal direction, from the notch, to the ends of the specimens (Fig. 4).

Welded Specimens

Type A Specimens—Solid 26Cr-1Mo Weld—The Type A specimens of Heat X were welded using the gas metal-arc welding (GMAW) method with solid 26Cr-1Mo filler metal. All of these specimens broke in a brittle manner during test. The controls used to prevent weld metal contamination were unsatisfactory. In fact, the argon purge gas on the torch contained 0.5 percent oxygen, which was believed, at the time of the tests, to be beneficial in preventing weld metal contamination. The backup purge gas inside the specimen was pure argon. Postweld heat treatment of these GMAW welded specimens did not improve their response to fracture or cause any fractures to become ductile. Of significance is the fact that in Specimens X-2 HAZ and X-3 HAZ, which were notched in the heat-affected zone, the cracks started in the heat-affected zone but quickly jumped into the weld metal (Fig. 5). Obviously, the weld metal was more brittle than the heat-affected zone.

Type A Specimens—Duplex 26Cr-1Mo/Hastelloy C-276 Weld—In order to develop a tough weld deposit, all of the rest of the welded specimens tested contained a dual weld metal deposit made using the gas tungsten-arc welding (GTAW) method. The weld deposit consisted of a root pass of 26Cr-1Mo (to retain the same internal corrosion resistance as the base

TABLE 2—Burst test results of Cr26-1Mo tubular material.

Specimen No.	Weld Deposit	Heat Treatment[a]	Test Temperature, °C (°F)	Burst Pressure, MPa (psi)	Type of Fracture
BASE METAL					
X-1	none	no	3 (+37)	86 (12 500)	ductile, 100% shear in notch only
X-2	none	no	−45 (−50)	86 (12 500)	brittle, 100% cleavage fracture for full 30-cm length; transverse branching on one end of brittle crack
X-3	none	no	−19 (−2)	88 (12 800)	ductile, 100% shear at 3.5-cm-long longitudinal tube defect (hot tear) 55% through wall; no crack at Charpy notch but some bulging
X-4	none	no	−1 (+30)	75 (10 900)	ductile, 100% shear in notch only
X-5	none	no	0 (+32)	83 (12 000)	ductile, 100% shear in notch only
Y-1	none	no	0 (+32)	138 (20 000)	brittle, ductile crack origin with brittle fracture extending from one end of notch to end of specimen
Y-2	none	no	0 (+32)	117 (17 000)	ductile, 100% shear in notch only
Y-3	none	no	18 (+65)	110 (16 000)	ductile, 100% shear in notch only
Z-1	none	no	0 (+32)	117 (17 000)	ductile, 100% shear in notch only
Z-2	none	no	−18 (0)	117 (17 000)	ductile, 100% shear in notch only
Z-3	none	no	−43 (−45)	121 (17 500)	brittle, ductile origin with brittle crack extending from one end of notch to end of specimen
WELDED SPECIMEN (TYPE A)					
X-1 HAZ	26-1	no	16 (+60)	17 (2 500)	brittle, 100% cleavage fracture through weld (not HAZ) 18.5 cm length, started at lack of weld penetration
X-2 HAZ	26-1	yes	0 (+31)	48 (7 000)	brittle, 100% cleavage fracture to one end of tube only; crack started in notch, went transversely to weld and followed weld to end of tube
X-3 HAZ	26-1	yes	−1 (+30)	62 (9 000)	brittle, 100% cleavage fracture, crack started in HAZ notch and jumped into weld after using about ⅔ of notch length; some transverse cracking
X-4W	26-1	yes	−1 (+30)	37 (5 300)	brittle, 100% cleavage fracture through weld; cracks both stopped in transverse cracks
X-5W	26-1	no	16 (+60)	62 (9 000)	brittle, 100% cleavage fracture through weld for 18-cm length; numerous transverse cracks in base metal

X-6W	26-1	yes	−2 (+29)	53 (7 700)	brittle, 100% cleavage fracture; cracks extended 2.5 cm beyond notch on one end and 5 cm beyond notch on other end
Y-1 HAZ	26-1/C-276	yes	0 (+32)	121 (17 500)	brittle, ductile crack origin with 6 to 7-cm brittle crack into base metal from one end of notch
Y-2 HAZ	26-1/C-276	yes	18 (+65)	121 (17 500)	ductile, 100% shear in notch only
Y-3 HAZ	26-1/C-276	yes	10 (+50)	110 (16 000)	ductile, 100% shear in notch only
Z-1 HAZ	26-1/C-276	yes	0 (+32)	103 (15 000)	brittle, fracture not in notch but along weld fusion line because of lack of proper fusion during welding
Z-2 HAZ	26-1/C-276	yes	18 (+65)	117 (17 000)	ductile, 100% shear in notch with 2-cm-long brittle crack into base metal from one end of notch
Z-3 HAZ	26-1/C-276	yes	27 (+80)	110 (16 000)	ductile, 100% shear in notch with 1-cm-long brittle crack extending into weld fusion line from one end of notch because of poor fusion
WELDED SPECIMEN (TYPE B)					
X-1*	26-1/C-276	yes	−2 (+29)	68 (9 800)	ductile, 100% shear in notch only
X-2*	26-1/C-276	yes	−1 (+30)	79 (11 500)	ductile, 100% shear in notch only
X-3*	26-1/C-276	yes	−1 (+30)	69 (10 000)	ductile, tube swollen and 100% ductile shear in notch; two short brittle cracks extending into base metal from weld end of HAZ notch
X-4*	26-1/C-276	yes	−18 (0)	79 (11 500)	brittle, fracture started tough and went brittle about 5 cm into both the HAZ and base metal ends of the Charpy notch
X-5*	26-1/C-276	yes	+18 (+65)	75 (10 800)	ductile, 100% shear in notch only
X-6*	26-1/C-276	yes	65 (+150)	69 (10 000)	ductile, 100% shear in notch only
Y-1*	26-1/C-276	yes	65 (+150)	121 (17 500)	ductile, 100% shear in notch with 1-cm brittle fracture extending into base metal from weld end of notch
Y-2*	26-1/C-276	yes	49 (+120)	103 (15 000)	ductile, 100% shear in notch only; specimen failed by creep mode because pressure held accidently, at about 103 MPA (~14 935 lb/in.^{2}) for 35 to 40 min, while specimen temperature was being raised
Z-1*	26-1/C-276	yes	65 (+150)	86 (12 500)	ductile, 100% shear in 1-cm-long crack in base of notch; low pressure and lack of full break because of weld defect
Z-2*	26-1/C-276	yes	65 (+150)	124 (18 000)	ductile, 100% shear in notch only

[a] All heat-treated specimens were introduced, two at a time, into a 980°C (1800°F) furnace, held at 980°C (1800°F) for 20 min and were water-quenched immediately upon removal.
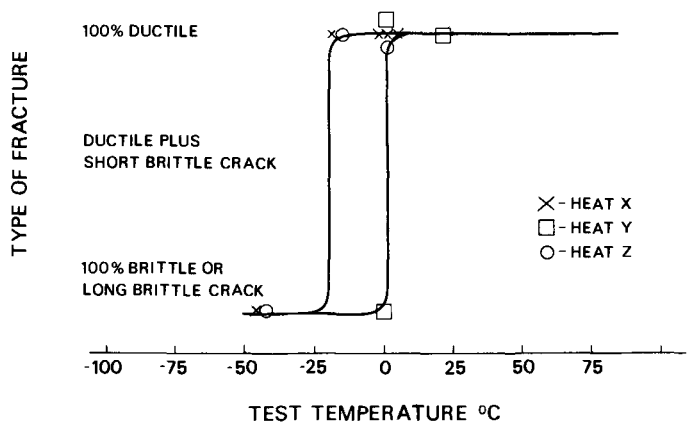
FIG. 3—*Base metal test specimens.*
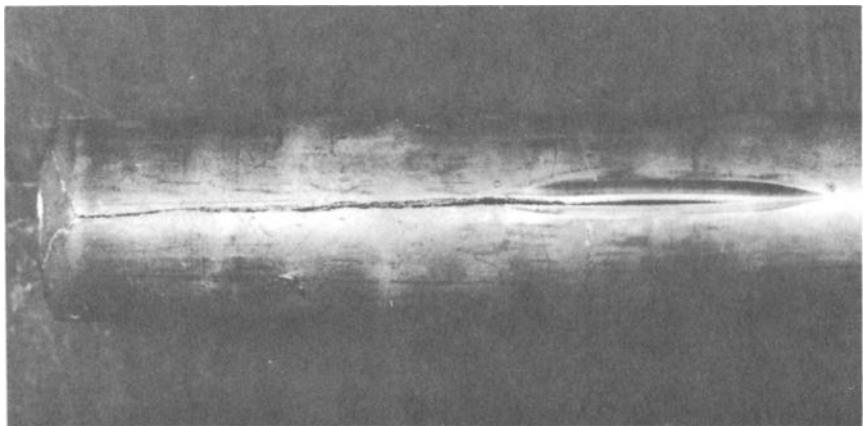
FIG. 4—*Base Metal Specimen Z-3, tested at −43°C, showing brittle fracture from the end of the notch to one end of the specimen. Note that the initial fracture in the notch was tough.*
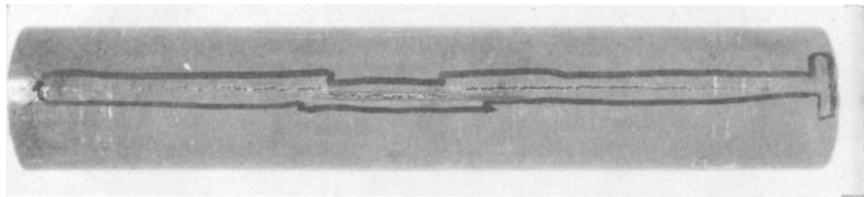
FIG. 5—*Specimen X-3 HAZ, tested at −1°C, showing cleavage fracture. The crack started in the HAZ notch and jumped into the weld after using about ⅔ of the notch length; some transverse cracking at one end of specimen.*

metal) followed by filler and cover passes of Hastelloy C-276 filler metal produced by the Stellite Division of Cabot Corp. Since the residual elements, carbon and nitrogen, were very low in the Hastelloy C-276, it appeared to have an interstitial-impurity level low enough to eliminate residual element diffusion into the HAZ of the 26Cr-1Mo base metal. Hastelloy C-276 has good low-temperature toughness. The main disadvantages in using Hastelloy C-276 weld metal were its high cost and low melting point. The Hastelloy C-276 melts at a considerably lower temperature than does the 26Cr-1Mo base metal; consequently, the welder must be careful to properly melt the Hastelloy C-276 filler metal into the sidewall of the 26Cr-1Mo base metal, or a lack of sidewall fusion will result. The welding procedure is shown in Table 3. The specimens were given a postweld heat treatment consisting of 20 min at 980°C (1800°F) followed by a water-quench.

The results for all of the Type A specimens are shown in Fig. 6.

The results of the burst tests for Heat Y revealed that this material had an apparent DBTT between 10 and 0°C (50 and 32°F). Specimen Y-1 HAZ, which was tested at 0°C (32°F), had a long brittle crack that extended from one end of the notch into the base metal (Fig. 7). The other specimens (Y-2 HAZ and Y-3 HAZ) exhibited only ductile, 100 percent shear in the notch only.

Heat Z, Specimen Z-1 HAZ, tested at 0°C (32°F), failed in a brittle manner with the crack being about 150 mm (6 in.) long in the weld. Microscopic examination showed lack of fusion. The cracks in Z-2 HAZ and Z-3 HAZ tested at 18 and 27°C (65 and 80°F), respectively, both started in 100 percent shear in the notch and then exhibited 10 to 20-mm-long 3½ to ¾ in.) brittle cracks into the base metal or weld fusion line (Fig. 8).

*Type B Specimens—Duplex 26Cr-1Mo/Hastelloy C-276 Weld—*The results of the tests on the Type B specimens are shown in Fig. 9. In these specimens, the weld, HAZ, and base metal were tested at the same time. If the weld had ductility or strength properties which were worse than the HAZ, the crack would then jump over into the weld as the Type A GMAW welded specimens had previously shown. Inasmuch as Hastelloy C-276 gives a tough, strong weld deposit, it was unlikely that the crack

TABLE 3—*Welding procedure for 26Cr-1Mo.*

1. GTAW method for all welds
2. 0.4-mm root gap
3. Foot-controlled rheostat used to limit heat input to the lowest amount to obtain good fusion
4. Pure argon purge of 0.28 1/s on the torch and 0.08 1/s for the backup flow
5. 3.2-mm diameter 2% thoriated tungsten electrode
6. 19-mm nozzle diameter
7. 160 A direct current straight polarity
8. Root pass of 1.5 to 2.0-mm depth with E-BRITE 26-1 filler metal
9. Filler and cover passes of Hastelloy C-276 filler metal
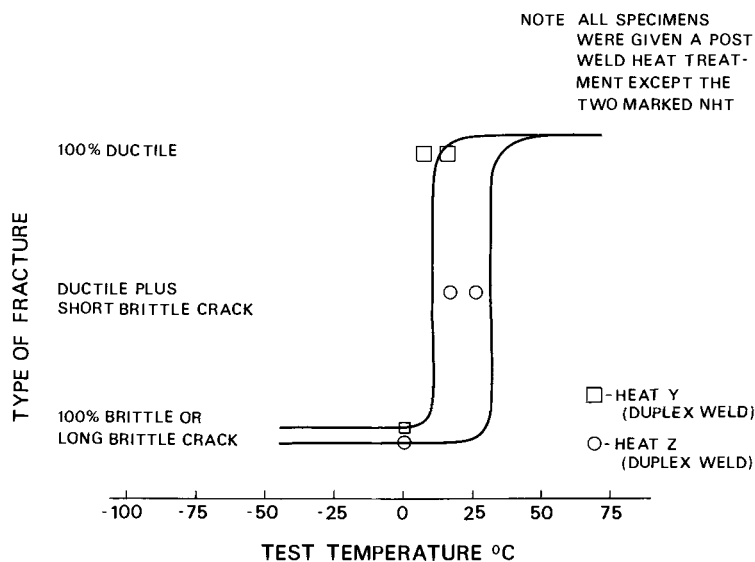
FIG. 6—*Type A test specimens.*
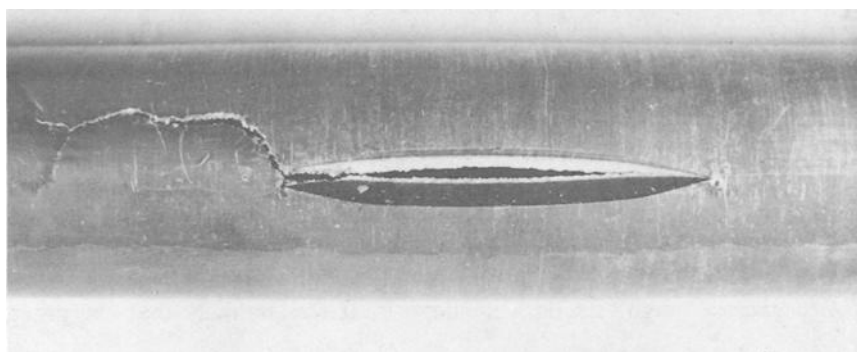
FIG. 7—*Specimen Y-1 HAZ, tested at 0°C, showing ductile failure in notch with a brittle fracture extending 6 to 7 cm into the base metal.*

would propagate into the composite 26Cr-1Mo/Hastelloy C-276 weld deposit.

The Type B specimens of Heat X showed that the material had an apparent DBTT of very near 0°C (32°F). The specimens of Heat Y showed that the DBTT was less than 65°C (150°F) if the abnormality of Specimen Y-1* could be explained. This specimen failed in a completely ductile
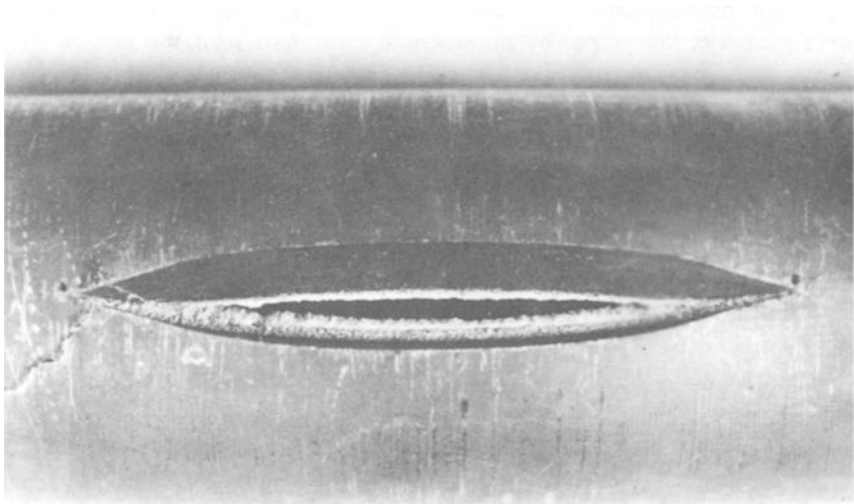
FIG. 8—*Specimen Z-2 HAZ, tested at +18°C, showing 100 percent ductile shear failure in the notch along with a short brittle 2-cm-long crack into the base metal.*
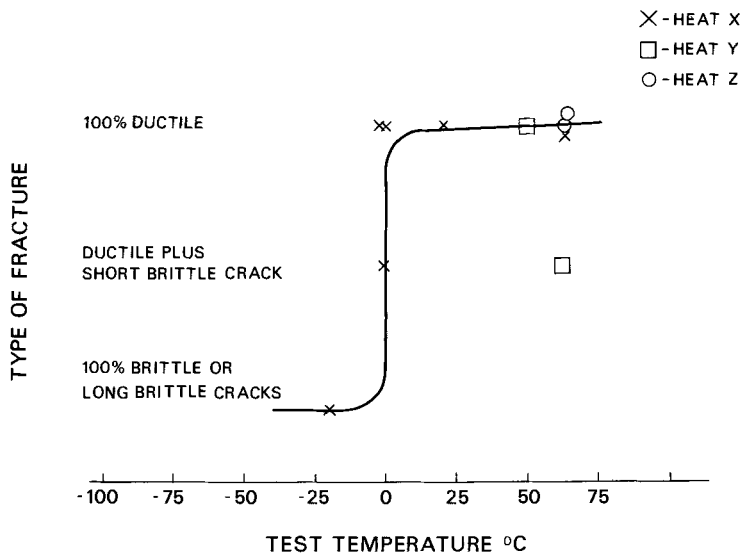
FIG. 9—*Type B test specimens.*

manner except for a short, 1-cm-long (½ in.) brittle crack which extended into the base metal from the weld end of the notch (Fig. 10). Certainly the brittle fracture started in the HAZ, but there was no area of tough shear that was detectable by microscopic examination of the end of the crack in the base metal. The Type B specimens of Heat Z showed 100 percent ductile behavior, and the DBTT was less than 65°C (150°F).

Impact Tests

Charpy impact data of specimens from both Heats Y and Z revealed that the 980°C (1800°F) postweld heat treatment did not significantly increase the DBTT when tested using the Charpy V-notch method. The data are shown in Fig. 11. All of the base material before or after heat treatment showed a DBTT of about −45°C (−50°F).

Duplicate half-size Charpy impact specimens were made from the longitudinal duplex welds of failed specimens of both Heats Y and Z. The impact data ranged from 18 to 60 J (13 to 45 ft-lb) at both −18 and −45°C (0 and 50°F). It is expected that the range of impact values for a Hastelloy C-276 weld deposit would be of the order of 40 to 70 J (30 to 52 ft-lb) for half-size specimens in this same temperature range. The fracture surfaces of these specimens showed ductile tearing for the Hastelloy C-276 and brittle fractures for the 26Cr-1Mo root pass and HAZ. The fractured specimens contained about 80 percent Hastelloy C-276 weld metal and 20 percent 26Cr-1Mo weld metal.

Discussion

The results of the burst test data on the unwelded base metal specimens showed that the material, as supplied by the manufacturer, was tough
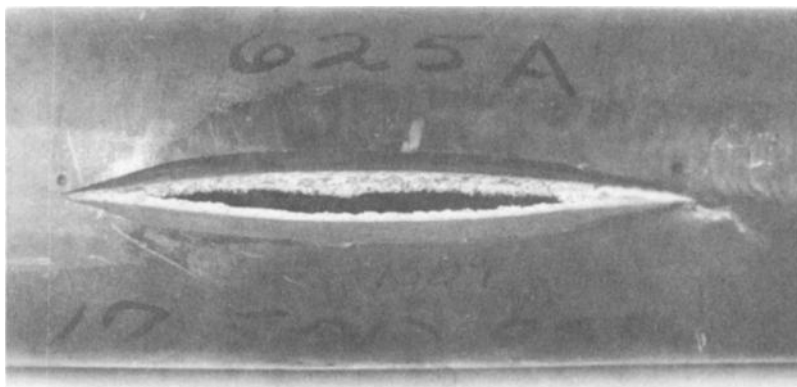
FIG. 10—*Welded Specimen Y-1*, tested at 65°C, showing ductile shear in the notch and 1-cm brittle fracture extending from the end of the notch in the HAZ into the base metal.*
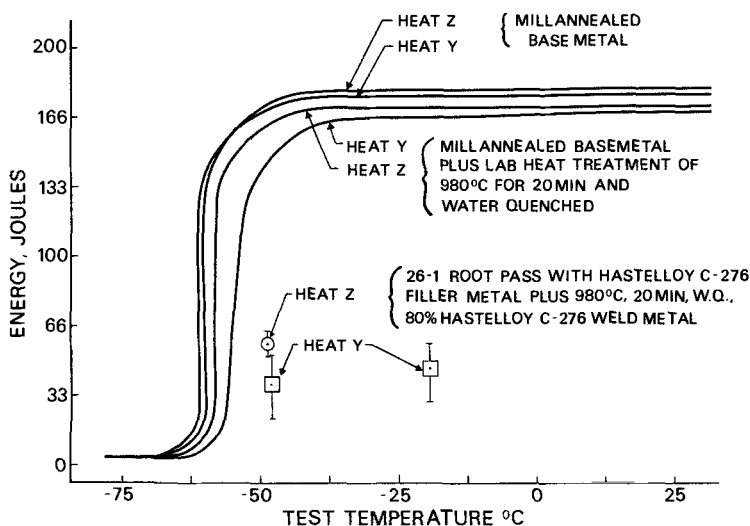
FIG. 11—*Charpy V-notch impact test data.*

down to 0°C (32°F) and perhaps to as low as −40°C (−40°F). It is interesting to note that the Charpy V-notch data for Heats Y and Z would predict a DBTT of −59°C (−75°F) for the unwelded base metal.

Apparently, the burst test was a more severe method of determining the DBTT than was the Charpy V-notch specimen. This may be because there was more chance for triaxial stress concentration in the large, tubular, burst test specimen than there was in the small impact test specimen.

The analyses of the burst test specimens would have been much easier if the specimens had failed by either a 100 percent brittle fracture mechanism or 100 percent ductile shear mechanism; however, this was not the case. Three of the "ductile" fractures that occurred in the specimens contained small brittle fractures extending into either the base metal or into the HAZ. These specimens are plotted in Fig. 9 halfway between the ductile and brittle fracture types. These three specimens showed considerable deformation (swelling of the tube) before failure. The initiation of the brittle cracks in the ductile mode plus their short length suggest that the material would have been sufficiently elastic to redistribute the stresses which could lead to brittle failure. The fact that the small brittle cracks did form is still puzzling—especially since they arrested in the base metal without showing any ductile tearing at the tips. Perhaps the amount of air compressed inside the specimen was insufficient to drive the cracks farther; however, other specimens did show full-length brittle cracks that contained corresponding amounts of bulging.

Since embrittled ferritic stainless steels have low notch impact strength,

the use of a postweld heat treatment should be beneficial if it removes the embrittlement. Most likely, 475°C (885°F) embrittlement did occur in the HAZ zone because of the temperature profile in the base metal during welding. Therefore, a postweld heat treatment at 980°C (1800°F) was used to remove any 475°C (885°F) embrittlement caused during welding. The facts that two of the Type A, Heat X specimens were notched in the HAZ and that the crack initiated in the notch and jumped into the weld suggested that the postweld heat treatment did improve the HAZ properties; however, in this group of specimens the weld was so contaminated by oxygen from the welding gas that the specimens would have probably always exhibited brittle failure in the weld.

The ductile burst specimens which contained brittle cracks and which were welded properly seem to show that the heat treatment was beneficial. These specimens were notched in the HAZ, yet the brittle cracks which started there ran into the base metal, with one exception, and did not propagate along the HAZ. The one exception, Z-3 HAZ, had a short brittle fracture along the fusion line because of poor sidewall fusion, which directed the brittle crack into the mechanically weakest area. Therefore, it appeared that the postweld heat treatment did improve the HAZ properties sufficiently to direct any short brittle cracks to run out into the base metal instead of remaining in the HAZ, where they initiated. The properties of the HAZ may have been better than the base metal, as the data indicate, but it was more likely that the HAZ allowed the brittle crack to initiate and then, because the HAZ and base metal had about equivalent toughness, the crack was free to follow any path of low toughness.

Conclusion

The burst test provided a good technique for determining the brittle fracture tendency of the weld metal, heat-affected zone, and base metal. It was very easy to differentiate between a ductile or tough rupture. Ductile fractures were gray and featureless whereas brittle fractures were shiny and faceted. The burst test appears to be very suitable for the evaluation of tubular products. Composite 26Cr-1Mo/Hastelloy C-276 weld deposits in 26Cr-1Mo base material provided a weld with very good toughness.

After the weld was made tough by using Hastelloy C-276 filler metal, the properties of the HAZ became important. Certainly the HAZ of 26Cr-1Mo material needs to be studied more closely before the full potential of the material can be realized.

C. W. Vigor[1]

Effect of Cold-Working on Impact Transition Temperature of 409 and E-4 Stainless Steels

ABSTRACT: When Type 409 stainless steel (11 percent chromium, balance iron, titanium stabilized) was specified for rectangular mechanical tubing for structural components, brittle fracture concerns were not anticipated because the tube wall thickness was in the plane-stress regime. However, low-temperature impact tests indicated that brittle fractures often occurred in the corner areas of the rectangular tubing, suggesting that residual cold-work influenced impact strength. Laboratory impact tests showed cold-working to strongly affect the ductile-to-brittle transition temperature (DBTT) of 409 stainless. A novel impact specimen allowed direct evaluation of the DBTT of the cold-worked tubing corner, confirming results obtained in conventional Charpy tests. An acceptably low DBTT for heavily cold-worked sections was found for a low-carbon ferritic stainless (11Cr-1Ni-0.03C-Fe) obtained from Crucible Steel Corp. under the trade designation of E-4. The as-welded toughness of E-4 is also improved over 409 due to the formation of low-carbon martensite in weld-heat-affected zones; in this application, however, only the base material properties were of interest.

KEY WORDS: brittle fracture, 409 stainless, rectangular tubing, low-temperature impact, tubing corners, cold-working, impact transition temperature, E-4 stainless, ferritic stainless steels, fracture toughness

In heavy sections where plane-strain conditions prevail, the ductile-to-brittle transition temperature (DBTT) of ferritic stainless steels can be relatively high. For sheet metal gages, however, plane-stress conditions prevail and problems due to brittle fracture of sheet metal fabrications are virtually unknown unless associated with weld heat-affected zone HAZ embrittlement. When AISI 409 stainless steel was considered for square and rectangular structural tubing applications for improved corrosion resistance, its low-temperature impact properties were believed to be ade-

[1] Departmental research engineer, Metallurgy Department, General Motors Research Laboratories, Warren, Mich. 48090.

quate as the tube wall thickness was within the plane-stress regime. In connection with weld process control testing, however, low-temperature cleavage fractures were noted in tube corner areas away from any weld (HAZ's).

This suggested that residual cold-work was affecting the DBTT for 409 stainless steel. As a result of this observation, an investigation was undertaken at the GM Research Laboratories to determine the severity of the embrittlement in the corners of the cold-formed tubing and to explore the behavior of possible alternative materials. One material investigated was an 11 percent chromium low-carbon ferritic stainless steel obtained from the Crucible Steel Division of Colt Industries under their trade designation of E-4. Because of its low-carbon content, typically 0.03 percent maximum, E-4 forms a low-hardness martensite in weld HAZ's which possesses good toughness at low temperature. Preliminary work at GM Research had indicated that the E-4 material also appeared to be more tolerant of cold-working. This paper presents the results of a study comparing the impact properties of 409 and E-4 as a function of the residual cold-work typically produced in the corner of a cold-formed rectangular tube.

The work was subdivided into several separate but related investigations:

1. Determination of baseline DBTT for as-received materials of 409 and E-4.

2. Determination of the degree of cold-work in the tube corner in order to give impact test specimens a like amount of deformation and to determine the effect on the DBTT for both 409 and E-4.

3. Determine whether heat treatment could produce a recovery of the DBTT.

4. Establish a correlation between DBTT found for cold-worked test bars and the DBTT for the corner area of the rectangular tubing.

To provide the correlation between notch-bar impact tests and properties in the cold-worked tube corner, Item 4 just given, a novel impact test specimen was devised which allowed direct evaluation of the DBTT of the cold-worked tube corner material.

Chemical Composition

Types 409 and E-4 stainless steel both contain ~11 percent chromium with the balance essentially being iron. The compositions of the two materials are compared in Table 1.

Despite the similarity of compositions, the fundamental metallurgical behavior of these two materials is markedly different.

Metallurgical Characteristics

Type 409 is an 11 percent chromium ferritic stainless which is stabilized against transformation to austenite at high-temperature to prevent hard-

TABLE 1—*Composition of 409 and E-4 stainless steels.*

	409, weight %	E-4, weight %
Carbon	0.08 max	0.03 max
Manganese	1.00 max	0.30 to 0.70
Silicon	1.06 max	0.35 to 0.55
Sulfur	0.045 max	0.03 max
Phosphorus	0.045 max	0.03 max
Nickel	0.50 max	0.70 to 1.00
Chromium	10.5 to 12.5	10.5 to 12.5
Titanium	6 × C min	none
	0.75 max	

ening in weld HAZ's and in mill processing. Because even small amounts of carbon cause steel containing 11 percent chromium to be intensely air-hardening, titanium is added to form the stable compound, titanium carbide, thus removing carbon from its role in austenite formation.

The microstructure of 409, shown in Fig. 1, consists of equiaxed ferrite grains with a random scattering of Ti(C,N) particles.

E-4 is a specialty alloy and does not have an industry-type designation. Like 409, it is nominally an 11 percent chromium stainless but differs from 409 in that the carbon is not combined with a stabilizing element. Its metallurgical hardening response is essentially the same as carbon steel. Unlike carbon steel, however, martensite hardening occurs on slow cooling from above 760°C (1400°F). Because of the low carbon content, typically 0.02 to 0.03 percent, the hardness does not exceed approximately HRC-20. At this low hardness, martensitic weld HAZ's have excellent toughness which is retained to subambient temperatures.

Because of the high hardenability due to the combined effect of the nickel and chromium content, martensitic hardening occurs on cooling of hot-rolled coils. A subcritical anneal is required before further mill reductions. Sections thinner than about 5 mm (0.2 in.) are produced by cold-rolling. A final subcritical anneal is given all material to achieve formability.

The microstructure of E-4 is shown in Fig. 2. Like 409, its matrix structure is a solid solution of chromium in iron. Unlike 409, E-4 has a dispersion of chromium and iron carbides. The grain size of E-4 is typically finer than 409, reflecting the different mill processing.

Properties

The properties of 409 and E-4 are compared in Table 2.

The mechanical properties of 409 and E-4 are essentially equivalent, although E-4 tends to have a slightly higher mean yield strength and hardness.
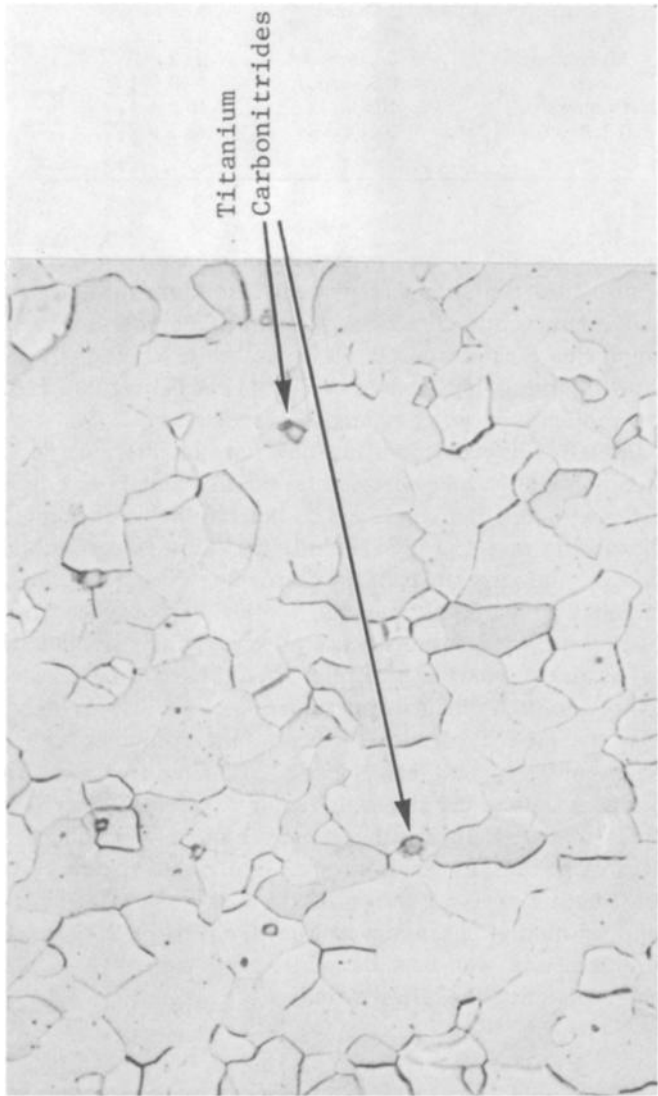
FIG. 1—*Microstructure of 409 stainless steel. Etchant: Glyceregia* (×500).
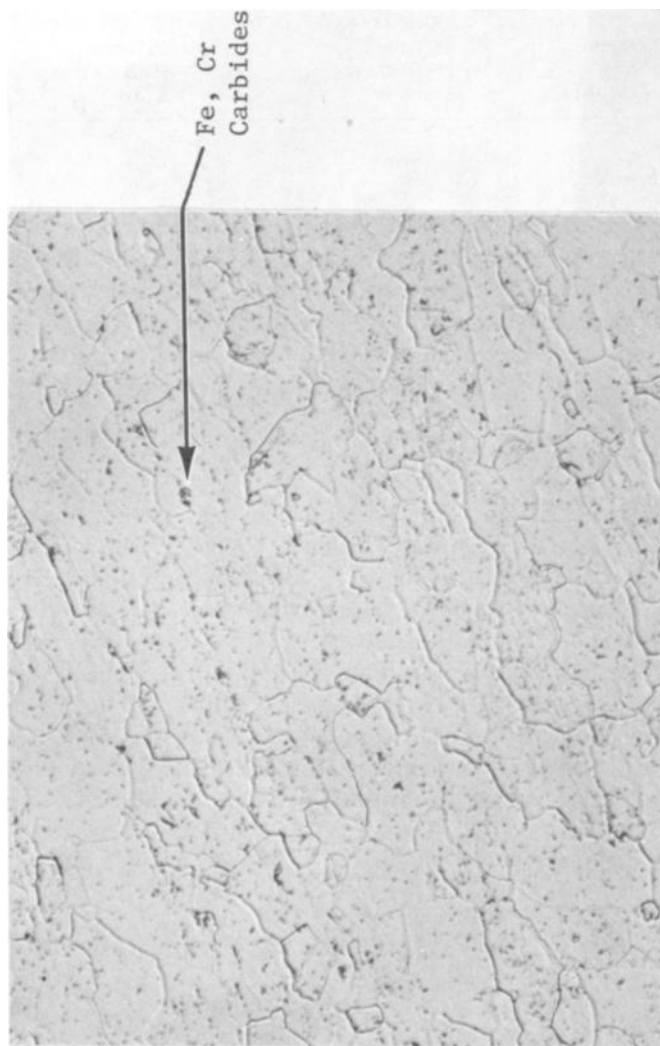
FIG. 2—Microstructure of E-4 stainless steel. Etchant: Glyceregia (×500).

TABLE 2—*Mechanical properties of 409 and E-4.*

	409	E-4
Tensile strength	393 to 517 MPa	414 to 517 MPa
	(57 000 to 75 000 lb/in.^{2})	(60 000 to 75 000 lb/in.^{2})
Yield strength	207 to 330 MPa	241 to 303 MPa
	(30 000 to 48 000 lb/in.^{2})	(35 000 to 44 000 lb/in.^{2})
Elongation (50.8 mm)	24% min	28% min
Hardness	HRB-80 max	HRB-85 max
Grain size (ASTM E-112)	5 to 8	5 to 8

Materials Source

All materials tested were commercially obtained. Subsize impact test specimens for 409 were prepared from 2.77-mm-thick (0.109 in.) stock and for E-4 from 2.36-mm (0.093 in.) stock. The special tube corner impact test specimens were prepared from commercially made tubing of both E-4 and 409. The dimensions of the tube cross section are noted in Fig. 3.

Impact Testing

Impact tests were conducted in accordance with recommended practices of ASTM Notched Bar Impact Testing of Metallic Materials (E23-72). For subambient tests, specimens were cooled in an ethanol bath which had been chilled to the desired test temperature with dry ice. The bath was maintained in an open-mouth vacuum flask. All specimens were maintained in the bath at the test temperature for a minimum of 5 min before testing as specified by E23-72. Tests were conducted within 2 to 4 s after removal from the cooling bath (a maximum of 5 s is allowed in E23-72). The temperature of the bath was maintained within ±0.5 deg C of indicated test temperature. To facilitate speedy specimen transfer and the accuracy of
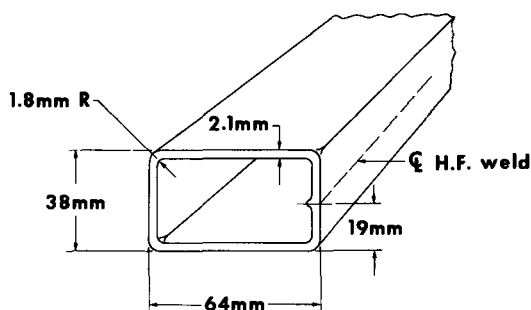
FIG. 3—*Dimensions of tube.*

specimen positioning in the impact machine, special specimen tongs were constructed as recommended by E23-72.

A Riehle Model PI-2 Combination Impact Test Machine was used for all tests. The hammer mass was 6.8 kg (15 lb), the drop height 0.61 m (2 ft), the impact velocity 3.44 m/s (11.3 ft/s), and the maximum available energy 40.7 J (30 ft-lb).

Test Specimens

The minimum-thickness test specimen recommended by E23-72 is 2.5 mm (0.098 in.). Test specimens of as-received materials were 2.77 mm (0.109 in.) thick, which slightly exceeded the minimum thickness, and test specimens of cold-worked materials were 2.36 mm (0.093 in.) thick, which was slightly less than the minimum thickness. All specimens were prepared so as to cause the fracture to occur in a direction parallel to the rolling direction. Standard 45-deg, 0.25-mm (0.010 in.) root radius V-notch geometry was used. Notches were formed by precision grinding and checked for accuracy on a shadowgraph.

Cold-Working of Impact Test Specimens

In order to assess the effect of cold-work on impact transition temperature, the strain in the tube corner had to be determined so that impact test specimens could be given a like strain. The material's hardness response was used to relate the two methods of inducing strain. Figure 4 shows typical results of microhardness measurements made in the corner of 409 and E-4 tubes. The E-4 material has a higher work-hardening rate than 409. As may be seen, the greatest amount of work-hardening on both materials occurs on the inner or compression side of the bend. This is
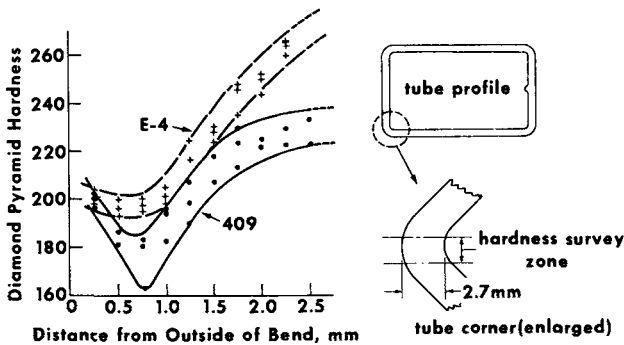
FIG. 4—*Hardness survey of cold-formed tube corner. Upper right, tube profile; lower right, location of survey zone; left, hardness of E-4 and 409 measured from outside to inside of bend.*

consistent with geometric considerations in the tube fabrication process where a round section is first formed for purposes of high-frequency welding and then re-formed into the rectangular section. Both steps involve compressive strain on the inner tube surface.

Impact test specimens were cold-worked by indentation between cylinders of 19-mm (0.75 in.) radius, as shown in Fig. 5. Indentations of 5, 10 and 15 percent reduction in thickness were made. Typical hardness distribution patterns along the centerline of a section specimen for 5 and 15 percent reductions are shown in Fig. 6. The hardness in the transverse direction was found to be uniform.

The 15 percent reduction indentation produced a hardness which was about 75 percent of the maximum at the inner corner for the 409 tube and 60 percent of the maximum for E-4 as shown in Fig. 7. The 15 percent reduction was chosen as the reduction to be given the impact specimens as it appeared to be fairly representative of the amount of cold-work in each material. A greater reduction would more severely cold-work the 409 material than was desired and a lesser reduction would not work the E-4 enough. An impact test specimen which had been reduced 15 percent in thickness in its midsection is shown in Fig. 8. The notch was ground after the cold-working operation.

Tube Corner Test Specimen

The impact test specimen devised from the tube corner is detailed in Fig. 9. The tubing was transversely sectioned into 12-mm-wide (0.47 in.) slices. From this an equal-length leg section was prepared from the side and top portions of the tube away from the weld (top left and right, Fig. 9). The legs of the specimen were bent upward 45 deg as shown in the middle left of Fig. 9. A jig was used to avoid further straining of the tube corner. Two such members were faced together and spot-welded securely (middle right, Fig. 9). The specimen was then finished to standard Charpy
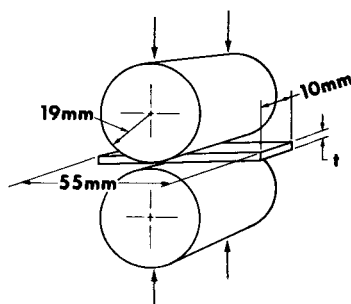
FIG. 5—*Method of cold-working impact test specimens.*
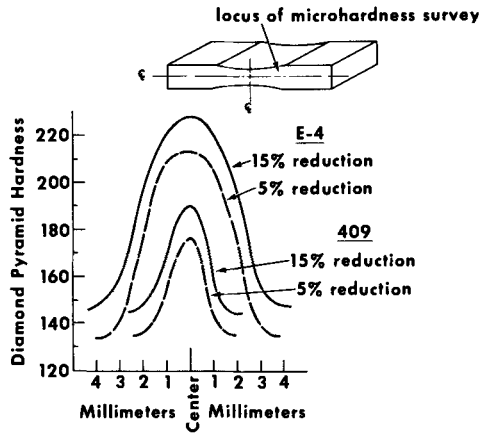
FIG. 6—*Microhardness response to indentations of 5 and 15 percent reduction in thickness for 409 and E-4. Hardness survey was made on sectioned and polished specimen. (Data have been averaged and smoothed for presentation purposes.)*
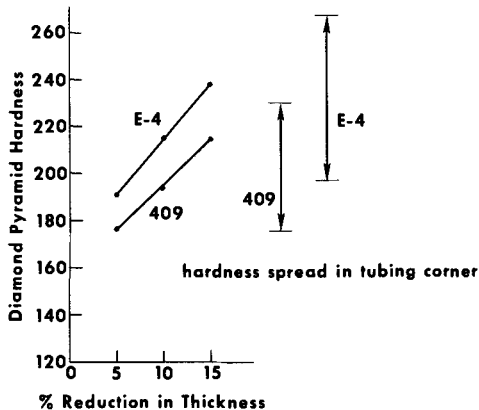
FIG. 7—*Peak hardness produced by roll indentation compared with hardness spread found in tubing corner.*

length, width, and notch configuration. In testing this specimen, the pendulum hammer strikes both upper and lower members simultaneously, thus balancing the rotational moment due to the offset of that portion of the specimen containing the corner bend. Figure 10, top, shows the tube corner specimen prior to test. Above the ductile-to-brittle transformation temperature, Fig. 10, middle, the specimen deformed without fracture. Below the DBTT, Fig. 10, lower, the specimen fractured at the notch location without discernible prior plastic deformation. In the immediate
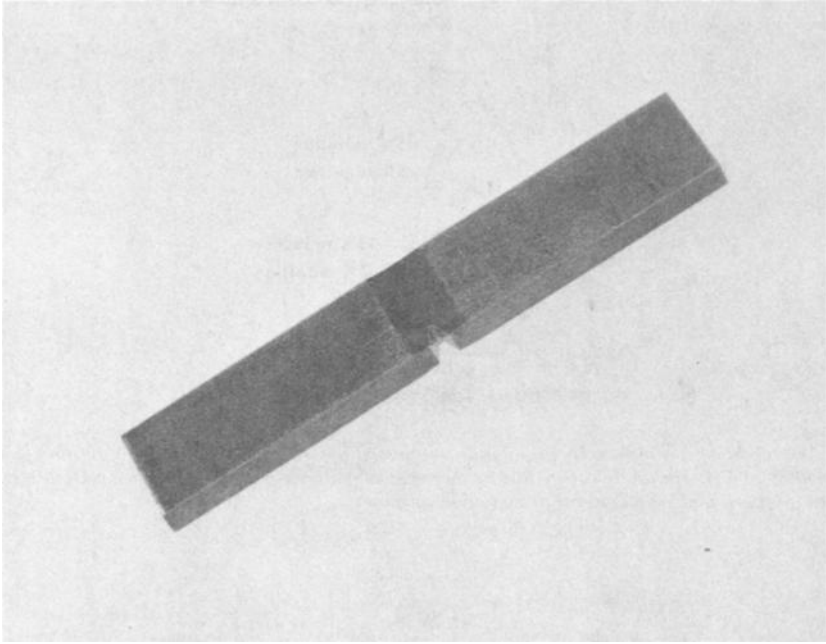
FIG. 8—*Impact test specimen cold-reduced 15 percent in midsection with standard Charpy V-notch (×1.5).*
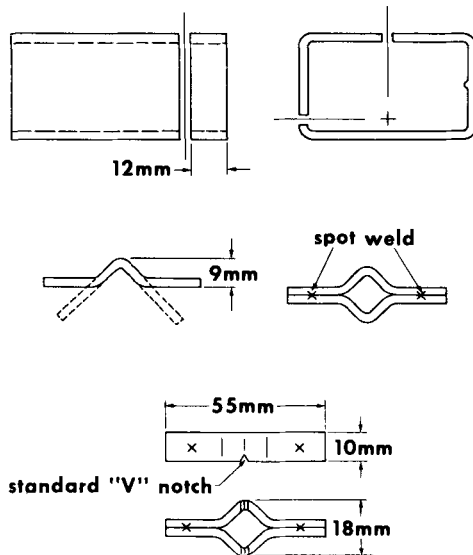
FIG. 9—*Preparation of tube corner impact test specimen.*
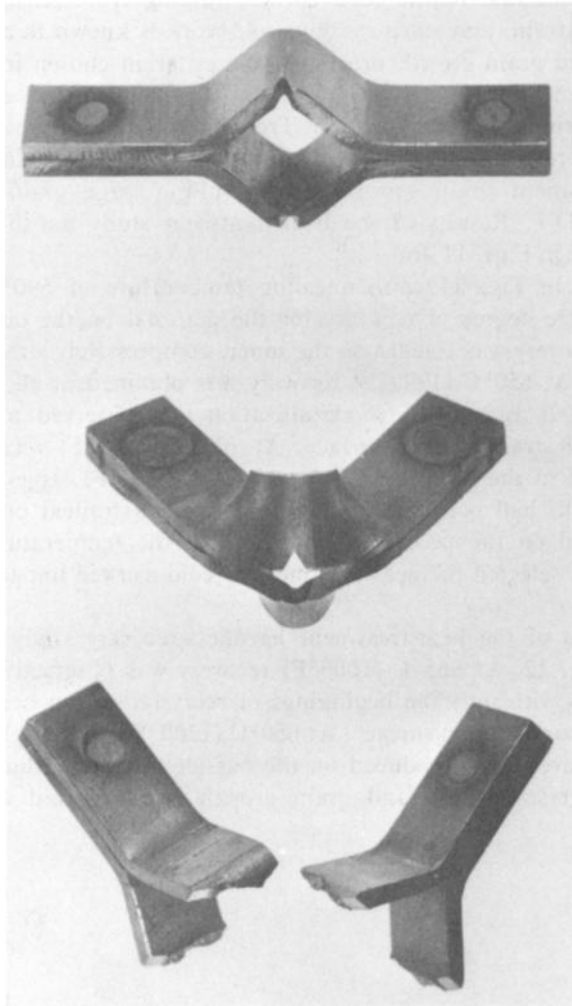
FIG. 10—*Tube corner impact specimen. Top: prior to test; middle: above transition temperature—no fracture; bottom: below transition temperature—fracture.*

neighborhood of the transformation temperature, some degree of plastic deformation preceded fracture.

Heat Treatment

The effect of heat treatment on the restoration of impact properties was evaluated. To determine an appropriate treatment temperature, the material's hardness response was again used. Since a considerable range

of cold-work existed in the tube corner, varying from tension strain to compressive strain, and since residual cold-work is known to affect recrystallization and grain growth processes, the criterion chosen for a suitable heat treatment was based on hardness recovery without encountering substantial primary recrystallization. Treatments producing massive recrystallization were avoided because of the tendency of 409 stainless steel to exhibit germinant grain growth. The resulting large grain size would raise the DBTT. Results of the heat-treatment study for the two alloys are presented in Figs. 11 and 12.

As shown in Fig. 11, an annealing temperature of 590°C (1100°F) produced some degree of recovery for the material on the outside of the bend. No recovery was evident on the inner, compressively strained portion of the tube. At 650°C (1200°F) recovery was obtained in all cold-worked areas. A small amount of recrystallization was observed at the inside compressively strained tube surface. At 700°C (1300°F) recrystallization had occurred in the whole section. At 760°C (1400°F) large-grained germinant growth had occurred in the outer tension-strained portion of the corner. Based on the preceding observations, the temperature of 650°C (1200°F) was selected for heat treatment of cold-worked impact test specimens of 409.

The results of the heat-treatment hardness-recovery study for E-4 are shown in Fig. 12. At 565°C (1050°F) recovery was observed for all cold-worked areas with only the beginnings of recrystallization being observed at the inner compression surface. At 650°C (1200°F), only slight additional hardness recovery was produced on the outside and midradius while considerable recrystallization and grain growth had occurred at the inner
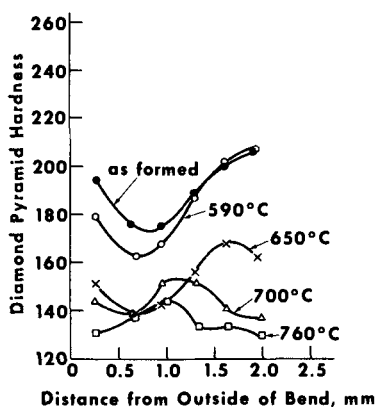
FIG. 11—*Effect of annealing temperature on hardness in tube corner for 409 stainless, 1 h at temperature.*
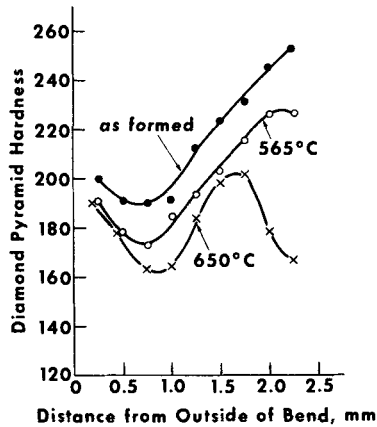
FIG. 12—*Effect of annealing temperature on hardness in tube corner for E-4 stainless. 1 h at temperature.*

compression surface. An annealing temperature of 565°C (1050°F) was chosen for cold-worked E-4 impact test specimens.

Baseline Impact Properties of 409 and E-4

The notched bar impact behavior of 409 and E-4 in the as-received condition is compared in Fig. 13. Because of slight specimen thickness differences, 2.77 mm for 409 and 2.36 mm for E-4, the comparison is based on fracture energy per unit area of cross section at the notch. When
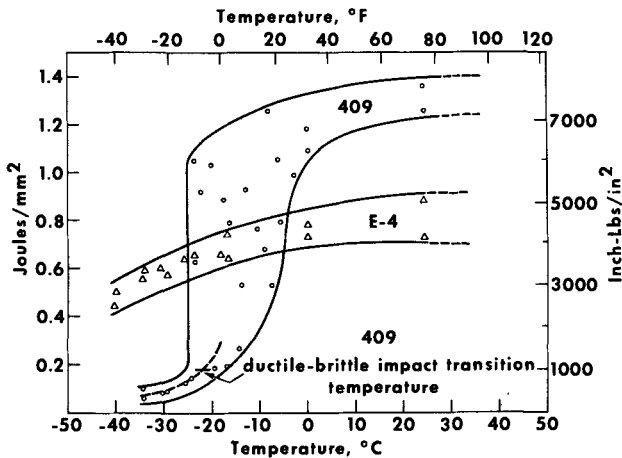
FIG. 13—*Impact properties of as-received materials.*

evaluating subsize Charpy impact tests, the DBTT is generally regarded to have occurred at a value of 0.175 J/mm^2 (1000 in-lb/in.^{2}). Judged by this criterion, the DBTT for 409 steel is $-22°C$ ($-7.5°F$). The impact-energy-versus-temperature curve is typical for a ferritic steel, although displaced upward in temperature compared with a plain carbon steel.

E-4 stainless did not show an impact transition down to $-40°C$ ($-40°F$), which was the lowest temperature tested. The slight decrease in impact energy with decreasing temperature displayed by E-4 rather than an abrupt drop may be likened to the behavior of tempered martensite structures.

Impact Properties of Cold-Worked Specimens

Impact results for Type 409 specimens which had been reduced 15 percent in thickness in the notched area, as in Fig. 8, are shown in Fig. 14. The cold-working increased the DBTT to 20°C (68°F). Also shown in Fig. 14 for comparison purposes is the impact test results for as-received material. The net change in the DBTT due to the 15 percent reduction in cross section was 42 deg C (76 deg F).

Impact test results for E-4 similarly cold-worked 15 percent are presented in Fig. 15. In this instance a DBTT was present at $-27°C$ ($-17°F$).

Tubing Corner Test Specimen

Impact test results for the special tubing corner test specimens, Figs. 9 and 10, are presented in Fig. 16. For both materials there was an abrupt transition from no fracture, that is, the specimen deformed, to fracture
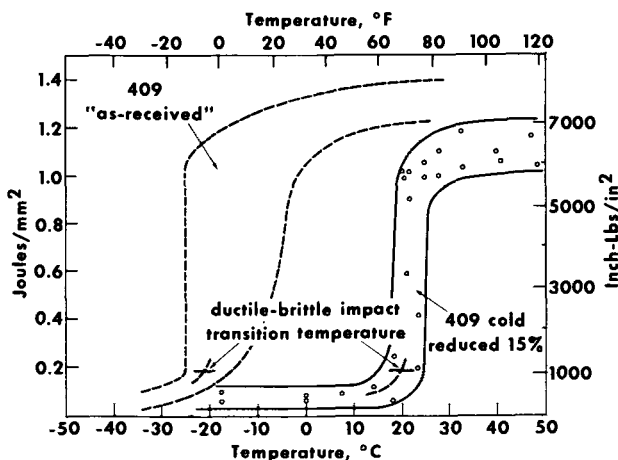
FIG. 14—*Impact properties of cold-worked 409 compared with as-received condition.*
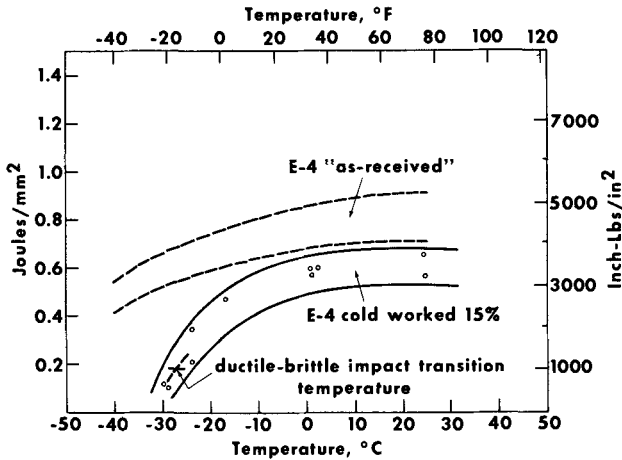
FIG. 15—*Impact properties of cold-worked E-4 compared with as-received condition.*
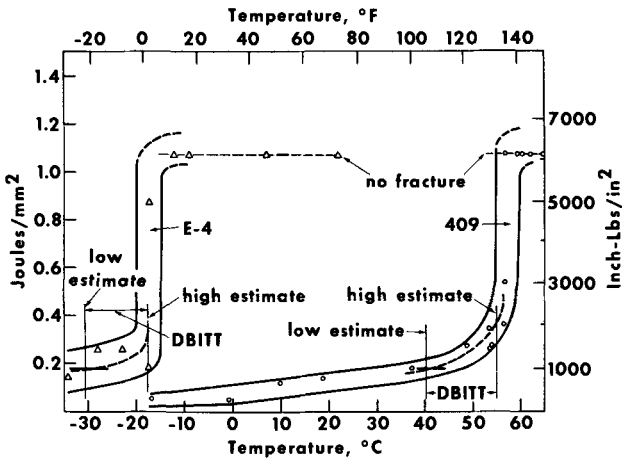

FIG. 16—*Impact properties of tubing corner test specimen.*

in a narrow temperature range. In conventional impact tests, the impact transition temperature is generally regarded to be at the lower knee of the curve. As indicated in Fig. 16, this locates the DBTT somewhat above the 0.175-J/mm² (1000 in-lb/in.²) criterion for subsize Charpy bars. As a result, the DBTT for the nonconventional tube corner specimen cannot be precisely defined; therefore, a high and low estimate of the DBTT was made. For 409 the low and high estimates for the DBTT are 40 and 55°C (104 and 131°F), respectively. The low and high estimated for the DBTT of E-4 are −30 and −17°C (−22 and 1.4°F).

Effect of Heat Treatment on Impact Properties

Heat treatments which produced hardness recovery but avoided excessive recrystallization were used for each of the materials, Figs. 11 and 12. Tests of heat-treated specimens were made sufficient only to evaluate the temperature range between the "as-received" test results and the 15 percent cold-worked test results.

Impact test results of the cold-worked 409, 15 percent reduction, after annealing at 650 °C (1200 °F) for 1 h are shown in Fig. 17. As may be seen, the heat treatment produced some recovery of impact properties but did not restore the material to the level of the as-received properties.
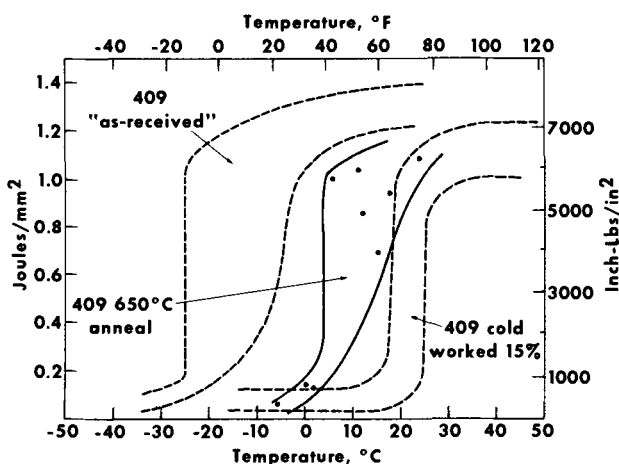
FIG. 17—*Impact properties of cold-worked and annealed 409.*

Impact test results of cold-worked and annealed E-4 are shown in Fig. 18. At the 565 °C (1050 °F) anneal temperature, impact recovery was only intermediate between the as-received and 15 percent cold-worked curves. At an annealing temperature of 650 °C, limited tests indicated that recovery approached the as-received properties.

Impact test results for a Type 409 tube corner specimen annealed at 650 °C (1200 °F) and E-4 annealed at 565 °C (1050 °F) are presented in Fig. 19. Shown for comparison purposes are the results for unannealed tube corner specimens. The transition temperature of the 409 was lowered to approximately −10 °C (+14 °F), which is close to the −22 °C (−7.6 °F) of as-received flat material shown in Figure 13. The 565 °C (1050 °F) annealing temperature on the E-4 tube corner specimens has effected a complete recovery as fracture could not be obtained down to −50 °C.
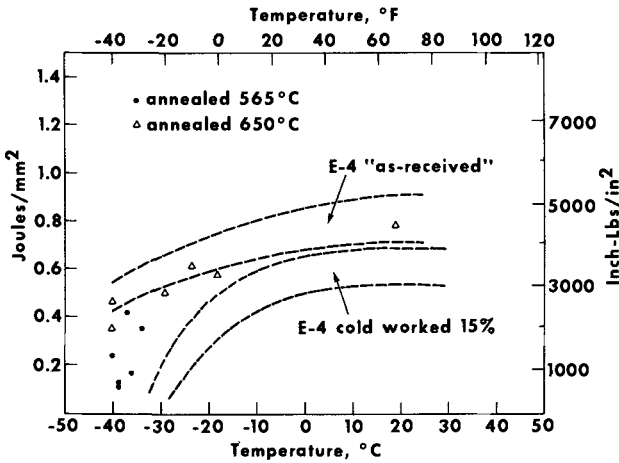
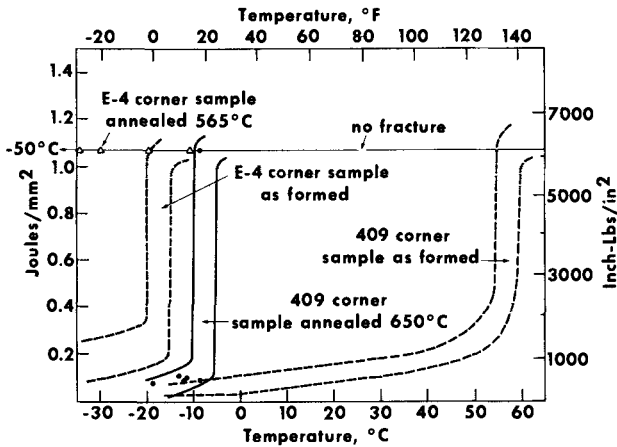FIG. 18—*Impact properties of cold-worked and annealed E-4.*

FIG. 19—*Impact properties of annealed tubing corner test specimen.*

Discussion

As demonstrated in this study, cold-working has a marked effect on raising the DBTT for 409 stainless steel. The low-carbon ferritic stainless, designated E-4, appears to be an acceptable alternative material to escape the effects of cold-working of the DBTT of 409 ferritic stainless. Annealing produced only a partial recovery of impact properties for 409 but complete recovery in E-4.

Increases in the DBTT occur in ferritic stainless steels in weld HAZ's, the effects of which are better documented in the literature[2] than the effects of cold-work. The good low-temperature toughness of welds made in E-4 is due to formation of a low-carbon martensite in weld HAZ. The finding that E-4 also possessed an improved impact behavior when cold-worked was somewhat surprising, as toughening due to a martensitic microstructure was not involved.

DISCUSSION

C. R. Thomas[1] (*written discussion*)—The corrosion resistance of E-4, particularly the heat-affected zone, would be of critical importance in many possible applications of a 12Cr steel. Since the HAZ would be martensitic, with presumably a lower corrosion resistance than the annealed ferritic steel, does the author have any comment to make on the use of E-4 in a fairly aggressive environment? Such an environment is encountered underground in South African mines—pH 4, chloride ion, 1200 ppm, temperature 30°C (86°F).

C. W. Vigor (*author's closure*)—The difference in corrosion resistance between annealed material and the weld HAZ in E-4 appears to be much less than for higher carbon hardenable stainless. In general, the corrosion resistance of 12Cr stainless steels is just sufficient to resist rusting in mild or moderately severe environments. Whether E-4 would be suitable under the conditions cited is questionable. However, one test is worth many opinions.

[2]"Wrought Stainless Steels," *Metals Handbook*, 8th ed., ASM Committee on Wrought Stainless Steels, T. Lyman, Ed., American Society for Metals, Metals Park, Ohio, 1961, p. 427.

[1]Cranfield Institute of Technology, Department of Materials, Cranfield, Bedford, U.K.

J. J. Eckenrod[1] and C. W. Kovach[1]

Development of a Low-Chromium Stainless Steel for Structural Application

ABSTRACT: A new stainless steel is described which provides a good combination of mechanical properties and corrosion resistance for structural applications where welding is required. Development of this steel was based upon utilizing a 12 percent chromium, 0.85 percent nickel chemical composition which produces a tough, fine-grain size, ferrite-carbide microstructure in the mill-annealed condition. When welded with austenitic filler metal, a martensitic heat-affected zone microstructure is produced which also has good toughness resulting from its low-carbon nickel martensite composition. Data are given illustrating the composition balance and mill processing required to achieve these properties for this steel. The alloy has seen application in cargo container and mass transit vehicle structurals where good toughness, strength and corrosion resistance are required in the base metal and welds.

KEY WORDS: stainless steels, mechanical properties, toughness, corrosion resistance, welding, heat-affected zone, microstructure, ferritic stainless steels, fracture toughness

When stainless steel is needed in sheet form for structural applications, austenitic grades have been the usual choice because of their strength and toughness properties, particularly in the cold-worked condition. They are, however, relatively expensive and can be subject to stress corrosion cracking under some conditions. Conventional ferritic grades have not been satisfactory alternatives because of toughness limitations in welds, nor have martensitic grades because of mill production difficulties and toughness limitations with martensite at normal carbon levels. The need for an economic structural stainless steel that could be produced in sheet form suggested the development of ferritic stainless steels which transform to low-

---

[1] Supervisor stainless steels and technical director stainless steels, respectively, Crucible Research Center, Pittsburgh, Pa. 15230.

273

carbon martensite in welds. The strength of low-carbon martensite can compare favorably with the strength of stable austenitic structures. The development of this type of improved structural stainless was, therefore, based upon optimizing base metal toughness through composition and mill processing control, and on adjusting composition such that the weld and heat-affected zone (HAZ) would have strength and toughness properties compatible with the base metal. This paper describes a steel which has been developed with useful properties for sheet structural applications. The steel has been named Crucible E-4 stainless and contains nominally 12 percent chromium and 0.85 percent nickel with low carbon for optimum toughness. The steel can also have a somewhat higher carbon content if a carefully controlled amount of titanium is added.

Materials and Evaluation

To minimize the cost of the steel but provide the necessary corrosion resistance, a 12 percent chromium alloy was selected to determine the chemical composition and processing required to provide a stainless steel suitable for structural applications. Laboratory ingots of 22.5 kg (50 lb) were heated at 1176°C (2150°F) for 2 h, forged to 63.5-mm-thick (2½ in.) sections, reheated to 1176°C (2150°F), hot-rolled to 6.35-mm-thick (¼ in.) sheet, and heat-treated by simulated mill anneals. Commercial materials were from mill-processed coils produced from either electric arc or argon-oxygen decarburization (AOD) refined 90-t (100 ton) heats. Tables 1 and 2 give the chemical composition of the laboratory and commercial heats studied.

Tensile properties were determined in the longitudinal direction using standard test specimens and procedures. Notch toughness was evaluated by impact testing one-half-size 5.0-mm (0.197 in.) Charpy V-notch specimens removed transverse to the rolling direction. The ductile-to-brittle transition temperature (DBTT) was determined either by fracture appearance (50 percent shear) or the 10.2-J (7.5 ft·lb) minimum ASME Boiler Code Charpy V-notch energy requirement for half-size specimens of fully de-oxidized carbon and low-alloy steels having tensile strengths between 448 and 517 MPa (65 and 75 000 psi) [1].[2]

Base Metal Properties

For welding applications, 12 percent chromium stainless steels are normally stabilized with titanium to minimize austenite formation during welding, to provide good weld ductility, and to provide good intergranular corrosion resistance in weld HAZ's [2,3]. However, these steels in the mill-

---

[2] The italic numbers in brackets refer to the list of references appended to this paper.

TABLE 1—Chemical composition of laboratory steels.

Heat No.	Weight %										
	C	Mn	Si	Ni	Cr	Ti	Mo	Cu	Al	N_2	Ti/C Ratio
2232	0.070	0.56	0.20	0.39	11.70	0.20	N/A	0.19	0.014	0.027	2.9
1C25	0.046	0.54	0.34	0.26	11.69	0.24	0.21	0.13	N/A	0.018	5.2
2225	0.068	0.57	0.24	0.76	11.78	0.17	0.23	0.17	N/A	0.020	2.5
2227	0.063	0.56	0.30	0.85	11.73	0.44	0.23	0.23	0.028	0.018	7.0
1B94A	0.066	0.54	0.51	0.73	11.31	0.54	0.18	0.11	0.035	0.009	8.2
1C12	0.063	0.37	0.33	0.24	12.68	N/D	0.12	0.17	N/A	0.014	0.0
2223	0.056	0.54	0.23	0.78	11.78	N/D	0.22	0.18	N/A	0.024	0.0

N/A = not analyzed.
N/D = not detected.

TABLE 2—*Chemical composition of commercial heats.*

| Heat No. | Weight % | | | | | | | | | | Ti/C Ratio |
	C	Mn	Si	Ni	Cr	Ti	Mo	Cu	Al	N_2	
632733	0.057	0.59	0.42	0.79	11.15	0.06	0.24	0.05	0.010	0.022	1.1
651254	0.018	0.65	0.38	0.94	11.24	0.0	0.23	0.05	0.010	0.021	0.0
632734	0.054	0.63	0.28	0.84	11.88	0.09	0.15	0.05	0.010	0.034	1.7
120902	0.056	0.68	0.50	0.89	11.37	0.15	0.16	0.05	0.011	0.023	2.7
121164	0.070	0.55	0.32	0.82	11.38	0.17	0.19	0.08	0.014	0.018	2.4
632736	0.033	0.68	0.35	1.02	11.64	0.24	0.17	0.04	0.006	0.026	7.3
632804	0.054	0.60	0.25	0.82	11.37	0.17	0.33	0.05	0.010	0.035	3.1
139011	0.060	0.60	0.38	0.75	11.64	0.22	0.20	0.12	0.03	0.014	3.7
128392	0.049	0.50	0.57	0.67	11.25	0.59	0.11	0.15	0.085	N/A	12.0
653583	0.024	0.56	0.55	0.82	11.26	0.0	0.28	0.07	N/A	0.022	0.0

N/A = not analyzed.

annealed condition do not normally provide the properties desired for structural applications, particularly in heavy sections. For example, a 12 percent chromium steel having a titanium-to-carbon ratio of 12 exhibited in the mill-annealed condition a yield strength of 303 MPa (44 000 psi) and a DBTT of 15°C (60°F) for 5-mm-thick (0.197 in.) half-size Charpy V-notch specimens. More importantly, the DBTT of the weld HAZ was about 65°C (150°F). The as-hot-rolled, mill-annealed, and weld HAZ microstructure of this steel was fully ferritic. Evaluating the mechanical properties and microstructures of a number of titanium-stabilized 12 percent chromium stainless steels suggested that steels having lower than normal titanium-to-carbon ratios and increasing amounts of martensite in the as-hot-rolled microstructure result in higher than usual yield strength and improved toughness in the mill-annealed condition.

A series of 12 percent chromium laboratory heats was used to further explore the effects of titanium-to-carbon ratio on hot-rolled microstructures and resulting annealed properties. Hot-rolled specimens of these alloys were subjected to various anneals. The mechanical properties and DBTT of the steels studied are listed in Table 3.

Figure 1 shows typical microstructures of residual nickel steels having titanium-to-carbon ratios of 2.9 and 5.2. The as-hot-rolled microstructure of the 2.9 titanium-to-carbon ratio steel was predominantly martensite, and subsequent annealing produced a uniform fine-grained ferrite-carbide microstructure. Annealed yield strength was 370 MPa (53 600 psi) and the DBTT was below −62°C (−80°F). The higher titanium-to-carbon ratio material contained about equal amounts of ferrite and martensite in the hot-rolled microstructure. Subsequent annealing produced a coarser-grained less-uniform ferrite-carbide microstructure than the lower titanium-to-carbon ratio steel. Annealed yield strength was lower, 285 MPa (41 300 psi); the DBTT was about −23°C (−10°F). Thus, the steel having the predominantly martensitic hot-rolled microstructure provided higher annealed yield strength and a lower DBTT.

Since a predominantly martensitic hot-rolled microstructure appeared necessary for producing the desired properties, and nickel promotes the development of martensite in 12 percent chromium steels, a series of steels having about 0.5 percent nickel added over normal residual levels was evaluated. Figure 2 shows the effects of the nickel addition on the microstructure of hot-rolled and annealed material having varying titanium-to-carbon ratios. As hot-rolled, the steel having a 2.5 titanium-to-carbon ratio was fully martensitic. Annealing this material produced a fine-grained uniform ferrite-carbide microstructure. The yield strength was 338 MPa (49 000 psi) and the DBTT −62°C (−80°F). Increasing the titanium-to-carbon ratio to 7 resulted in some ferrite developing in the microstructure. Annealing produced a slightly coarser-grained ferrite-and-carbide microstructure and the material had a yield strength of 310 MPa (45 000 psi)

TABLE 3—Mechanical properties of annealed, 760 to 870°C (1400 to 1600°F) 12 percent chromium stainless steels with varying nickel contents and titanium-to-carbon ratios.

| Heat No.	Ti/C	%Ni	Hardness, R_B	Yield Strength, MPa	(ksi)	Tensile Strength, MPa	(ksi)	Elongation in 50.8 mm (2 in.), %	DBTT, °C	(°F)
				residual Ni						
2232	2.9	0.39	86	370	(53.6)	525	(76.2)	26.0	<−62	(<−80)
1C25	5.2	0.26	76	284	(41.3)	456	(66.1)	31.0	−23	(−10)
				Ni modified						
2225	2.5	0.76	81	343	(49.8)	530	(73.8)	33.5	<−62	(<−80)
2227	7.0	0.85	80	311	(45.1)	497	(72.1)	29.5	−57	(−70)
1B94A	8.2	0.73	80	302	(43.8)	481	(69.8)	31.0	−51	(−60)
				no Ti—0.06% C						
1C12	0	0.24	79	316	(45.8)	502	(72.8)	22.0	−57	(−70)
2223	0	0.78	86	370	(53.7)	552	(80.0)	27.5	−62	(−80)
				no Ti—0.02% C						
651254	0	0.94	81	279	(40.4)	481	(69.7)	29.0	...	...
635693	0	0.72	...	259	(37.5)	474	(68.7)	31.0	...	...
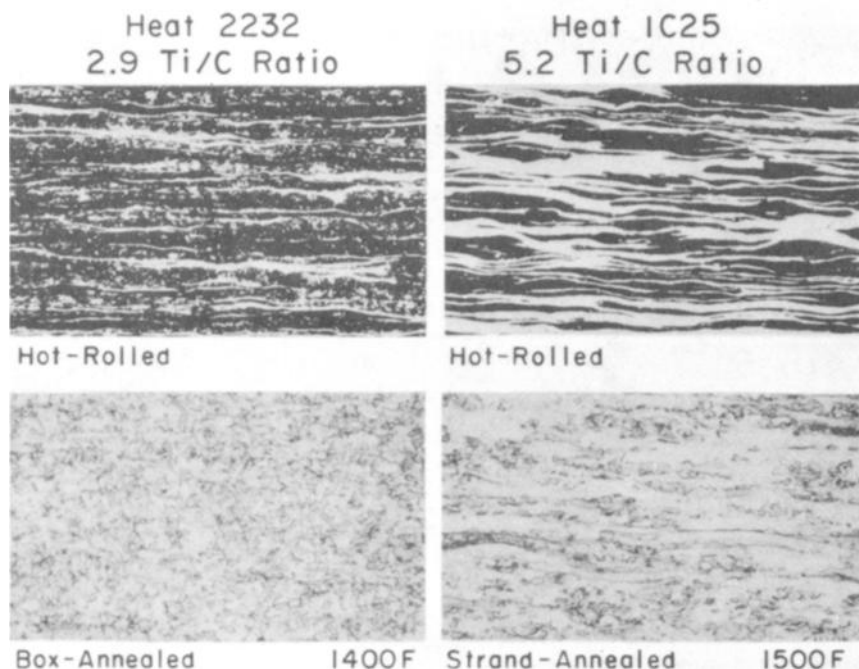
FIG. 1—*Microstructures of 12Cr stainless steels with variable titanium-to-carbon ratios* (×*170*). *Etchants: Steads reagent for as hot-rolled. Vilellas reagent for annealed.*

and a DBTT of −57°C (−70°F). Further increases in the ratio produced additional ferrite in the hot-rolled microstructure. Annealing this material resulted in a still coarser grained microstructure, lower yield strength, 302 MPa (43 800 psi), and slightly higher DBTT, −51°C (−60°F).

These results, in addition to confirming the need for a martensitic hot-rolled microstructure, show that the nickel addition to the steel provides improved toughness. The microstructure of hot-rolled residual nickel steel with a titanium-to-carbon ratio of 5 was similar to that of the nickel-bearing steel having a ratio of about 8, but the DBTT of the nickel-bearing steel was about 28 deg C (50 deg F) lower. The nickel addition also seems to provide some grain refinement to the annealed material.

To further explore the effect of nickel on the microstructures developed in and the properties of 12 percent chromium steels, two low-carbon titanium-free steels with residual and 0.75 percent nickel were evaluated. The resulting microstructures are shown in Fig. 3. The nickel addition provided a fully martensitic hot-rolled microstructure and a uniform fine-grained annealed microstructure. The resulting annealed yield strength was 370 MPa (53 700 psi) and the DBTT was below −62°C (−80°F). The residual nickel steel had a mixed hot-rolled microstructure, a less-uniform
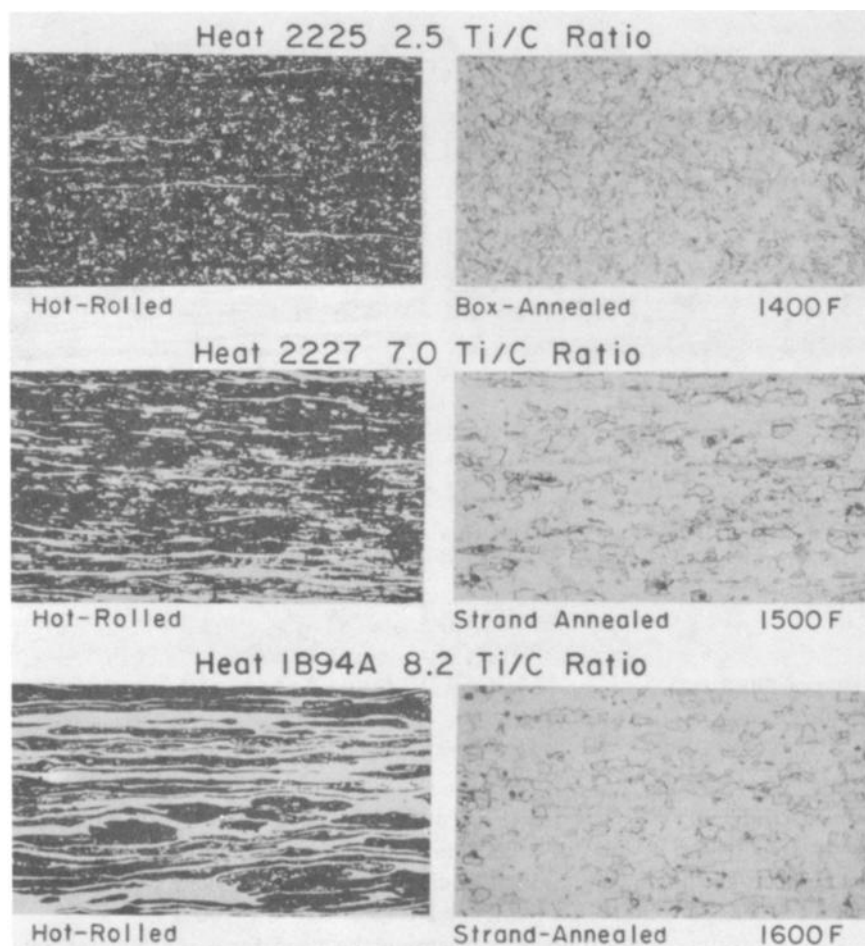
FIG. 2—*Microstructures of 12Cr-0.80Ni stainless steels with varying titanium-to-carbon ratios (×170). Etchants: Steads reagent for as hot-rolled. Vilellas reagent for annealed.*

annealed microstructure, a lower yield strength, 316 MPa (45 800 psi), and a slightly higher DBTT, −57°C (−70°F).

The nickel addition to these steels provides several important benefits. First, in the as-hot-rolled microstructure it promotes the development of martensite, which is necessary to provide the desired strength and toughness. Second, finer-grained annealed microstructures result which also promote higher strength and better toughness. Third, there appears to be some inherent improvement in the toughness from the nickel addition itself.

The nickel content and the titanium-to-carbon ratio are particularly critical toward developing the desired properties. Nickel and the titanium-
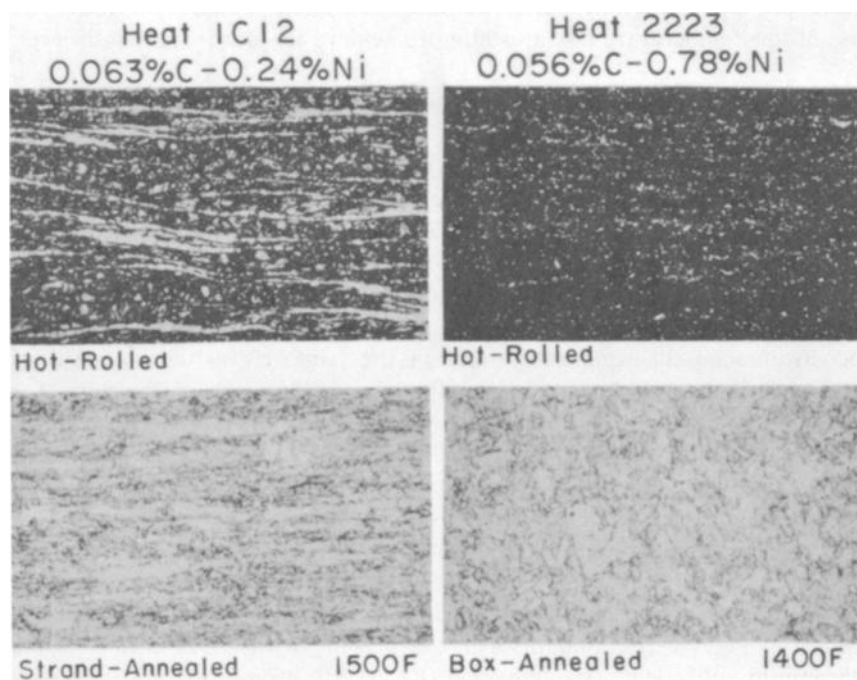
FIG. 3—*Microstructures of residual-nickel and nickel-modified 12 percent chromium stainless steels (×170). Etchants: Steads reagent for as-hot-rolled, Vilellas for annealed.*

to-carbon ratio control the amount of martensite in the steel and its annealing response. In general, the lower the nickel content and the higher the titanium content, the higher will be the ferrite content. In addition, the presence of nickel in more than a residual amount retards softening of the martensite in the steel during annealing. With nickel-bearing steels, the annealing temperature required to achieve desired strength levels depends primarily upon the specific ferrite-martensite balance, which is in turn determined by the titanium-to-carbon ratio. More specifically, for nickel-bearing steels with a titanium-to-carbon ratio below 4, having essentially martensitic microstructures, box-annealing at 760 to 815°C (1400 to 1500°F), near the lower critical temperature of the steel, is required to temper the martensite sufficiently to achieve the desired strength and ductility. Nickel-bearing steels with titanium-to-carbon ratios of about 4 to 7 contain more ferrite and must be box-annealed at lower temperature, 650 to 760°C (1200 to 1400°F), to achieve the desired strength. Nickel-bearing steels having still higher titanium-to-carbon ratios contain substantial ferrite, and short-time continuous annealing within the temperature range of 816 to 871°C (1500 to 1600°F) is required. For these high-titanium

steels the rapid softening due to the increased ferrite content precludes the use of low-temperature box-annealing to achieve the desired strength level.

Weld Heat-Affected Zone Toughness

Both laboratory and commercially produced nickel-bearing steels with varying titanium-to-carbon ratios were used to evaluate the microstructure, hardness, and toughness of weld HAZ's. The steels were joined by single-pass gas metal-arc or shielded metal-arc welding using Type 309 stainless steel filler metal. The joint design and the location in the Charpy V-notch specimen are shown in Fig. 4. The welds were made to produce minimum penetration on the square-edge side of the joint. Using these conditions and techniques, the fusion line on the square-edge side of the joint was reasonably straight so that by lightly etching the Charpy V-notch specimen blanks the notch could be consistently located in the HAZ. The tested specimens were examined and any fractures that occurred in the weld metal were disregarded.

The weld HAZ properties at −29°C (−20°F) are listed in Table 4 in descending energy absorption values. The weld HAZ impact properties and hardness of those steels can be interpreted in terms of the microstructures shown in Fig. 5. The amount of ferrite present in the HAZ relates to the chromium equivalent[3]; steels having the lowest chromium equivalent contain no ferrite whereas, for those with higher chromium equivalent, ferrite begins to appear in the microstructure. For those steels having the highest
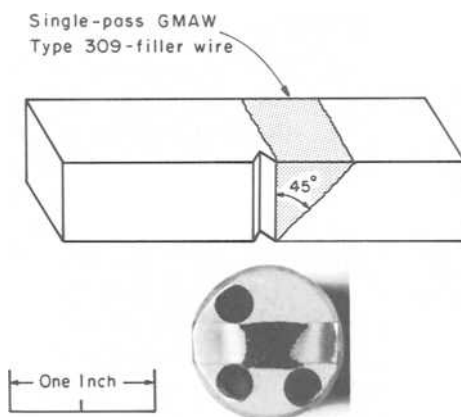
FIG. 4—*Joint design and location in the Charpy V-notch specimens for studies on the weld heat-affected zone properties (1 in. = 25.4 mm).*

[3]Chromium equivalent [4] = %Cr + %Si + 2(%Mo) + 10(%Al) + 16(%Ti) − %Cu − %Ni − 30(%C + %N).

TABLE 4—Results of Charpy V-notch, 5.0-mm (0.197 in.) specimen impact tests at −29°C (−20°F) on nickel-bearing 12 percent chromium stainless steel weld heat-affected zones.

Heat No.	%C	%Ti	Ti/C Ratio	Cr Equivalent	Hardness		Impact, J	Energy, (ft · lb)
					Base Metal, R_B	Heat-Affected Zone, R_C		
2515	0.078	0.0	0.0	8.7	91	38.5	27.8	(20.5)
2508	0.072	0.13	1.8	9.4	83	39.5	23.0	(17.0)
2223	0.056	0.0	0.0	9.2	86	40.0	17.0	(12.5)
632733[a]	0.057	0.06	1.1	9.6	85	38.5	13.6	(10.0)
651254[a]	0.018	0.0	0.0	10.3	81	35.5	10.8	(8.0)
632734[a]	0.054	0.09	1.7	10.4	76	36.0	10.2	(7.5)
120902[a]	0.056	0.15	2.7	11.4	82	38.0	9.5	(7.0)
2507	0.068	0.29	4.3	13.1	85	35.0	8.8	(6.5)
121164[a]	0.070	0.17	2.4	11.4	87	38.5	8.1	(6.0)
632736[a]	0.033	0.24	7.3	12.9	77	33.0	7.5	(5.5)
632804[a]	0.054	0.17	3.1	11.2	79	35.0	6.8	(5.0)
2227	0.063	0.44	7.0	16.3	82	20.0	6.8	(5.0)
2228	0.065	0.53	8.1	17.8	96	96 R_B	6.8	(5.0)
139011[a]	0.060	0.22	3.7	13.2	84	32.0	5.4	(4.0)

[a] 90-t (100 ton) commercial heats.

Heat 2515   Cr Eq. 8.7%
20.5 ft-lb at −20°F

Heat 632733   Cr Eq. 9.6%
10 ft-lb at −20°F

Heat 2507   Cr Eq. 13.1%
6.5 ft-lb at −20°F

Heat 2227   Cr Eq. 16.3%
5 ft-lb at −20°F
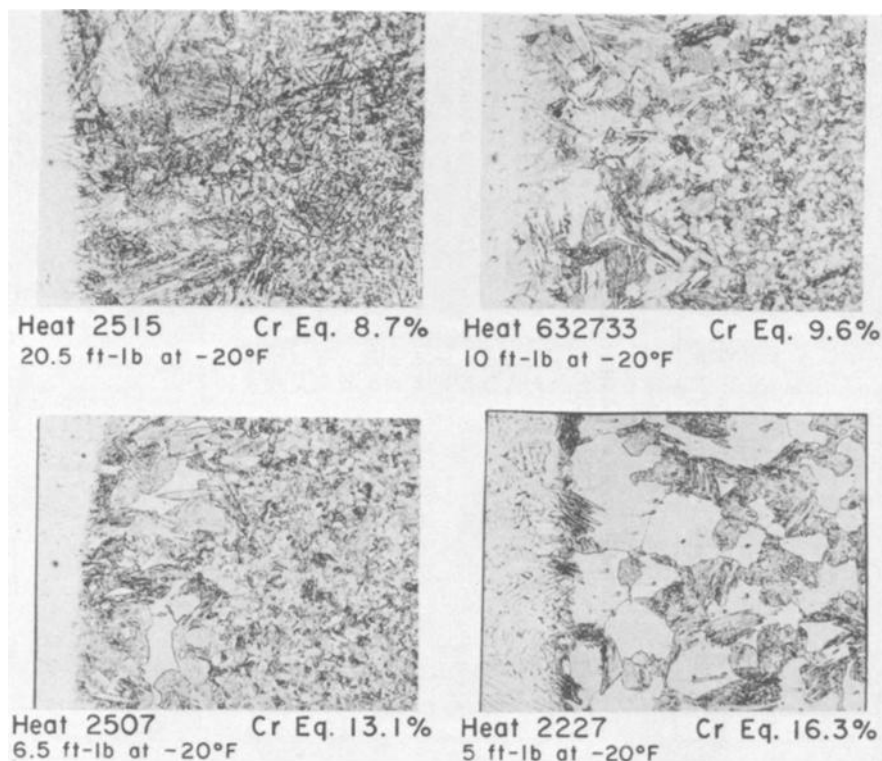
FIG. 5—*Microstructures of 12 percent chromium nickel-bearing stainless steel heat-affected zones (×145). Etchants: Kallings + 2 percent Picral.*

HAZ impact properties, the microstructure is predominantly martensitic with only a trace of ferrite. For those steels having impact values in the middle range, more of a coarse-grained blocky-type ferrite begins to develop in the microstructure which again relates to the chromium equivalent. Those steels having the lowest impact values develop considerable ferrite in the HAZ and have the higher chromium equivalent.

A graphical relationship between alloy balance, which is controlled by the chemical composition (chromium equivalent), and the HAZ impact properties is illustrated in Fig. 6. There is a decrease in the impact values with increased chromium equivalent, which in turn controls the microstructural balance. Thus, to provide a satisfactory impact value at −29°C (−20°F), the steel should have the lowest possible chromium equivalent that will provide the required strength, ductility, and corrosion resistance. Base metal and weld HAZ Charpy V-notch impact properties typical for low-carbon no-titanium Crucible E-4 stainless steel are shown in Fig. 7.
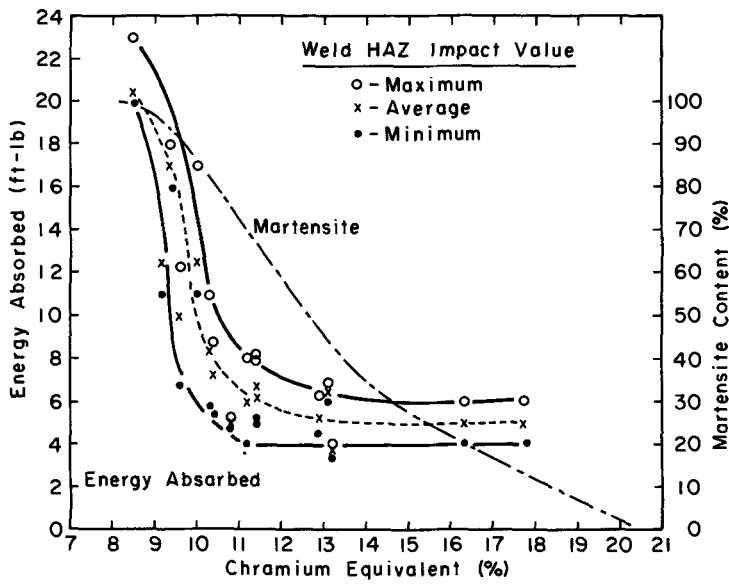
FIG. 6—*Effect of chromium equivalent on martensite-ferrite balance and the Charpy V-notch impact properties of nickel-bearing 12 percent chromium stainless steel heat-affected zones at* $-29\,°C\ (-20\,°F)$.
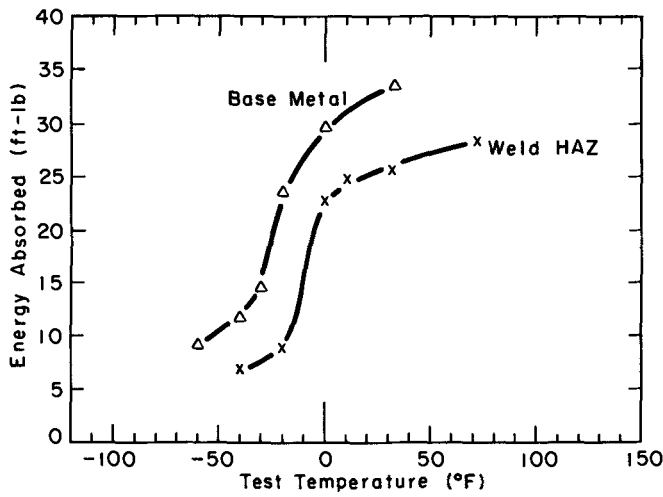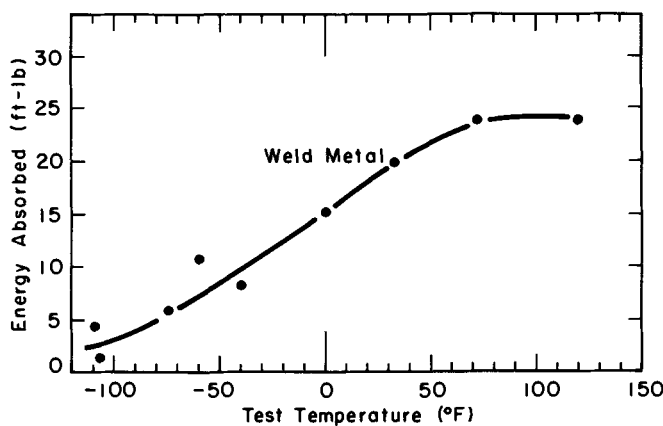

FIG. 7—*Charpy V-notch impact test results on low-carbon titanium-free nickel-bearing 12 percent chromium stainless steel. One-half-size, 5-mm (0.197 in.) specimen.*

Using the 10.1-J (7.5 ft·lb) evaluation criteria, the DBTT is below −51°C (−60°F) for the base metal and about −40°C (−40°F) for the weld HAZ.

Weld Metal Properties

Filler metals are often not required for welding thinner materials and gas tungsten arc (GTA), high-frequency resistance or friction welding techniques can be used. To evaluate the weld metal properties, 3.2-mm (0.125 in.) specimens of low-carbon no-titanium Crucible E-4 were GTA welded. The weld toughness was evaluated by testing quarter-size Charpy V-notch impact specimens prepared so that the apex of the notch was located in the center of the weld. The results of the impact tests are shown in Fig. 8. No abrupt change was observed in the energy values, with decreasing temperature making it difficult to determine the DBTT; however, the fracture appearance (50 percent shear) and lateral expansion values, 0.51 mm (0.020 in.), indicate that the DBTT is at least −40°C (−40°F). The GTA welds displayed excellent bend ductility, and the flareability and flangeability of some GTA welded tubing produced from steels having a similar chemical composition were also excellent as shown in Fig. 9.

High-frequency welded tubing has been produced and the weld area and HAZ microstructure are predominantly martensitic. This tubing also displays excellent ductility and flareability as shown in Fig. 9.

Mechanical Properties

As has been demonstrated, tough 12 percent chromium steels can be produced by chemical composition and process control so as to develop a

FIG. 8—*Charpy V-notch impact test results on a gas tungsten-arc weldment in low-carbon titanium-free nickel-bearing 12 percent chromium stainless steel. One-quarter-size, 2.5-mm (0.098 in.) specimens.*
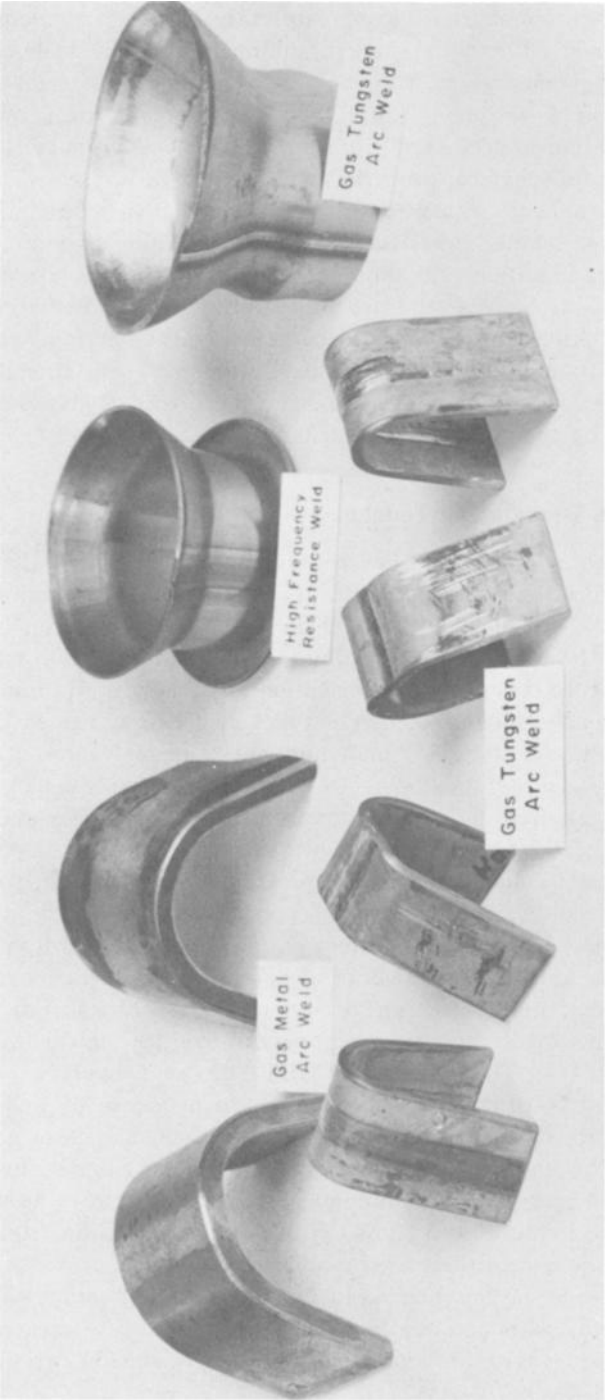
FIG. 9—Bend, flare, and flange test results on welded nickel-bearing 12 percent chromium stainless steels.

tempered low-carbon martensite microstructure. The desired microstructure can be obtained either by a small titanium addition to steels containing 0.03 to 0.07 percent carbon, thus effectively reducing the carbon content to a low level, or by producing low-carbon (0.02 percent) steel, making the titanium addition unnecessary. Both approaches will produce the desired toughness, but mechanical properties will be slightly different. The higher-carbon titanium-bearing steels have higher annealed yield strength because of the improved tempering resistance, that is, annealing response, provided by the titanium addition. Titanium carbides, especially the extremely small ones observed in these steels, are probably more effective strengtheners than are the chromium carbides in the non-titanium-bearing steels. Thus, the higher-carbon titanium-bearing steels will have yield strengths about 310 MPa (45 000 psi) or higher, whereas those with low carbon and no titanium will be about 276 MPa (40 000 psi).

Discussion on Strength and Toughness

The toughening effect of nickel in iron, carbon steels, and alloy steels is widely recognized and the mechanisms may be similar in stainless steels [5]. The nickel-toughening mechanisms in carbon and alloy steels are considered to be related to solid solution strengthening, grain refinement, and the influence of nickel on deformation and fracture [6]. Solid solution strengthening effects for the 0.8 percent nickel in these 12 percent chromium stainless steels are probably small and not a major factor. The grain-refining effect of nickel in alloy steels is attributed to the lower austenitizing temperature required for nickel-containing steels. There is a downward shift in the DBTT associated with nickel-induced grain refinement, but grain refinement could not account for all the shift; that is, for a given grain size, nickel-bearing steels had lower DBTT [7-10]. The nickel-containing stainless steels are also finer-grained than those without nickel. Here again the contributing effect of nickel may relate to the change in the austenite field and resulting transformation product. Nickel is unique in its beneficial effect on the fracture toughness of iron [6] and high-chromium stainless steels [11]. The reduction of DBTT in steel is explained by nickel-facilitating cross-slip [12,13] decreasing the dependence of yield strength on temperature [14] and strain rate [13] and raising the cleavage strength [15]. Thus, the observed beneficial effects of nickel on the strength and toughness of 12 percent chromium stainless steels appear to be parallel to those observed in nickel-iron alloys and nickel-bearing carbon steels.

A martensitic microstructure is necessary in autogeneous welds and weld HAZ's to provide the toughness and ductility required without a postweld heat treatment. Although martensitic welds and HAZ's are contrary to those thought necessary for good bend ductility [3], the low-carbon marten-

site that does develop in these low-titanium or titanium-free nickel-bearing steels is sufficiently ductile without heat treatment to allow simple bending as illustrated earlier. The chemical composition of the steel, particularly the titanium and carbon contents, is especially critical to insure low-carbon martensite. This can be achieved by producing low-carbon steel balanced with other elements to provide a fully martensitic weld and HAZ. Higher-carbon steels will develop fully martensitic microstructures, but the resulting bend ductility may be marginal. Therefore, higher-carbon steels need a small amount of titanium to combine with carbon to provide a low-carbon martensite.

Commercial Implications

The results of these studies led to the development of Crucible E-4 stainless steel. Crucible E-4 stainless steel contains about 11.5 percent chromium, about 0.85 percent nickel, and may contain about 0.20 percent titanium depending upon properties required for specific applications. Two compositions have been produced, one containing about 0.06 percent carbon and about 0.20 percent titanium, the other about 0.02 percent carbon and no titanium. Yield strength of the higher-carbon titanium-containing steel will be about 310 MPa (45 000 psi) or higher whereas yield strength of the lower-carbon alloy will be about 276 MPa (40 000 psi). Based on a 10.2-J (7.5 ft·lb) minimum energy requirement for one-half-size Charpy V-notch specimens, the DBTT for the base metal will be at least $-40°C$ ($-40°F$) for either composition.

Crucible E-4 stainless steel has been used in cargo boxes and mass transit vehicles where good toughness, strength, and corrosion resistance is required in the base metal, weldments, and weld HAZ's.

Conclusions

A 12 percent chromium stainless steel having a unique combination of properties has been developed. With appropriate chemical composition, the one-half-size specimen Charpy V-notch DBTT of the steel will be at least $-40°C$ ($-40°F$), with yield strength ranging from about 276 to 310 MPa (40 000 to 45 000 psi). Weld and weld HAZ notch toughness and ductility are adequate without the necessity of postweld heat treatments. The unique combination of properties is attained by a nickel-bearing steel having a fine-grained microstructure as annealed and a predominantly low-carbon martensitic weld or HAZ microstructure. The improved properties of the steel are attributed to the effect of nickel additions on strength and toughness of the ferrite and in developing tough, ductile low-carbon martensitic weldments and heat-affected zones.

References

[1] ASME Boiler and Pressure Vessel Code, Section VIII, Rules for Construction of Pressure Vessels, Division 1, 1974 edition, p. 45.

[2] Pollard, B. and Aronson, A. H., *Metals Engineering Quarterly,* Aug. 1973, p. 28.

[3] Kaltenhauser, R. H., *Metals Engineering Quarterly,* May 1971, p. 41.

[4] Mehta, J. M., Colt Industries, Crucible Research Center, Pittsburgh, Pa., Report 4-458-31, 18 April 1974.

[5] Lefevre, J., Tricot, R., and Castro, R., *Revue de Metallurgie,* April 1973, p. 259.

[6] Johnson, R. J., *Metals Engineering Quarterly,* Aug. 1975, p. 1.

[7] Kranzlein, H. H., Burton, M. S., and Smith, G. V., *Transactions,* American Institute of Mining, Metallurgical, and Petroleum Engineers, Vol. 233, 1965, p. 64.

[8] Stoloff, N. S., *Fundamental Phenomena in the Materials Science,* Vol. 4, 1967, p. 197.

[9] Gensamer, M., *Transactions,* American Institute of Mining, Metallurgical, and Petroleum Engineers, Vol. 215, 1959, p. 2.

[10] Hodge, J. M., Manning, R. D., and Reichold, H. M., *Transactions,* American Institute of Mining, Metallurgical, and Petroleum Engineers, Vol. 185, 1949, p. 233.

[11] Bond, A. P., Dundas, H. J., Ekerat, S., and Semchyshen, M. in *Proceedings,* Stainless Steel '77, London, England, R. Q. Barr, Ed., Climax Molybdenum Co., p. 197.

[12] Jolly, W., *Journal of the Iron Steel Institute,* Vol. 206, 1968, p. 170.

[13] Jolly, W., *Transaction,* American Institute of Mining, Metallurgical, and Petroleum Engineers, Vol. 242, 1968, p. 306.

[14] Wullart, R. A., "The Effect of Nickel on the Microstructure and Mechanical Properties of Ferritic Steels," AD-861-803, National Technical Information Service, Department of Commerce, Springfield, Va., 1969.

[15] Floreen, S., Hayden, H. W., and Devine, T. M., *Metallurgical Transactions,* Vol. 2, 1971, p. 403.

E. L. Creamer [1]

885 °F Embrittlement in 12Cr Steel Distillation Column Tray *

ABSTRACT: A crude distillation column tray, fabricated supposedly from Type 410 stainless steel, failed in an extremely brittle manner after exposure to conditions which could induce 474°C (885°F) embrittlement. An investigation confirmed that the tray had experienced 474°C (885°F) embrittlement. Although the material met, according to analysis, Type 410 stainless steel composition requirements, it also contained a significant concentration of titanium, raising the suspicion that the alloy was Type 409 stainless steel. Results of the investigation tend to reinforce the concept advanced by others that titanium promotes 474°C (885°F) embrittlement in the straight chromium steels. Additional work is required to define the chromium and titanium levels which can lead to embrittlement.

KEY WORDS: ferritic stainless steels, fracture toughness, embrittlement

A tray from a crude distillation column, supposedly fabricated from Type 410 stainless steel, was found to have failed in an extremely brittle manner. Because of continuing interest in all details of the behavior of the 12 percent chromium (12Cr) steels exposed for long periods of time to service temperatures in the general temperature range of 371 to 510°C (700 to 950°F), a metallurgical investigation to determine the cause of the failure and the condition of the metal was conducted. The tray had been exposed to conditions which could be expected to lead to 474°C (885°F) embrittlement in a susceptible alloy. The condition, known as "885°F embrittlement," although not fully understood, is believed to involve the precipitation of a submicroscopic phase. It can affect various grades of straight chromium steels following extended exposure in the 371 to 510°C (700 to 950°F) range. The effect is maximized in Type 446 (27Cr) stain-

---

* Original experimental data were measured in English customary units.

[1] Senior staff research metallurgist, Shell Development Co., Houston, Tex. 77001.

less steel and in the 468 to 482°C (875 to 900°F) exposure range. The embrittlement subsequently can be eliminated by annealing the metal at a temperature well above that at which embrittlement occurred.

The appearance of the fracture surface of the tray sample suggested that the metal possessed very little ductility. The microstructure consisted of ferrite and extremely fine and uniformly distributed carbides (Fig. 1). Room-temperature tension test results showed that tensile and yield strength values were considerably higher than are normally found for this alloy (Table 1). Tensile ductility values were acceptable but elongations approached the lower limits specified in ASTM Specification for Heat-Resisting Chromium and Chromium-Nickel Stainless Steel Plate, Sheet, and Strip for Fusion-Welded Unfired Pressure Vessels (A 240-75a) Type 410 (Table 1).

Results

Because ductility and toughness in 400-series stainless steels which have experienced 474°C (885°F) embrittlement can be restored by suitable heat treatment, a portion of the tray was heat-treated for 3 h at 593°C (1100°F). As anticipated, the microstructure was not altered appreciably by the heat

FIG. 1—*Representative microstructure of Type 410 stainless steel distillation column tray (as-received condition). (×200; etchant: Vilella's)*

TABLE 1—*Room temperature tension test results for Type 410 stainless steel distillaton column tray.*

Condition	Tensile Strength, N/mm^2 (ksi)	Yield Strength, N/mm^2 (ksi)	Elongation, %	Reduction in Area, %
As received	672.3 to 674.3 (97.5 to 97.8)	574.4 to 586.1 (83.3 to 85.0)	22.5 to 25.0	62.2 to 64.6
Heat-treated 3 h at 593°C (1100°F)	445.4 to 455.1 (64.6 to 66.0)	275.1 to 284.1 (39.9 to 41.2)	34.1 to 34.9	72.4 to 73.9
Specification ASTM A 240 Type 410	448.2 (65.0) min	206.8 (30.0) min	20.0 min. ...	... ...

treatment (Fig. 2). However, mechanical properties after heat treatment were in the range more frequently associated with Type 410 stainless steel in the annealed condition (Table 1). Average tensile strength approached the minimum acceptable level of 448.2 N/mm^2 (65.0 ksi) but was still above the minimum of 413.7 N/mm^2 (60.0 ksi) for the titanium-containing, slightly lower chromium ASTM A 176 Type 409 steel. The reduction in strength and increase in ductility resulting from the heat

FIG. 2—*Representative microstructure of Type 410 stainless steel distillation column tray [heat treated 3 h at 593°C (1100°F)]. (×200; etchant. Vilella's).*

treatment strongly indicate that the steel had experienced 474°C (885°F) embrittlement. This was also shown by results of hardness tests performed on a gradient bar prepared from a portion of the tray (Fig. 3). Between exposure temperatures of approximately 510 and 566°C (950 and 1050°F), hardness decreased sharply from the 165 HB range to the 110 HB range. Impact tests were not performed because of the limited thickness of the material.

Chemical analysis of a section of the tray showed the material to conform to composition requirements of ASTM A 240 Type 410 stainless steel (Table 2). (As the aluminum concentration was only 0.07 percent, the alloy was not a Type 405 stainless steel.) However, the titanium concentration (level not specified in ASTM A 240 Type 410) was found to be relatively high—0.5 percent—indicating that the alloy, except for chromium concentration, also conformed to the ASTM A 176 Type 409 specification. (Permissible concentrations for chromium, carbon, and other elements for Types 405, 409, 410, and CA15 stainless steel are listed in Table 3.)
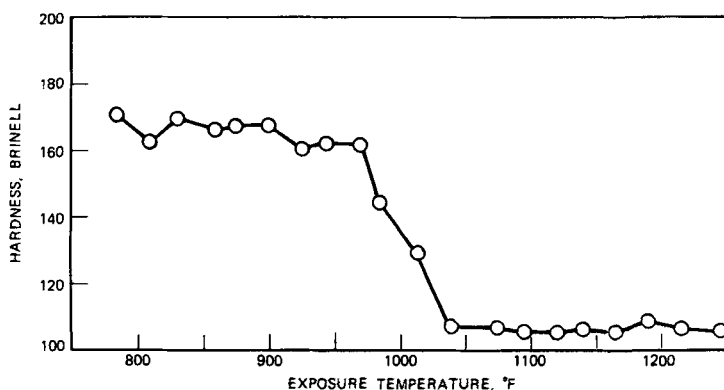
FIG. 3—*Effect of exposure temperature (3-h exposure) on hardness of Type 410 stainless steel distillation column tray.*

TABLE 2—*Chemical analysis results for Type 410 stainless steel distillation column tray.*

	Cr, % (weight)	Ni, % (weight)	Mn, % (weight)	Al, % (weight)	Ti, % (weight)	C, % (weight)
Tray sample	13.4	0.23	0.40	0.07	0.50	0.09
Specification ASTM A 240 Type 410	11.5 −13.5	0.75 max	1.00 max	...	...	0.15 max

TABLE 3—Partial composition requirements for wrought 12Cr-type stainless steels.

Designation	Form	ASTM Specification	Cr, % (weight)	C, % (weight)	Ni, % (weight)	Ti, % (weight)	Al, % (weight)
Type 405	wrought	A 240 Type 405	11.50–14.50	0.08 max	0.60 max	…	0.10–0.30
		A 176 Type 405	11.50–14.50	0.08 max	0.60 max	…	0.10–0.30
		A 268 TP 405	11.50–13.50	0.08 max	0.50 max	…	0.10–0.30
Type 409	wrought	A 176 Type 409	10.50–11.75	0.08 max	0.50 max	6 × C, min	…
Type 410	wrought	A 240 Type 410	11.50–13.50	0.15 max	0.75 max	0.75 max	…
		A 176 Type 410	11.50–13.50	0.15 max	0.75 max	…	…
		A 268 TP 410	11.50–13.50	0.15 max	0.50 max	…	…
CA15	casting	A 296 Grade CA15	11.50–14.00	0.15 max	1.00 max	…	…
E410	weld electrode	E 410[a]	11.00–13.50	0.12 max	0.60 max	…	…

[a] American Welding Society.

Conclusion

Because of numerous successful applications of Types 405, 410, and CA15 stainless steel under conditions which are known to be favorable to development of 474°C (885°F) embrittlement, results of this study suggest that the titanium concentration, perhaps coupled with the relatively high chromium level, was influential in producing 474°C (885°F) embrittlement. The role of titanium in accelerating 474°C (885°F) embrittlement in 17Cr-type steels has also been alluded to by Grobner.[2] In other work,[3] the role of titanium in embrittling steels containing 15 to 28 percent chromium was investigated. Titanium levels were relatively high (0.9 to 3.18 percent), and 474°C (885°F) embrittlement occurred only at chromium levels above 15.5 percent. If results of additional investigative work should reveal that titanium does, in fact, play a decisive role in causing 474°C (885°F) embrittlement in steels of the 12Cr type, it is foreseen that it may be appropriate to restrict use of Type 409 stainless steel to service conditions which do not involve 371 to 510°C (700 to 950°F) exposure. It may likewise be necessary to add a maximum permissible titanium concentration to the existing specifications for Types 405, 410, and CA15 steel and it is even conceivable that revisions of limits on chromium concentration may be indicated.

Meanwhile, this brittle failure experience involving the 12Cr-type steel crude column tray can serve to alert producers and users of this class of alloys to the possibility that titanium-containing 12Cr-type steels may be considerably more susceptible to 474°C (885°F) embrittlement than otherwise might have been anticipated.

[2] Grobner, P. J., *Metallurgical Transactions,* Vol. 4, Jan. 1973, pp. 251–260.
[3] Szczepanski, M., *The Brittleness of Steel,* Wiley, New York, 1963, pp. 253–254.

G. J. Rosenberger[1] and R. N. Wright[2]

Toughness and Fabrication Response of Fecralloy Strip

ABSTRACT: Alloys of iron-chromium-aluminum-yttrium possess extraordinary oxidation and cyclic oxidation resistance and are attractive for automobile emission control hardware applications. They are, though, less tough than most ferritic stainless steels and care must be exercised in their general handling. Extensive practical use of light-gage strip is possible, however. This paper presents fundamental fracture mechanism observations on an Fe-15.9Cr-4.9Al-0.3Y alloy strip together with a detailed discussion of the fabrication of such Fecralloy strip en route to the manufacture of automobile emission control hardware. The implications for steel strip production practice are discussed and an assessment of light-gage strip fabrication latitude is presented.

KEY WORDS: toughness, fracture mechanisms, strip fabrication capability, catalytic converter applications, ferritic stainless steels, fracture toughness

The reduction of motor vehicle emissions by automotive catalytic converters is of considerable environmental and economic benefit. Since the somewhat controversial introduction of control devices in 1974, the levels of carbon monoxide (CO), hydrocarbons (HC), and nitrogen oxides (NO_x) in many urban areas have decreased [1].[3] The materials requirements of these devices are imposing. In particular, the support onto which the catalytic mixture of alumina and noble metals is applied must possess some unique properties. These include the ability to remain mechanically intact under conditions of (1) extreme temperatures occasionally in excess of 1200°C, (2) rapid thermal and vibrational cycling, and (3) varying atmospheres. In addition, the support surface must be capable of securely bonding the high-surface-area alumina. Finally, all these properties must

---

[1] Development chemist, Matthey-Bishop Inc., Malvern, Pa. 19355.
[2] Materials Science Department, Rensselaer Polytechnic Institute, Troy, N. Y. 12185.
[3] The italic numbers in brackets refer to the list of references appended to this paper.

be maintained for a Federally mandated 80 000-km (50 000 mile) minimum service life.

The only material which had been proven to be a suitable support was ceramic, either a pellet bed or monolithic honeycomb. The possibility of using metallic-supported auto catalysts had been pursued [2-4] but with only marginal success. There are several distinct advantages to using metallic rather than conventional ceramic substrates, and these are outlined in Table 1. Most importantly, metallic units offer equivalent or superior catalytic performance at reduced volume and weight. Initial efforts into metal catalysts were limited by the lack of an alloy with the desired properties. Other than meeting the aforementioned criteria demanded of a catalytic support, obvious considerations of cost and large-scale availability (possible 1000 metric tons yearly) enter into choice of the alloy. With this in mind, several steels were evaluated according to their resistance to the high-temperature/corrosive atmosphere of engine exhaust [5]. As the data in Table 2 indicate, Fecralloy (15Cr-5Al-0.5Y) had exemplary oxidation characteristics when compared with the other steels. Similar compositions (25Cr-4Al-1Y), in sheet form, have been reported to withstand several thousand hours at 1200°C in air with no significant deterioration [6].

Ferritic stainless steels display impressive levels of oxidation resistance, particularly when alloyed with aluminum. Moreover, the oxidation resistance of iron-chromium-aluminum alloys can be further improved through

TABLE 1—*Advantages of metal- versus ceramic-supported catalyst.*

Lower volume and weight required
Resistance to cracking upon thermal shock
Better heat transfer, which influences catalytic performance
Better mechanical strength for handling in a production environment
More flexibility to change catalyst design

TABLE 2—*Engine exhaust corrosion data [5]*
on 0.050-mm steel sheet.

	Temperature, °C				
Alloy	950	1000	1050	1085	1200
Armco 18 SR	F-390	F-215	F-30	F-0	. . .
AISI 310	F-625	F-420	F-30	F-0	. . .
Kanthal DSD	G-615	G-420	G-30	F-0	. . .
Fecralloy	G-625	G-420	G-30	G-185	G-300

F = failure—number of hours of test; failure criterion as appreciable metal deterioration and loss of catalytic performance.

G = good—number of hours of test; good criterion as the metal intact with good catalytic performance.

the addition of reactive metals such as yttrium, thorium, calcium, and cerium [7]. An extensive amount of work has been performed on "Fecralloy," or alloys based on the iron-chromium-aluminum-yttrium system [6,8,9]. It appears that the addition of yttrium improves oxidation resistance, particularly cyclic oxidation resistance, by increasing the adherence of the Al_2O_3 layer which forms at the alloy surface. This may reflect a mechanical "locking" effect produced by intergranular subscale formation of Y_2O_3 [8].

Nonetheless, Fecralloy has important limitations. Firstly, like all ferritic stainless steels, strength is quite limited above 500 to 600°C [9]. Beyond this, Fecralloy has generally less toughness than most ferritic stainless steels. Aluminum shows a marked tendency to increase the ductile-to-brittle transition temperature (DBTT) in ferrite. The effect has been attributed to cross-slip inhibition, and a tension test DBTT increase of 85 deg C can be associated with an 8 percent addition of aluminum to iron [10]. In fact, because of toughness and ductility considerations, aluminum alloy contents beyond 7 percent have generally not been investigated for Fecralloy. Aside from aluminum, the toughness is thought to be compromised by the presence of yttrium. Until gross oxidation occurs, yttrium is present nominally as YFe_9 (unpublished microprobe analyses have shown that actual compositions of this intermetallic compound fall in the range of Fe-10Cr-6Al-15Y). There is little solubility of yttrium in ferrite and, even at high temperatures, no more than 0.1 percent is likely to be in solution. Upon solidification of dilute iron-yttrium alloys, a eutectic structure of YFe_9 and ferrite forms at around 1350°C [11]. In Fecralloy, the as-cast structure is referred to as having intergranular and interdendritic films of YFe_9. The intermetallic morphology reverts to a distribution of large globular and even angular particles during ingot soaking and the early stages of primary processing. During rolling, some of the YFe_9 particles fracture and stringers of fractured "YFe_9" can be seen in the rolling direction. Not all particles fracture, however, and the dispersion of YFe_9 in strip consists of both stringers and large globular particles. The relative amounts of stringers and globular particles vary and may reflect such factors as hot-working finish temperature. An example of such a Fecralloy microstructure is shown in Fig. 1 for Heat A of the composition given in Table 3. The globular YFe_9 particles are particularly prominent in the transverse section, whereas the longitudinal section clearly reveals the presence of stringers. Note that the stringers involve extensive particle-matrix interface decohesion. The intermetallic constituent morphologies clearly suggest possibilities for crack initiation in brittle fracture and for rapid void development in ductile fracture. Little fundamental work on fracture mechanisms has been undertaken, however. Of course, the YFe_9 component is intrinsic to the alloy design and not simply a constituent that can be removed by careful refining technique.
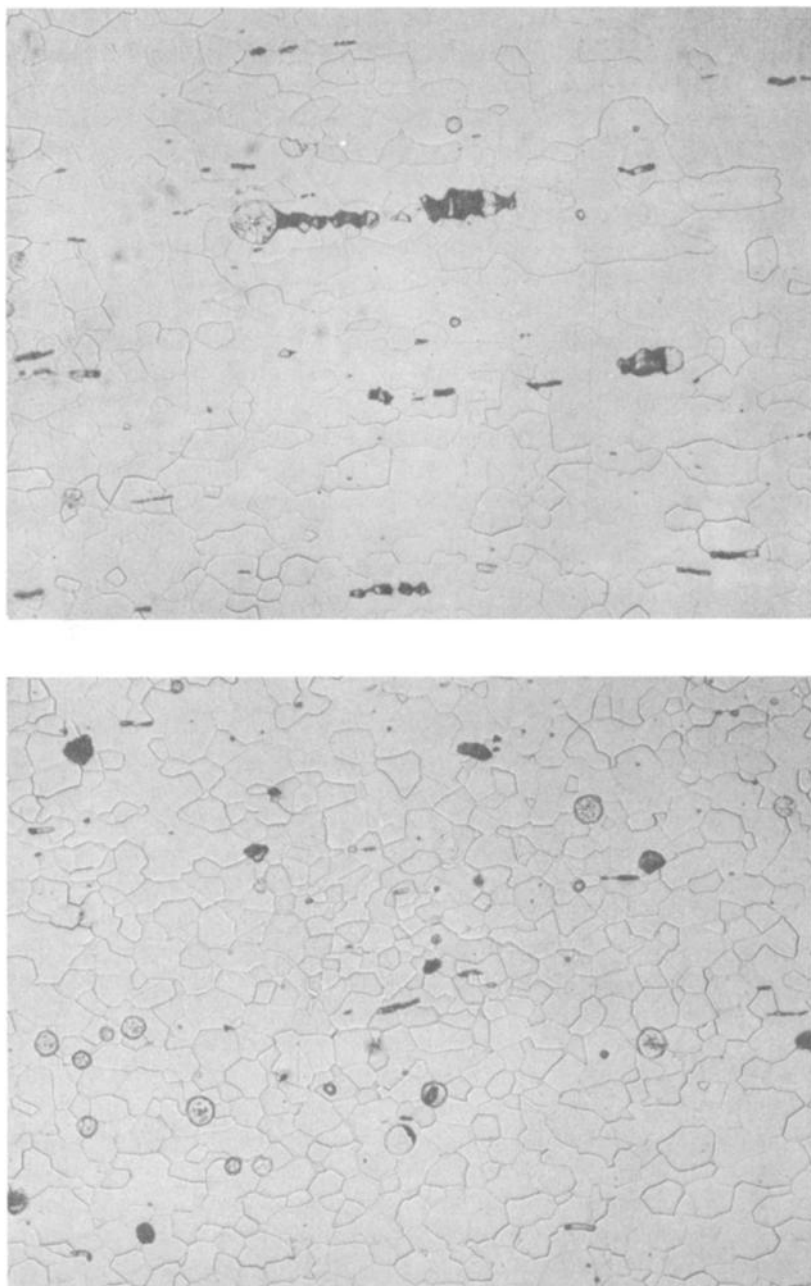
FIG. 1—*Optical micrographs of mill-annealed structure of Heat A:* (top) *longitudinal section and* (bottom) *transverse section* (×250).

TABLE 3—*Chemical compositions of the subject alloys in weight percent.*

Heat	Cr	Al	Y	Si	C	S	P	Ni	Mn
A	15.9	4.82	0.31	0.24	0.02	0.003	<0.01	0.08	<0.10
B	15.9	4.91	0.26	0.24	0.018	0.002	<0.01	0.07	<0.10

Beyond probable embrittlement through high matrix aluminum and YFe_9 content, Fecralloy is more or less susceptible to classic ferritic stainless steel embrittlement problems such as "475°C embrittlement," σ-phase embrittlement, and the problem attendant to carbon and nitrogen (C + N) content [12-14].

Despite limited toughness, Fecralloy can be successfully used in a number of high-technology products. This is due in large part to two factors. First, the vacuum induction melting technique makes it possible to improve toughness by restricting (C + N) levels. Second, it is quite clear that ductile-to-brittle transition temperature (DBTT) is a very sensitive function of strip thickness [15,16] and that light-gage Fecralloy can be extensively processed with little fear of brittle fracture.

In this context, this paper presents the first fundamental observations on fracture mechanisms in Fecralloy strip, together with a detailed discussion of the fabrication of Fecralloy strip en route to the manufacture of automobile emission control hardware.

Materials

The fabrication discussion concerns experience with cold-rolled 0.050 mm foil. It is difficult to perform a meaningful fracture study on such material, however, and the basic fracture evaluation was conducted on 1.4 to 1.5-mm-thick cold-rolled and mill-annealed commercial Fecralloy strip of the chemical composition give in Table 3. The materials have been vacuum induction melted and the basic microstructure is shown in Fig. 1. The grain size is two or three ASTM grain sizes finer than observed at this gage in many ferritic stainless steel mill products, and the grain size, per se, is clearly not a limitation on toughness. The size of the globular YFe_9 particles is roughly the same as the grain size. For comparison, the microstructures of cold-rolled and annealed 0.050-mm strip are shown in Fig. 2.

There is, of course, some question as to whether the fracture behavior as annealed at 1.4-mm gage is truly relevant to that as cold-rolled at 0.050-mm. The DBTT should be much lower for the lighter-gage strip except for the problematical effect of the cold-work. Of course, the as annealed 1.4-mm gage condition is more relevant to toughness considerations of steel mill processing. In any event, the two gages will be compared wherever practical.
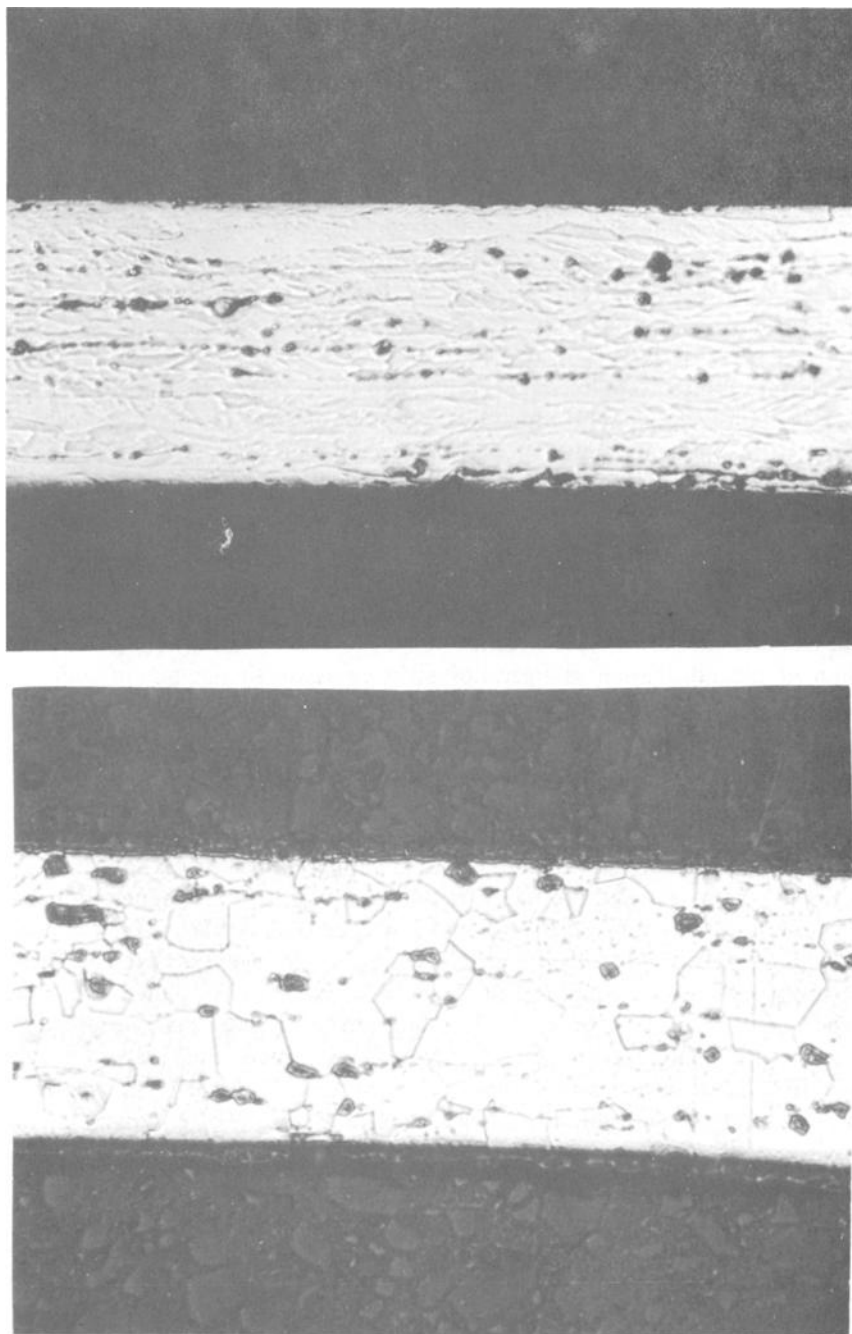
FIG. 2—*Optical micrographs of longitudinal sections of 0.002-in. Fecralloy foil:* (top) *as cold-rolled and* (bottom) *as-annealed at 850°C for 7 min* (×750).

General Mechanical Properties

The tensile properties for the cold-rolled 0.050-mm strip to be considered in the fabrication discussion are, typically, those given in Table 3. The low elongation is not necessarily a sign of brittleness, but rather reflects the early onset of necking. Bending strains far in excess of 1% can be achieved as discussed in the following.

Longitudinal and transverse tension tests were undertaken on 1.4-mm strip of Heat A at a strain rate of 0.05/min. These results are also presented in Table 4. The flow stress reflects the considerable solid solution hardening of the chromium and aluminum content. In spite of the presence of the YFe_9 inclusions, the ductility is only a little below typical ferritic stainless steel grades (T430, T434, T409, etc.) at similar gages. The presence of stringers is manifested in the lower transverse ductility.

The hardnesses of the 1.4 to 1.5-mm materials were R_b 84 and R_b 88 for Heats A and B, respectively.

The DBTT for a 1.5-mm strip of Heat A was evaluated by means of subsize Charpy impact testing. The testing was carried out on a Physmet subsize impact testing machine according to ASTM Specification for Notched Bar Impact Testing of Metallic Materials (E 23-72) [17], except for the nonstandard 1.4-mm thickness. Charpy testing was undertaken throughout a range from −80 to +99°C using liquid nitrogen, 2-methyl butane, ethanol, and water as heat-transfer media. Ten longitudinal and six transverse specimens were tested. A sharp transition was indicated in both cases in the range of 0 to 10°C. It is unlikely that the transverse DBTT was any more than 10 deg C higher than the longitudinal DBTT. The upper-shelf energy was perhaps 25 percent higher for the longitudinal case.

The tests confirm, of course, the brittleness of Fecralloy relative to other ferritic stainless steel alloys of comparable melting practice. The DBTT is even higher than those of electric-furnace-melted, titanium-stabilized grades. A comparison is made in Table 5 [15,16]. Even so, the DBTT value at 1.5 mm is sufficiently low to suggest that the DBTT range value is extremely interesting and clearly suggests that the YFe_9 *stringers* are not substantially involved in the DBTT process.

TABLE 4—*Tensile properties of the subject alloys.*

Material	0.2% Offset Yield Strength, MPa	Ultimate Tensile Strength, MPa	Elongation in 25 mm, %
0.050-mm Foil (typical)	930	987	1
Heat A (longitudinal)	421	573	25
Heat A (transverse)	462	614	21

TABLE 5—*A comparison of subsize Charpy DBTT values at a gage of about 1.5 mm.*

Material	DBTT
Fecralloy, Heat A	+5°C
EB 26-1	< −100
26-1S	−20 to −70
T439	−35 to −100
T409	< −100

Fracture Mechanism Study

Fracture initiation observations were made through a study of sub-critical microcrack appearance on the electropolished surfaces of tension specimens pulled to fracture in the DBTT range. Strip tension specimens were lapped, cleaned, ground with 600-grit silicon carbide and electro-polished for 90 s at 10 V in a solution of 30 percent concentrated nitric acid in dry methanol at −30 to −40°C. Tension testing was performed on a Instron machine specially outfitted with a test fixture submersed in a dewar flask. Testing media were the same as used in Charpy testing. The mechanical results of these tests are presented in Table 6. Yield points were noted on most of the tests, with the yield point behavior becoming more pronounced at lower temperatures. It is obvious that the tension test DBTT range is at least 150 deg C below the Charpy test DBTT range, re-flecting the lower strain rate and the absence of notch constraint. Again the transverse and longitudinal DBTT values are apparently comparable, with the upper-shelf ductility being somewhat lower for the transverse orientation.

After testing, the electropolished surfaces were examined by light micros-copy. In general with this approach, the as-tested strip surface reveals gross strain markings (orange-peel effects, shear bands, etc.), grain bound-

TABLE 6—*Low-temperature tensile behavior of electropolished specimens of Heat B.*

Test Temperature, °C	Orientation	0.2% Offset Yield Strength, MPa	Ultimate Tensile Strength, MPa	Elongation in 25 mm, %
−40	transverse	628	787	17
−72	transverse	718	828	19
−90	transverse	758[a]	869	21
−130	transverse	842[a]	925	17
−150	transverse	821[a]	876	7
−130	longitudinal	780[a]	883	25
−150	longitudinal	842[a]	890	8

[a] Denotes appearance of yield point.

aries, slipbands, mechanical twinning, second-phase particles, and populations of subcritical microcracks. The microcracks often reveal crack initiation and arrest sites, enabling assessment of the roles of the microstructural elements in the fracture process. The behavior in the present case is rather unequivocal. About 10 percent of the YFe_9 globules can be observed to contain microcracks. Generally the globules seem to have fractured on cleavage planes as shown in Fig. 3. Primary globule cracking tends to be perpendicular to the tensile axis, although secondary cracks parallel to the tensile axis may be observed. Little evidence of particle-matrix interface decohesion was observed. The material displayed in Fig. 3 underwent a tensile strain of about 17 percent and it is clear that the brittle YFe_9 particles are simply pulled apart by the adhering ductile matrix.

The cracks in the YFe_9 particles can, potentially, propagate throughout the matrix to bring about brittle fracture (presumably only one such case actually occurs for a given specimen fracture). In a few cases a cracked inclusion was seen to be associated with a crack that had propagated through one or two grains before arrest and blunting at a grain boundary. Mostly, however, the stress concentrations presented by the YFe_9 cracks are relieved by intense slip or mechanical twinning in the adjacent matrix, as shown in Fig. 4.

In some instances microcracks were observed which were not identifiable with a cracked YFe_9 globule. Presumably such cracks arise from subsurface YFe_9 particles. About 50 percent of the surface cracks were associable with visible inclusions. In a few instances microcracking could obviously be associated with YFe_9 stringers such as shown in Fig. 5. In general, however, the stringers seem to play little role in the brittle fracture mechanism. This observation is fully consistent with the similarity in longitudinal and transverse DBTT ranges. Of course, stringers may be associated with voids in the as-received conditions as shown in Fig. 1. Perhaps it is the sharp, fresh cracks that develop in the large globules that possess the most stress-raising capability.

Thus, it seems fair to conclude that YFe_9 inclusions are, in fact, fundamental to the poor fracture toughness or high-DBTT range displayed by Fecralloy or both. On the other hand, it is the globules and not the stringers that seem to be the most common crack initiation sites. This is borne out both in terms of microscopic evidence and in terms of a comparison of transverse and longitudinal DBTT values. The stringers do seem to play a role in accelerating the *ductile* fracture process insofar as upper-shelf energies and elongations are reduced in the transverse direction. There is some question as to whether the low-temperature tension test observations are truly representative of fracture behavior at the higher DBTT ranges associable with higher strain rates, notch effects, and heavier gages. Certainly fracture mechanism evaluation should be undertaken under these conditions as well. The evidence for the condition studied is, however,
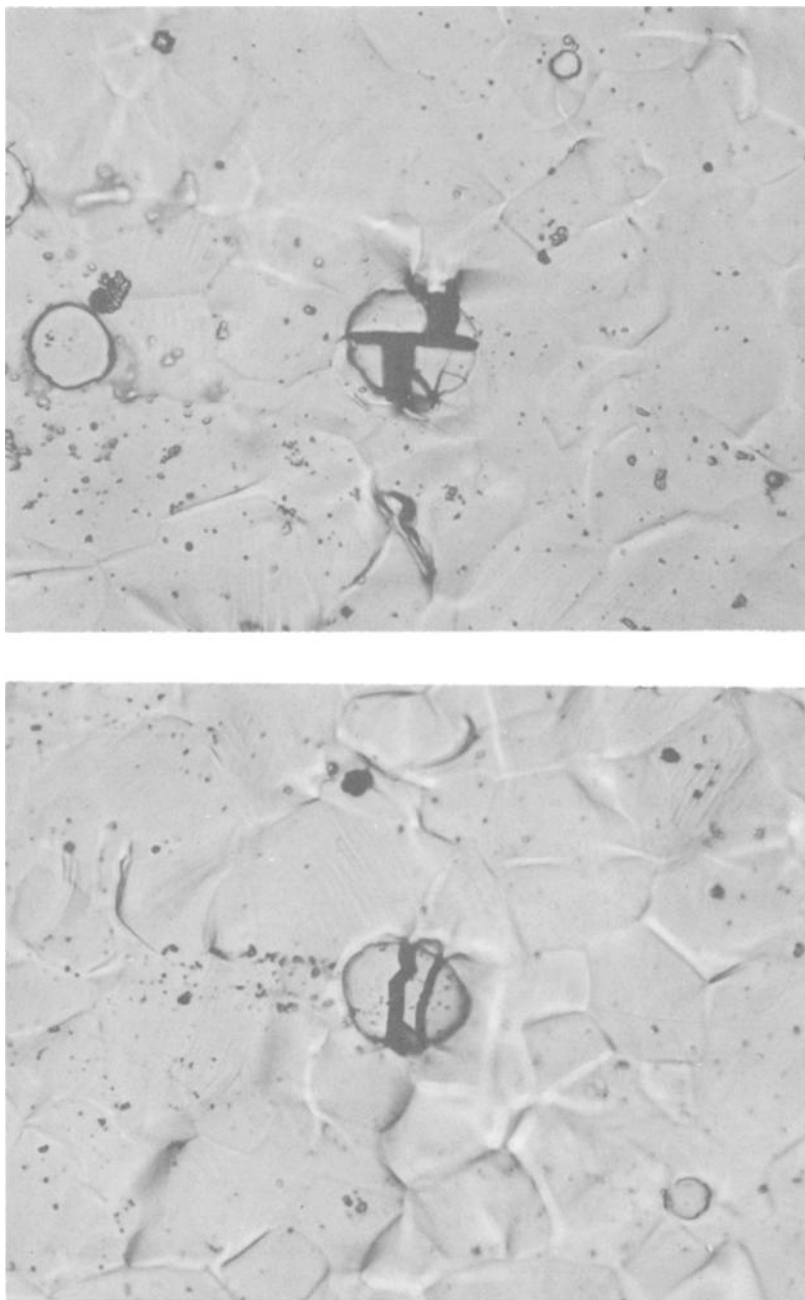
FIG. 3—*Optical micrographs showing cleavage of YFe₉ globules in Heat B, tested at* −*130°C in the transverse direction; tensile axis is horizontal* (×750).
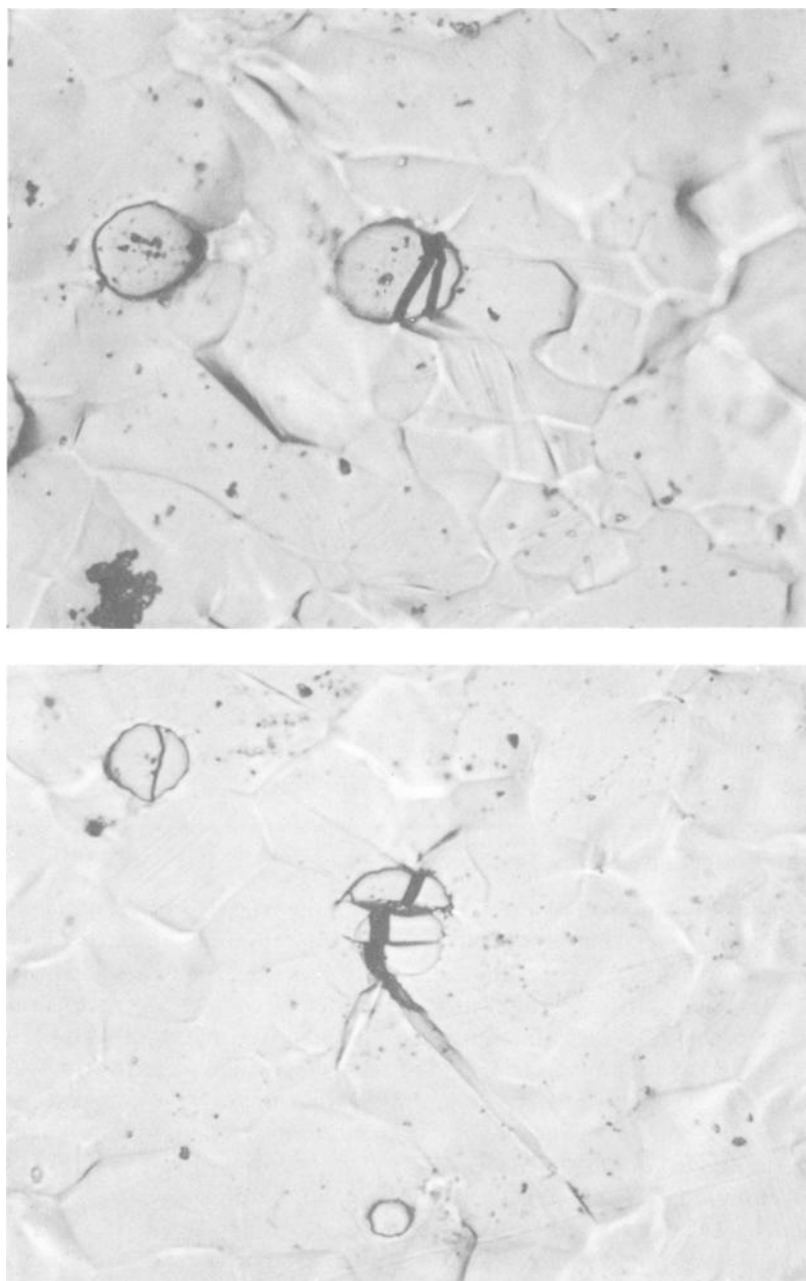
FIG. 4—*Optical micrographs showing stress relief and crack blunting through slip* (top) *and twin formation* (bottom) *in the ferrite matrix; Heat B, tested at* −130°C *in the transverse direction; tensile axis is horizontal* (×750).
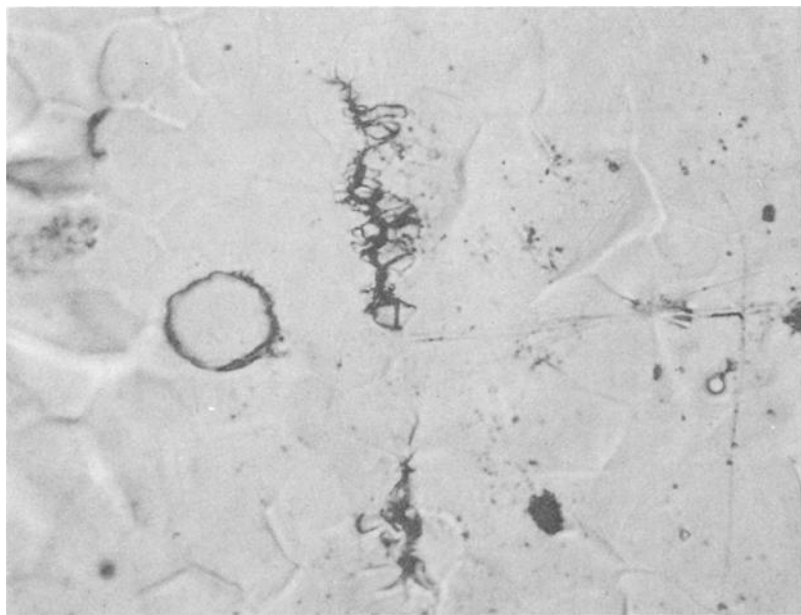
FIG. 5—*Optical micrograph showing cracking associated with YFe₉ stringer in Heat B, tested at −130°C in the transverse direction; tensile axis horizontal (×750).*

sufficiently clear-cut to suggest that the YFe₉ inclusions dominate a wide range of DBTT behavior.

Steel Production Practice Implications

Quality-control metallographers tend, quite rightly, to be concerned with general inclusion levels and stringer configurations in particular. In this context, it is important to note that YFe₉ inclusions are intrinsic to Fecralloy and must be dealt with as a matter of course. Moreover, unless second-order differences in transverse ductility are important, the present study suggests that YFe₉ stringers are relatively benign as far as the DBTT is concerned. In fact the most severe-looking microcracks are associated with *round* globules. Thus, even preoccupation with angular versus globular particles seems unwarranted.

It is highly likely that YFe₉ distribution and morphology can be manipulated by soaking and hot-rolling practice variation. Again, concern with stringer development may be unwarranted. A much more promising approach would appear to be that of refining YFe₉ globule size. The fractured particles are typically 0.025 mm in diameter and cracks in smaller globules would almost certainly provide less stress concentration. The

benign nature of stringers may simply lie in the small size of the stringer particles. Careful evaluations of ingot structure and soaking effects may provide clues to microstructural refinement.

Fabrication Capability

Successful fabrication of Fecralloy foil is possible despite its inherent brittleness and low ductility. The metal can be cold-worked into sheet or wire and fabricated into shapes, much like ferritic stainless steel. Upon bend testing (per ASTM Guided Bend Test for Ductility of Welds (E 190-76) of 0.050-mm strip, no cracks were observed (at $\times 10$ magnification) in a 180-deg bend down to mandrel widths of 0.2 mm in both the longitudinal and transverse directions. Such testing is likely to be more severe than any real-world situation; thus Fecralloy strip would be expected to withstand any reasonable bending or stamping fabrication without cracking.

A schematic flow diagram of the fabrication of Fecralloy strip into auto catalysts is shown in Fig. 6. A typical assay of a one-metric-ton heat of incoming material is given in Table 7. Once approved, the metal is unwound and fabricated. This is followed by a surface cleaning step and a proprietary enhancement step which makes the surface compatible with the alumina coating. Finally, the catalytic coating is applied and fixed by a

```
                        QC Check of 3-6" Strip

                           at .050 mm
                               |

                           1.  Unwinding
                           2.  Spot Weld to Mandrel
        Fabrication   {    3.  Corrugation
                           4.  Outer Skin + Face Welds

                               |

                           5.  Degreasing
        Pretreatment  {    6.  Temperature/Atmosphere
                               Enhancement Step

                               |

                           7.  Alumina and Platinum Group Metals
        Coating       {    8.  Fix by Firing

                               |

                           Assembled into Stainless
                           Steel Cans and Placed
                           in the Auto Exhaust Train
```
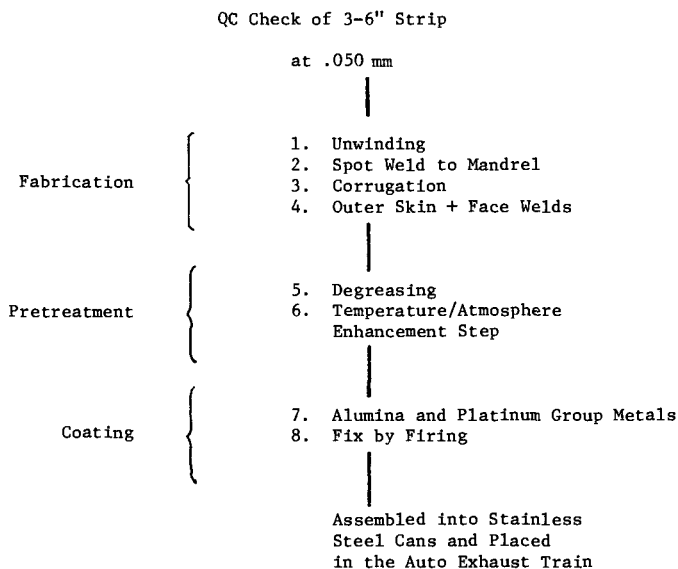
FIG. 6—*Schematic of converter fabrication.*

TABLE 7—*Typical assay of incoming Fecralloy.*

CHEMISTRY

Cr	15.80 weight %	C	135 ppm
Al	4.95	N	30
Y	0.25	O	40
Ni	0.15	P	100
Mn	0.07	S	15
Si	0.29	...	...

MECHANICAL

Tensile strength	918 MPa
Yield strength	870 MPa
Elongation in 25 mm	1.0%
HKN, 50 g	280
ASTM grain size	9.0
Bend test (0.1 mm)	pass

firing process. Examples of fabricated substrate are shown in Fig. 7. The metal configurations may be achieved by stamping or crimp rolling, which are similar to paper corrugation. The two state-of-the-art designs are the interleaf, whereby one strip of metal is coiled under the tension of a flat interleaf layer, and the helical, in which two corrugating sheets are formed at small opposite angles to the edge of the sheet. As listed in Table 1, an advantage in using metal for auto catalysts is the ease with which the cell geometry and cell density may be changed, as opposed to ceramic monoliths, which cannot be easily altered. With metal, such modifications can be made simply by changing a stamp or corrugating roll. The frequent design changes required by improvements in the continuous modeling/testing phase make use of Fecralloy metal strip attractive.

Summary

A fundamental fracture mechanism study of Fecralloy strip has indicated that fracture initiation in the DBTT range occurs primarily by cleavage of globular YFe_9 particles. YFe_9 stringers appear to play a secondary role in the brittle fracture process, although transverse "upper-shelf" ductility and fracture energy are reduced by the stringers. Implications for steel production suggest toleration of stringer arrays and attention to refinement of YFe_9 globules. Moreover, it has been shown that fabrication of light-gage strip can be accomplished. This fact, combined with the remarkable oxidation resistance, makes Fecralloy ideal for high-temperature applications such as supports for automotive emission catalyst.
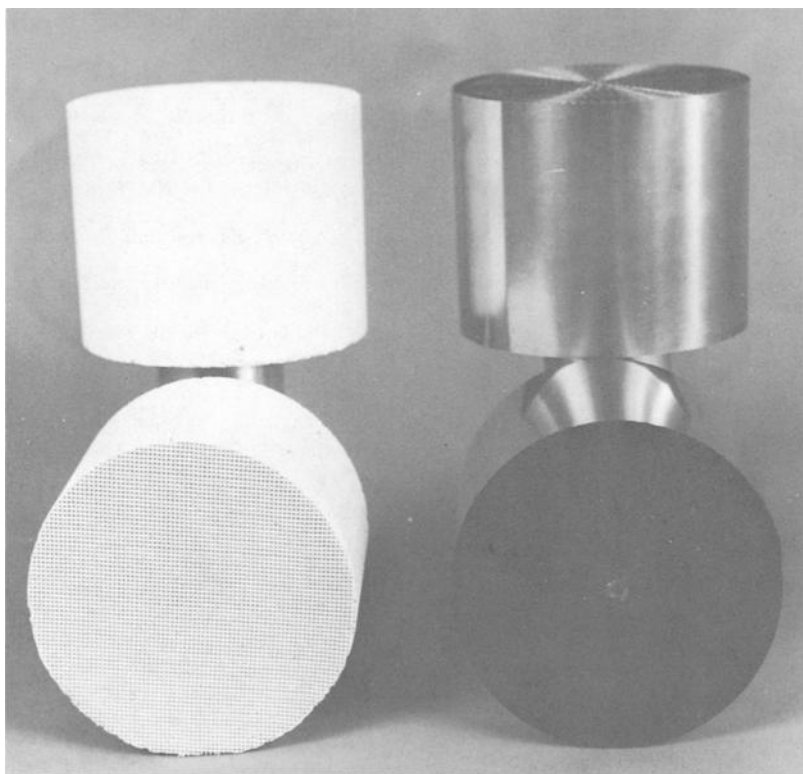
FIG. 7—*Conventional ceramic monoliths and Fecralloy steel substrates.*

Acknowledgment

The extensive fracture mechanism study effort of John F. Grubb of Rensselaer Polytechnic Institute is gratefully acknowledged.

References

[1] Pierrard, J. M., and Snee, R. D., "Relating Automotive Emissions and Urban Air Quality," presented at the National Meeting of Air Pollution Control Association, Denver, Colo., 1974.
[2] U.S. Patent 3,891,575.
[3] French Patent 2,240,049.
[4] Lacroix, R. in *Proceedings,* Symposium on Scientific Bases for the Preparation of Heterogeneous Catalysts, Societie Chemique de Belgique, Brussels, Belgium, Oct. 1975, Paper No. G21.
[5] Dulieu, C. A., Evans, W. D. S., Larbey, R. E., Verall, A. M., Wilkins, A. J. J., and Povey, J. H. in *Proceedings,* International Automotive Engineering Congress and Exposition, Detroit, Mich., Society for Automotive Engineers, March 1977, Paper No. 770299.

[6] Wukusick, C. S., "The Physical Metallurgy and Oxidation Behavior of Fe-Cr-Al-Y Alloys," ISAEC Contract No. AT(40-1)-2847, General Electric Co. NMPO Report No. GEMP-414.

[7] Collins, J. F., Calkins, V. P., and McGurty, J. A., *The Rare Earths*, Wiley, New York, 1961, Chapter 20.

[8] Wukusick, C. S. and Collins, J. F., *Materials Research & Standards*, Vol. 4, 1964, p. 637.

[9] Bartos, J., Perkins, R., and Robertshaw, F., "Mechanical Properties of Fe-Cr-Al-Y Alloys," ISAEC Contract No. AT(40-1)-2847, General Electric Co. NMPO Report No. GEMP-711.

[10] Stoloff, N. S. in *Fracture: Proceedings of Conference on the Physical Basis of Yield and Fracture*, Physical Society, London, 1966, p. 68.

[11] Domagala, R. F., Rausch, J. J., and Levinson, D. W., *Transactions*, American Society for Metals, Vol. 53, 1961, p. 137.

[12] Grubb, J. F. and Wright, R. N., "The Role of C and N in the Brittle Fracture of Fe-26Cr," in process of publication.

[13] Plumtree, A. and Gullberg, R., *Journal of Testing and Evaluation*, Vol. 2, No. 5, 1974, p. 331.

[14] Plumtree, A. and Gullberg, R., *Metallurgical Transactions*, Vol. 7A, 1976, p. 1451.

[15] Wright, R. N., *Welding Journal Research Supplement*, Vol. 50, 1971, p. 434s.

[16] Lula, R. A., *Metal Progress*, Vol. 110, No. 2, 1976, p. 24.

B. Mintz[1] *and J. M. Arrowsmith*[1]

Impact Properties of Fe-13Cr Thick Plate

ABSTRACT: The impact properties of an Fe-13Cr ferritic stainless steel at gages of 250 and 125 mm have been examined. Because these steels have notoriously coarse grain sizes, it is found that, on hot-rolling to thick plate, poor impact properties are often developed. Because only partial transformation to austenite is achieved on heat-treatment, it is not possible to refine the ferritic grain size and so improve impact performance. It has been found, however, that simple heat treatments can refine the grain boundary carbides and this action gives rise to as much as a 60 deg C fall in transition temperature. The various heat treatments given to the plates after hot-rolling are discussed and their impact properties compared with those obtained in the hot-rolled condition.

KEY WORDS: ferritic stainless steels, fracture toughness

Thirteen percent chromium ferritic stainless steels (AISI Grade 405), are the least expensive stainless steels available and are used for heat- and wear-resistant applications where corrosion requirements are a minimum; for example, in runners for turbines in hydroelectric power stations, coal hoppers, and for the lower parts of fractionating columns in petroleum refining processes. Often all that is required for these applications is a thin surface layer of stainless steel on boiler quality steel and such cladding results in considerable cost saving. Because of the presence of thin non-porous adherent oxide films on stainless steels, they cannot be readily roll-bonded to boiler quality steel. However, explosive bonding has been found to be a very successful technique in bonding stainless to boiler quality steels. In the Colclad process [1],[2] a 12-mm low-carbon steel plate is explosively bonded to a 250-mm ferritic stainless steel slab, the former being the "flyer"

---

[1] Section manager and departmental manager, respectively, British Steel Corp., Scottish Laboratory, Meadow Road, Motherwell, Scotland.

[2] The italic numbers in brackets refer to the list of references appended to this paper.

or "plating" plate. The plated slab is then rolled to an insert plate (50 to 13.5 mm). The low-carbon steel layer of the insert plate is finally roll-bonded to a thick boiler plate in a composite pack and rolled so that the final product is a boiler steel plate which has a thin cladding of stainless steel on one surface.

Whereas no problems are encountered with the austenitic stainless steels, the 13 percent chromium ferritic stainless steels, being sensitive to brittle fracture, are prone to shatter during the high-strain-rate explosive bonding process. To some extent this is alleviated by preheating the slab prior to bonding, but, as explosive bonding takes place in the open and as the explosives themselves must be guarded against preignition, the preheat temperature is restricted to the region of 150°C. This in itself is not always sufficient to prevent brittle failure. An investigation has therefore been carried out to establish whether the impact properties of Fe-13Cr slab at 250-mm gage can be improved by further processing and or heat treatment and this paper reports the findings.

Experimental

The ferritic stainless steel chosen for examination came from a cast in which all the slabs had cracked on explosive bonding. The cast analysis (weight percent) of this ferritic stainless steel (slab analysis was almost identical) was as follows

C	Si	S	P	Mn	Ni	Cr	Mo	V	Sol. Al	N
0.018	0.50	0.015	0.024	0.32	0.16	13.1	0.042	0.07	0.19	0.039

The steel was made by electric furnace and cast as 7620-kg ingots and rolled to 1020-mm-wide by 250-mm-thick slabs, the finish rolling temperature being 1020°C. One slab was commercially tempered at 640/680°C for 8 h at temperature, this being the condition the plate is supplied in prior to explosive bonding. The impact transition curves derived from Charpy tests taken from the mid-thickness position in the rolling direction are given in Fig. 1, slab coded HR250, and it can be seen that the impact properties are very poor, the 50 percent fracture appearance transition temperature (50 percent FATT) being as high as +150°C and the 54 J impact transition temperature (ITT) being +120°C. It is not surprising therefore that this slab subsequently shattered on explosive bonding. Examination of the microstructure, Fig. 2, shows the presence of very coarse grains enveloped by a coarse grain boundary network of carbides and small islands of tempered transformation product. Notwithstanding these grain boundary networks, brittle failure was always classical cleavage, Fig. 3.

Two approaches were used in an attempt to improve impact behavior: (1) grain refinement by increasing rolling reduction and (2) grain boundary carbide refinement by heat treatment.
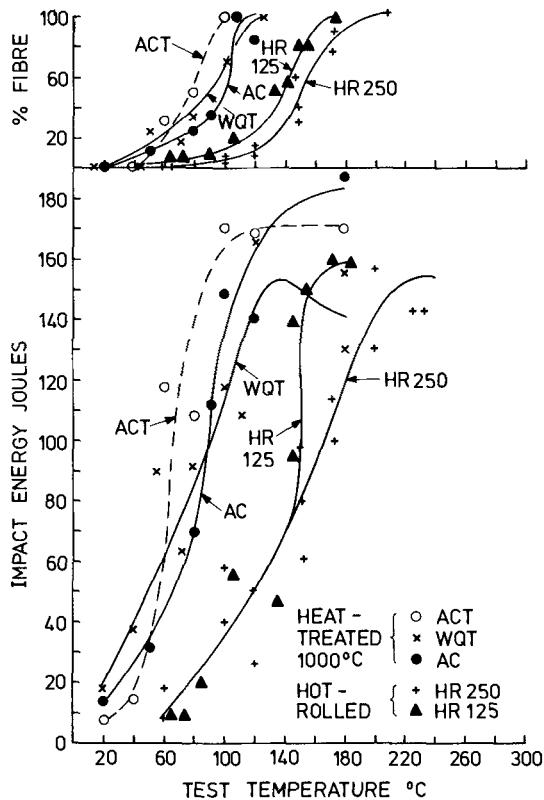
FIG. 1—*Impact transition curves for hot-rolled and tempered plates HR250 and 125 and heat-treated at 1000°C plates AC, ACT, and WQT.*

Grain Refinement by Increase in Rolling Reduction

Because only partial transformation to γ-phase occurs on heat-treating these ferritic stainless steels, grain size control and particularly grain refinement are often very difficult compared with ferrite/pearlite steels. Furthermore, as explosive bonding is an expensive process, any decrease in slab thickness adds significantly to cost. A further 50 percent rolling reduction from 250 to 125 mm, finish rolling at ~1000°C, was given to the final slab in this cast. As can be seen from Fig. 1, however, the 125-mm plate, coded HR125, after tempering at 680°C for 2½ h showed only slightly improved impact behavior, due to only a small additional grain refinement being achieved (grain size reduced from 750 to 550 μm). This slab as expected cracked on explosive bonding. It should be noted that the measured cooling rates for the 250 and 125-mm slabs after finish rolling at ~1000°C would be 2 and 3½ deg C/min, respectively, for the temperature range 800 to 400°C [2].
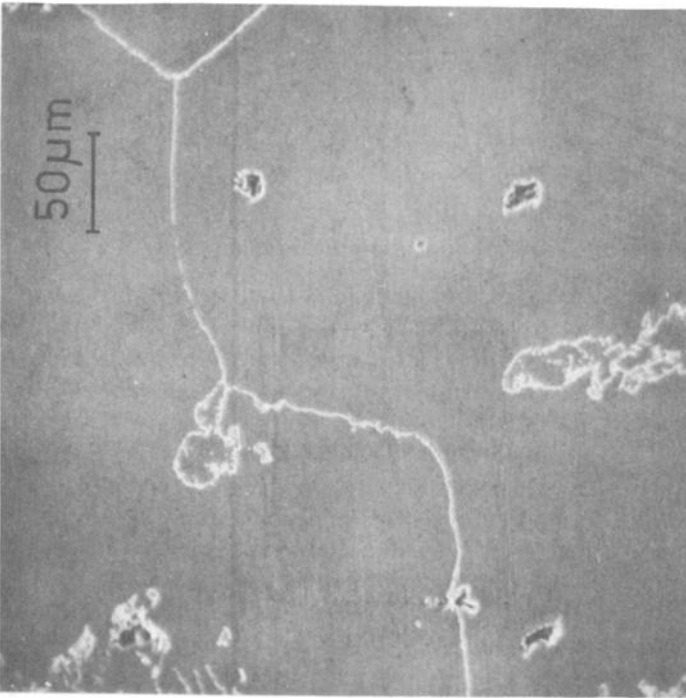
FIG. 2—Coarse grains enveloped by a grain boundary network of carbides with small islands of tempered transformation product.
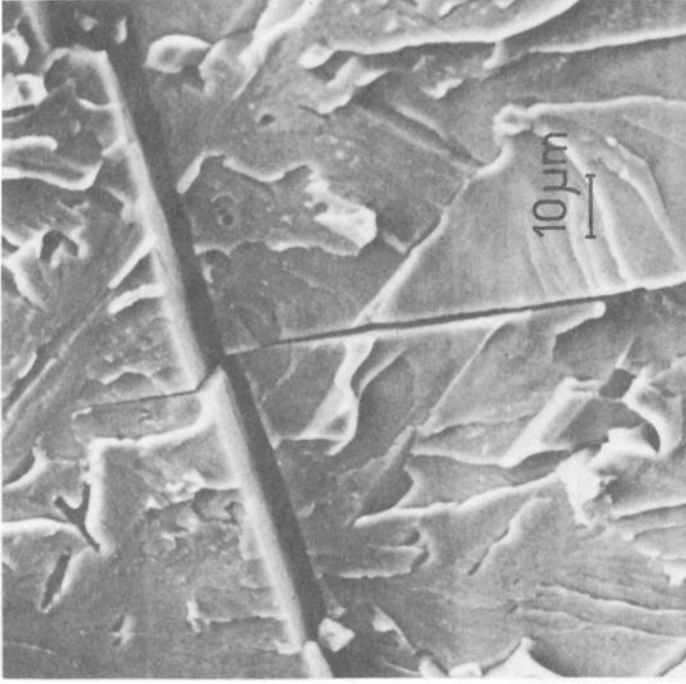
FIG. 3—Typical area on a fracture surface showing cleavage facets.

Grain Boundary Carbide Refinement by Heat Treatment

Small specimens were taken from the 250-mm-thick slab, HR250, and annealed in an argon atmosphere for 1 h at 800, 950, 1000, and 1100°C followed by air-cooling at a rate of 5 deg C/min. As would be expected from a steel having no conventional phase transformation, no grain refinement occurred on heat treatment. Using the optical microscope with oil immersion, however, considerable refinement of the grain boundary carbides was found to occur in the temperature range 950 to 1000°C.

As a result of this preliminary work an annealing temperature of 1000°C was chosen for heat treatment. The following heat treatments were then given to three blocks 165 by 165 by 125-mm cut from the 250-mm-thick slab HR250. (Note that thermocouples were inserted into the center of all the blocks so that temperature could be monitored accurately.)

1. One block, coded AC, was annealed for 5 h at 1000°C and air-cooled at a rate of 7 deg C/min in the temperature range 800 to 400°C. It should be noted that this cooling rate is somewhat faster than that for the 125-mm hot-rolled plate (namely, 7 deg C/min compared with 3½ deg C/min). No subsequent tempering treatment was given.

2. The second block, coded ACT, was annealed for 5 h at 1000°C, followed by air-cooling to room temperature as in treatment 1, and then tempered for 3 h at 690°C and air-cooled.

3. The remaining block, coded WQT, was annealed for 5 h at 1000°C and water-quenched (cooling rate 140 deg C/min in temperature range 800 to 400°C). The block was then tempered for 2 h at 550°C and air-cooled. This treatment was chosen because previous work on ferrite/pearlite steels had suggested that water-quenching and tempering at low temperatures might give very fine carbides [3,4].

Impact and tensile data were obtained, longitudinal Charpies and transverse tensiles being taken from the mid-thickness positions in the blocks. In addition, the following microstructural measurements were made on the three heat-treated blocks (AC, ACT, and WQT) and on the hot-rolled and tempered 250-mm slab and 125-mm plate (HR250 and 125, respectively)

1. Grain size (mean linear intercept).

2. Volume fraction of martensite[3] (point counting), and

3. Average grain boundary carbide thickness of a random 100 carbides, measured using the scanning electron microscope (SEM) by the method described in the paper by Mintz et al [3]. The etchant used for all this metallographic work was a 50/50 mixture of picral and 5 percent hydrochloric acid in meths.

In addition to the preceding measurements, microhardness measure-

---

[3] The term "martensite" used in the text refers to the transformation product from the austenite and includes both tempered and untempered martensite as well as other tempered lower transformation products.

ments were carried out on the martensitic regions using a Leitz microhardness tester with a 50-g load. Carbon extraction replicas were also taken from selected specimens so that the particles at the grain boundaries could be identified by diffraction.

Results

The impact transition curves for all the conditions examined are given in Fig. 1. The impact and tensile data are summarized in Table 1 and grain boundary carbide thickness, grain size, volume fraction martensitic product, and microhardness measurements in Table 2. It can be seen from Fig. 1 that while the additional hot reduction gives only a small improvement to impact properties (compare curve for HR250 with HR125), the various heat-treated conditions result in similar marked improvements in impact behavior (curves AC, ACT, and WQT). The additional heat treatment at 1000°C thus results in a 55 to 70 deg C lowering of the 50 percent FATT and ITT for 54 J. It should be noted that no grain refinement occurred on heat treatment (Table 2). The microstructures for the hot-rolled and heat-treated conditions are shown in Figs. 2 and 4 and Figs. 5-7, respectively. The hot-rolled 125-mm plate has slightly more martensitic product present in the structure than the 250-mm hot-rolled slab, and the heat-treated plates have even greater amounts of martensitic product present; see Table 2. Grain boundary carbides were found to be thick and in continuous networks in the hot-rolled and tempered conditions but were considerably refined after heat-treatment. (See Table 2 and also compare Figs. 8 and 9 with Figs. 10-12 for hot-rolled and heat-treated 1000°C conditions, respectively.) The grain boundary carbides were identified by electron diffraction to be $M_{23}C_6$. Water-quenching produced no significant further refinement of the grain boundary carbides but gave rise to a considerable reduction in the amount of carbide outlining of the boundaries (Fig. 12). In addition, this heat-treated plate had the greatest amount of martensitic product present, and more was concentrated within the ferrite matrix than for the other heat-treated conditions.

In the case of the hot-rolled 250-mm slab, the γ-phase had transformed to small islands of coarse carbides, many of which were not associated with the ferrite grain boundaries (Figs. 2 and 13). The hot-rolled 125-mm plate, although in the main having these coarse islands of carbides present in the microstructure, also had some finer-tempered carbide islands and finer grain boundary carbides (Fig. 14). The martensitic islands in this plate were now mainly situated at the ferrite grain boundaries (Fig. 4). The untempered plate air-cooled from 1000°C (AC), Fig. 15, had the transformation product present as untempered martensite. Water-quenching and tempering at 550°C produced tempered martensitic islands containing very fine carbides (Fig. 16). The air-cooled plate tempered at the higher tem-

TABLE 1—Summary of impact and tensile data.

Sample Code	Condition	0.2% Proof Stress, N/mm²	UTS, N/mm²	% Reduction of Area	50% FATT, °C	54 J, ITT, °C	27 J, ITT, °C	Shelf Energy, J
HR 250	hot-rolled and tempered	260	352	45	150	125	95	154
HR 125	hot-rolled and tempered	260	365	47	135	125	90	159
AC	heat-treated, 1000°C, air-cooled	230	353	50	94	70	43	180
ACT	as above and tempered	230	343	46	78	58	43	170
WQT	heat-treated, 1000°C, water-quenched and tempered	280	398	43	93	52	28	145

TABLE 2—*Summary of microstructural and microhardness measurements.*

Sample Code	Condition	Grain Size mm$^{-1/2}$	Grain Size μm	Average Carbide Thickness (t), μm	Volume Fraction of Martensite Product	Micro-Hardness Measurements Ferrite Matrix, HV	Micro-Hardness Measurements Martensite Islands, HV
HR 250	hot-rolled and tempered	1.15	750	0.65	4.6	165	197
HR 125	hot-rolled and tempered	1.35	550	0.58	6.7	169	207
AC	heat-treated, 1000°C, air-cooled	1.15	750	0.30	8.4	147	390
ACT	as above, tempered	1.15	750	0.30	10.0	147	221
WQT	heat-treated, 1000°C, water-quenched and tempered	1.15	750	0.28	13.0	144	281
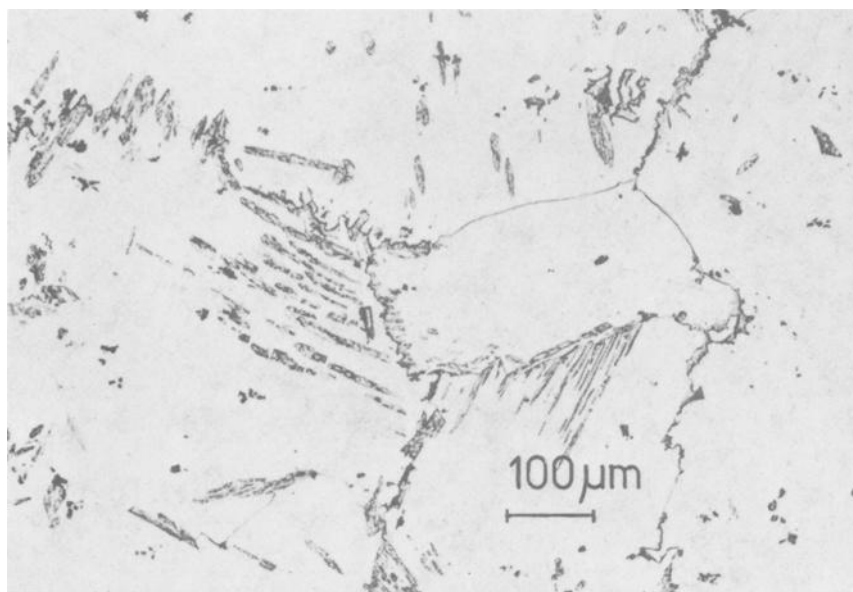
FIG. 4—*Photomicrograph of hot-rolled and tempered 125-mm plate.*
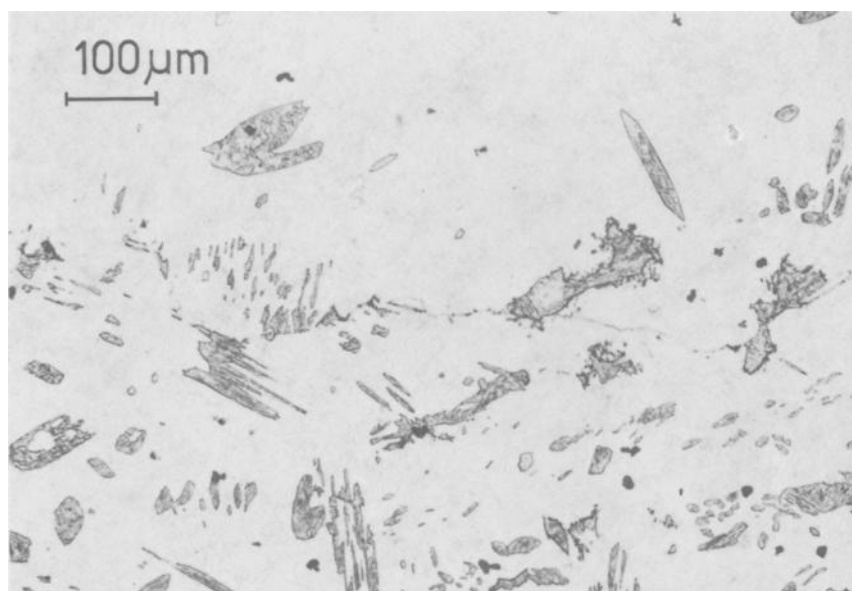
FIG. 5—*Photomicrograph of heat-treated plate AC, annealed at 1000°C and air-cooled. Note the greater amount of second phase in the structure.*
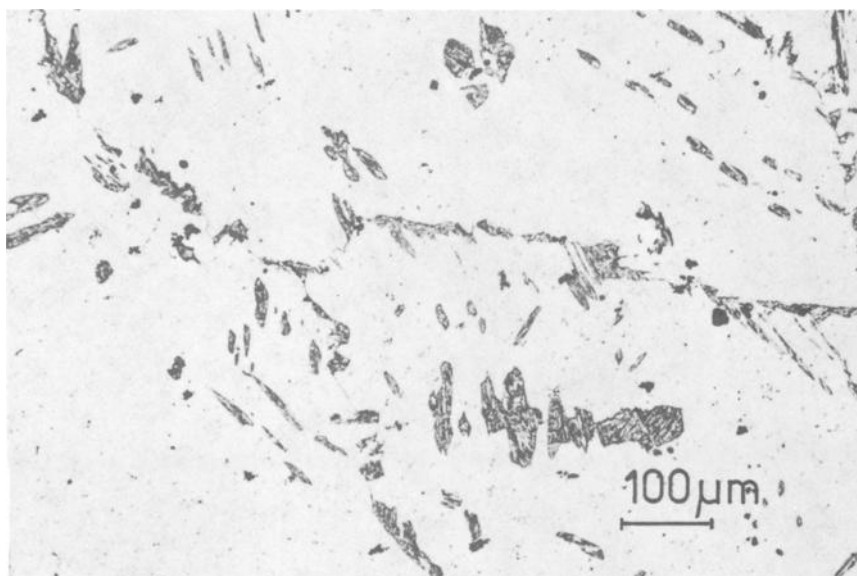
FIG. 6—*Photomicrograph of heat-treated plate ACT, annealed at 1000°C and tempered at 690°C.*
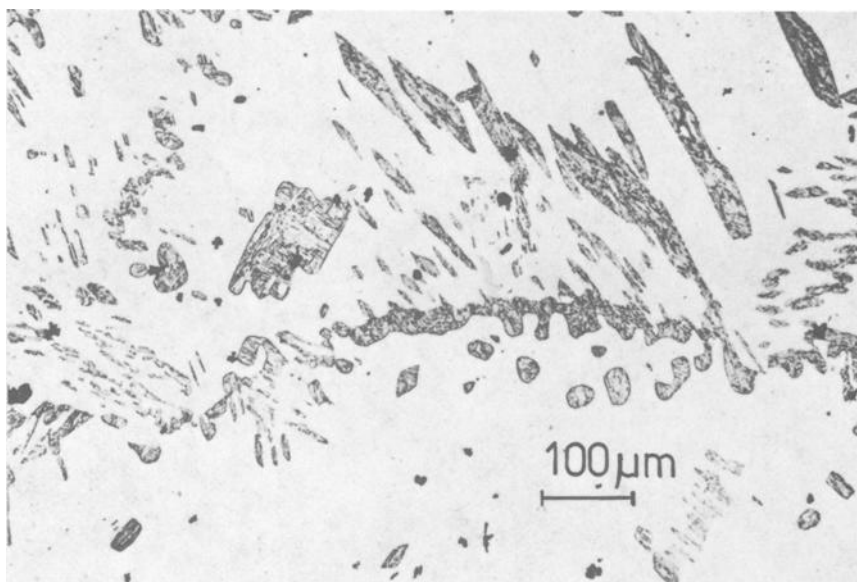
FIG. 7—*Photomicrograph of heat-treated plate WQT, annealed at 1000°C, water-quenched and tempered at 550°C.*

FIG. 9—Typical coarse grain boundary carbides found in the hot-rolled and tempered 125-mm plate HR125.

FIG. 8—Typical coarse grain boundary carbides found in the hot-rolled and tempered 250-mm plate HR250.
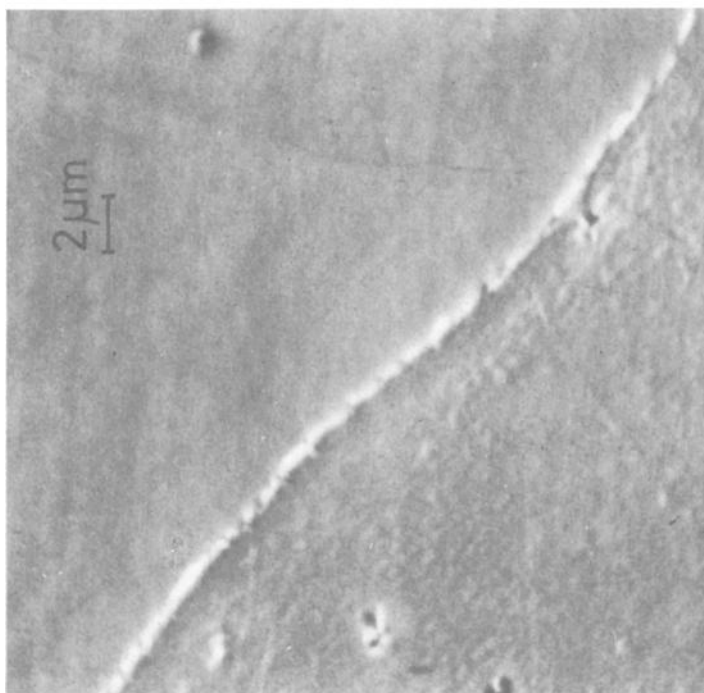
FIG. 10—*Typical finer grain boundary carbides present after heat-treating at 1000°C and air-cooling (Plate AC).*
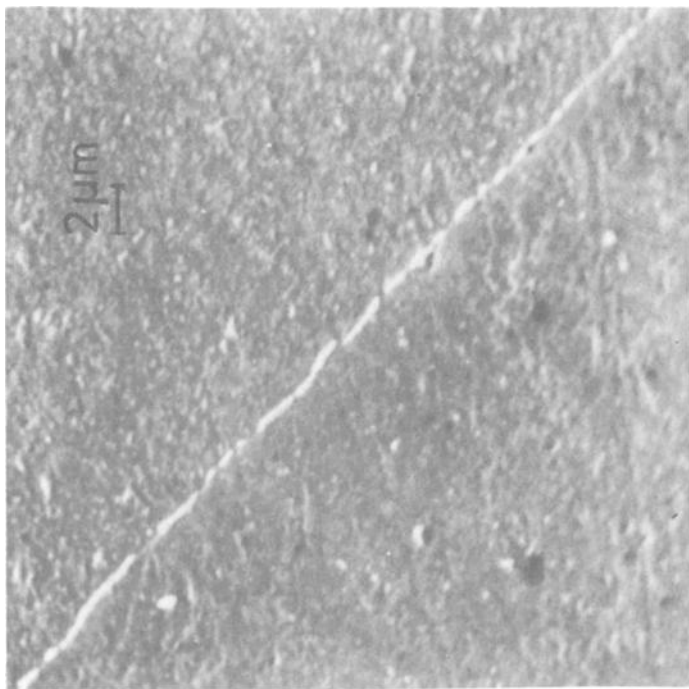
FIG. 11—*Typical fine grain boundary carbides present after heat-treating at 1000°C, air-cooling, and tempering at 690°C (Plate ACT).*

FIG. 13—Coarse carbide formations found in hot-rolled and tempered 250-mm plate.

FIG. 12—Typical fine isolated grain boundary carbides present after heat-treating at 1000°C, water-quenching, and tempering at 550°C (Plate WQT).

FIG. 15—Scanning electron micrograph of martensitic islands found at ferrite grains in the heat-treated to 1000°C and air-cooled plate (AC).

FIG. 14—Example of tempered martensitic islands found at ferrite boundaries in the hot-rolled and tempered 125-mm plate.

perature of 690°C showed the transformation product present as well-tempered martensite, the matrix carbides now being significantly coarser than those present at 550°C, Fig. 17, and similar to some of the islands in the hot-rolled and tempered plate at 680°C (the 125-mm plate HR125, Fig. 14).

Microhardness measurements are given in Table 2. These indicate that the hardness of the ferrite matrix is significantly higher in the hot-rolled and tempered conditions (~20 HV higher than for the heat-treated conditions). The hardness of the martensitic islands was very high for the untempered martensitic conditions (390 VPN) and softened with increase in tempering temperature (namely, 281 HV at 550°C and 221 HV at 690°C).

Discussion

The benefits to impact properties derived from increase in rolling reduction at high finish rolling temperatures of 1000°C can be seen to be minor compared with the benefit from heat treatment. It must be stressed, however, that this conclusion is likely to apply only at high finish rolling temperatures. Where mills are capable of rolling to low temperatures (namely, 700°C), the warm-worked structures produced should readily recrystallize on normalizing and, provided low normalizing temperatures are used, finer grain sizes with improved impact properties should be obtained. This was not the case in the present instance and the discussion therefore is centered entirely on the manner in which heat treatment alone can improve impact behavior.

Influence of Microstructure on Impact Properties

The major changes in microstructure and properties that occur on heat treatment can be summarized as follows:

1. Heat treatment results in significantly finer grain boundary carbides being produced.
2. There is a softening of the ferrite.
3. There is an increase in the amount of martensitic product in the structures.

Influence of Carbide Refinement on Impact Transition Temperatures— The influence of microstructure on impact behavior is generally difficult to quantify. Work by Gladman et al [5] and Allen et al [6] has shown the importance of grain boundary carbide thickness in controlling the impact behavior in very low-carbon steels (≤0.05 percent carbon). The latter work has shown, as in the present investigation, that a low carbon content of 0.02 percent, in the presence of a coarse grain size, can give extensive networks of grain boundary carbide films. Recent work by Mintz et al [3] on
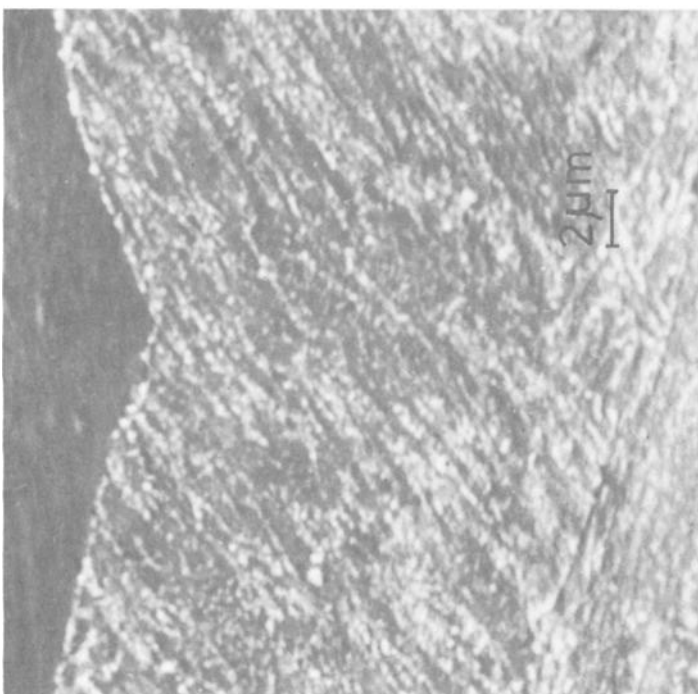
FIG. 17—Typical example of a well-tempered martensitic island in the heat-treated to 1000°C, air-cooled, and tempered at 690°C plate, ACT.

FIG. 16—Typical appearance of second phase in the heat-treated to 1000°C, water-quenched, and tempered at 550°C plate, WQI, showing it to be lightly tempered martensite.
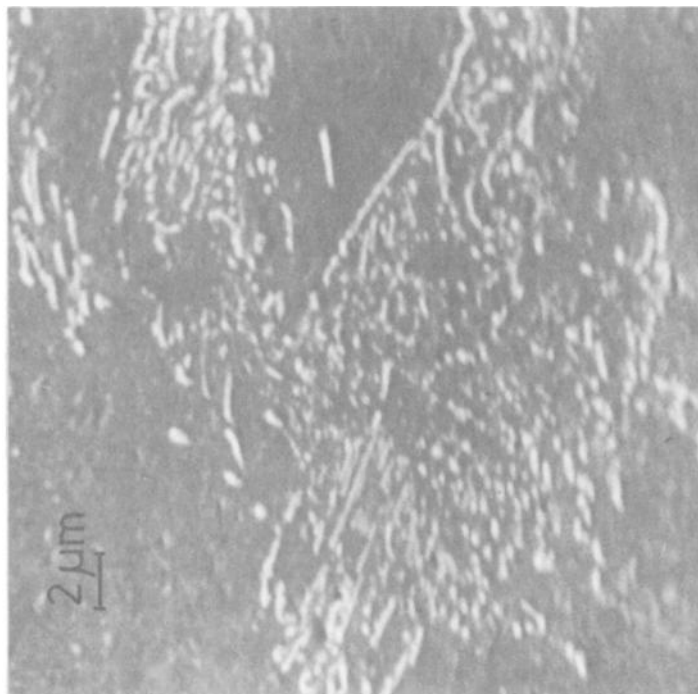
ferrite/pearlite steels and low-carbon pearlite/free steels has attempted to quantify the influence of grain boundary carbide thickness on impact behavior. Their work covered the grain size range 4 to 13-mm$^{-1/2}$ and was able to successfully differentiate between the influence of grain boundary carbide thickness and the influence of grain size on impact properties. Again, the present work is particularly interesting in that as the grain size remains constant a direct measure of the influence of grain boundary carbide thickness on impact behavior can be obtained. In the paper by Mintz et al it was shown that increasing the grain boundary carbide thickness (t) causes an increase in transition temperature, a unit increase of $t^{1/2}$ (μm$^{+1/2}$) being accompanied by an increase in transition temperature of 131 and 193 deg C for 50 percent FATT and 54 J impact criteria, respectively. Using these factors, the change in carbide thickness from 0.65 to 0.3 μm which results from heat treatment would cause a 35 and 50 deg C fall in 50 percent FATT and 54 J impact transition temperatures, respectively.

Influence of Heat-Treatment at 1000°C on Ferrite Matrix Strength—The changes in 50 percent FATT and 54 J that have been calculated as due to differences in carbide thickness are less than the observed fall in ITT of 55 to 75 deg C. However, some softening of the ferrite matrix (~20-VPN fall in hardness) also occurs on heat-treating at 1000°C, and this will also lead to some lowering of the transition temperature. The difference in strength and matrix hardness between the hot-rolled and heat-treated conditions is most likely due to differences in retained dislocation densities, it being difficult to anneal out dislocations in these steels due to the formation of stable subgrain boundaries [7].

Work by Mintz [8] has shown that the influence of dislocation hardening and precipitation hardening on the ITT is very similar, factors of 0.4 to 0.5°C/N/mm^2 having been quoted. Assuming that the 30-N/mm^2 difference in proof stress (Table 1) is due to differences in dislocation density, then heat-treating at 1000°C would give rise from this source to ~13°C fall in transition temperature. Thus the combined fall in transition temperature from grain boundary carbide refinement and softening of the ferrite matrix would be in the region of 50 to 65 deg C which is close to the observed range of 55 to 73 deg C.

Although the 0.2 percent proof stress of the water-quenched and tempered plate WQT is significantly higher than for the air-cooled conditions, AC and ACT, it is noticeable that the ferrite matrix hardness values (Table 2) are the same for all the heat-treated 1000°C conditions. This suggests that the increase in proof stress and ultimate tensile strength (UTS) observed in this steel, WQT, may possibly be related to the presence of the martensitic products influencing work-hardening rates. Exactly why this should be so is not clear, but it could be a combination of a greater volume fraction of martensitic product as well as a more uniform dispersion within

the ferrite grain matrix. This increase in proof stress meant that this plate had the best combination of impact and tensile properties.

Influence of Martensitic Product on Impact Behavior—Although the introduction of a certain amount of γ-phase into the structure is believed to play a crucial part in refining the grain boundary carbides, as explained later in this discussion, the form and volume fraction of martensitic product resulting from γ-phase decomposition do not appear to influence impact behavior. Thus the presence of 8 percent volume fraction of martensite in the form of untempered martensite islands at the ferrite grain boundaries in Plate AC, Fig. 15, did not appear to adversely influence impact properties, the impact properties being similar to those given by the air-cooled and tempered plate, ACT, in which the islands consisted of temper carbides in a ferrite matrix, Fig. 17. This may suggest that it is easier to crack non-coherent carbides at the ferrite grain boundaries than the more coherent martensitic islands. The increase in volume fraction of martensitic product in the heat-treated plated from 8 to 13 percent (Table 2) also seemed to have little influence on impact behavior.

Cause of Carbide Refinement

From the work of Baerlecken et al [9], both carbon and nitrogen have a very marked effect in expanding the γ-phase loop in the iron-chromium system, nitrogen being slightly more potent (Fig. 18a and 18b, respectively). From their work it can be seen that if in the present steel the carbon and nitrogen are all in solution (that is, 0.018 percent carbon and 0.039 percent nitrogen), then the structure at a 1000°C would be expected to have a high volume fraction of austenite. In fact a specimen which was rapidly cooled (~700 deg C/s) after a prolonged soak at a 1000°C produced only 13 percent martensite. This indicates, as would be expected from the high aluminum level, that a significant amount of the nitrogen is probably combined as aluminum-nitride in both the hot-rolled and heat-treated conditions. The equilibrium diagram is therefore most probably of the type, shown in Fig. 18c [10], in which only carbon is present in solution in the γ-phase. From this diagram it can be seen that, for the range 12 to 13 percent chromium, raising the temperature to the range 850 to 1000°C introduces γ-phase into the structure, the maximum amount occurring at temperatures in the region of 1000°C, that is, the heat-treatment temperature. The initial observation that the grain boundary carbides were refined in the temperature range 950 to 1000°C indicates that the refinement of carbides is related in some manner to the introduction of γ. A possible explanation to account for refinement of carbides could be that, because of the much greater solubility of carbon in γ, the introduction of γ will redistribute most of the carbon from the ferrite to the austenite and this will leave less carbon to precipitate out at the ferrite grain boundaries. Such an explana-
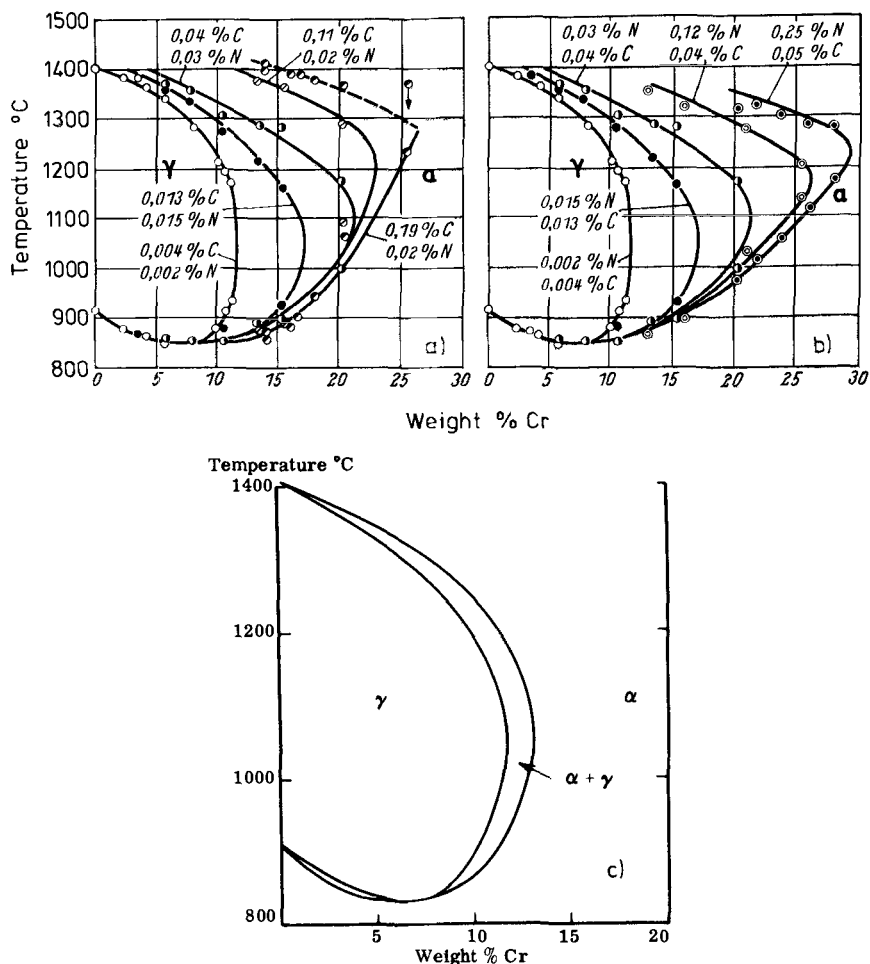
FIG. 18—*Equilibrium diagrams for iron-chromium system showing* (a) *influence of carbon and* (b) *influence of nitrogen in expanding the γ loop (after Baerlecken et al* [9]); (c) *is the diagram for an 0.01 percent carbon steel which is probably more representative of the steel under examination (after Bungardt et al* [10]).

tion, however, does not account for the experimental observation that there is no significant refinement of grain boundary carbides as the volume fraction of entrapped γ increases from 8 to 13 percent (AC to WQT in Table 2), although this increase markedly reduces the amount of carbon available for precipitation as shown by the reduction in the amount of grain boundary carbide (compare Fig. 12 with Fig. 10).

Previous work on ferrite/pearlite and pearlite-free steels [3] has shown that the grain boundary carbide thickness is determined by the cooling

rate, composition, and the presence or absence of pearlite. Because the heat-treated blocks had undergone faster cooling rates through the transformation than the hot-rolled plates, the influence of cooling rate on grain boundary carbide thickness was examined in more detail using small specimens heated to 1000°C and cooled in the range 1 to 100°C/min. The results are given in Fig. 19. It can be seen from this curve that cooling rate has a very pronounced effect on grain boundary carbide thickness but only over a very narrow range. For cooling rates < 5 deg C/min (which is equivalent to the cooling rate of 100-mm air-cooled plate) the grain boundary carbides are coarse and average around 0.6 μm. Above 5 deg C/min, carbides are fine, averaging 0.3 μm in thickness. Indeed it can be seen that the apparent reason for the heat-treated plates having better impact properties than the hot-rolled plates is that the hot-rolled plates spanned the cooling range 2 to 3½ deg C/min while the heat-treated plates spanned the cooling range 7 to 140 deg C/min, Fig. 19. However, the very abrupt change in grain boundary carbide thickness which occurs at 5 deg C/min and the absence of a significant influence of cooling rate in the range 5 to 140 deg C/min, together with carbide refinement being related to the presence of γ, suggest that there is another factor in addition to cooling rate which is responsible for this refinement. Possibly this other factor could be, as has been observed with ferrite/pearlite steels, the introduction on cooling through the transformation of a critical amount of second phase. For example, it has been found that in carbon/manganese steels [3] with low carbon content, the last γ to trans-
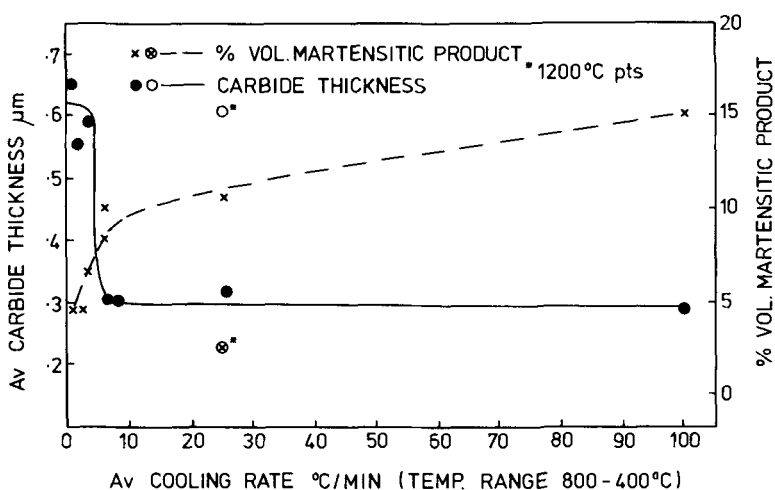
FIG. 19—*Carbide thickness and volume fraction second phase as a function of cooling rate for specimens heated to 1000°C for 2 h and cooled at rates in the range 1 to 100 deg C/min. Asterisked points are for the 1200°C treatment.*

form has too small a volume fraction to form a distinct phase, and cementite forms only at grain boundaries giving coarse carbides. Raising the carbon content increases the volume fraction of γ prior to final transformation, resulting in pearlite formation, and this for the same cooling rate causes a finer carbide distribution at the grain boundaries. The filamental grain boundary carbides in this case are believed to be the tails of the pearlite colonies [11]. With pearlitic steels it has also been shown that when the γ volume fraction is small, degenerate coarse pearlite is formed, whereas large volume fractions of γ give rise to fine lamellar pearlite [11]. This is probably because there is insufficient free energy available to create the extra surfaces required for lamellar pearlite in small volume fractions of austenite [12]. A schematic diagram to illustrate the proposed mechanism of carbide refinement is shown in Fig. 20. Although the present situation is different in the sense that the phase formed from the larger volume fractions of γ is martensite rather than pearlite, similar arguments may be relevant. In Fig. 19 the volume fraction of martensitic product against cooling rate is plotted, and from this it can be seen that fine carbides are present when the entrapped γ content exceeds about 8 percent.

In order to critically test this theory, one specimen was heated to 1200°C and cooled at a faster rate than 5 deg C/min, namely, 26 deg C/min. This
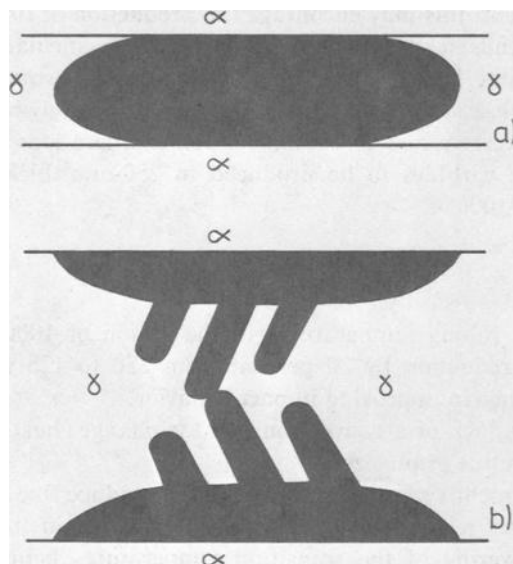
FIG. 20—*Schematic diagram illustrating a possible way in which a carbide refinement may occur: (a) at low volume fractions of γ, a thin film forms around the ferrite boundaries which collapses from α/γ interfaces to form thick grain boundary carbides; (b) with larger volume fraction of γ, film is thicker, allowing pearlite formation and finer grain boundary carbides to form because collapse is now from separate α/γ interfaces.*

resulted in only small amounts of γ being trapped at the ferrite grain boundaries and, in accord with the theory, coarse grain boundary carbides were produced (see Fig. 19). Thus the introduction of a critical amount of γ seems to be the factor which controls the carbide thickness, and cooling rate is only important because it can control the amount of γ trapped in the structure.

Summarizing, with the present composition it would seem that, provided the cooling rate is in excess of about 5 deg C/min, that is, the cooling rate for 100-mm or thinner air-cooled plate, sufficient γ is always entrapped to ensure fine grain boundary carbides. For cooling rates less than 5 deg C/min the rates are so slow that most of the γ present at 1000°C can retransform to ferrite during cooling, resulting in a low volume fraction of γ available for carbide formation and hence coarse grain boundary carbides. Thus for the 250 to 125-mm-thick plates, air-cooling from 1000°C is not in itself sufficient to produce fine grain boundary carbides. Some accelerated cooling, either water-quenching (cooling rates of 15 to 45 deg C/min) [2] or possibly forced air-cooling, may be sufficient. For plates < 100 mm, air-cooling by itself should be adequate.

Composition would be expected to influence the amount of γ which can be retained prior to carbide formation, and reducing the chromium or increasing the carbon contents, for example, would increase the amount of γ at 1000°C and this may encourage the production of fine grain boundary carbides. Indeed the slabs examined had particularly low carbon contents and came from a cast which had one of the worst records of all the ferritic stainless steel casts which have been explosively bonded. Further work is therefore required to examine whether alterations to composition will enable fine carbides to be produced in 250-mm-thick slab which is air-cooled from 1000°C.

Conclusions

1. For finish rolling temperatures in the region of 1000°C, increasing the hot-rolling reduction by 50 percent from 250 to 125 mm has only a marginal influence in improving impact behavior.

2. Due to the lack of a conventional phase change, heat treatment cannot be used to refine grain size.

3. Heat treatment can, however, be used to produce fine grain boundary carbides and this results in substantial improvement in impact behavior, a 60 deg C lowering of the transition temperatures being achieved. To achieve this improvement, heat treatment at 1000°C is required, followed by cooling at rates faster than 5 deg C/min (equivalent to air-cooling 100-mm plate). For the 250-mm slab, water spray quenching would give the required cooling rate although it is possible that forced air-cooling may be adequate. However, adjustment to composition rather than in-

creased cooling rate may be the long-term solution to the problem of obtaining satisfactory impact behavior in thick slab.

4. The refinement in grain boundary carbides is believed to be due to the heat treatment introducing a certain amount of γ into the structure, this controlling in some way the form in which the carbides subsequently precipitate out at the boundaries.

5. Annealing the hot-rolled plates in addition to being able to refine carbides also produces some softening of the ferrite, presumably due to a reduction in dislocation density. This softening also contributes significantly to improving impact behavior.

6. Martensite islands at ferrite grain boundaries in amounts up to 8 percent volume fraction are not detrimental to impact behavior.

References

[1] British Steel Corp. Brochure on Colclad® process, in press.
[2] Watson, D., private communication, British Steel Corp., Ladgate Lane Laboratories. Middlesbrough, U.K.
[3] Mintz, B., Morrison, W. B., and Jones, A., Metals Technology, Vol. 6, Part 7, 1979, p. 252.
[4] Cochrane, R. C., ISI Special Report 145, Iron and Steel Institute, 1971, p. 101.
[5] Gladman, T., Holmes, B., and McIvor, I. D., ISI Special Report 145, Iron and Steel Institute, 1971, p. 68.
[6] Allen, N. P., Rees, W. P., Hopkins, B. E., and Tipler, H. R., Journal of the Iron and Steel Institute, Vol. 174, 1953, p. 108.
[7] Gladman, T., private communication, British Steel Corp. Sheffield Laboratories, U.K. England.
[8] Mintz, B. in Proceedings. Institution of Metallurgists Spring Residential Course, Metal Society, London, Series 3, No. 7, March 1977, p. 47.
[9] Baerlecken, E., Fischer, W. A., and Lorenz, U. K., Stahl und Eisen, Vol. 12, 1961, p. 778.
[10] Bungardt, K., Kunda, E. and Horn, E., Archiv für das Eisenhüttenwesen, Vol. 29, 1958, p. 193.
[11] Hillert, M., Transactions. American Institute of Mining, Metallurgical, and Petroleum Engineers, 1961, p. 197.
[12] Davy, L. G. T. and Glover, S. G., Journal of the Australian Institute of Metals. Vol. 13, 1968, p. 71.

Summary

The papers in this publication deal with fundamental and applied research data on the toughness of ferritic stainless steels.

The initial paper, "The Toughness of Ferritic Stainless Steels," is a keynote address by Wright (Rensselaer Polytechnic Institute), serving to review past work on ferritic stainless steel toughness and to summarize the present state of understanding. Emphasis is placed on the micromechanisms of fracture and on effects on the ductile-to-brittle transition consistent with the Cottrell crack nucleation model. The general effects of strain rate, plastic constraint (including gage effect), and grain size are set forth. The basic fracture behavior of body-centered-cubic metals, iron, and iron-chromium solid solutions is summarized. Primary emphasis is placed on the role of second phases in the ferritic stainless steel fracture process, including extended discussions on carbides, nitrides, martensite, α'-precipitation, and σ and χ phases. The role of titanium and columbium as gettering agents for carbon and nitrogen (C + N) is considered. The effects of cold-work are set forth and a brief outline is made of annealing guidelines for optimized toughness. Finally the fracture behavior of welds and weld heat-affected zones (HAZ's) is discussed and approaches to improved as-welded toughness are reviewed.

The balance of the first session concerns current research on ferritic stainless steel fracture. Plumtree and Gullberg present their latest work on the influence of interstitial and some substitutional alloying elements on the toughness of ferritic steels. Vacuum-melted Fe-25Cr and Fe-18Cr-2Mo alloys with 40 to 1000 ppm (C + N) were studied using notched-bar impact tests. They found molybdenum and chromium to have little effect, but that combined (C + N) must be maintained below 150 ppm for a low ductile-to-brittle-transition temperature (DBTT) and a high shelf energy. While the DBTT changes rapidly with (C + N) in this range, it is much less sensitive to (C + N) changes at levels well below and well above 150 ppm. When one increases the interstitial (C + N) content to the 150-ppm range, a great increase is seen in the amount of second phase present, particularly at the grain boundaries. The second-phase particles enhance cleavage fracture by reducing surface energy. The tendency toward brittle fracture with increased interstitial content and larger grain size is explained by Plumtree and Gullberg in terms of the Cottrell theory for brittle fracture. Nickel additions are seen to decrease DBTT levels while slightly diminishing

upper-shelf energy. The addition of titanium to alloys with 270 to 570 ppm (C + N) lowers DBTT and increases shelf energy.

Grubb, Wright, and Farrar presented a paper on the micromechanisms of brittle fracture in titanium-stabilized and α'-embrittled ferritic stainless steels. Fe-26Cr alloys, with and without titanium stabilization, were studied with particular emphasis on microscopic observations of electropolished strips pulled in the DBTT range. Embrittlement due to α'-precipitation seems related to flow stress increase and the α'-precipitation is seen to bring about a gross change in slip character leading to the development of relatively few, extremely intense slipbands. It is clear that at total (C + N) levels in the 550-ppm range the effect of titanium is to lower the DBTT through removal of (C + N) (Plumtree and Gullberg, in the foregoing, noted similar behavior for compositions in the 270 to 520-ppm range). At total (C + N) levels of about 75 ppm, however, titanium lowers the DBTT for material that has undergone lengthy low-temperature heat treatment but raises the DBTT in all other cases. The embrittling effect of titanium is associated with intergranular microcrack formation and may reflect embrittling titanium segregation to the grain boundary or oxygen intergranular embrittlement due to extensive carbon gettering.

The fourth paper of this session is authored by Saito et al. This paper concerns fracture in Fe-30Cr-2Mo alloys and carefully considers stress state as well as metallurgical condition. By means of a "hydrostatic" tension test using Bridgman-type specimen designs, it is shown that this alloy is more sensitive to triaxial or hydrostatic stress state than a carbon steel would be. The implications of this for hot-rolling under conditions of high centerline tension are examined. The sensitivity to hydrostatic stress state is believed related to the role of twinning in the crack propagation process, and prestraining is discussed as a possible means of limiting the twin-related cleavage fracture. Grain size reduction through combinations of hot-working and normalizing treatments is set forth as a basis for improved toughness. Lastly, calcium additions are considered as means for modifying oxide and sulfide morphology in ways conducive to improved toughness.

The balance of the papers deal with the properties of commercial and developmental ferritic steels. Based on their chromium content, these steels can be divided in three groups: the high-chromium steels (26 to 28 percent), intermediate chromium (16 to 18 percent), and low chromium (10 to 12 percent).

A paper by Deverell deals with the impact properties of low interstitials: VIM melted E-BRITE[1] 26Cr-1Mo alloy, 29Cr-4Mo, and 29Cr-4Mo-2Ni-Fe alloys using the 50 percent shear fracture (FATT$_{50}$) (fracture appearance

---

[1] Registered trademark, Allegheny Ludlum Steel Corp.

transition temperature) of Charpy V-notch (CVN) impact specimens as the toughness measurement. Full-size (10 mm) CVN specimens of each alloy can show a $FATT_{50}$ below room temperature if heat-treated properly. The transition temperature decreases with lighter-gage material. Slow cooling from the annealing temperature or exposure at intermediate temperature increases the transition temperature substantially in comparison with water-quenching. This effect is felt also in the heat-affected zone (HAZ) of welds. Welding with adequate shielding and preparation results in similar weld, HAZ, and base metal transition temperature. The addition of nickel in 29Cr-4Mo-2Ni alloy has a beneficial effect on toughness.

Ohashi et al reports on the toughness of the extra-low interstitial alloys 18Cr-2Mo, 26Cr-1Mo, and 29Cr-2Mo, all columbium stabilized. Specimens with machined and natural cracks were used. In the as-annealed condition and, using machined notches, these materials have good toughness as indicated by transition temperature. In the presence of sharp notches or when exposed to temperatures where σ or Laves phases are formed, the transition temperature increases above room temperature. Thin-gage, fine-grain size and nickel addition have beneficial effects on toughness. The authors conclude that these types of steels have good resistance to crack initiation but relatively low resistance to crack propagation. The toughness of low-interstitial 18Cr-2Mo stabilized with columbium was studied by Nakazawa et al, using standard impact specimens and K_c values determined on specimens with sawed notches. Based on the test results obtained, it is concluded that this steel in thicknesses up to 12 mm can be safely used in welded structures at 0°C or higher. Embrittling factors are "475°C embrittlement" and phase precipitation at 750 and 950°C.

The Wood paper deals with the influence of residual elements carbon, nitrogen, manganese, silicon, nickel, copper, and molybdenum on the mechanical properties, including toughness, of 18Cr steel titanium-stabilized in thin-gage sheet 1.27 mm (0.050 in.) thick. The residual elements influence the mechanical properties of this steel especially in the welds. High (C + N), typical of electric-arc furnace melting, has much higher transition temperature than the (C + N) levels attained in vacuum melting or vacuum oxygen decarburization and AOD melting. Titanium also increases the transition temperature. In a similar study, Redmond reports on the influence of stabilizing elements niobium, titanium, (Nb + Ti), and (Cb + Al) and of residual elements sulfur, manganese, and silicon on the toughness of 18Cr-2Mo with low (C + N) (0.015 + 0.015). Impact transition temperature and crack-opening displacements (COD) measurements and COD transition temperature were determined. The sheet tested was 3.2 mm (0.125 in.) thick. Silicon, manganese, and sulfur had only a minor influence on the base metal and weld metal toughness. The base metal $FATT_{50}$ was below room temperature for all compositions examined. The

base metal toughness was best for niobium-stabilized steels followed by mixed niobium-titanium and titanium stabilization. In weldments, however, the order was titanium stabilization best followed by columbium-titanium and titanium. Increasing the total stabilizer content contact tends to increase the impact transition temperature. The importance and complexity of stabilizing elements is all too evident. Stabilization is, of course, mandatory in order to prevent intergranular corrosion.

The toughness of E-BRITE 26Cr-1Mo welded pipe 50.8 mm (2 in.) in diameter by 4.7-mm (0.187 in.) wall was studied by Scribner. The pipes were provided with machined notches and burst tested. The visual appearance of the fracture surface was used as a toughness rating. The transition temperature is above room temperature in both weld and HAZ when using E-BRITE filler metal. With C-276 filler metal, only the HAZ has transition temperatures above room temperature.

Krysiak's paper deals with the weld properties of 26Cr-1Mo-Ti and 29Cr-4Mo steels in relatively heavy gage 3.27 to 3.81 mm (0.129 to 0.150 in.). Sound welds have been made in both alloys. The need for careful gas shieldings and cleanliness is being emphasized to prevent carbon, nitrogen, and oxygen pickup. The best weld toughness was obtained with austenitic filler metal followed by a low-interstitial ferritic and then 26-1Mo-Ti. The transition temperature of 26Cr-1Mo-Ti weld metal was found to lie above room temperature.

The Fecralloy alloy described by Rosenberger and Wright is less tough than the other ferritic steels and, consequently, is used primarily in very thin strip.

The balance of the papers deal with the low-chromium (10 to 12 percent) steels which are frequently used in structural applications requiring good toughness. The influence of cold-working in increasing the transition temperature of Type 409 is discussed by Vigor. A low-carbon martensitic stainless steel is, however, not susceptible to this deterioration in toughness. Eckenrod and Kovach describe a new steel, E-4, which in the annealed condition has a fine-grained ferritic structure while the weld is low-carbon martensite. This combination insures good toughness in both base metal and weld. Thomas deals with the weld and HAZ of Type 409. Grain growth in the HAZ raises the transition temperature. Martensite formation also raises the transition temperature besides lowering the resistance to corrosion. Mintz in his paper discloses a method of circumventing the grain size effect on toughness in heavy-gage plate, consisting in a heat treatment which can refine the grain boundary carbides and lower the transition temperature appreciably. Creamer in a failure analysis paper demonstrated that 474°C (885°F) embrittlement has produced a brittle failure in a ferritic steel with 13.5 percent chromium and 0.5 percent titanium.

In conclusion, this symposium is the first forum for discussion and

assessment of the toughness of an emerging family of stainless steels which, based on their unique corrosion properties, are raising considerable industrial interest. The papers presented make a positive contribution to the understanding of the mechanism of fracture in these steels and of the influence of composition, structure, second phases, grain size, gage, cold-work, and welding. In light gages the toughness problems are minimized but, as the gage increases, the foregoing factors have to be taken into consideration in a cautious approach in engineering utilization.

R. A. Lula

Allegheny Ludlum Steel Corp., Brackenridge, Pa. 15014; editor.

Index